Novel process of hydrogen production from liquids of biomass origin

Panagiota Pimenidou

Submitted in accordance with the requirements for the degree of
Doctor of Philosophy

The University of Leeds
School of Process, Environmental and Material Engineering/
Energy and Resources Research Institute

December, 2010

The candidate confirms that the work submitted is her own, except where work which has formed part of jointly- authored publications has been included. The contribution of the candidate and the other authors to this work has been explicitly indicated below. The candidate confirms that appropriate credit has been given within the thesis where reference has been made to the work of others.

Chapters 4, 5, 7 and 8 within the thesis have been based on work from jointly authored publications. These jointly authored publications are:

Pimenidou P.[(a)], Rickett G.L., Dupont V. and M.V.Twigg. 2010. Chemical looping reforming of waste cooking oil in a packed bed reactor. Bioresource Technology. **101**(23) pp.6389- 6397.

Pimenidou P.[(b)], Rickett G.L., Dupont V. and M.V.Twigg.2010. High purity H_2 by sorption- enhanced chemical looping reforming of waste cooking oil in a packed bed reactor, Bioresource Technology. **101**(16), pp.9279- 9286.

Pimenidou P., Rickett G.L. and V. Dupont. 2009. In- situ CO_2 capture for unmixed steam reforming (Abstract). Oral presentation at WCCE8 (8th World Congress of Chemical Engineering). August 23- 27 2009, Montreal, Canada

All work contained within these publications are directly attributable to the candidate except for the non- isothermal FORTRAN kinetic calculations program, the excel balances flowsheets and the thermodynamic equilibrium calculations which are attributable to Dr. Valerie Dupont, while all authors have editing responsibilities.

December, 2010 The University of Leeds Panagiota Pimenidou

Acknowledgements

This research has been carried out by a team which has included Dr Valerie Dupont and Dr. Gavin Rickett. My own contributions, fully and explicitly indicated in the thesis, have been on everything except for the non- isothermal FORTRAN kinetic calculations program, the excel balances flowsheets and the thermodynamic equilibrium calculations which are attributable to Dr. Valerie Dupont.

My thanks to the Engineering and Physical Research Science Council (EPSRC), to Johnson Matthey for the catalyst material and to WBB Minerals for the dolomite.

Abstract

This thesis aims to investigate for the first time the chemical mechanism and efficiency of the process of unmixed steam reforming (also known as chemical looping reforming in a packed bed reactor) in producing hydrogen when utilising liquids of waste biomass origin as the feedstocks, in particular waste cooking oil. Moreover, the optimisation of unmixed steam reforming is investigated by incorporating a natural CO_2 sorbent, calcined dolomite, in the reactor bed material, resulting in the process called Sorption Enhanced Unmixed Steam Reforming, which operates by shifting the reactions toward more favourable thermodynamics.

The characteristic properties of three liquids of waste biomass origin (waste cooking oil, and fast pyrolysis oils from EFB -palm empty fruit bunches- and pinewood), are examined, including their decomposition kinetics by numerical modelling for the first time. The sorbent's efficiency, as expressed by its extent of CO_2 intake and release is examined at both 'micro'- and 'macro'-scales (i.e, from few mg to few g samples) through the kinetics of the carbonation and calcination reactions in conditions simulating sorption enhanced unmixed steam reforming, in addition to its durability in both set ups. These are compared to the sorbent's performance during the sorption enhanced unmixed steam reforming of the waste cooking oil throughout several chemical loops or cycles.

The chemical looping (cyclic operation) of both processes is assessed using the Ni-NiO and CaO-$CaCO_3$ 'loops', and compared against the equivalent process in thermodynamic equilibrium. The production from waste cooking oil of a nearly pure H_2 stream (>96% vol), with a hydrogen yield enhancement of between 29 and 120 %, with long periods of autothermality per cycle, at lower molar steam to carbon ratios (2.5 and 4) and lower temperatures (by 200 °C) than the literature to date on steam reforming of equivalent virgin vegetable oils is shown. This investigation thus demonstrates the success in producing H_2 from waste cooking oil using these advanced steam reforming processes, auguring promising results for similarly challenging organic waste liquid fuels.

Contents

Abbreviation		
$N_{o,MgCO_3}$	initial molecular amount of $MgCO_3$	mol
$N_{o,CaCO_3}$	initial molecular amount of $CaCO_3$	mol
MW_{MgO}	molecular weight of MgO	40.30
MW_{CaO}	molecular weight of CaO	56.07
$m_{i(MgCa(CO_3)_2)}$	initial mass of the $Mg(CaCO_3)_2$ in the fresh dolomite	g
a^i	molar conversion of $CaCO_3$ at any time in **TD_b** or CaO in **CRB**	%
M^o	initial mass of dolomite	g
$\overline{W_{CO_2}}$	Molar mass of CO_2	44.01 g mol^{-1}
P^i_{sorb}	percentage mass of the sorbent (oxide + carbonate; $CaO.CaCO_3$) remaining in the TGA crucible at step *i*	%
M^i_{sorb}	mass of sorbent remaining in the TGA at any time during the experiment of index '*i*'	g
$M^{f,i-1}_{sorb}$	mass of sorbent remaining in the TGA from the experiment prior to index '*i*' (*i*-1)	g
$N^{f,i-1}_{sorb}$	number of mol of the reactant sorbent species (carbonate if *i* is odd, oxide if *i* is even)	mol
$N^{f,i}_{CaCO_3}$	final molecules of $CaCO_3$ by step **TD_a**, **TD_b** or **TD**	mol
$N^{f,o}_{CaO}$	final molecules of CaO by step **TD_a**, **TD_b** or **TD**	mol
$\alpha^{f,i}$	Final molar conversion of $CaCO_3$ in **TD_b** or conversion of CaO in **CRB**	%
$N^{f,i-1}_{CaCO_3}$	final molecules of $CaCO_3$ from the	mol

	previous step **TD_a**, **TD_b** or **TD** in **CRB**	
$N_{CaO}^{f,i-1}$	final molecules of $CaCO_3$ from the previous step **CRB** in **TD_a**, **TD_b** or **TD**	mol
P_{CaO}	percentage of CaO in the sorbent	%
$\overline{W_{CaO}}$	molar mass of CaO	
$N_{CaCO_3}^{f,o}$	Number of $CaCO_3$ molecules at the end of the 1st thermal decomposition (i= 1)	mol
$N_{CaO}^{f,o}$	Number of CaO molecules at the end of the 1st thermal decomposition (i= 1)	mol
A	pre- exponential factor (Arrhenius),	s^{-1}
f(α)	differential conversion function	
E	activation energy	kJ mol^{-1}
$T_{CaCO_3\,(i)}$	initial temperatures during the calcinations (**TD**)	K
$T_{CaCO_3\,(f)}$	final temperatures during the calcinations (**TD**)	K
$T_{MgCa(CO_3)_2\,(i)}$	Initial temperature of $MgCa(CO_3)_2$ thermal decomposition	K
$T_{MgCa(CO_3)_2\,(f)}$	final temperature of $MgCa(CO_3)_2$ thermal decomposition	K
$T_{i(TD)}$	initial temperature of thermal decomposition of $CaCO_3$	K
$\%\alpha_{MgCO_3}^{TDi}$	conversion of $MgCO_3$ during the i^{th} step of TD (calcination)	%
ΔN_{CO_2}	number of CO_2 molecules evolved during **TD** or consumed during **CRB**	mol
N_{MgCO_3}	number of $MgCO_3$ mol in the as-	mol

	received fully carbonated dolomite	
$\alpha_{CaCO_3}^{i}$	conversion of $CaCO_3$ during TD_b or TD	%
$N_{CaCO_3}^{f,i-1}$	number of $CaCO_3$ molecules produced during the **CRB** or remained after **TD**	mol
$x_{CO_{2,out}}$	dry molar fraction of CO_2	
$\dot{N}_{dry,out}$	total dry molar flowrate of the gases leaving the reactor (CO_2, N_2)	mol min^{-1}
$\dot{N}_{N_2,in}$	molar flowrate of N_2 entering the reactor	mol min^{-1}
$N_{CaCO_3}^{f,i}$	number of $CaCO_3$ molecules at the end of TD	mol
$N_{CaO}^{f,i}$	number of CaO molecules at the end of TD	mol
α_{CaO}^{i}	molar conversion of CaO during CRB	%
$N_{CaO}^{f,i-1}$	available number of mol of CaO at the beginning of CRB	mol
$\dot{N}_{CO_{2,in}}$	molar flowrate of CO_2 supplied in the reactor during CRB	mol min^{-1}
P_{CO_2}	CO_2 partial pressure in CO_2/ N_2 mixture	kPa
$\dot{V}_{N_2}$	volumetric flowrate of N_2 supplied in the reactor	L min^{-1}
$\dot{V}_{C_nH_mO_k}$	volumetric flowrate of waste bio- oil entering the pre- heater	m^3 s^{-1}
$\dot{V}_{H_2O}$	volume flowrate of liquid water prior to vaporisation	m^3 s^{-1}
$m_{i\ (fresh\ catalyst)}$	mass of catalyst	kg
y_{CH_4}	dry molar fraction of CH_4	

y_{CO}	dry molar fraction of CO	
y_{CO_2}	dry molar fraction of CO_4	
y_{O_2}	dry molar fraction of O_2	
y_{H_2}	dry molar fraction of H_2	
y_{N_2}	dry molar fraction of N_2	
$\dot{n}_{out,dry}$	total dry molar flowrate of the gases	mol min^{-1}
$\dot{n}_{N_2,in}$	molar flowrate of nitrogen	mol min^{-1}
$X_{C_mH_nO_k}$ or X_{WCO}	waste cooking oil's conversion	
$\dot{n}_{WCO,in}$	inlet dry molar flowrate of WCO	mol min^{-1}
$\dot{n}_{WCO,out}$	inlet dry molar flowrate of the WCO	mol min^{-1}
$SEL_{CO\ or\ CH_4\ or\ CO_2\ or\ H_2\ or\ NiO}$	selectivity to the gaseous products (CO, CH_4, CO_2, H_2) or NiO	
$\dot{n}_{NiO\rightarrow Ni,FF}$	reduction rate of the NiO catalyst	mol min^{-1}
k	mole fraction of oxygen in the WCO	
$\dot{n}_{c,oxidation}$	rate of oxidation of the deposited carbon	mol min^{-1}
X_{O_2}	fraction of O_2 conversion	
$WHSV$	weight hourly space velocity	h^{-1}
S:C	steam to carbon ratio	
$\eta_{H_2\ purity}$	purity of hydrogen	
$\dot{v}_{H_2\ or\ CO_2\ or\ CO\ or\ CH_4}$	volumetric concentration fraction of H_2 or CO_2 or CO or CH_4	
$\dot{n}_{H_2O,out\ (H_2,red)}$	produced $H_2O_{(g)}$	mol min^{-1}
$X_{NiO\rightarrow Ni,red}$	reduction fraction of the NiO particles conversion	
$X_{Ni\rightarrow NiO}$	extent of Ni conversion to NiO	%

$X_{WCO,SS}$	Steady State waste cooking oil's conversion	
$X_{WCO,PB}$	Pre- Breakthrough waste cooking oil's conversion	
$X_{WCO,BT}$	Breakthrough waste cooking oil's conversion	
$\dot{n}_{CO_2,carb}$	rate of carbonation	mol min^{-1}
T_{middle} or T_{bottom}	temperature of the middle or bottom reactor's bed	K
$dt_{100\%\,CO_2}$	difference in time between the onset of the H_2 curve and the onset of the CO_2 curve	
$n_{CO_2,ads,BT}$	rate of adsorbed CO_2 from breakthrough to steady state	mol min^{-1}
t_{FR}	Time for the full catalyst's reduction	
R_{red}	% of the ratio of the NiO reduction rate	%
$\eta_{H_2,eff}$	H_2 yield efficiency	

Chapter 1
Introduction

The current technologies in the chemical and energy industrial fields use feedstocks of carbon origin, such as coal, oil and natural gas. Upon direct or indirect application of these materials, carbon dioxide (CO_2) emissions are produced, which lead to climate change. In addition, the international community seeks the exploration of the necessary natural sources to support the needs that have arisen in the past two centuries in the energy and transportation sectors, since fossil fuels are depleting. These concerns are further amplified by an upcoming economic crisis which alarms the Western countries' governments in order to undertake the patronage of promising future technologies.

Sustainable or green energy covers the needs of humanity for the supply of renewable energy or energy from renewable sources that will continue to supply energy to future generations. These sources originate in plants, in solar, wind, wave, hydro and geothermal energy. Biomass combustion and geothermal energy are regarded as first generation technologies, solar heating and wind power as second generation whereas biomass gasification, biorefinery technologies, concentrated solar thermal power and ocean power are considered as third generation technologies (IEA). Low carbon technologies on the other hand refer to the technologies that result in CO_2 emissions which do not harm the atmosphere and therefore they can be regarded as sustainable.

CO_2 as a by-product of general power-generation industries and the transport sector, has been the focus of attention, spurring on initiatives such as the Kyoto Protocol (UNFCC: Undated). The latter aims to reduce UK emissions of greenhouse gases by 8% of the 1990 baseline figures by the 2008-12 period. In general, in the past 3 decades special attention has been given to the prevention of the CO_2 emissions both in its pre- or post- production stages, by the development of alternative energy sources that may consequently cause the emergence of new technologies either in their processing or application.

Solar and wind energy have been considered to produce electricity for stationary applications but difficulties have been noticed in their uptake as they

require large areas. In the transportation sector one of the most promising and environmentally friendly fuels is hydrogen (H_2) as its heat of combustion is -285.5 kJ mol^{-1} -caused by an energy content of 142.9 kJ mol^{-1}, and produces water. Hydrogen's environmental friendliness relies on the fact that it is considered to be the energy carrier that offers most mitigation in NO_X and CO_X emissions when used in fuel cells (**Wee, 2010; Aki et al., 2006; Sun et al., 2004**) and hydrogen internal combustion engine (H_2 – ICE) applications (**Yamada et al., 2010; Verhelst et al., 2009; White et al., 2006; Ford report on the business impact of climate change: Media.Ford.com, 2009**).

The hydrogen economy is the term that is presently utilised by governments and organisations when they deal with the prospective utilisation of hydrogen as the alternative fuel for transportation. International policies are built around the hydrogen economy whose technology will change the scenarios for the future as currently known, in the way coal and steam did at the beginning of the Industrial Age. Unfortunately, most of the hydrogen economy studies are classified as visions which are not supported by conclusive theories (**Hisschemöller et al., 2006**). At this point it needs to be underlined that there are certain practical barriers that hinder the realization of the hydrogen economy such as the technological immaturity of on-board storage, the lack of hydrogen refuelling infrastructure, the limited lifetime and the high cost of the fuel cells which is encumbered by their deficiency in low carbon hydrogen production.

Hydrogen is abundant on earth in the form of water, fossil fuels and as a component of every living organism while in its elemental form is present in the order of parts per million in the atmosphere. The industrial scale production of hydrogen is currently based on hydrocarbons such as natural gas, naphtha and coal, combined with water, where natural gas and coal are already used as primary energy sources. Other methods are water electrolysis and the Bosch or water gas process, which consists in passing steam on white hot coke. Hydrogen is often found in oil refineries as a by- product. All these processes are analytically presented in **Chapter 2** where all current trends in the production of hydrogen are discussed.

The need for new or improved technologies for hydrogen production from sustainable sources becomes apparent as society and industry demands grow.

While fuel cells are developed for their better and durable performance, still the problem of finding sustainable sources of hydrogen remains, as it is at present extracted from fossil fuels. On one hand, alternative sources of hydrogen are sought, whereas on the other, energy efficient and low CO_2 emissions technologies need to be established. Hydrogen-derived technologies can be improved by sequestering the carbon dioxide that results in the production of that particular hydrogen energy carrier, or by using renewable sources. CO_2 that is industrially captured can currently be stored in geological formations like depleted oil and gas fields (**Rydén M. Et al., 2008**) or deep saline aquifiers (**Lyngfelt A., 2001**).

The global dependence on fossil fuels as a main energy source has led to a serious energy crisis and has had several implications on some of the key-players in oil production and exportation (**Ni et al., 2006**). In the most dramatic studies it is reported that the United Arab Emirates could fail to meet their share in the oil and natural gas demands by 2015 and 2042 respectively (**Kazim, A et al: 2001**). Fossil fuel energy dependency in 2003 in the US reached 86% with a projected increase of 1.5% till 2015 (**Muradov et al., 2008**). In addition to the reduction of existing fossil fuel resources, the combustion of fossil fuels will release substantial amounts of controlled greenhouse gases, such as CO_2, SO_2 and NO_X.

These indications were considered to favour the concept of the hydrogen economy and the preservation of the planet's fossil fuel reserves. Currently, hydrogen production in the United States heavily depends on hydrocarbon based fuels, with 95% of the hydrogen being produced from the steam reforming of methane (U.S. Department of Energy, 2008). Despite the benefits of hydrogen combustion, it is still being produced through non-environmentally friendly methods and from depleting natural resources, such as the steam reforming of natural gas, coal and naphtha which are accompanied by net atmospheric CO_2 emissions production. Consequently, in the long run, focus is given on the production of hydrogen from biomass sources or waste feedstocks without a net CO_2 increase (**Medrano et al., 2009**).

Biomass is suggested as a renewable source of energy while the net CO_2 emissions generated from the combustion of biomass or biomass-derived fuels are minimised as they are near-carbon neutral. In addition, the use of biomass as energy sources diminishes the dependence on fossil fuels. Intense investigation of

the steam gasification of biomass or biomass-derived products (**Toonssen et al., 2008; Hauserman, W. B, 1994**), their fast pyrolysis (**Ni et al., 2006; Czernik et al., 2004**) and the steam reforming of biofuels or bio-oils (**Iordanidis et al., 2006; Marquevich et al., 2000**) has commenced, as it combines the H_2 extraction from both organic feedstocks and water, allowing water to become a hydrogen source through thermochemical means at higher energy efficiency than that required by water splitting alone. Biomass gasification is coupled with shift converting or steam reforming of the product hydrocarbon gas, and followed by purification to achieve a clean product stream (**Toonssen et al., 2008; Mahishi et al., 2007**). Furthermore, biomass derived fuels (**Rioche et al., 2005; Vagia et al., 2008**) and sunflower oil (**Dupont et al., 2007; Marquevich et al., 2000**) had their share of attention in the steam reforming process as a transition technology for cleaner hydrogen. Non-reforming technologies such as water and steam electrolysis are still not economically feasible due to their high cost in production and distribution especially when electricity delivery is considered (**Mueller- Langer et al., 2007**).

Vagia et al. (2008) and **Czernik et al. (2007)** carried out research that further illustrated the viability of hydrogen production from the steam reformation of bio-oils and/or their fractions, and found that a hydrogen rich product gas stream can be obtained. **Vagia et al. (2008)** achieved 50% conversion of acetic acid (a component of the aqueous fraction of bio-oil) with a hydrogen yield of 35% at a temperature of 823 K (550°C), and at higher temperatures of 923 K (650°C) and 1023 K (750°C) observing full conversion of acetic acid and a yield of 90%. **Czernik et al. (2007)** achieved a stoichiometric yield of 70- 80% at 1123 K (850°C) and for a S:C of 5.8. **Rioche et al. (2005)**, despite achieving a hydrogen yield of 60- 70% in their work on the steam reforming of the model components of bio-oil's, noted an observable gradual deactivation of the catalyst. **Vagia et al. (2008)** confirmed the formation of carbonaceous species that deposited on the catalyst surface that led to a serious side effect of the steam reformation of fast pyrolysis bio-oils, diminished effectiveness of the catalyst and resulted in reactor blockage which reduced the hydrogen yield. Despite the favourable hydrogen yields that were obtained from the whole bio-oil over the aqueous carbohydrate-derived fraction of the bio-oil, the economics of steam reforming all of the bio-oil were deemed less encouraging by **Czernik et al. (1999)**.

The feasibility of hydrogen production from a biomass originated feedstock such as sunflower oil (**Marquevich et al., 2003**) was demonstrated by attaining hydrogen yields within the range of 65.6-72.3% while the conversion fractions of the feed oil to product gases ranged from 0.2 to 0.95. The divergence in the conversion of the feed oil to product gases was highly dependent on the S:C (molar steam to carbon) ratio, temperature and type of catalyst used. **Dupont et al. (2007)** observed full conversion (100%) of sunflower oil for S:C= 1.8 at 973 K despite high carbon deposition as the $C_{(s)}$ selectivity reached 39.9%, thanks to a self-regenerating process making use of chemical looping which featured an oxidative step.

The "Novel Process of Hydrogen Production from Liquids of Biomass Origin" looks primarily into the unmixed steam reforming (USR) of waste cooking oil and the suitability of two fast pyrolysis oils as future feedstocks for this process. The preliminary study of all three oils is discussed in **Chapter 6**, based on their chemical and kinetics characterisation investigated via a series of small studies. The novelty of USR was based on the unmixed combustion concept as laid out first by **Lyon and Cole (2000)**, who observed the potential for the catalyst's utilisation as a mass transfer material (MTM), in this case for the transfer of oxygen, therefore supporting any endothermic reactions that are involved in the conventional steam reforming process via the oxidation of the catalyst (**Lyon and Cole, 2000**). Unmixed Steam Reforming (USR) is the process that combines cyclically alternated feeds of air with fuel and steam feeds in a single reactor packed with particles of an oxygen transfer material (OTM) which doubles as a steam reforming catalyst. In the investigation by **Dupont et al., (2007)**, this oxygen transfer material or OTM was nickel, which oxidised under air flow thus releasing heat, and reduced while still hot under fuel and steam flow, becoming active for steam reforming.

The uniqueness of the USR relies on the fact that it aims to (i) utilise fuels of biomass or waste origin without cumulative poisoning by carbon deposits (**Pimenidou et al., 2010[(b)]; Pimenidou et al., 2010[(b)]; Dupont et al., 2008; Dupont et al., 2007**) (ii) increase the purity of the end product stream by N_2 separation from the air caused by the oxidation of the OTM catalyst under air feed, and increase it further when the OTM catalyst bed is mixed with a solid CO_2 sorbent, by CO_2 capture via the process of 'sorption enhancement' (**Pimenidou et**

al., 2010[(b)]; Dou et al., 2009; Dupont et al., 2008; Dupont et al., 2007) (iii) by combining exothermic and endothermic reactions at the heart of the process, and by shifting the equilibrium of the steam reforming and the water gas shift reactions via in-situ CO_2 capture, decrease the operating temperature (**Pimenidou et al., 2010[(a)]; Pimenidou et al., 2010[(b)]; Dou et al., 2009**) and overall to decrease the energy consumption or even achieve autothermality (e.g. no external heat input is required) of the process. For the sake of operating with favourable thermodynamics of the steam reforming reaction, the process is best operated at atmospheric pressure. Moreover, any carbon depositions from the steam reforming of the fuel on the catalyst are removed during the AF feed step (**Pimenidou et al., 2010[(a)]; Dupont et al., 2007**). USR may have an additional advantage with regards to sulphur tolerance of the catalyst when compared to the conventional steam reforming process. This was observed by **Lyon and Cole (2000)** when they found that the sulphur in the fuel was oxidised to gaseous SO_2 by application of the air flow feed (AF), thus preventing the cumulative poisoning of the catalyst by surface sulphates. Therefore, it becomes apparent that gaseous or liquid fuels that were hitherto poor H_2 feedstocks via conventional catalytic steam reforming can now be considered as possible candidates for unmixed (also termed 'chemical looping') steam reforming. Methane (**Dupont et al., 2008**) and sunflower oil (**Dupont et al., 2007**) can achieve high conversions to H_2 under the USR process, as glycerol USR did when sorption enhanced (**Dou et al., 2009**).

The USR process comprises two alternating half cycles of fuel feed (FF) and air feed (AF). Both the FF and AF feed steps make up a full cycle. When used in packed bed configuration, two reactors would need to be employed in order for each half cycle (that is FF and AF), to operate in parallel and generate a continuous H_2 output. With a single reactor, the H_2 production is intermittent and corresponds to the FF feed step. The fuel feed (FF) step involves the steam reforming of the fuel which passes over the catalyst particles with steam. The mechanism of the FF and AF steps are presented in **Chapter 2**. The catalyst is initially pre-reduced in order to serve as an oxygen transfer material (OTM) that results in a better heat transfer in the entire reactor's volume in order to enhance the highly endothermic reactions which are involved. The OTM catalyst is then oxidised by air via a highly exothermic reaction which heats up the bed, and then reduced by the organic gases

present during the fuel and steam feed (e.g. the fuel itself and its decomposition products such as CH_4, CO and hydrogen) thus becoming catalytically active for the steam reforming process. Another advantage that this process offers is the initiation of the water gas shift (WGS) reaction which further promotes the conversion of CO into hydrogen (H_2) and CO_2 (**Dupont et al., 2008; Kumar et al., 1999**).

During the air feed (AF) step, the NiO is formed by the direct contact of the reduced Ni catalyst with oxygen while any solid carbon that had deposited on the catalyst during the FF step is removed by oxidation as a gaseous oxide of carbon product. When a carbonated CO_2 sorbent is present, the temperature rise caused by the oxidation reactions of the air feed also result in the calcination of the sorbent (i.e. its regeneration). The USR process is pertinent to the chemical looping combustion (**Ishida et al., 1987; Rizeq et al., 2003**), featuring the same chemistry, albeit in packed bed configuration with alternate flows, as opposed to the dual fluidised bed configuration and interchanging material flows most common in the literature for chemical looping. Chemical looping was proposed primarily for the combustion process as a boosting power station efficiency system as well as to sorption-enhance gasification and circulated fluidised bed reforming. These processes' relevance relies on the cyclic chemistry of the OTM and the Ca based sorbents, and separation of the fuel and air at different stages. At present, the most common terminology found for the unmixed fuel process in the literature is 'chemical looping in a packed bed'.

The present study's breadth is to scrutinize and prove the viability of producing hydrogen from waste vegetable cooking oil when the USR process is applied (**Chapter 7**). The quantitative parameters that will be examined are the hydrogen yield, the purity of the gas product with and without the use of a CO_2 sorbent, and the possibility of an autothermal process. The secondary parameters that will aid the derivation of the process's primary outcomes are: the volume flow rates of the product gases, reduction and oxidation rates of the catalyst as well as the selectivity of the system to the different gaseous products.

As mentioned earlier, the experimental procedure initially involves a hydrogen reduction step on the fresh catalyst which is, as received from the manufacturer, in an oxidised form (NiO) on an alumina support. This initial step which is conducted only once and at the very beginning of a single experiment is

then followed by a steam reforming (fuel-steam feed or 'FF') step and then an oxidation step (air feed or AF). In total six FF cycles and six AF cycles will be conducted in a cyclic manner. This allows scope for comparison of the hydrogen yields obtained with the use of an OTM only and with combination of an OTM and a CO_2 sorbent.

A sorbent can be applied in the USR process, to potentially capture CO_2 when at the same time steam reforming occurs (FF step). In the case a sorbent is employed within the catalyst bed, the process of USR becomes 'sorption enhanced' (SEUSR- Sorption Enhanced Unmixed Steam Reforming). The sorbent's presence can, through Le Chatelier's principle, aid the water gas shift (WGS) reaction by driving the reaction forward (Dupont et al., 2008) resulting in enhanced production of H_2. Therefore, a high purity (over 90%) H_2 reformate can be potentially produced as an outcome of the in-situ N_2 and CO_2 separation as well as of the beneficially promoted WGS reaction (less unreacted CO). In the AF step the exothermic catalyst oxidation reaction elevates the temperature within the reactor bed to levels that match the sorbent's thermal decomposition, which is accompanied by CO_2 release, thereby regenerating the CO_2-sorbent for the following cycle.

Again according to Le Chatelier's principle, the use of a sorbent can further assist the reforming of the fuel in the presence of steam due to the enhanced consumption of CO resulting from the increased water gas shift, this further contributes to increasing the purity and yield of H_2 in the reformate by decreasing the concentration of unreacted fuel. This was observed for the SEUSR of the waste cooking vegetable oil (**Chapter 8**). In order to better investigate the sorption enhancement effect, two studies of the CO_2 capture and release (carbonation and calcinations) of a natural sorbent in both a small and bench scale reactors ('micro' and 'macro') were conducted in the absence and presence of steam. These pre-studies are presented in **Chapter 4** ('micro'- study) and **Chapter 5** ('macro'- study) (**Pimenidou et al., 2009**), and gives an insight in the sorbent's performance for its CO_2 capture capacity in conditions simulating those of unmixed steam reforming. The latter observation is critical, as distinction of these two different actions during the FF step is necessary for a better understanding of the SEUSR process, as discussed in **Chapter 8**.

In a nutshell, this study investigates and demonstrates the viability of the USR to produce H_2 from waste cooking oil (WCO) with optimised energy efficiency, via the cyclic reduction and oxidation of the catalyst (OTM) in the absence and presence of a cheap, natural high temperature solid CO_2-sorbent. The challenge of using this fuel to sustain the efficiency of chemical looping reforming is attested. Furthermore, the sorbent's presence is shown to produce a high purity H_2 reformate over repeated cycles when at the same time SEUSR reaches large intervals of its cycle where very little or no external heat is supplied to the process, demonstrating autothermal behaviour for long periods of time within each cycle.

Chapter2
H_2 production

Hydrogen is a promising primary energy material for replacing fossil fuels in many applications, as well as a secondary one, as for example in producing electricity. The majority of the Western countries' Research and Development programs invest in research towards the hydrogen economy since the fuel cells technology using hydrogen as a fuel, offers an environmentally and economically friendly alternative to current fossil fuel economy.

Until today, industrial hydrogen production relies on fossil fuels applying methods such as steam reforming, coal gasification and partial oxidation as the oldest and most economic processes. In terms of operation, all these methods are highly energy consuming and they produce large amounts of carbon oxides (CO_x) as well as sulphur oxides (SO_x).

Carbon dioxide (CO_2) and methane (CH_4) are considered to be two of the major contributors in the global warming phenomenon and possibly in the future might have financial and regulatory effects for the hydrogen production companies. Consideration is taken for the utilization of the non-renewables produced in these processes. Processes like biomass pyrolysis and gasification are quite similar to steam reforming and gasification of fossil fuels.

Essentially, the need for renewable sources of hydrocarbons as hydrogen carriers is emphasized as well as the development of less energy intensive processes that will limit or eliminate the by-production of global warming gases.

This project aims to study the production of high purity hydrogen from liquid fuels of waste biomass origin with high energy efficiency by the Unmixed Steam Reforming (USR) process and by Sorption Enhanced Unmixed Steam Reforming (SEUSR) using coupled Ni- and Ca- chemical looping in a single packed bed reactor under alternated cyclic air feeds with fuel and steam feeds. In order to demonstrate the advantages of the USR and the SEUSR processes, it is necessary to explore the current methods of hydrogen production.

2.1 H_2 production history

It is very interesting to revise the chronicles of hydrogen technology related to hydrogen technology in order to realise the progress made in the last 50 years.

Robert Boyle in 1670 produced hydrogen from acid reaction on metal. The water gas shift reaction ($CO + H_2O \rightarrow CO_2 + H_2$) was discovered in 1780 by Felice Fontana. Antoine Lavoisier, in 1783, was the "godfather" of hydrogen, where the term is based on "hydro" for 'water' and "genes" for 'born of'. In the same year Lavoisier and Pierre Laplace measured the heat of combustion of hydrogen. The steam iron process ($3Fe + 4H_2O \rightarrow Fe_3O_4 + 4H_2$) of Lavoisier and Meusnier (1784) was the first process of hydrogen production from water passed over a bed of hot iron at 600°C. In 1789, Jan Rudolf Deiman and Adriaan Paets van Troostwijk succeeded in water electrolysis by using a Leiden jar, which created static electricity between two electrodes in the inside and outside of a jar. William Nicholson and Johann Ritter decomposed water with use of a voltaic pile. In 1806 François Isaac de Rivaz engineered the first internal power combustion engine by using hydrogen and oxygen. The same Swiss inventor at the end of 18th century experimented with steam powered vehicles. In 1834, Michael Faraday publishes his law on electrolysis. In the same year Benoît Paul Émile Clapeyron developed the ideal gas law. Two years later, in 1836, John Frederic Daniell invented a primary cell in which hydrogen decomposed producing electricity. The fuel cell principle was firstly presented by Christian Friedrich Schönbein (1839) in the "Philosophical Magazine". The "Philosophical Magazine" was the first published (1798) scientific journal. In 1893 Friedrich Wilhelm Ostwald by conducting experiments, described the operation of fuel cells. Jackson D.D. and Ellms J.W.in 1896 were the first to mention hydrogen production by microalgae (anabaena), as representatives of the Massachusetts Board of Health. In 1898, James Dewar liquefied hydrogen mainly with the aid of his invention, the vacuum flask (Royal Institution of London). The Linde-Frank-Caro process (1909) was developed for hydrogen production by removing H_2 and CO_2 from water gas by condensation. In 1910 Fritz Haber patented the Haber process for ammonia production ($N_2 + 3H_2 \rightarrow 2NH_3$).

At this point it is important to emphasize that till the World War Two, hydrogen for ammonia production in Europe was mainly sourced from the electrolysis of water and not from the steam reforming of natural gas as we know it

today. In particular, the Vermok hydroelectric power plant of 60 MW produced solely hydrogen via electrolysis which was exclusively intended for ammonia production.

The hydrocracking process (the catalytic cracking of heavy hydrocarbons into smaller more desirable fractions in the presence of hydrogen) was launched in 1920 in a plant in Germany (Leuna) for the commercial hydrogenation of brown coal. The first synthetic methanol was produced by BASF in 1923 by the steam reforming method. In the same year J. B. S. Haldane envisaged and recorded in Daedalus (or Science and the Future) that "great power stations where during windy weather the surplus power will be used for the electrolytic decomposition of water into oxygen and hydrogen". Three years later the partial oxidation process (hydrocarbon+O_2→CO+H_2) was developed at the University of Illinois by Vandeveer by using oxygen instead of air for the production of syngas.

In 1937 the Heinkel HeS 1 (Heinkel-Strahltriebwerk 1; German for Heinkel Jet engine 1) was the first experimental gaseous hydrogen fuelled (centrifugal) jet engine built as well as the first working jet engine. In 1943 hydrogen liquid was tested as rocket fuel at Ohio University. 1939 - Hans Gaffron discovered that algae can switch between producing oxygen and hydrogen.

2.2 Available methods and current trends in H_2 production

The main current energy carriers are electricity, gasoline and natural gas while 1/3 of the energy carriers end up to the consumers in a solid form as coal and biomass. The sustainable energy policies prefer more economical and renewable sources for the end users. Electricity and hydrogen are considered as the main future energy carriers. The production processes of hydrogen from fossil fuels are the oldest and the cheapest. Their major drawbacks are the large carbon dioxide emission production and the energy penalties the present processes entail. The CO_2 emissions awareness is further discussed in **chapter 3**.

Light hydrocarbons (natural gas, refinery gases, LPG (propane, butane), naphtha) are used as the sources of hydrogen in the current industrial processes by applying steam reforming for the light hydrocarbons or partial oxidation for the

first and second set of feedstock. The main hydrogen by-products are carbon monoxide (CO) and carbon dioxide (CO_2). Consideration is given to the utilization of the non-renewables produced in these processes. Econometric models are built in order to predict the duration of the remaining reserves of fossil fuels. It is estimated that oil, coal and gas will last for 35, 107 and 37 years respectively based on the Klass model (**Shafiee et al.; 2009**). The only fossil fuel that will be available after 2042 will be coal. On the other hand, the speculations of IEA (International Energy Agency) based on the coal consumption rate in 1998 showed that the current reserves will be depleted globally within 224 years and within 237 years in the OECD (Organisation for Economic Co- Operation and Development) countries (**Alpern et al., 2002**).

2.2.1. Current methods

The industrial processes that are mainly employed in hydrogen plants are selectively presented based on their contribution to global hydrogen production. The worldwide hydrogen production is estimated at 0.1 Gtonnes and is vastly consumed in oil refineries and in ammonia and methanol production.

2.2.1.1 Natural Gas Steam Reforming

In the conventional steam reforming process of methane (SMR- Steam Methane Reforming), the fuel is reformed via a highly endothermic reaction at a high temperature and pressure (500- 950°C; around 3 - 25 atm respectively) in order to produce a mixture of hydrogen (H_2) and carbon monoxide (CO).

$$CH_4 + H_2O \rightarrow 3H_2 + CO \qquad \Delta H_{298.15K} = +206 \text{ kJ mol}^{-1}$$

The main hydrocarbons are cracked into H_2, CO and CO_2 usually on Ni catalyst particles dispersed on catalyst supports (such as silica, alumina, titanium, ceria and zirconia) which are packed in the reformer tubes (**Diskin et al., 1998**). The high temperatures that are applied in the reformer result in the use of heavy and expensive materials such as high alloy nickel- chromium steel, in addition to the irreversible formation of carbon and the high energy consumption.

Many researchers focused on alternative catalysts for lowering the operating conditions as they believed that the current catalysts (Ni or Ru on Al_2O_3 or SiO_2; **Sato et al., 2007**) are not effective in the steam reforming of hydrocarbons at temperatures lower than 1073 K (800°C). Additionally, the enhancement of Ni catalysts with mineral substances such as Mg (**Nagaoka et al., 2007**) for fuel cells pre-reformers was confirmed and the potential of autothermal CH_4 conversion to H_2 was investigated (**Takehira et al., 2004**) while catalysts enriched by potassium (K) addition (**Stefanescu et al., 2007**) exhibited lower coke formation. In the past, attempts were made in manufacturing Ni catalysts that will allow lower operating temperatures i.e. supported on zirconia (**Matsumura et al., 2004**) or that will promote lower steam to carbon ratios (**Marquevich et al., 2001**) in the steam reforming process to economise on the energy and material burden of raising steam from purified water.

Steam in the reformer is in excess in order to prevent thermal cracking and coking. The steam and carbon monoxide can further react to produce additional hydrogen in the mildly exothermic reaction called water gas shift (WGS reaction);

$$CO + H_2O \rightarrow CO_2 + H_2 \qquad \Delta H_{298.15K} = -41 \text{ kJ mol}^{-1}$$

The steam reforming and reverse water gas shift reactions are catalytic. The methane fuel passes through zinc oxide or activated carbon beds to adsorb any sulphur it may carry (usually as H_2S) and to avoid the catalyst's deactivation.

Following the steam reformer, two different temperature shift converters are employed in order to enable water gas shift reactions that will enhance the H_2 production by conversion of CO and steam to CO_2 and H_2. The water gas shift reaction (WGSR) is a slightly exothermic reaction which means that its equilibrium constant decreases with increasing temperature and thus that as it proceeds and releases heat, it raises the reaction temperature which then limits its progress. For thermodynamic and kinetic reasons it is industrially performed in two stages with cooling in between which restores the loss in activity from its exothermicity. The low temperature shift converter (473- 523 K) succeeds the high temperature shift converter (583- 803 K). It is very important to monitor the temperature of the catalyst beds in both the high and low temperature shift reactors in order to maintain optimum CO conversion. In the high temperature shift reaction, Fe_3O_4/

Cr_2O_3 catalysts are used, leaving a 2.5 vol % dry CO concentration at the exit, whereas in the low one, the catalysts that are employed are Cu- ZnO- Al_2O_3, resulting in a 0.2 vol% dry CO concentration.

The low temperature shift converters' catalysts are sensitive to chloride and sulphur poisoning. Periodic checking of the inlet gas composition is necessary. Chlorides' presence may be due to leaking water from upstream heat exchangers.

The steam reforming of methane is completed with the purification of hydrogen from CO, CO_2 and N_2 via a PSA (Pressure Swing Adsorption) or TSA (Temperature Swing Adsorption) process. Alternatively, chemical adsorption can be applied by using an amine contactor combined with methanation in order to eliminate CO and CO_2. Finally any CO_2 surplus can be removed from the high H_2 purity (99.99%) product by isolation. Analysis of syngas purification from CO_2 is given in **chapter 3**. It is worthy of noting that the maximum theoretical yield of hydrogen via steam methane reforming followed by complete water gas shift is 4 mol H_2 per mol of CH_4, or 50 wt % of the CH_4 fuel, the highest from hydrocarbon sources.

2.2.1.2 Partial oxidation (POX)

The partial oxidation of light and heavy hydrocarbons is applied, even though it is a quite similar process to the SMR. In partial oxidation, methane is oxidized directly, by pure O_2. In partial oxidation, the oxidative material that is required for methane is less than the stoichiometric requested for the complete combustion of the hydrocarbon fuel. The product of this process is a syngas (synthesis gas) stream that primarily consists of hydrogen and carbon monoxide.

Partial oxidation of methane is described by the following reaction:

$$CH_4 + \frac{1}{2} O_2 \rightarrow CO + 2H_2 \qquad \Delta H = -36 \text{ kJ mol}^{-1}.$$

The partial oxidation contends the total oxidation reaction which is the following:

$$CH_4 + 2\,O_2 \rightarrow CO_2 + 2H_2O \quad \Delta H = -890 \text{ kJ mol}^{-1}.$$

Additionally, nitrogen oxides are produced (**Guo et al., 2007; Otsuka et al., 1998**) resulting in further cleaning of the produced hydrogen gas.

Preheated methane or natural gas (750 K) and oxygen (450 K) are fed in the reactor. Both gases are mixed by a burner and react in a turbulent diffusion flame. The high temperatures (1650 K; 1377°C) of the produced syngas are maintained by the refractory lined reactors. In autothermal reforming, partial oxidation and steam reforming, methane reacts with steam and oxygen in the presence of a catalyst.

Coke formation is avoided by (i) high temperatures, (ii) short resident times and (iii) control of the oxygen feed to the required stoichiometric ratio. A catalyst is not needed even though its presence could enhance the process's yield as well as reducing the operating temperature.

The POX reactor design is simpler compared to the one used in the SMR in which case the methane is burned in the reactor rather than heated separately as it occurs in the SMR; hence less heat transfer is required through the reactor compared to the steam reformer.

Despite the fact that this process presents certain advantages in terms of the H_2:CO ratio and of its slight exothermicity, it still encounters drawbacks in the methane conversion which occurs in two steps. The first one involves the complete combustion of methane with oxygen into CO_2 and water while the second step results in CO_2 formation and steam reforming of the residue methane by the first step and the final production of syngas. Due to the overall exothermic methane oxidation, "hot spots" (**Koh et al., 2007; Chen et al., 2007**) may be created on the catalyst bed which can melt its support material leading to the catalyst's deactivation. The process is considered to be non-catalytic even though particular attention has been given in later years to the catalytic partial oxidation (CPO) which is more promising economically (**Corbo et al., 2007**). Still the CPO indicates that the process is efficient in terms of H_2 selectivity when a Ni- based catalyst is used, but the potential of its activity loss may be caused by the extremely high resulting temperatures. On the other hand, the application of a Pt- catalyst ensures the stable performance of the process but does not exhibit high H_2-selectivity (**Corbo et al., 2007**).

Careful control and design of special reactors is required for the partial oxidation process. If the previous parameters are not encountered at the required level, thermal runaways or possible explosions can occur during the feed- gas pre-mixing (**Chen et al., 2007**).

From hydrogen yield point of view, the partial oxidation of methane to CO and H_2 only yields 2 mol of H_2 per mol of CH_4, or 25 wt% of the fuel, i.e. half of the hydrogen yield from steam methane reforming. As a result, SMR is more appealing economically over the partial oxidation process despite some of its advantages as previously described. Even though the partial oxidation's reactor is cheaper in construction, it is more expensive in operation than the SMR's due to significant heat losses.

2.2.1.3 Autothermal reforming (ATR)

The common steps between the ATR and the SMR are:

- Natural gas compression and purification i.e. from sulphur,
- Catalytic steam reforming of methane to H_2 and CO,
- Water gas shift conversion of CO into CO_2 and additional H_2,
- Hydrogen product stream purification.

Autothermal reforming combines partial oxidation and adiabatic steam reforming. In this process the reactor is divided into three sections. The first one consists of a refractory lined pressure vessel with a burner that is followed by a combustion chamber where the partial oxidation of the preheated natural gas or methane with the preheated oxygen takes place. In the final section, the syngas is reformed on a catalyst bed. The produced syngas is at 1300 K (1027°C) which is dictated by the catalyst's operating conditions.

Table 1 Main industrialised hydrogen production processes' operating conditions and pre- purification H_2/ CO product ratios

Method	Operating conditions		H_2/ CO
	Temperature (K)	Pressure (bar)	
SMR	1023- 1173	15- 40	3- 5
POX	1123- 1273	20- 40	1.6- 2.65
ATR	1473- 1773	20- 150	1.6- 3

In **Table 1** the main characteristics of syngas production methods are presented. From the H_2:CO ratios it appears that the more attractive process is that of SMR. On the other hand despite of the fact that the POX reactor is more compact, the ATR reactor is less expensive and more flexible in terms of H_2:CO ratios of the produced syngas.

2.2.1.4 Coal gasification

Coal gasification on the other hand follows the SMR principle. The chemistry of coal gasification can be quite extensive due to the operating conditions and the reactants that are applied. In particular, coal is pre-treated with steam (1330°C) under high pressure (25 bar) for syngas to be produced while heat is supplied,

$$Coal + H_2O \rightarrow H_2 + CO + impurities$$

The oxygen is regulated to result in incomplete combustion of the fuel compared to the oxygen that is supplied in a combustor. Any minerals that are contained in the feedstock leave the gasifier as an inert slag. A smaller fraction of these solids is blown out from the gasifier as flying ash downstream.

The catalytic shift conversion of CO as well occurs in a shift reactor:

$$CO + H_2O \rightarrow CO_2 + H_2$$

giving a 60% H_2 in the product that also contains CO_2 residues of CO and impurities (i.e. CH_4, O_2, N_2 and H_2O) depending on the composition of the syngas.

Finally the produced hydrogen is purified from sulphur- containing products (99.99% removal of H_2S) by physical adsorption followed by the PSA. In the case that isolation is required, secondary adsorption removes the remaining CO_2.

Several products may be contained in the produced syngas as H_2O, CO and CH_4 and traces (i.e. H_2S, NH_3) which vary upon the applied process and the organic and inorganic content of the feedstock. The cost of the produced hydrogen via coal gasification depends on the employed technologies and whether CO_2 sequestration is involved or not (**Stiegel et al., 2006**). In coal gasification, the purification of oxygen contributes significantly in increasing its cost.

Therefore, the competitiveness of coal gasification strictly depends on the newly developed technologies' reliability and cost. The term "newly developed technologies" aims to describe any incremental developments that are made to well established technologies (i.e. CFB (Circulated Fluidised Beds); **Li X.T. et al., 2004**) or materials (i.e. catalysts; **Wang J. et al., 2010; Zhang et al., 2010** or feedstock; **Asadullah et al., 2010**) in the gasification process. In general, there are several aspects in the gasification, gas cleaning and gas separation technologies that need to be resolved in regard to the previously mentioned concerns. More particularly, an issue that arises in respect to the certainty of any new developments at the various stages of the coal gasification are for example the need for extra protection of the reactor's material due to sulfidation and corrosion at high temperatures.

2.2.1.5 Biomass gasification

Production of hydrogen from biomass can be obtained either by applying direct gasification or pyrolysis to produce liquid bio-oil for reforming. Biomass is an organic material originated in (i) agriculture including hardwood, softwood (ii) and in waste including municipal solid waste or sewage. Despite the fact that biomass is supported by many (**Kirubakaran et al., 2009**) to be a renewable source of energy due to high availability of agricultural fields in developing countries' economies, it is thought by many that these food sources could be used in alleviating the ever-present poverty faced by the majority of the population in those countries.

Direct biomass gasification is similar to the coal gasification process. More particularly it involves partial oxidation of the biomass with air, oxygen and/ or steam leading to the formation of a syngas of which the main gaseous product is H_2. The biomass is treated with steam in a gasifier where syngas containing hydrocarbon gases, hydrogen, CO, CO_2, tar and water vapour are produced. The char that is left in the gasifier is then treated with oxygen, steam and hydrogen. Shift reaction and purification follow the gasification step.

The efficiency of biomass steam gasification for the hydrogen production is reported to be enhanced by using a CO_2- sorbent because the tars can be reformed. In spite of this, the maximum yield that is achieved is 62.2% (**Madhukar et al., 2007**).

Waste sludge and woodchips biomass gasification for H_2 production was carried out by **Sato et al. (2007)**. Ni/ MgO- CaO (based on dolomite) catalyst that was doped with WO_3 applied to resist sulphur poisoning. This catalyst showed big tar reforming performance, plus it proved its resistance to coking, sulphur poisoning and was stable even in the presence of hydrogen sulphide (**Sato et al., 2007**).

Overall the application of the biomass gasification either in moving bed or fluidised bed reactors either exhibits a non- uniform temperature profile or results in deviation from chemical equilibrium respectively. Both effects result in low carbon conversion or in decreased quality of the product gas (**Li et al., 2004**)

2.2.1.6 Biomass pyrolysis

Liquid bio- oils are produced by biomass pyrolysis which involves depolymerization of cellulose, hemicelluloses and lignin. During pyrolysis, biomass is endothermically decomposed at 450- 550°C to oxygenated organics and water in order to produce food additives and special chemicals (**Bridgwater, 1999**). Longer residence times and wider temperature ranges are applied for producing liquid bio-fuels (**Bridgwater et al., 1999**).

$$Biomass + Energy \rightarrow Bio - oil + Char + Gas\ impurities$$

The bio-oil is then reformed via steam (Magrini-Bair et al., 2003) in the presence of a nickel catalyst at 750-850°C.

$$Bio - oil + H_2O \rightarrow CO + H_2$$

Following up, CO is converted into CO_2 by water shift reaction:

$$CO + H_2O \rightarrow CO_2 + H_2$$

Zhao et al. (2010) attempted to optimise hydrogen rich syngas by combination of biomass pyrolysis and steam reforming of the bio- fuel at elevated temperatures (975- 1275 K), while **Magrini- Blair et al. (2003)** performed the steam reforming of the pyrolysis bio-oil in a fluidised bed reactor.

2.2.2 Current trends

Currently hydrogen is produced from fossil fuels. Still, 95% of hydrogen is produced from non-renewable sources. Biomass and waste biomass origin oils are considered in steam gasification and steam reforming (**Prasad et al., 1985; Idem et al., 1996; Marquevich et al., 2000, 2001; Czernik et al., 2004, Maher et al., 2007; Gornay et al., 2009**) as an intermediate step towards a more sustainable path of hydrogen production until newly emerging technologies such as plasma reforming and steam electrolysis are better established. Water electrolysis is reconsidered as a potential hydrogen production method which is presently pushed forward by photovoltaic (PV) cells or wind turbines. Other renewable sources for solar hydrogen production are plants, microalgae, and organic wastes. State of the art advancements in renewable hydrogen production technologies such as plasma reforming are examined in the following section.

2.2.2.1 Plasma reforming

The idea of plasma is based on the fact that when a gas is ionised it can release high energy as it is led to a higher state of electrical conductivity. This is the reason that this principle becomes attractive to many technologies including reforming. Non-thermal plasma is currently in the spotlight compared to non-isothermal plasma due to its lower energy consumption. Non-thermal plasma can assist reforming as promising results in efficiency, feedstock rate of conversion and

H_2 yield were exhibited (**Petitpas et al., 2007**). Despite this, it is considered an immature technology since aspects such as cold start-up and shut down are not well established as well as NO_x production when air is used. Still **Whitehead (2010)** supported that non-thermal assisted catalysis could lessen the NOx presence among with CO. These achievements could reduce the system's energy requirements while the catalyst's durability could be enhanced.

2.2.2.2 Electrolysis

The principle of water electrolysis relies on two electrodes, an anode and a cathode which are immersed into water. In between the two electrodes an electrolyte is placed. A direct current (voltage) is supplied in order to maintain the balance of electrons flow from the negative charged side to the cathode where negatively charged hydrogen ions are consumed for the hydrogen production. According to **de Levie (1999)** the water electrolysis principle was discovered and investigated by Troostwijk and Deiman, when Pearson in1797 duplicated this experiment. Later-on, Volta's battery supplied direct voltage enabling the analysis of the anodic and cathodic electrolysis products separately.

So far, the water electrolysis technology is not considered a competitive process in hydrogen production due to its high consumption of electricity and is limited to small scale installations (**Wei et al., 2010; Zeng et al., 2010**). A new revival of the water electrolysis as a potential hydrogen production process is considered due to the development of the fuel cells technology (**Kelly et al., 2008; Grigoriev et al., 2009; Dubey et al., 2010; Wei et al., 2010; Zeng et al., 2010; Li et al., 2010**). Safety issues may arise (**Grigoriev et al., 2009**) in water electrolysis when applied in the PEM (Proton Exchange Membrane) fuel cells as the operating pressures are high (up to 70 bar) and gas cross permeation limits are reached that may lead to explosive mixtures (O_2 and H_2).

Dubey et al. (2010) chose to use carbon nanotubes in order to enhance the energy efficiency of the water electrolysis when **Wei et al. (2010)** examined the stability of the MEA (Membrane Electrode Assembly) for such a process and how dilute acid washing can enhance it on an industrial scale. Several drawbacks to the applied technologies were noticed and still work needs to be done towards the

direction of producing efficient electrolysers, electrocatalysts (**Zeng et al., 2010**) in addition to noise problems and polymers that are resistant when applied in high pressure systems (**Kelly et al., 2008**).

Further attempts, to boost water electrolysis performance with the aid of solar energy lead to thermochemical water splitting and biomass decomposition, solar water thermolysis and solar thermochemical biomass decomposition (**Guo et al., 2009**).

2.3 Steam reforming and unmixed steam reforming

Steam reforming is a well established process in the industry for hydrogen production. It was preferred over water electrolysis (1920's) due to its efficiency and lower cost. The steam methane reformer uses natural gas as feedstock which mainly consists of CH_4 in order to produce synthesis gas. The high operating temperatures (700- 900°C) and pressures (15- 31bar) make it an energy intensive process. The end product is a mixture of H_2 and CO at a ratio of 5:1 with other gases present such as CO_2 and nitrogen. These values are typical for a S:C ratio ranging from 2.8 to 3.2. The water gas shift reactions are based on stoichiometry of $H_2O_{(g)}$:C in order to avoid soot formation. The product stream that results from the high and low temperature water gas shift reactors contains 75% in H_2 on a dry basis.

The principle of unmixed steam reforming was derived from the work of **Lyon and Cole (2000)** on unmixed combustion. The unmixed combustion involved alternate feeds of the air and fuel on the catalyst as a metal or oxidised metal respectively. Unmixed combustion referred to catalytic combustion that enabled the mix of fuel and air by using the applied catalyst as a mass transfer material. Additionally it was demonstrated that when the catalyst is used as a mass transfer material, it contributes to efficient heat transfer by conduction compared to the large surface areas that are needed in industrial combustion processes. The "Method and apparatus for unmixed combustion as an alternative to fire" was earlier patented by **Lyon (1996)**.

Kumar et al. (1999) studied the cyclic effect of unmixed steam reforming of methane in terms of its efficiency in H_2 production and of the deficiencies carbon formation on the catalyst could potentially have. It was concluded that the efficiency of the NiO as an oxygen transfer material (OTM) while alternating between two reactors from which one performed the steam reforming step and the second regenerates the catalyst, was maintained. Despite the fact that so far Ni based catalysts were considered to be active in their reduced form during the steam reforming process (**Ruy et al., 2007**), it was earlier established that NiO creates a reactive environment (**Dupont et al., 2007; Dou et al, 2009**) through a self-reducing process.

Unmixed steam reforming (USR) performance depends on the exothermic oxidation of a metal based catalyst occurring under air flow. The produced heat is utilised for the highly endothermic steam reforming reaction which occurs under fuel and steam flow. Under the fuel and steam flow a rich hydrogen gas flow is produced, while the catalyst is reduced (**Dupont et al., 2007**).

One of the advantages of this process is the insensitivity it presents when fuels prone to coking are used. This is as long as complete burning of any deposited carbon on the catalyst that is produced during the steam reforming reaction, is completed during the air flow step. Additionally, any sulphur that might be contained in the fuel is believed to be oxidised under air flow according to **Lyon and Cole (2000)**, preventing any poisoning of the catalyst. Based on these advantages the process offers, fuels that were unfriendly to hydrogen production can now be studied as steam reforming feedstocks.

The vaporised fuel and steam are the reactant gases. The dry gaseous effluent (reformate) is rich in H_2 (>80%) and contains as by- products CO, CO_2 and sometimes CH_4. The USR can potentially produce a hydrogen stream (H_2) of up to 90% based on the methane study of **Dupont et al. (2007)** when a suitable carbon dioxide (CO_2) adsorbent is chosen. The sorbent's regeneration relies on the air-flow feed step. The produced carbon dioxide (CO_2) and nitrogen (N_2) leave the reactor as a separate flow from that of hydrogen; hence they (CO_2 and N_2) can be separated (if CO_2 storage is desired) or then vented.

In particular, during the USR on a nickel based catalyst the reactions that occur can be categorised into the alternated **fuel- steam feed** and **air feed** half-cycles and are as follows:

FF step:

When the catalyst is at its initial as received form (NiO) or after its oxidation during the air feed step,

$$C_nH_mO_k + \left(2n + \frac{m}{2} - k\right)NiO \rightarrow nCO_2 + (\frac{m}{2})H_2O + \left(2n + \frac{m}{2} - k\right)Ni$$

(R1)

Given enough reduced Ni present, the steam reforming occurs catalytically by the following mechanism,

$$C_nH_mO_k + (n-k)H_2O \rightarrow nCO + (n + \frac{m}{2} - k)H_2$$

(R2)

Note that reactions (R1) and (R2) also apply to the intermediate products of the fuel's thermal or catalytic decomposition such as $C_{(S)}$ (n=1, m=k=0), CH_4 (n=1, m=4, k=0), CO (n=k=1, m=0), and H_2 (m=2, n=k=0) where each can act either as NiO reducing agent or as steam reforming feedstock, with equal production rates of Ni or H_2 per mole of fuel whether they carry out R1 or R2. In the case H_2 as the reducing agent, the reaction is exothermic except for the temperature interval of 640- 790 K (367- 517°C).

Water gas shift then takes place by CO resulting from reaction **R2** and the supplied steam,

$$n \times (CO + H_2O \leftrightarrow CO_2 + H_2)$$

(R3)

Thermal cracking of the fuel may be involved,

$$C_nH_mO_k \rightarrow (n-k)C_{(S)} + \left(\frac{m}{2}\right)H_2 + kCO$$

(R4)

The produced solid carbon by reaction **R4** or the produced CO in **R2** can proceed to reaction with evolved hydrogen by exothermic methanation,

$$C + 2H_2 \rightarrow CH_4 \text{ and/ or } CO + 3H_2 \rightarrow CH_4 + H_2O \text{ (reverse SR)}$$

(R5)

The catalyst's reduction by the produced H_2 is given by the following reaction equation, which is a special case of (**R1**), and is commonly employed in industry as a method of metal oxide reduction avoiding carbon deposition.

$$NiO_{(s)} + H_{2\ (g)} \rightarrow Ni_{(s)} + H_2O_{(g)}$$

(R6)

The exothermic Boudouard reaction may also occur,

$$2CO \leftrightarrow CO_2 + C$$

(R7)

The Boudouard reaction (CO disproportionation) may lead to coking of the catalyst (**Koh et al., 2007**).

The overall enthalpic balance of the under Fuel- steam Flow (FF) cycle is endothermic.

AF step:

In this step, air is the reactant and the gaseous effluent is oxygen- depleted air that contains carbon dioxide (CO_2). The main two reactions that occur during the air feed (AF) step are the catalyst's oxidation and the solid carbon oxidation. Both

reactions aim to convert the reactor materials (Ni→NiO, C→CO_2) in order to heat up the bed in preparation for the subsequent catalytic endothermic step (positive contribution to autothermality), as well as carrying out separation of the N_2 from the air by bonding the O_2 to the nickel bed (positive contribution to H_2 purity in the reformate).

The catalyst (Ni) is oxidized in the presence of air (20.9% vol O_2/ N_2)

$$Ni + \frac{1}{2}O_2 \rightarrow NiO$$

(R8)

Such a reaction is accompanied by high heat release (highly exothermic), providing the necessary energy to the current step and to the overall process (USR).

During steam reforming carbon $C_{(S)}$ species are produced and deposited on the catalyst. These solid carbon ($C_{(S)}$) particles, can be fully oxidized to CO_2 (**R8**) and/ or to CO (**R11**),

$$C_{(S)} + O_2 \rightarrow CO_2$$

(R9)

$$C_{(S)} + \frac{1}{2}O_2 \rightarrow CO$$

(R10)

Both complete and incomplete carbon oxidations (**R9**, **R10**) are exothermic reactions (especially **R9**).

In this step, and according to **R2** where the fuel is $C_{(S)}$, solid carbon deposits can react with NiO particles, via two reactions,

$$C_{(s)} + NiO \rightarrow CO + Ni$$

(R11)

and/ or

$$C_{(s)} + 2NiO \rightarrow CO_2 + 2Ni$$

(R12)

The total enthalpic balance of the under air flow (AF) cycle is exothermic (**Dupont et al., 2007**). The heat generated throughout the cycle can be sufficient so

that little or no external heating is necessary. The overall process's balance (global balance) can potentially be zero (autothermal process; **Dupont et al., 2007**), when appropriate timing is set for each cycle (AF and FF), as well as suitable amounts of metal catalyst and CO_2- sorbent are chosen.

In particular, it was shown that the hydrogen production efficiency as well as the gases' production selectivity is the same as that of the conventional steam reforming bound with the catalytic partial oxidation when methane was used. When continuous hydrogen production is considered, two reactors can run in parallel.

The reactions previously mentioned differ significantly from those described by **Lyon and Cole. (2000)**. Specifically, the primary difference is that the steam reforming and the fuel decomposition occur simultaneously, leading to a high concentration of H_2 product (when methane is used: 75 vol%) even in the absence of CO_2-sorbent, but the fuel decomposition route to H_2 production is less productive than the steam reforming (carbon by-product may oxidise under air flow rather than steam-gasify under fuel flow). Secondly, carbon undergoes an approximately complete burn under the air feed step, supplying heat for the endothermic reactions of the process. Thirdly, the steam reforming reaction is initiated only when a sufficient amount of the metal catalyst is regenerated.

A main trend in the current and new hydrogen technologies is their decarbonisation, which is further discussed in **chapter 3**. The production of CO_2-free syngas can be achieved by the chemical looping (CL) of a CO_2-sorbent. Chemical looping focuses in near and mid- term solutions for hydrogen production with reduced environmental effects. Furthermore, CO_2 sequestration can be incorporated within biomass conversion into hydrogen processes.

Chemical-looping (CL) is a technology with inherent separation of the greenhouse gas CO_2. It was initially considered in the power generation industry in order to increase the thermal efficiency of stations. In the past three decades (**Richter et al., 1983; Ishida et al., 1987**) chemical looping started to be encountered as a potential CO_2 separation technique with a low energy penalty. This technique involves the use of a metal oxide as an oxygen carrier. The metal oxide transfers oxygen from air to the fuel, hence direct contact between air and fuel is avoided.

In combustion applications, the products of chemical looping are CO_2 and H_2O. When the latter is condensed, a pure stream of CO_2 is ready for sequestration without any additional separation systems that will result penalties. The outlet gas from the fuel reactor consists of CO_2 and H_2O, and almost a pure stream of CO_2 is obtained when water is condensed.

The chemical looping technology has been so far applied in the combustion and fluidized bed technology. In the latter, two inter-connected fluidized beds, a fuel reactor and an air reactor, are used in the process. In the fuel reactor, the metal oxide is reduced by the reaction with the fuel, and in the air reactor the reduced metal oxide is oxidized with air. When using chemical looping with packed bed configuration, the bed materials remain always in the reactor, and the flows are alternated between oxidising and reducing conditions.

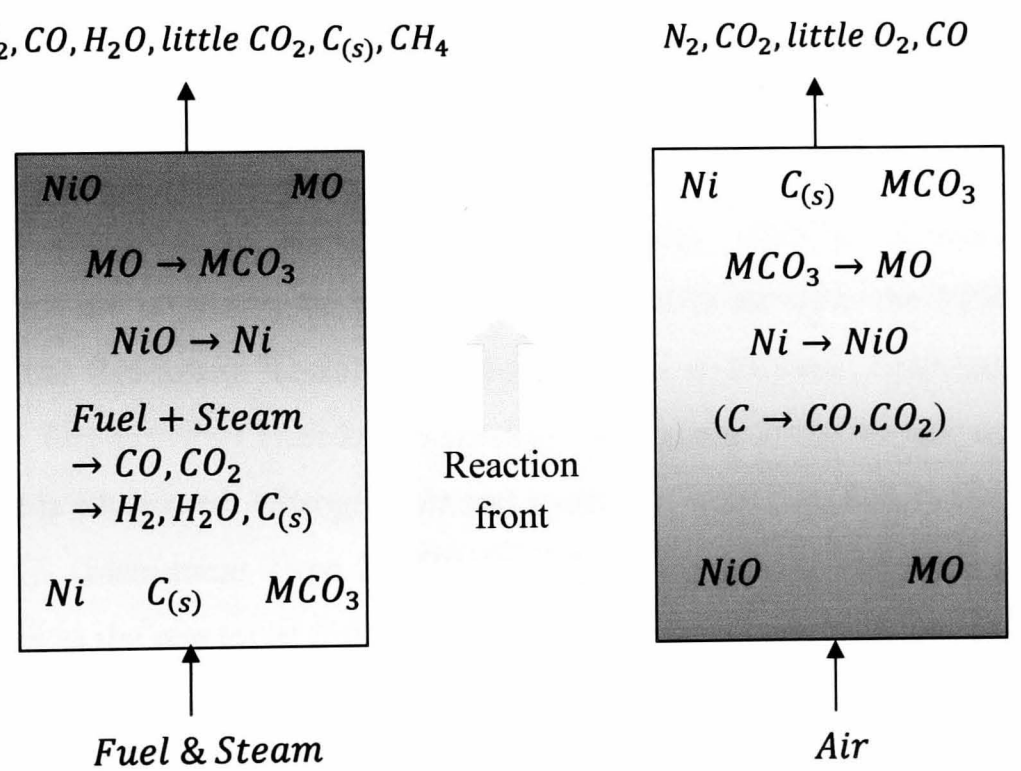

Figure 1 Main mechanisms of chemical looping reforming in packed bed configuration (or unmixed steam reforming) (**Dupont et al, (2008)**).

The previous work carried out by **Kumar et al. (1999)** and **Lyon and Cole (2000)** essentially demonstrated another application of the unmixed combustion by combining it with steam reforming, which was the capability of the process to remove within a single bed reactor any produced CO_2 and to produce a high purity

hydrogen product by cyclic unmixed steam reforming. Therefore, chemical looping reforming (CLR) in a single bed reactor was implemented. Consequently, the current study investigates the use of an OTM (Oxygen Transfer Material) which performs as a steam reforming catalyst when in it is reduced within the chemical looping of unmixed steam reforming (USR) as illustrated in **Figure 1**.

During the FF step the produced CO_2 via reaction mechanisms **R1** and **R3**, can removed in-situ by a metal oxide solid CO_2 sorbent, which needs to operate successfully under the pressure and temperature conditions of this step,

$$M_xO_{y(s)} + CO_{2(g)} \rightarrow M_xCO_{(y+2)(s)}$$

(R13)

Under the AF step the carbonated metal, is regenerated in order to perform under the FF step as described by reaction **R13**,

$$M_xCO_{(y+2)(s)} \rightarrow M_xO_{y(s)} + CO_{2(g)}$$

(R14)

The experimental set-up for the USR and SEUSR chemical looping experiments are implemented in a bench scale reactor set up in the ERRI/ SPEME (Energy and Resources Research Institute/ School of Process, Environmental and Materials Engineering) (Leeds University). In **Figure 2** the bench scale reactor apparatus is illustrated. Nitrogen, air and hydrogen were supplied to the system by three MKS (Instrument Type 247C) mass flow controllers. The three gases were introduced to the reactor at different steps of the process and they are controlled by manually switched solenoid valves. The bio-oil and deionised water were fed to the two pre- heaters with the aid of two peristaltic pumps (Watson Marlow 5058). The reactants entered the reactor by two co- axial injectors with the fuel on the outside.

The temperature of the reactor bed material was monitored by three Eurotherm temperature controllers with closed loop burst firing. Three type K sheathed thermocouples were used for the temperature measurement within the reactor. For the chemical looping USR and SEUSR process experiments, the thermocouple that controlled the reformer's temperature was placed in the centre of

the reactor bed, whereas the other two were placed 5cm above and below the centre.

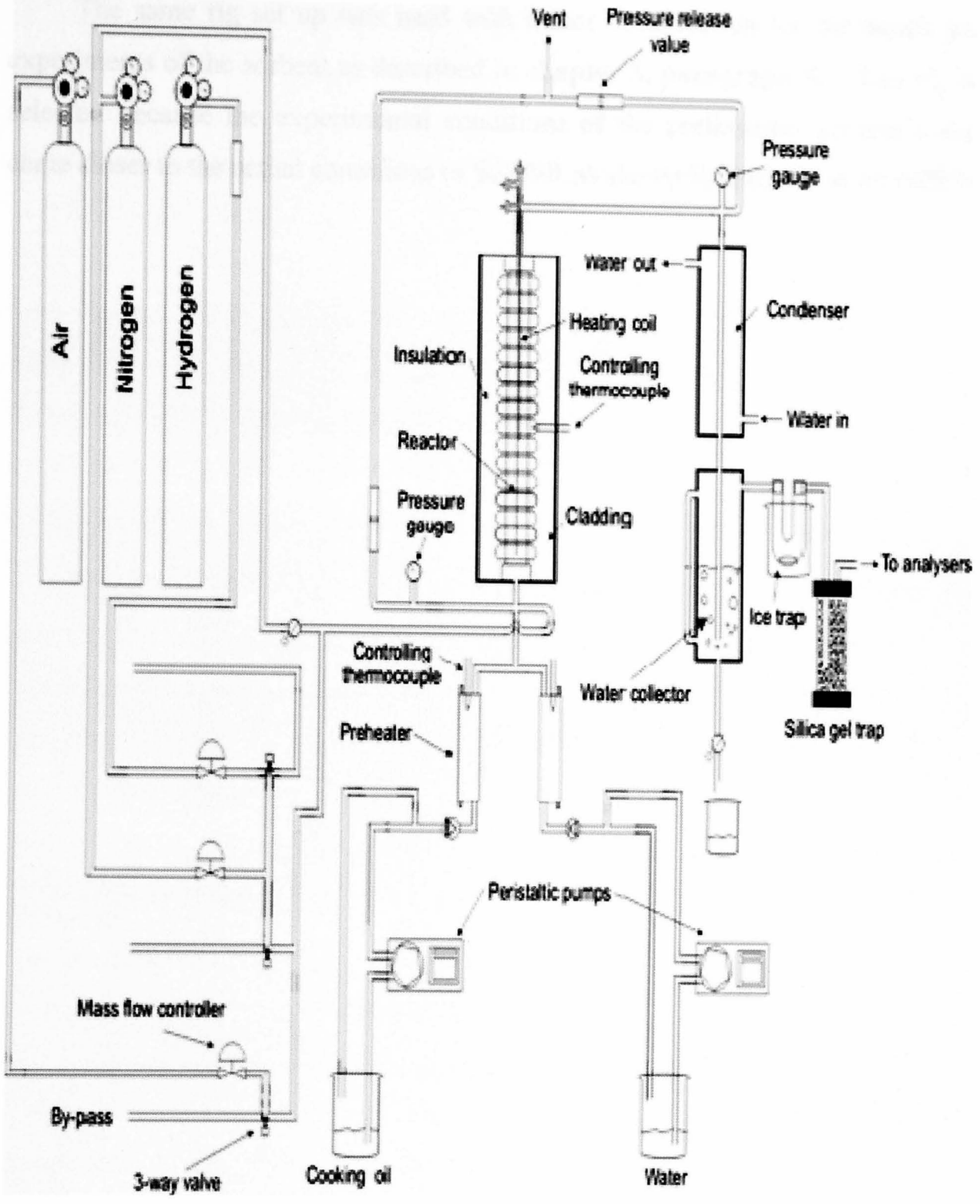

Figure 2 USR and SEUSR experimental rig

Any unreacted steam that left the reactor was condensed and collected. The produced gases were first cooled down and any moisture removal was ensured prior to their online analysis by ABB Advanced Optima analysers. The Uras 14 absorption non- dispersive infrared sensor (NDIS) analyzer monitored CO, CO_2

and CH_4 while the Caldos 15 thermal conductivity analyser measured H_2 and the Magnos 106 paramagnetic susceptibility analyser monitored the O_2.

The same rig set up was used with minor modification for the bench scale experiments of the sorbent as described in **chapter 5, paragraph 5.1**. This rig was selected because the experimental conditions of the preliminary sorbent's study came closer to the actual conditions of SEUSR as shown by **Dupont et al. (2007)**.

Chapter 3
CO_2 capture

Carbon dioxide emissions reduction is one of the key issues in today's agenda of most of the developed countries. This has led to the setting up of national, transnational collaborative agencies (Act on CO_2, U.K., International Environmental Agency) and the establishment of organisations (European Environmental Agency) for the purpose of coordinating worldwide efforts and collecting data in central locations. The Kyoto protocol (United Nations Framework Convention on Climate Change) is the most well known international agreement on the reduction of greenhouse gases. This topic is of particular priority in the framework of sustainable energy and low-carbon energy technologies.

Despite the public's attention in limiting the CO_2 emissions in transportation as the main anthropological climate change contributor, accounting for a 72% of the greenhouse gases (**Gielen et al., 1998**), still a considerable amount of its production is sourced in the current industrial applications. The CO_2 emissions from electric power generation accounts for a significant portion of the greenhouse gases emissions on which the countries who signed the Kyoto protocol agreed to reduce. (**Hammons, 2006**).

Consequently a market for a low carbon economy emerged with power supply and car companies participating in this scheme claiming bigger stakes in such a market through competition (**Dagoumas et al., 2010; Shimada et al., 2007; Bing et al., 2010; Gomi et al., 2009; Mathews et al., 2008; Nader et al, 2009; Peace et al., 2009; Liu K. et al., 2010; Cranston et al., 2009**).

Most of the current energy, which is mainly fossil fuels' sourced, and industrial sector processes, contributes up to 100% of the produced carbon dioxide. Especially in combustion processes when complete burning of hydrocarbons is involved, carbon dioxide is the main gaseous by-product. In incomplete reactions, as in pyrolysis, carbon monoxide is as well present.

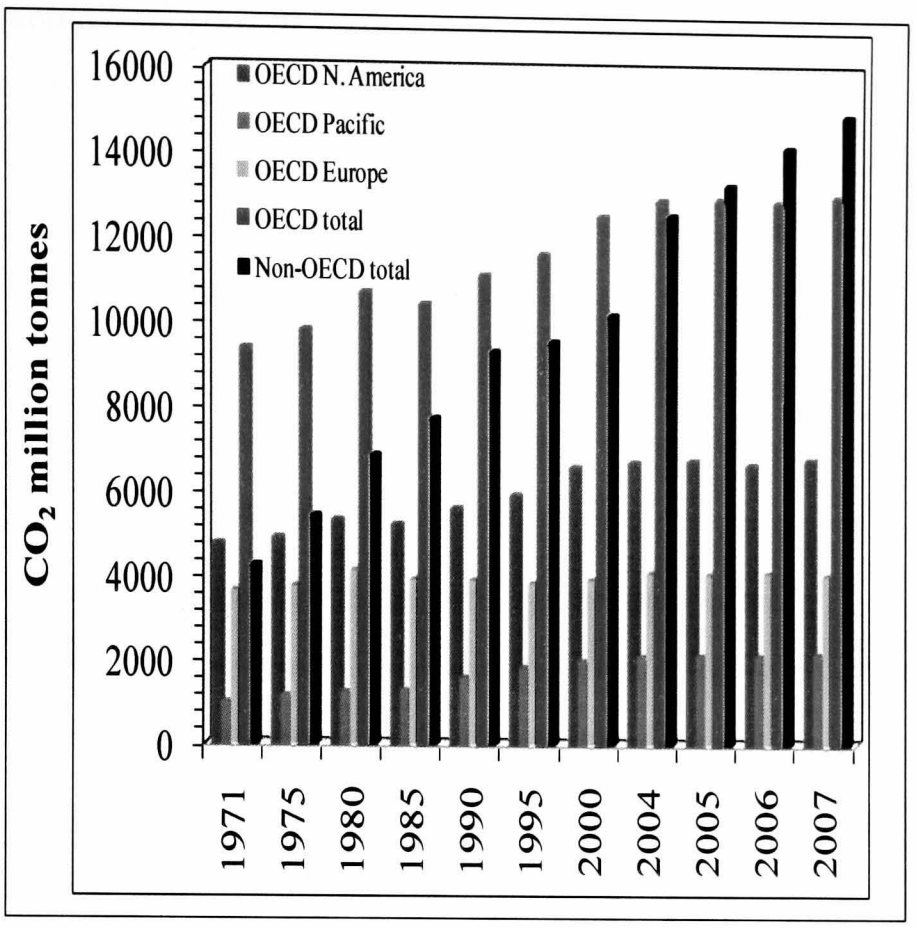

OECD: Organisation for Economic Co-operation and Development

Figure 3 : Global CO_2 production over the period 1971- 2007 based on "CO_2 emissions from fuel combustion 2009- Highlights" (free publications papers) from the IEA (International Environmental Agency) website (http://www.iea.org/co2highlights/co2highlights.pdf)

The majority of the industrial emissions come from the cement, iron and steel industries, while fewer emissions are produced by intensive oil recovery and gas processing industries. In **Figure 3**, the CO_2 production based on fuel combustion for the period of 1971 to 2007 is shown. It is evident that despite the fact that the majority of the OECD countries, including the heavily industrialised ones, have signed the Kyoto protocol (1997) which entered it into force in 2005, the CO_2 emissions are not greatly reduced, mainly due to the lack of appropriate technology that can support this policy. As a result of the current industrial status, sustainable sources of energy are researched in order to limit the emissions of CO_2 (**Chiu et al., 2009**).

Several studies focus on the energy consumption and CO_2 emissions of petroleum and biomass products processes (**Ren et al., 2009**), of which the medium scaled ones account for the 10-15% CO_2 worldwide production (**Hendriksa, 2009**).

CO_2 capture and storage is the aspect that is considered as a short term answer to minimise its emissions. Considerations on the utilisation of the unwanted CO_2 are looked into, with regard to the cost of its capture, storage (**Chen et al., 2009**) and transportation; the energy requirements for its conversion; the demand of the market for a product such as CO_2 and the enhancement of motivation on the CO_2 policy that society and economy need (**Song, 2006**).

In the production of hydrogen, (which is encountered as the "future" fuel), the challenge is greater and triple targeted:

- a sustainable/ renewable hydrocarbon source,
- a process with lower energy demand than the current ones,
- a method/ material that removes CO_2.

For the above reasons a lot of attention has been given to the potential of natural materials, such as dolomite and limestone, as well as to synthetic materials that promise or intend to exhibit enhanced performance compared to the readily available natural ones in terms of the CO_2 removal and durability under harsh conditions compared to the natural materials used in some industrial processes.

3.1 Materials for CO_2 removal

The materials that are used in the CO_2 capture depend on the process in which it is incorporated. Particularly, the applied technology needs to follow the conditions of the process for maximum efficiency for the removal of CO_2. For instance, in the electrical power production sector where power is generated either (i) by pulverised coal firing or (ii) from a natural gas combined cycle or (iii) in an integrated coal gasification combined cycle or (iv) by fuel cells, the CO_2 removal may be best performed either pre- or post- combustion. In case (i), chemical post-combustion CO_2 removal is applied by scrubbing the combustion products with monoethanolamine (MEA), which has very high steam requirements and is more efficient in low CO_2 partial pressures; alternatively, adsorption (pressure or temperature swing (physical) adsorption), low temperature distillation (freezing technology) and membranes can be applied. Regarding the natural gas combined cycle, any CO_2 that is produced at different stages of the production is usually

accompanied by post processes of absorption. Currently, in this particular process the chemical looping concept is considered for reduction of the produced CO_2. In general all the previous electricity production methods incorporate steam treatment of CO on the pre-combustion level for maximising the CO_2 production when a chemical adsorption technique is applied at post combustion. In fuel cells any produced CO_2 is removed by means of physical solvents, membranes or adsorbents. In the hydrogen production plants the best established method of CO_2 capture is the PSA (Pressure Swing Adsorption) system where materials such as active carbon (**Plaza et al., 2007**) and zeolites (**Belmabkhout et al., 2009; Montanari et al., 2008; Weinberger et al., 2009**) are used to physisorb the CO_2. The PSA system is far more efficient in treating combustion emissions than any wet scrubbing method in a conventional steam reforming by natural gas plant as it treats H_2 at a feed pressure while it provides heat to the reformer furnace (Union Carbide, 1966). Recently, systems of MEA/ MDEA (Monoethanolamine/ methydiethanolamine) have been proposed for the same purpose by increasing the power supply to the plant by using, for instance, steam turbines. Alternatively, a new solvent, the AMP (2- amino- 2- methyl- 1- propanol) has been proposed over the MEA due to the fact that it offers reduction of the regeneration energy requirement while it has an increased occupying capacity (**Abu-Zahra et al., 2009**). From the last point made, it is important to know not only the suitability and efficiency of a CO_2 removal system but the overall economy it creates in the process that is applied (**van de Broek et al., 2009; Rubin et al., 2007**).

It is accepted that, the materials that are applied in the previously described processes for CO_2 capture are costly during production when their application is so energy consuming while the effluent gas needs to be pretreated before entering the purification system (**Romeo et al., 2009**).

Numerous studies have been performed in fluidized bed reactors for CO_2 capture by application of CaO sorbents. (**Solieman et al., 2009; Abanades et al. 2010**). The fluidized bed reactors technology has been known since the 1920s and is mainly used in the petroleum industry.

In the table that follows (**Table 2**), the cost of the most common natural and synthetic CO_2 adsorbents, that will be further discussed in **paragraph 3.1.1** and **3.1.2**, are presented. For comparison reasons in the second column the cost of the

sorbents for removing 1 mole of CO_2 is mentioned. Finally the operating conditions in terms of temperature and pressure are presented in order to decide on their suitability for the current process (SEUSR- Sorption Enhanced Unmixed Steam Reforming) under study.

Table 2 Manufacturing and operating cost and operating conditions (pressure-temperature of natural and synthetic CO_2 adsorbents

	Material	Unit cost ($/ kg)	Unit cost per one CO_2 mole ($/ kg)	temperature (K)	pressure (bar)
Natural	$CaCO_3$	0.005[2004]	0.0015[2004]	873[1]	0.0032
				923[2]	0.15
	hydrotalcite	2.0[2004]	4.0[2004]	273-400[3]	0-1
				676[4]	0.3984
	limestone	1.43[5]		1023-1123[6]	1
	dolomite			1023-1153[7]	1
Synthetic	MEA	1.250[8]	0.544[8]	393[9]	0.0001-1
	zeolites	1[2004]	0.2[2004]	298- 378[10]	0-15
	modified	2.0[2004]	4.0[2004]	573-723[4]	0.05-1.31
	activated	0.5[2004]	0.25[2004]	251- 298[11]	19.06-64.01
				273- 348[12]	0-8

[1] Solieman et al., 2007
[2]Florin et al., 2008
[3] Ding et al., 2001
[4] Oliveira et al., 2008
[5] Romeo et al., 2009
[6] Stanmore et al., 2005
[7] Chrissafis et al.(b), 2005
[8] Rao et al., 2002
[9] Hao et al., 2010
[10] Liang et al., 2009
[11] Molina- Sabio et al., 1995
[12] Pellerano et al., 2009

3.1.1 Synthetic material

Zeolites (from the greek words ζέω (zeo) = boil and λίθος (lithos) = stone, rock) have for long been used as an adsorptive material for various applications. By 1970 only 27 zeolites were known. By the 5th edition (2008) of the "Atlas of Zeolite Structure Types" the number of zeolites, rose to 133, whereas in 2008 they were 175 as classified by Webmineral Zeolites, Dana Classification. The synthetic

zeolites are mainly used as binders in detergents whereas only 8% of them are used in catalysis and 6% as adsorbents/ desiccants (Minerological Society of America-International Zeolite Association, 2009). Their structure is based on a molecular sieve which allows the accommodation of cations such as Ca^{+2}, Mg^{+2}, Na^{+}, K^{+} which can be exchanged with others when in contact with a solution. In hydrogen production the purification of the H_2 stream relies on the zeolites' selectivity to be permeated by H_2 molecules but not by CO_2 molecules. Zeolites are mainly used in the PSA systems for such a scope and are more efficient under high pressures, low temperatures and high gaseous concentrations. The properties of various zeolites and their CO_2 removal capability was studied by **Inui et al. (1995)** who concluded that 13X zeolites were the most appropriate ones. In contrast, **Kumar et al. (2003)** showed that the NaY zeolite exhibited better regenerative capability than the 13X.

The zeolites and carbon based adsorbents are at their optimum when applied in a PSA system when the feed stream to be purified is at about 393 K (≈120°C). Other materials such as lithium silicate, calcium and other metal oxides were applied in PSAs at a temperature range of 773- 973 K (≈500- 700°C) (**Singh et al., 2009**).

Materials that are based on organic templates on which amine groups exist, react with CO_2 via an acid-base reaction (chemisorption) rather on physisorption (no bonding between the gas-solid molecules). Such materials are most appropriate for a VSA (Vacuum Swing Adsorption) System. (**Chaffee et al., 2007**). NaX zeolites are preferred in the PSA systems as they exhibit a high working capacity, equilibrium selectivity and low purge requirements (**Mosca et al., 2008**).

MEA (Monoethanolamine) is a solvent that is known for its property to remove CO_2 for over 60 years. Yet, it is still considered for post- combustion CO_2 removal at low temperatures (**Abu- Zahra et al., 2009**), despite the fact that in contact with O_2 it causes corrosion and because of problems in its regenerative capability.

Pre-combustion (or fuel decarbonisation) sorbents such as lithium silicates (Li_4SiO_4) are applied at high temperatures (473-823 K; 200-550°C), at pressures between 0 and 20 atm and for CO_2 concentrations between 0 and 20% (**Figueora et al., 2008**).

Activated carbons on the other hand, due to their high surface area, are very efficient in CO_2 capture at high concentrations of CO_2 whereas at room temperature they lose their removal capacity (**Sarkar et al., 1997**). They are mainly treated carbon, sourced in coal or biomass, in order to give a highly porous product (**Wigmans, 1989**). Mesopores develop under the conditions where micropore development is restricted, and vice versa.

Carbon fibre composite molecular sieves (CFCMS) have been tested on their adsorptive capacity at atmospheric pressure and temperatures of 303, 333 and 373 K (30, 60 and 100°C) and were found to be the best among other carbon based adsorbents as they had higher affinity (**Yong et al., 2002**). These pure porous adsorbents chemical modifications allow such materials to adsorb effectively CO_2 without being restricted by the surface area even at high temperatures. Hence, physisorption is not the only phenomenon that is observed under such conditions by the CFCMS material.

Hydrotalcite like materials are based on the structure of natural hydrotalcites that are altered by adding other compounds which will enhance their CO_2 absorbency (**Yong et al., 2002**). Such additional compounds are aluminum (Al) and the type of ion (CO_2^{2-} and OH^-). The effect of steam was presented over repeated cycles in the same study (**Yong et al., 2002**) based on a previous investigation of **Hufton et al. (1999)**. It was shown that initially the steam had a positive effect up to the 14th cycle, when the mol CO_2 kg^{-1} of the modified hydrotalcite was the same as in absence of steam. **Oliveira et al. (2008)** tested modified natural hydrotalcite extrudates by isotherms formation at 579, 676 and 783 K (306, 403 and 510°C) in the presence of steam, in order to enhance their CO_2 sorption reproducibility.

Ion transport membranes (ITM) were proposed as a material for removing carbon dioxide from the syngas production process of methane by partial oxidation. Their principle relies on the fact that at a temperature of above 973 K (700°C) they allow the permeation of O_2 only, as the steam that is produced is then removed by condensation (**Foy et al., 2005**). There are three main ceramics that are applied in this technology: perovskite, fluorite and a mixture of these two.

3.1.2 Natural material

Natural materials that have the potential of being used as CO_2 adsorbents are zeolites, dolomites, limestone, and hydrotalcite. The first ones are normally formed in volcanic rocks and are rarely found in pure form. They are nevertheless found in a mixture with other minerals, quartz and metals. For these reasons they are not considered in industrial applications where zeolites of high purity are required.

The hydrotalcites were originally used in the industry as catalyst pre-cursors while in the past years they are considered as materials for CO_2 removal. Hydrotalcite is one of the materials that is proposed as one of the adsorbents that could be used in a PSA system (**Singh et al., 2009**). This is so as the hydrotalcites work better at low temperatures (up to 300°C) (**Yong et al., 2002**) which is the technological application field that the PSA technology (**paragraph 3.2.2.1**) is based on.

Ding et al. (2001) and **Singh et al. (2009)** studied natural hydrotalcites. Hydrotalcites in their natural form are not chosen to be investigated as the anions present in the interlayer do not allow the determination of trends (TGA; DTA; CRTA-controlled rate thermal analysis) and characteristics (**Vágvölgyi et al., 2008**). The hydrotalcites capacity in CO_2 adsorption has been studied for temperatures of 481- 575 K (208- 302°C) which was found to be at 0.8 mol kg^{-1} in the presence of 30% vol $H_2O_{(g)}$.

A study reporting the efforts to incorporate hydrotalcite in oxygen fired circulating fluidized bed (CFB) and its carbonation-calcination cycles were presented (**Alstom Power Inc., 2004**). Lime has been studied by Abanades's group (**Abanades et al., 2003** and **Abanades et al., 2004**) as a material to remove CO_2 from coal combustion systems in terms of the performance of the sorbent over repeated cycles, that of the system and that of the plant. In both studies, the necessary energy for the material's calcination in a high temperature combustor was compared to that of its calcination when performed at low temperatures under steam.

3.2 Techniques for H_2 product stream purification

The technologies that are applied for the removal of CO_2 must ensure that when recovered, it is as pure as possible for transport and storage reasons. These technologies can be classified into three categories. These are: pre- combustion, post- combustion and oxyfuel. The latter is an expensive method due to its intense energy consumption. It involves the use of pure oxygen instead of air and is currently performed in the cryogenic separation of air. During this process the air is cooled down in order to prevent the separation of the liquefied oxygen, nitrogen and argon. Nevertheless, the oxyfuel CO_2 capture is not further explored here as its conditions are far from the unmixed and sorption enhanced unmixed steam reforming process (USR and SEUSR).

3.2.1 Pre-combustion

Usually the pre-combustion technology is applied in coal power plants and especially in the ISCC (Integrated coal Gasification Combined Cycle) technology. The pre-combustion technology refers to removal of CO_2 prior to combustion by conversion of the fuel into CO_2 and H_2, thus de-carbonising the fuel The fuel is steam reformed and then water gas shift conversion of the syngas further converts CO into CO_2 and H_2O into H_2. Then, the produced CO_2 is adsorbed in a scrubber column. Scrubbing is more costly efficient when higher concentrations and pressures of CO_2 are fed through it. The optimum temperature range is at 523- 723 K (250- 450°C), leaving few available materials for this sorption technique (**Singh et al., 2009**). Pre-combustion equipment demands significant alterations; therefore such a technology is mostly suggested in new plants rather than in old ones due to investment cost.

An alternative pre-combustion treatment is the application of physical solvents (**Figueora et al., 2008**), i.e. polypropylene carbonate, whose efficiency in CO_2 capture relies on its partial pressure and on the selective non- adsorption of H_2. The regeneration of the solvent is performed at low pressures at which the bonding between the CO_2 and the solvent becomes weak. Attempts are made in order to improve the performance of the physical solvents at higher temperatures.

3.2.2 Post-combustion

Despite the fact that VSA (Vacuum Swing Adsorption) systems were initially abandoned for CO_2 removal on a plant scale due to operational and expenditure issues, they are expected to make a comeback as new materials are developed (**Chaffee et al., 2007**), which could make this system slightly more competitive. On an industrial scale the main physical adsorption methods that are performed are the pressure (PSA) and temperature swing adsorption (TSA).

3.2.2.1 PSA (Pressure Swing Adsorption)

PSA systems are employed in hydrogen production plants by steam reforming of natural gas as well as in cryogenic air separation systems in the steel industry (**Thambimuthu et al., 2002**), where the produced nitrogen serves as the regenerative gas for the CO_2 capture system. Normally in a PSA system, in every vessel the activated carbon is preferred to be placed at the entrance of the gases inlet whereas the zeolite is at the outlet. This is so because in a conventional natural gas steam reforming plant the product stream needs to be purified by any CO_2, CO, CH_4 and N_2 gases; carbon active is more selective with CO_2 whereas the 5A zeolite is more selective with N_2 (**Liu K. et al., 2010**). The adsorbents are efficient at low temperatures and at operating pressures that allow them to perform at optimum efficiency, while the temperature remains approximately constant. The regenerative ability of this system relies on the pressure change in the adsorption beds of materials in order to desorb any CO_2, CO, CH_4, H_2 and N_2, thus reducing the adsorption capacity. Over repeated cycles the system does not lose its efficiency as the pressure changes are fast resulting in big quantities of desorption of the unwanted gases (CO_2, CO, CH_4, and N_2) while the remaining ones are at low percentage. A cycle in a pressure swing adsorption system occurs in five steps: (i) adsorption, (ii) concurrent depressurization; (iii) countercurrent depressurization; (iv) purge at low pressure and (v) repressurization. In order for these steps to be followed at least five vessels have to be used. The adsorption of the high pressure gaseous stream impurities are removed by the material packed in the vessel, which is taken off line when its maximum capacity is reached. In order to minimize the H_2 adsorption by the different beds of adsorbents the concurrent depressurization step

is applied. During step (ii), the pressure is dropped in proportion to the flow of the product gas within the vessel in order to get a stream of high H_2 purity, which is then used to repressurize and purge the other adsorbent beds vessels. Countercurrent depressurization is performed so that the adsorbents are regenerated by depressurizing towards the feed end. The removed gases are led to the PSA off-gas. The purge step (iv) further assists the regeneration with high purity H_2 or another stream from concurrent depressurization. Before the vessel goes back to the adsorption step it needs to be repressurized. This is ensured by passing through the adsorbents the hydrogen from the concurrent depressurization step/ vessel. The vessel is ready for the next adsorption step once the pressure within is equal to the operating adsorption one.

The parameters that affect the design and capacity of the PSA system are: the feed (10-40 bar) and off-gas pressure (1-10 bar); the feed gas composition and the required product purity. The pressure drop along the vessel is very small (0.5 bar). The percentage of H_2 in the feed needs to exceed 50, otherwise the PSA system is not economic. In practice, the PSA unit is chosen based on the required hydrogen recovery and unit capacity. A four bed system is used for a feed of 5000 m^3 h^{-1} (STP) (small capacity) whereas for large capacity feeds (> 50,000 m^3 h^{-1} (STP)) a PSA system of three or more equalizations is required.

3.2.2.2 Temperature Swing Adsorption (TSA)

In the temperature swing adsorption (TSA) regenerative steps, the high temperature reduces the adsorptive capability of the materials used in order to remove the impurities that were adsorbed. The disadvantage of this process is that the repeated cycles of regeneration are not effective and are limited by the materials used due to the slow heating and cooling steps.

The key parameter in the TSA is the temperature that needs to be maintained within a range that establishes optimum performance of the adsorbents packed in the columns; otherwise an increase in temperature may result in a decrease in the quantity of the CO_2 that is adsorbed. On the other hand, a considerable increase in temperature causes the sorbents' regeneration which refers to the desorbed gases. At the same time it needs to be ensured that applied temperatures do not degrade

the adsorbents. The adsorption temperature is within the range of 313 K (40°C) when the regeneration temperature is around 393 K (120°C). On an industrial scale there are several vessels packed with adsorbents that work in parallel, in order to allow time for the adsorption- desorption cycles.

The main drawbacks of the TSA systems application is the large energy consumption it requires as well as large masses of adsorbents that are needed (**Bonjour et al. 2001**).

3.2.2.3 Anti-sublimation

Anti- sublimation (**Eide et al., 2005**) is another CO_2 capture process that can be used even at high CO_2 concentrations. The process relies on the fact that at a pressure of lower than 520 kPa and at temperatures between -78.5°C and 155.8°C which depend on the % v/v CO_2 concentration, CO_2 changes from a gaseous to a solid phase (anti- sublimation). This is because the CO_2 triple point is at 520 kPa, -56.6°C. The triple point of a compound refers to a specific temperature and pressure that the three phases of matter (solid, liquid, and gas) coexist under equilibrium.

3.2.2.4 Cryogenic distillation

Cryogenic distillation is economically feasible only when there are concentrations of CO_2 of 90% vol (**Ritter and Ebner et al., 2005**) which is not realistic in the steam reforming and in particular for this study in the USR process. This technique can be performed by either sublimation or condensation. Alternatively, cryogenic supported absorption can be performed which is similar to physical absorption. In every case, the option of cryogenic distillation is far more expensive than the available physical or chemical absorption techniques.

3.2.3 Calcium looping technology

The calcium looping technology was established as early as 1880 by duMotay who patented carbon gasification by lime (**Blamey et al., 2010**). High temperature solid looping cycles (**Morin et al., 2005; Li Y. et al., 2008; Blamey et al., 2010**)

involve the use of a solid reactant to transfer either CO_2 or O_2 from one reactor to another. Such a technology on an industrial scale can be applied on fixed and dual circulating fluid-bed reactors. High temperature carbonation/ calcination cycles are applied to remove CO_2 from reformed gas streams and solid bed redox loops that can combust a fuel on an oxygen transfer material (OTM).

The carbonation/calcination reactions occur at temperatures higher than those used in the steam cycle of conventional coal-fired power plants, so that it is theoretically possible to recover the heat used to regenerate the sorbent at temperatures suitable for highly efficient modern power generation. Any energy losses from firing the calciner and for compression of the captured CO_2 can be compensated by the fact that the process has intrinsic efficiency advantages as additional power can be generated from the capture system.

Although the favored sorbents, which are mainly $CaCO_3$ based natural rocks (i.e. dolomite, limestone), are abundant and cheap, the processes based on calcination/ carbonation have suffered from loss of reactive capacity after a number of cycles and from attrition of the sorbent material. Recent studies on sorbent reactivation (**Zeman, 2008; Manovic et al., 2008; Manovic et al., 2009; Romeo et al., 2009**), underline the role of the sorbent residual activity and the development of more durable synthetic sorbents (**Martavaltzi et al., 2008; Dennis et al., 2009**) have shown that calcium looping is feasible.

3.2.4 Chemical looping / In-situ CO_2 capture

All the previous techniques are very energy intensive and they contribute to the lower efficiency of the processes they are applied to, as for example in steam reforming for hydrogen production.

Several companies and research institutes (Centre for Coal Utilization in Japan, Areklett and Nygaard, General Electric) (**Eide et al., 2005**) have focused on in situ CO_2 capture. The Centre for Coal Utilization in Japan achieved CO_2 removal at 650°C and at a pressure above 12 MPa. The General Electric project investigated the CO_2 capture in a gasifier by a high temperature sorbent and the calcination of the sorbent in a separate reactor by burning the fuel by means of contact with an oxygen containing material.

In situ CO_2 capture in chemical processes involves the presence of a sorbent in the main reactor that will allow under the reaction conditions (i.e. at pressure of 1.5 MPa and temperature of 1023 K (750°C) for a FBMR- SMR (Fluidised Bed Membrane Reactor- Steam Methane Reforming; **Adris et al., 1997**) or at 1 bar and 1023 K (800°C) (**Dupont et al., 2007; Dupont et al., 2008**) the effective removal from the exit stream of a maximum load of CO_2. The temperature and pressure of the steam gasification/ reforming reaction of hydrocarbons, either in fluidised beds (**Hughes et al., 2004; Koppatz et al., 2009**) or fixed bed reactors (**Dou et al., 2009; Dou et al., 2010; Pimenidou et al.[(b)], 2010**) respectively, determine the material that gives the best efficiencies of adsorption and regeneration. Such a concept is met as early as in 1967 when **Curran et al.** proposed the CO_2 acceptor gasification process.

Due to the fact that all reforming, shift and CO_2 capture conditions need to be met simultaneously, the choice of the material that is used when the in-situ capture technology is applied is limited. Therefore, materials such as membranes that are mainly employed in cryogenic processes cannot be applied as they require high pressures or low temperatures (**Rao et al., 2001**). Hydrotalcites on the other hand have a very limited CO_2 removal capability at temperatures above 573 K (300°C) (**Yong et al., 2001**) which makes them suitable for water gas shift.

The suitability of metal oxides (Me_xO_y) in capturing CO_2 at temperatures between 823 K (550°C) and 1023 K (750°C) at atmospheric pressure (1 atm) has been demonstrated in the past 6 decades (**Curran et al., 1967; Feng et al., 2007; Rao et al., 2002**), and it is expressed by the reaction equation **R13** (**paragraph 2.3**).

The abundance of the metal oxides in rocks presents the cheapest option from an economic point of view. According to **Abanades et al. (2004)** CaO is more cost effective in CO_2 capture than MEA (see also **paragraph 3.1.1.1**).

The metal oxides that could be used in the USR process must satisfy the following criteria: (i) they must exhibit a high reactivity range between 823- 1023 K (550- 750°C) and (ii) their decomposition temperature has to be greater than 973 K (700°C) in order to be regenerated during the catalyst's oxidation (AF) step. The latter criterion that refers to the metal oxides' calcination temperatures excludes

metal oxides such as $MgCO_3$ (658 K; 385°C), $ZnCO_3$ (613 K; 340°C), $PbCO_3$ (623 K; 350°C), $CuCO_3$ (533 K; 260°C) and $MnCO_3$ (713 K; 440°C).

Deterioration of the adsorbent is also an aspect that is considered when choosing naturally formed metal oxides. It is expected that over repeated cycles of any process that encounters in-situ CO_2 adsorption, the reactivity between the CO_2 and the sorbent particles causes an accumulated decay through cyclic operation. Therefore, it is sensible to consider throughout the operation of such a process, the replenishment of a fraction of the sorbent's particles. Thus the need of a low cost sorbent becomes obvious. A number of synthetic oxides (Li_2ZrO_3: **Xiong et al., 2003**; Na_2ZrO_3: **Lopez- Oritz et al., 2004**) that have been tested to be durable over a large number of cycles of adsorption-regeneration were proven to be too expensive.

The in situ CO_2 removal incorporated in the steam reforming process is often referred to as sorption enhanced steam reforming (**Hildenbrand et al., 2006; Li Z. et al., 2007; Galucci et al., 2008; Florin et al., 2008; Rawadieh et al., 2009**). Many investigators (**Han and Harrison, 1994; Balasubramanian et al., 1999; Johnsen et al., 2006**) studied the enhancement of SMR process for H_2 production from a synthesis gas by the CO_2 capture reaction process.

3.3 Dolomite as CO_2 adsorption material

Because the USR is expected to be economical due to the use of a single reactor and of medium temperature materials, the choice of the reactor content was directed towards cheap and widely available chemicals. Calcined dolomite fulfils the requirements of high carbonation capacity, fast kinetics and low cost, but its stability under repeated decomposition-carbonation cycles has often been rated as poor, based on microbalance and TGA studies (**Chrissafis et al.[(a)], 2005; Chrissafis et al.[(b)], 2005**), that is, at small scale.

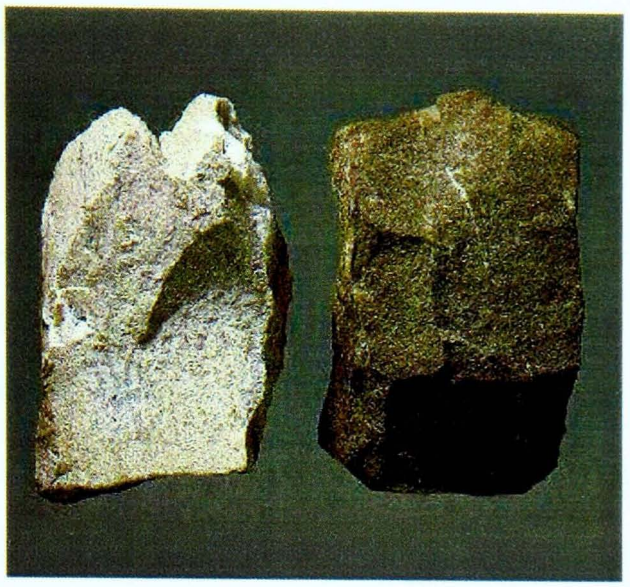

Figure 4 Dolomite aggregates

Dolomite is a naturally occurring sedimentary carbonate rock and mineral (**Figure 4**); which, both are calcium magnesium carbonate $CaMg(CO_3)_2$ formed and found in crystals. In the pages that follow, dolomite is reviewed with respect to the main reactions (CO_2 release or calcination/ CO_2 capture or carbonation) by which it is involved in the current CO_2 capture processes, the influence steam might have in these reactions and the mass of the material that is employed (micro- and macro- scale). Focus is maintained on these two fields of interest as they serve the scope of the SEUSR investigation that was introduced in **chapter 2**.

Dolomite is referred by numerous researchers to decompose into two stages (**Abanades, 2002; Alvarez et al., 2005; Aza et al., 2002; Beruto et al., 2003[(a)]; Beruto et al., 2003[(b)]; Bilinski et al., 1992; Bogahawatta et al., 2004; Braileanu et al., 1996; Caceres et al., 1997; Chrissafis et al.[(a)], 2005; Chrissafis et al.[(b)], 2005; Choudary et al., 1991; Choudary et al., 1994; Criado et al.,2004; Grasa et al., 2006; Hartman et al., 1996; Iwafuchi et al., 1983; Khan et al., 2001; Lee [(b)], 2004; L'vov et al., 2002; L'vov et al., 2004; Maitra et al., 2005; McCauley et al., 1999; McIntosh et al., 1990; McKenzie et al., 1993; Olszak- Humienik et al., 1999; Ozao et al., 1991; Samtani et al.[(a)], 2001; Samtani et al.[(b)], 2001; Stefaniak et al., 2002**) when in a CO_2 environment:

$$MgCa(CO_3)_{2(s)} \rightarrow MgO_{(s)} + CaCO_{3(s)} + CO_{2(g)} \quad \textbf{(R15)}$$

$$CaCO_{3(s)} \rightarrow CaO_{(s)} + CO_{2(g)} \quad \textbf{(R16)}$$

Reaction (**R15**) was confirmed by Beruto (**Beruto et al.[(b)], 2003**) by applying XRD after the half thermal decomposition of dolomite; it was noted that there was a solution of MgO in the calcite.

The calcination reaction (**R16**) is endothermic (ΔH^{o}_{923K} = 170.5 kJ mol^{-1}). CaO use for CO_2 capture was first mentioned by **DuMotay and Marechal** in 1867 in order to enhance the gasification of carbon by steam with lime (**Squires, 1967**).

The thermal decomposition reaction of $MgCa(CO_3)_{2(s)}$ (**R17**) (endothermic; ΔH^{o}_{298K} = 295.6 kJ mol^{-1}; **Hartman et al., 1996**) may occur in a single step (**Hartman et al., 1996; McIntosh et al., 1990; Olszak- Humienik et al., 1999; Samtani et al., 2002**) in an inert environment (100% N_2),

$$MgCa(CO_3)_{2(s)} \rightarrow MgO_{(s)} + CaO_{(s)} + 2CO_{2(g)} \quad \textbf{(R17)}$$

To date, many studies have been conducted on the thermal decomposition and carbonation of naturally formed dolomites (**Bandi and Krapf, 1976; Beruto et al., 2003; Braileanu et al., 1996; Caceres et al., 1997; Chrissafis et al.[(a)], 2005; Chrissafis et al.[(b)], 2005; Czernik et al., 2007; Khan et al., 2001; Lee, 2004; L'vov et al., 2002; Maitra et al., 2005; McIntosh et al., 1990; Myren et al., 2002; Samtani et al., 2001[(a)]; Samtani et al., 2001[(b)]**). The most common parameters that have been found to influence the thermal decomposition (calcinations) of dolomite are the partial pressure of the gas mixtures at which it is subjected as well as the heating rate (**Caceres et al., 1997**) and the way these parameters affect the dolomite decomposition kinetics (**Braileanu et al., 1996**). The influence of compaction and grinding have also been investigated for this reaction (**Czernik et al., 2007; Maitra et al., 2005**).

Dolomite is also a known material for the adsorption of unwanted gases, mainly carbon dioxide (CO_2) produced in chemical processes. The reversibility of reaction (**R16**) is confirmed by numerous investigators (**Curran et al., 1967; Barker, 1973; Chrissafis et al.[(b)], 2005**). Dolomite, calcite and magnesite carbonation behavior is a topic that has been investigated extensively for capturing CO_2 for environmental industrial purposes (**Herzog H., 2001; Shimizu T. et al., 1999; Silaban A et al., 1996; Balasubramanian B. et al., 1999**). The key reaction to this property of CaO (the capture of CO_2) is equation **R18**. The decomposition of dolomite, often referred to as calcination (exothermic; $\Delta H^{o}_{923\,K}$ = -170.5 kJ mol^{-1}) is

a reversible phenomenon regarding only the second half part of it; that is calcium oxide (CaO) can be regenerated back to calcium carbonate ($CaCO_3$) (carbonation) (**Samtani et al.[(a)], 2001**),

$$CaO + CO_2 \rightarrow CaCO_3 \qquad \textbf{(R18)}$$

This particular reaction is not only considered in processes for post-combustion or in-situ capture of CO_2 but for energy storage as well (**Barker 1973, 1974; Aihara et al., 2001**). CaO has been encountered in processes such as flue gas CO_2 separation (**Gupta et al., 2002**), in hydrocarbon and water gasification for H_2 production for CO_2 removal (**Lin et al., 2002**) and for in- situ CO_2 capture in steam methane reforming (**Lee et al., 2004**).

The carbonation reaction is a chemical adsorption (chemisorption) one as the substance thermodynamic properties shift the gas to attach itself to the solid material. Chemisorption is the adsorption when valence forces similar to the chemical compounds formation are involved. Additionally, the chemical structure of the adsorptive material can be altered by surface dissociation or reaction involving an activation energy; desorption of the original species can be recovered only at high temperatures. On the other hand, physisorption involves van der Waals forces and does not involve activation energy. Chemical adsorption is a monolayer process meaning that the adsorbed molecules are in contact with one layer of the adsorbent. Therefore it is very possible that when there are not enough CaO molecules on the external layer of a particle, the carbonation reaction will not be able to proceed to the internal layers of the particle and leaving incomplete the conversion of the available CaO molecules in the remaining mass of the sorbent.

The study of the behaviour of dolomite is extensive, especially when it comes to the above reactions. In all these studies, all the parameters that influence its decomposition are investigated, such as its preparation conditions (**Choudary et al., 1994; Stefaniak et al., 2002**), the way various carbonaceous rocks are influenced over repeated cycles of calcination/ carbonation (**Chrissafis et al.[(b)], 2005**) or the effect these cycles have on the sintering of the sorbent (**Chrissafis et al.[(a)], 2005**); the effect the decomposition has on its surface characteristics (porosity, surface area) affecting its adsorption capability (**Billinski et al., 1992**), the decrepitation that is affected by the particles' size (**McCauley et al., 1991**);

even the effect compaction and grinding has on its kinetics (**Maitra et al., 2005; Criado et al., 2004**). The most common parameters that are studied to influence the thermal decomposition of dolomite are the partial pressure of the gas mixtures at which it is subjected as well as the heating rate (**Samtani et al.[(b)], 2001**) and the role they play in deriving kinetics of its decomposition (**Olszak- Humienik et al., 1999**). The thermal stability of the adsorbents can ensure its durability over successive regeneration (calcinations)/chemisorption (carbonation) cycles. When it comes to experimenting with dolomite regarding industrial applications, the effect of successive heating-up and cooling-down in cycles on its efficiency in carbon dioxide (CO_2) intake was investigated (**Beruto et al.[(b)], 2003**; **Chrissafis et al.[(b)], 2005**).

Dolomite, calcite and magnesite carbonation behavior is a topic that has been investigated extensively for capturing CO_2 for environmental industrial purposes by **Herzog H. et al., 2001; Shimizu T. et al., 1999; Silaban A et al., 1996; Balasubramanian B. et al., 1999**.

The MgO in dolomite has been observed not to re-carbonate following initial full decomposition in previous studies (**McIntosh et al., 1990; Chrissafis et al.[(a)], 2005**), as in this one (**chapter 4**). While causing a drop in carbonation capacity compared to the fresh, uncalcined material, the inert MgO structure is believed to confer structural stability to the calcined dolomite during subsequent carbonations.

Kinetic studies of the main reactions (**R15-R18**) of dolomite and its constituents can give useful information about the rate of the previously mentioned reactions as well as they can give a more global understanding of the metal oxides. The kinetics of the calcination- carbonation reactions were sparsely studied, despite the fact that the main focus on the study of this material is given on its adsorptive capability of CO_2 and its thermal stability over repetition of the calcinations/ carbonation cycles. In **Table 3**, the kinetic parameters of the calcinations and carbonation reactions are presented, based on several kinetic models.

Many studies were produced based on readily available data, for predicting the kinetics of calcination and carbonation of calcium carbonate ($CaCO_3$) and calcium oxide (CaO) respectively. It was stated repeatedly that for different

calcium oxides the activation energies predicted vary significantly since they resulted from the decomposition of different dolomites/ calcites (**Lee, 2004**).

Table 3 Applied kinetic models and kinetic parameters for the calcination reaction (R17) and under non- isothermal experimental conditions and carbonation reaction (R18) under isothermal experimental conditions as found in the literature

	conditions	*model*	T_{range} *(K)*	*E (kJ mol^{-1})*	*A (min^{-1})*
Calcination	(non-isothermal)	n^{th} order[1]			
		0.75-1.0	983- 1083	121.17-109.73	4.32×10^{5}- 2.23×10^{3}
		0.85- 0.50	1083-1183	103.29-124.73	4.13×10^{5}-1.53×10^{2}
		0.33- 1.0	983-1183	133.17-126.33	1.83×10^{6}-8.53×10^{1}
		3rd law method[2]	298-825	245.5-246.8	-
		D1(one dimensional diffusion)[3]	293- 1273	219	1.52×10^{9}
		F1(random nucleation model)	293- 1273	390	3.98×10^{17}
Carbonation	Isothermal	Chemically reaction controlled[4]	823- 998	72.2- 72.7	1.03×10^{4}- 1.16×10^{4}
		Diffusion controlled[4]	823- 998	102.5- 189.3	1.57×10^{10}- 2.33×10^{5}

[1] Maitra et al., 2005 [2] L'vov et al., 2003 [3] Olszak- Humienik et al., 1999 [4] Lee et al., 2004

Extensive studies have been carried out on the kinetics of a variety of dolomite compositions (**L'vov et al., 2002; McCauley et al., 1991**). Comparisons in the mechanism of decomposition of magnesite, calcite and dolomite were carried out, concluding that calcite and dolomite follow the trend of a zero order reaction, whereas the magnesite's decomposition is a first-order mechanism.

Any change in the flow rate, the heating rate and samples' size did not influence the kinetic parameters and the mechanism of decomposition for all three materials (**Maitra et al., 2005**). Large variations are noted in the extensive research on dolomite's decomposition in the pre- exponential factor A (10^{2}- 10^{69} s^{-1}) and the activation energy E (110- 1600 kJ mol^{-1}) (**L'vov et al., 2002**). Predicting the rate of thermal decomposition of dolomite is also part of the whole dolomite's behaviour investigation (**Billinski et al., 1992**).

The kinetics of reaction (**R16**) have also been extensively studied in the past; **Lee et al. (2004)** noticed a reaction order dependence at higher temperature ranges; **Samtani et al. (2001)** studied the decomposition of $MgCO_3$, $CaCO_3$, $MgCa(CO_3)_2$; **L'vov et al (2002)** modeled the thermal decomposition of calcite using the third law method. More detailed references to previous studies on the kinetic studies of dolomite reactions (**R15**), (**R16**), (**R18**) are given in **chapters 4** and **5**.

A study of **Beruto et al., (2003)**[a] investigated the effect of H_2O and CO_2 in the high pressure regime of reaction (**R15**) for Ligurian dolomite in ancient ovens, and showed that during these TG-DSC (thermal gravimetric-differential scanning calorimetry) runs on sample masses of 55-57 mg, the rate limiting step of this reaction was the transfer of CO_2 on its interface, and that the presence of H_2O increased the rate of reaction as it plays the role of the $CO_{2(g)}$ carrier.

The effect of steam in DTA analysis of $CaCO_3$ decomposition in calcite and dolomite was examined by **McIntosh et al. (1990)**. It was shown that the decomposition occurred at lower temperatures in a wet nitrogen atmosphere and not in a dry one. It was expected that the kinetics of dolomite decomposition in wet carbon environment would be affected due to the apparent sintering of the dolomite's surface (**McIntosh et al., 1990**). This wet atmosphere would force the carbon dioxide to compete with water for sites exchanging and was expected to affect early reaction rates. This has been proven to be correct by the work carried out in this study.

In the work of **Bandi and Krapf (1976)**, it was noticed that the peak DTA (differential thermal analysis) temperature of 1 g of $CaCO_3$ under calcinations, was 300°C higher than expected for a 2 mg sample. The reason for this was that the sample generated its own carbon dioxide environment and the decomposition into calcite obeyed the thermodynamics laws according to the temperature and the partial pressure of CO_2 (**Bandi and Krapf, 1976**).

Chapter 4
Micro-scale study of CO_2 capture on dolomite for the USR (Unmixed Steam Reforming) process

CO_2 sorbents have been the object of extensive investigation due to their role in reducing carbon emissions from heat and power processes (**Balasubramanian et al., 1999; Herzog et al., 2001; Shimizu et al., 1999; Silaban et al., 1996**). The present study on calcined natural dolomite as a potential reversible CO_2 sorbent in hydrogen production was motivated by a larger programme of research into the process of unmixed steam reforming (USR) and sorption enhanced steam reforming (SESR) initiated by Dr V. Dupont (**Dupont et al., 2007, 2008, 2009**). In this chapter, the sorbent was tested in thermal decomposition and carbonation reaction conditions to investigate the effects it would have on the material conversion of the CO_2 partial pressure and repeated cycles.

4.1 Warmsworth dolomite

The sorbent under investigation is a naturally formed dolomite which originates from the Warmsworth quarry (**Figure 5**) in Doncaster (West Yorkshire) and it was excavated by WBB Minerals. According to the supplier, its composition as-received is summarised in **Table 4**,

Table 4 Chemical analysis of fresh dolomite's full calcination; CO_2 complete mass balance (**source: WBB Minerals datasheet**)

material	% mass
SiO_2	0.30
Fe_2O_3	0.27
Al_2O_3	0.10
MgO	21.30
CaO	30.70
CO_2	47.33

As long as the main component of the fresh dolomite is $MgCa(CO_3)_2$, the main reactions that are of interest in the purification of a gaseous stream by present CO_2 in the SEUSR process, are the ones capturing CO_2 (carbonation or '**CRB**') and

the regenerative step through the thermal decomposition reaction (calcinations or **'CLC' or 'TD'**).

Figure 5 Warmsworth dolomite quarry (Doncaster, West Yorkshire, UK)

Mass balances were carried out in order to define a formula for the initial molar amount of $MgCO_3$ ($N_{o,MgCO_3}$) and $CaCO_3$ ($N_{o,CaCO_3}$), based on the reaction equations (**TDa**) and (**TDb**) or (**TD**), as expressed by reaction equations (**R15**) and (**R16**) or (**R17**) respectively depending on the gaseous environment they take place in, and on the decomposed dolomite's composition (**Table 4**),

$$N_{o,MgCO_3} = \frac{\%\, wt_{MgO}}{MW_{MgO}} \times \frac{m_{i(MgCa(CO_3)_2)}}{100}$$

Eq.1

$$N_{o,CaCO_3} = \frac{\%\, wt_{CaO}}{MW_{CaO}} \times \frac{m_{i(MgCa(CO_3)_2)}}{100}$$

Eq.2

The initial mass of the $Mg(CaCO_3)_2$ in the fresh dolomite is denoted as $m_{i(MgCa(CO_3)_2)}$ when MW_{MgO} is the molar mass of MgO (= 40.30 g mol^{-1}) and the molar mass of CaO is MW_{CaO} (= 56.07 g mol^{-1})

4.2 Methodology and experimental set- up

The most appropriate method for the study of the sorbent was the thermogravimetric analysis (TGA). Thermogravimetry (TG) is mostly applied in the engineering sector for thermal analysis purposes of materials. Its principle relies on the recording of mass changes of a material's sample as a function of

temperature and time; sometimes these can be monitored in terms of pressure and gas composition.

Usually, a material sample (ranging from 1 mg to 100 g, depending on the apparatus) is placed on the arm of a recording microbalance (thermobalance) which is positioned into a furnace. The furnace's temperature is controlled by either a temperature- time profile or a temperature rate control mode. The sample's mass is recorded in the course of the temperature-time profile. The most common temperature profiles are:

- achieving an isotherm and maintain it there for a specific time ("soak");
- temperature ramping at constant rate (linear heating/ cooling);
- combination of ramping and "soak" segments.

The sample's gaseous environment can be: ambient air, vacuum, inert gas, oxidizing/ reducing gases, corrosive gases, carburizing gases, vapours of liquids or "self-generating atmosphere". The pressure can vary from high or controlled vacuum, through ambient, to elevated and high pressure; the latter is not practical due to the disturbances it might cause. The most common processes that are investigated by applying TG are: thermal stability and decomposition, dehydration, oxidation, determination of volatile content and other compositional analysis such as carbon residue and ash content, binder-burnout, high-temperature gas corrosion etc.

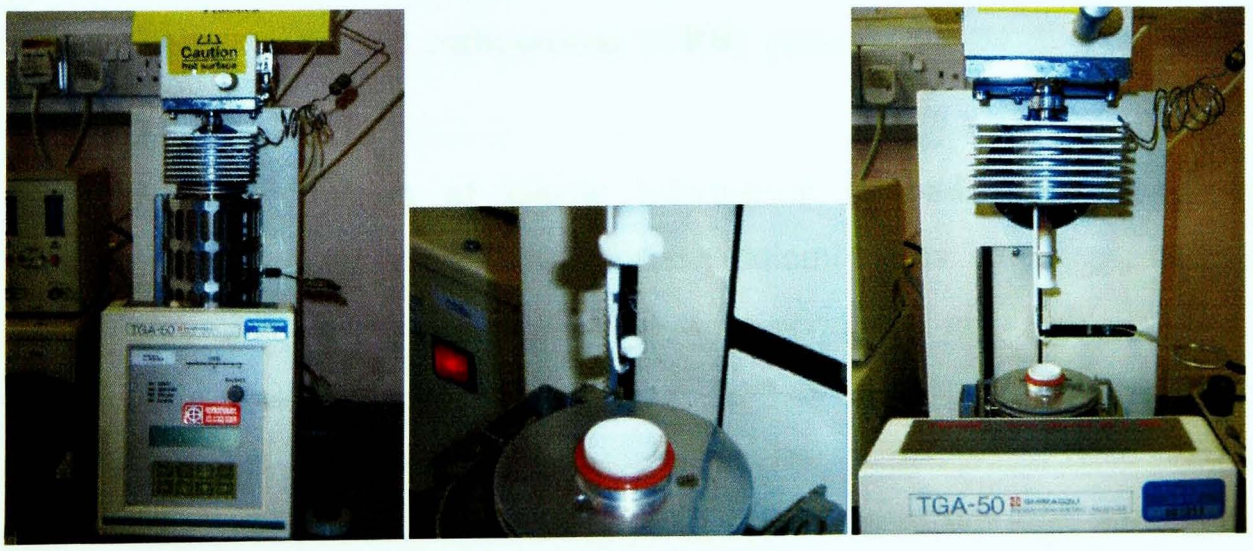

Figure 6 TGA- 50 (Shimadzu)

The 50 series TGA (**Figure 6**) utilizes a low mass thermobalance and furnace unit that minimizes dead volume, buoyancy and ensuring stable baselines. It also allows effective thermogravimetric analysis of samples in various gaseous environments.

In thermogravimetry (TG), any changes in the weight of the sample are measured and recorded while heating up or cooling down at a constant rate. Such a technique is effective for quantitative analysis of thermal reactions (decomposition, gas absorption) that are accompanied by mass changes. Any change in the sample's mass affects the balance's equilibrium. This imbalance is fed to the force coil that generates additional electromagnetic force to recover equilibrium. The mass change is proportional to the additional electromagnetic force. The Shimadzu TGA-50 is designed to minimize any noise and withstand any vibrations that may affect the measurement of changes in the sample mass, while high sensitivity is maintained.

The sorbent (dolomite) was for the present study investigated non-isothermally, by applying a heating rate of 10 K min^{-1}. Non-isothermal conditions were also chosen for the thermogravimetric analysis and the study of the sorbent in the USR (macro-scale) set-up, in order to determine the temperature range of the thermal decomposition of $MgCO_3$ and $CaCO_3$ and of the carbonation of CaO for the USR process.

At an early stage the initial mass of the sorbent was set at 10 mg and the heating-up and cooling-down steps were performed in gaseous mixtures of CO_2/ N_2 (**first set of experiments**). These experiments defined the temperatures at which the calcination (**TD**) and carbonations (**CRB**) occurred in the different gaseous mixtures.

For the production of kinetic information (**second experimental set; paragraph 4.4**) a mass of 3 mg of fresh dolomite was employed. Only the experiments under heating-up conditions were performed at a range of CO_2/N_2 ratios, while cooling down occurred in an inert environment (100% vol N_2), in order to avoid any carbonation of CaO while cooling, which would have generated data that could not be used for the modeling study. The model used the improved iterative Coats- Redfern method for non-isothermal data (**paragraph 4.1.2**). The Warmsworth dolomite kinetic study is of particular use not only for the process

under study (SEUSR), but also for the interest it presents in giving more insight in the behavior of dolomitic materials when used as high temperature CO_2 sorbents.

The same methodology was applied for the stability tests of the sorbent (5 mg) in the TGA apparatus (**third experimental set; paragraph 4.5**), whereas in the USR rig the calcination- carbonation cycles were performed in a representative CO_2/N_2 of the USR of methane under dry and 'wet' conditions, i.e. in the presence of steam of varying partial pressures (**chapter 5**).

In this study, the mass loss is linked to the evolution of CO_2 as seen in reactions $\mathbf{TD_a}$ **(R15)** and $\mathbf{TD_b}$ **(R16)/ TD (R17)** while the mass gain is based on the adsorption of CO_2 as in the **CRB** from the feed mixture. An alumina pan is placed in a furnace that is electrically heated; a thermocouple is placed to monitor the temperature and indirectly the heating rate. The maximum temperature that is reached by using such equipment is 1273 K. The first set of experiments was run with the maximum temperature available by the equipment (1273 K). Based on the temperature range of calcination and carbonation that resulted from the first set of experiments, the second set of experiments, which aimed to collect data for the kinetic parameters' calculation, was designed.

The gaseous mixtures supplied to the TGA furnace were monitored and switched on and off by an MKS Instrument Type 247C controller of a four channel readout; the resulted mixture could be further checked by a CSI 6000 Solid State calibration flowmeter. The control range was from 2 to 100% of full scale with an accuracy of ±1%. Two valves allowed the supply of either gas or both in different concentrations in the TGA analyzer, depending on the required mixture for the purpose of each experiment. The partial pressures of CO_2 used in all sets of experiments were of 5, 10 and 15 kPa, based on a total pressure of N_2 of 100 kPa.

The dolomite when received from the supplier was in the form of gravels. For the purpose of the TGA (Thermogravimetric Analysis) study, the fresh dolomite was ground and collected into particles of 1000-1400 μm by using stainless steel sieves (BS410).

4.2.1 Conversions' calculations for the TGA experimental set

For both experiments of the thermal decomposition (**TD**), represented by reaction $\mathbf{TD_b}$, and carbonation represented by reaction **CRB**, the conversion α (in %) at any time is defined by

$$\alpha^i(\%) = \frac{M^o}{\overline{W_{CO_2}}} \cdot \frac{(P^i_{sorb} - P^{f,i-1}_{sorb})}{N^{f,i-1}_{sorb}} \qquad \textbf{Eq.4}$$

$$\text{with } P^i_{sorb} = 100 \times \frac{M^i_{sorb}}{M^{f,i-1}_{sorb}} \qquad \textbf{Eq.5}$$

where P_{sorb} is the percentage mass of the sorbent (oxide + carbonate; $CaO.CaCO_3$) remaining in the TGA crucible at any time during a specific step of experiment of index '*i*'. *M0* is the initial mass of as-received fully carbonated dolomite (fresh dolomite) in the TGA crucible while M^i_{sorb} is the mass of sorbent remaining in the TGA at any time during the experiment of index '*i*'. The integer superscripts *i*-1 and *i* indicate preceding and present runs (steps) respectively. As the first experiment (*i*=1) is the calcination of the fresh (fully carbonated) dolomite, odd values of *i* refer to the thermal decomposition experiment, and even values refer to the carbonation experiment. The superscript '*f*' indicates the value reached at the end of a step and the superscript *f,i-1* denotes the value reached at the end of the previous step; *N* indicates the number of moles of the reactant sorbent species (carbonate if *i* is odd, oxide if *i* is even) at the beginning of the experiment (which is the same at the end of the previous experiment, including the purge N_2 step in cooling mode) and $\overline{W_{CO2}}$ is the molar mass of CO_2.

By the end of the thermal decomposition, either described by $\mathbf{TD_a}$, $\mathbf{TD_b}$ or **TD**, the final molecules of $CaCO_3$ ($N^{f,i}_{CaCO_3}$) and CaO ($N^{f,o}_{CaO}$) in the sample are calculated by equation 5 and 6, when $(-1)^i < 0$,

$$N^{f,i}_{CaCO_3} = \left(1 - \frac{\alpha^{f,i}}{100}\right) . N^{f,i-1}_{CaCO_3} \qquad \textbf{Eq.6}$$

$$N^{f,i}_{CaO} = \left(1 - \frac{\alpha^{f,i}}{100}\right) . N^{f,i-1}_{CaCO_3} + N^{f,i-1}_{CaO} \qquad \textbf{Eq. 7}$$

The total number of calcium carbonate ($CaCO_3$) molecules at the end of the carbonation step ($(-1)^i > 0$) are,

$$N_{CaCO_3}^{f,i} = \frac{\alpha^{f,i}}{100}.N_{CaO}^{f,i-1} + N_{CaCO_3}^{f,i-1} \qquad \textbf{Eq.8}$$

$$N_{CaO}^{f,i} = (1 - \frac{\alpha^{f,i}}{100}).N_{CaO}^{f,i-1} \qquad \textbf{Eq.9}$$

The initial boundary conditions (first step; thermal decomposition) are,

$$N_{CaCO_3}^{f,o} = \frac{P_{CaO}}{\overline{W_{CaO}}}.\frac{M^o}{100} \qquad \textbf{Eq.10}$$

$$\text{and } N_{CaO}^{f,o} = 0 \qquad \textbf{Eq.11}$$

with P_{CaO} as the percentage of CaO in the sorbent that is presented in **Table 6** and $\overline{W_{CaO}}$ as the molar mass of CaO.

4.2.2 Kinetic model for non-isothermal kinetic data

In order to set-up a kinetic model for the Warmsworth dolomite's decomposition and regeneration based on the collected data of the 2nd set of experiments in the TGA and the data generated by its study in the USR rig runs (**chapter 5**), the improved iterative version of Coats- Redfern method **(Urbanovici et al., 1999)** was applied to evaluate non-isothermal kinetic parameters and identify the best models simulating the mechanism at work.

In non- isothermal experiments, the differential equation that is set for a linear heating program is

$$\frac{d\alpha}{dT} = (\frac{A}{\beta}).f(\alpha).\exp[-\frac{E}{RT}], \qquad \textbf{Eq.12}$$

where A : pre- exponential factor (Arrhenius),

E: activation energy,

f(α): differential conversion function.

After integration, the integral conversion function is,

$$g(\alpha) = (\frac{A}{\beta}) \int_0^T \exp[-\frac{E}{RT}] dT \,. \qquad \textbf{Eq.13}$$

which can be used for deriving non- isothermal kinetic parameters, when integral methods are applied.

The right- hand side of the integral can be approximated by the following equation:

$$\int_0^T \exp[-\frac{E}{RT}] dT = (\frac{R}{E}) T^2 \exp[-\frac{E}{RT}] Q(x) \,, \quad \textbf{Eq.14}$$

where x= (E/RT),

and $Q(x)$ the function that changes slowly to x and is close to unity, which is given by,

$$Q(x) = \frac{x^3 + 10x^2 + 18x}{x^3 + 12x^2 + 36x + 24}$$

By substituting **eq.14** into **eq.13** and rearranging,

$$F_1 = \ln\left(\frac{g(\alpha)}{T^2 \times Q(x)}\right) = \ln\left(\frac{AR}{E\beta}\right) - \frac{E}{RT}$$

When F_1 is plotted against T^{-1} a linear plot is obtained. For the calculation of F_1 the values of $Q(x)$ are used based on the A and E values from the previous iteration. $Q(x)$ is equal to 1 for the first iteration; this condition corresponds to the original Coats- Redfern solution. The activation energy (E) and the pre-exponential factor (A) are respectively calculated from the gradient and the intercept of the line that is produced by the plot of F_1 vs T^{-1}. The iterations stop when the values of E and A or ln$A$ no longer change. The maximum correlation coefficient is chosen as the factor that determines the best fit of experimental conversions over the increasing temperature (i.e. heating rate= 10 K min^{-1}) as well as the best choice of model for the mechanism ($g(\alpha)$; **Table 5**) to explain the studied reactions.

Each model can potentially give the best simulation of the experimental data as a temperature function for both **TD_b** and **CRB** in both the micro- and macro-scale studies based on the iterations' best correlation coefficient activation energy (E), the pre-exponential factor (A or $\ln A$) and the calculated n when the reaction order mechanism is applied.

Table 5 Reaction mechanisms applied in the improved iterative Coats-Redfern method for non-isothermal data based on the Fortran 77 program by Dr. V. Dupont

Reaction mechanism	**Mechanism's equation g(α)**
3D (Jander) diffusion	$[1-(1-\alpha)^{\frac{1}{3}}]^2$
Power law	$\alpha^{\frac{1}{m}}$, for m=1,2,3 and 4
n^{th} order reaction special cases of n: contracting volume (shrinking) model and contracting surface model	$\frac{[1-(1-\alpha)^{1-n}]}{1-n}$ for n=1, $g(\alpha)=-\ln(1-\alpha)$

The best mechanism was identified by the closeness of its correlation coefficient to 1 and was then used to reproduce the conversion vs. temperature profiles. The ability of the modelled conversions to mirror the experimental ones was then considered as the ultimate criterion for validating if the model chosen was the 'best fit'.

4.3 Preliminary dolomite study: effect of mass and CO_2 partial pressure

The parameters to be chosen for the preliminary study of the sorbent in regard to its application in the USR process were the mass and partial pressure of CO_2 as they affect the extent and the conditions (temperature range) of the main reactions of dolomite (**TD, TD_a, TD_b; CRB**).

4.3.1 1st experimental set: 10 mg thermogravimetric analysis (TGA)

The dolomite's thermal decomposition (**TD_a** and **TD_b**) and carbonation performance (**CRB**) was studied in dry (steam absence) gaseous atmospheres of 5%, 10% , 15%, 25% (not shown), 50%, 75% vol CO_2/ N_2 and 100% vol CO_2 when

an initial mass of 10 mg of 1000- 1400 μm particles were used. The heating rate applied was set at 10 K min^{-1} for calcination (thermal decomposition steps), while the carbonation steps were performed when the sample was in cooling down mode. The temperature interval for the heating- up and cooling down cycles was set between 873 K (600°C) and 1273 K (1000°C). If every thermal decomposition and carbonation step made up one cycle, then for every different gaseous environment, four (4) cycles were produced.

The TGA mass loss curves for the m_i= 10 mg runs are selectively presented in **Figure 7**, in gaseous atmospheres of 100% vol N_2, 5%, 15%, 50%, 75% vol CO_2/ N_2, 100% vol CO_2,

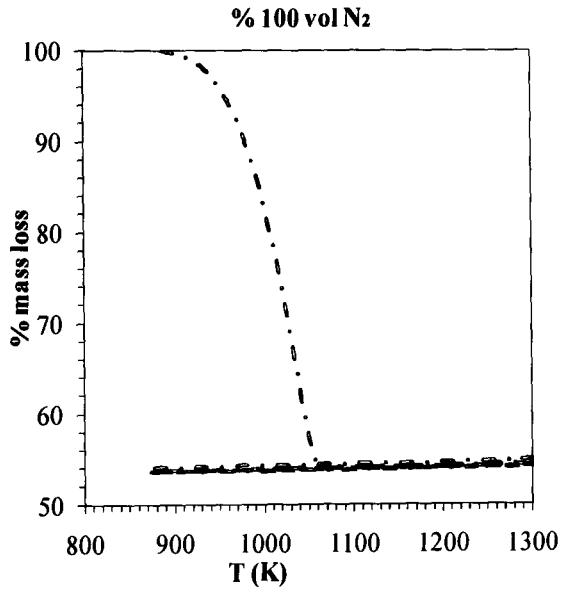

(a) Heating/ cooling cycles in inert gas (N_2)

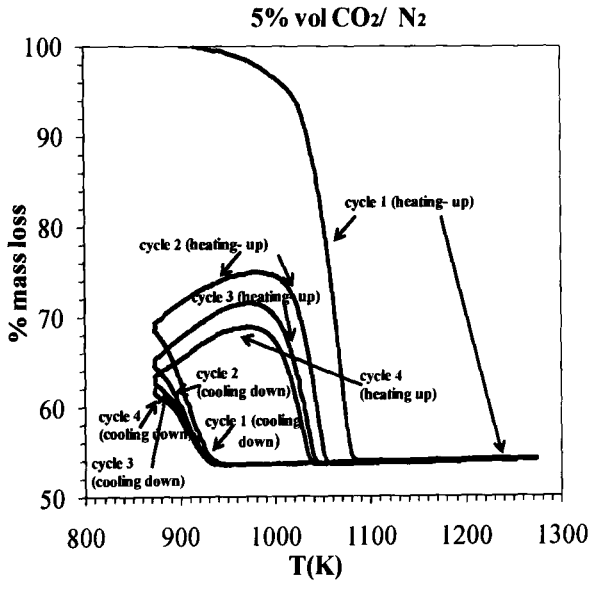

(b) Heating/ cooling cycles in low CO_2 concentrations (5% vol CO_2/ N_2)

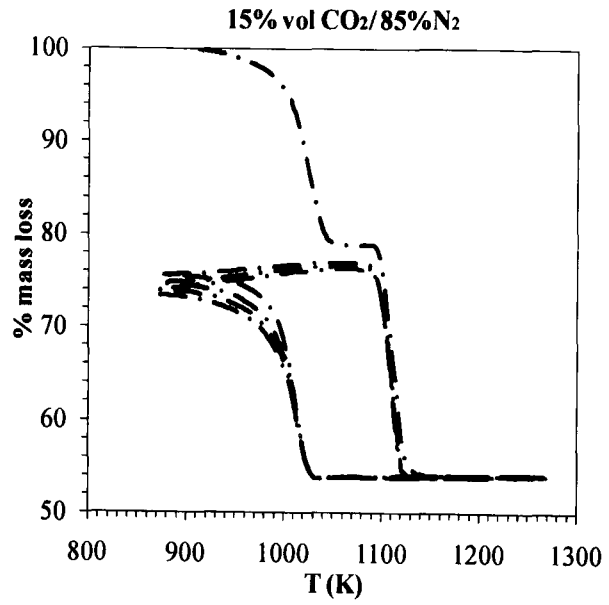

(c) Heating/ cooling cycles in low CO_2 concentrations (15% vol CO_2/ N_2)

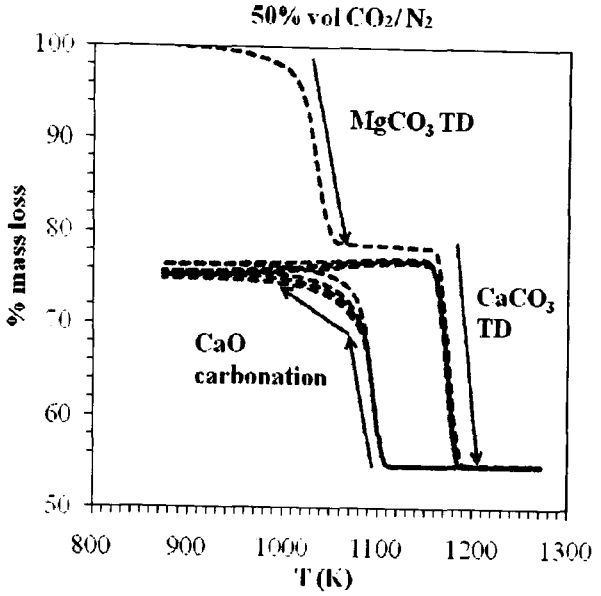

(d) Heating/ cooling cycles in intermediate CO_2 concentrations (50% vol CO_2/ N_2)

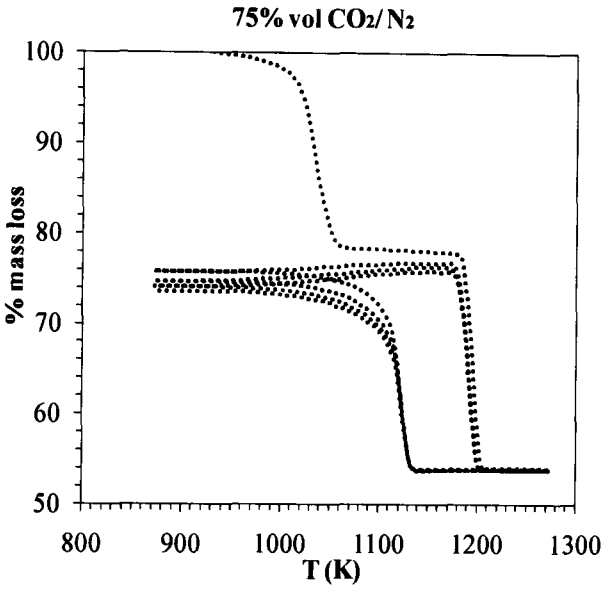

(e) Heating/ cooling cycles in high CO_2 concentrations (75% vol CO_2/ N_2)

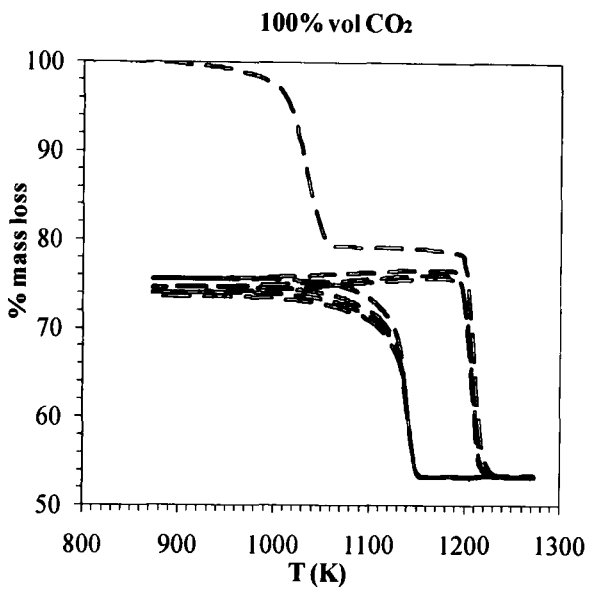

(f) Heating/ cooling cycles in high CO_2 concentrations (100% vol CO_2)

Figure 7 Calcination/ carbonation cycles of Warmsworth dolomite for four heating and cooling cycles in a TGA apparatus

From **Figure 7(a)** it becomes apparent that the thermal decomposition of $MgCa(CO_3)_2$ proceeds in a single curve (step) based on the percentage of the initial mass loss value that the percentage of $MgCa(CO_3)_2$ at the beginning of the experiment corresponds to 100%. The mass loss after the first thermal decomposition (TD1) of the fully carbonated fresh dolomite and following the first carbonation (C1) indicated that all the material had fully decomposed and only the CaO was active and able to recarbonate while the MgO remained inert. During the

cooling down steps (from 1273 K → 873 K) in an inert environment (100% vol N_2), it is proven that CaO cannot recarbonate back to $CaCO_3$, as earlier investigators (**McIntosh et al., 1990; Chrissafis K.[(a)], 2005**) confirmed. Recarbonation of MgO was not established under a variant CO_2 environment (**Figure 7(b), (c), (d), (e) and (f)**) as it would be expected (**McIntosh et al., 1990; Chrissafis K.[(a)], 2005**). Under low flow of CO_2 (2.63 mL min^{-1}) as in the 5% vol CO_2/ N_2 experiments (**Figure 7(b)**), the thermal decomposition of $MgCa(CO_3)_2$ was represented by a single curve with no apparent distinction between the $MgCO_3$ and $CaCO_3$ decomposition stages as in the rest of the experimental runs (**Figure 7 (c), (d), (e), (f)**).

The temperature ranges of the first thermal decomposition of $CaCO_3$ in the first heating- up step and those of $CaCO_3$ (after it was regenerated during cooling down) varied significantly in the different gaseous environments which were applied, as it can be seen in **Table 6**.

Table 6 Initial and final thermal decomposition temperatures (in K) of fresh dolomite and recarbonated CaO ($CaCO_3$) of 4 heating cycles as presented in **Figure 7** (TGA analysis) in various % vol CO_2/ N_2 mixtures

(a) Initial and final thermal decomposition (TD_a) temperatures (in K) of $MgCO_3$ calcination (in fresh dolomite- 1st heating- up)

	15% CO_2		50% CO_2		75% CO_2		100% CO_2	
Calcination	$T_{MgCO3\,(i)}$	$T_{MgCO3\,(f)}$	$T_{MgCO3\,(i)}$	$T_{MgCO3\,(f)}$	$T_{MgCO3\,(i)}$	$T_{MgCO3\,(f)}$	$T_{MgCO3\,(i)}$	$T_{MgCO3\,(f)}$
1	911	1044	912	1051	939	1057	897	1055

(b) Initial and final thermal decomposition (TDa) temperatures (in K) of $MgCa(CO_3)_2$ calcination (in fresh dolomite) (only for 5% vol CO_2/ N_2; **Figure 7(b)**) and of recarbonated CaO ($CaCO_3$) of 4 heating cycles as presented in **Figure 7(b)**, **(c)** and **(d)**

	5% CO_2		15% CO_2		50% CO_2		75% CO_2	
Calcination	$T_{MgCa(CO3)2\,(i)}$	$T_{MgCa(CO3)2\,(f)}$	$T_{CaCO3\,(i)}$	$T_{CaCO3\,(f)}$	$T_{CaCO3\,(i)}$	$T_{CaCO3\,(f)}$	$T_{CaCO3\,(i)}$	$T_{CaCO3\,(f)}$
1	910	1080	1080	1132	1144	1191	1174	1205
	$T_{CaCO3\,(i)}$	$T_{CaCO3\,(f)}$						
2	985	1058	1080	1130	1153	1189	1171	1204
3	973	1050	1077	1129	1163	1187	1167	1204
4	970	1043	1073	1127	1164	1188	1165	1204

The thermal decomposition of $MgCO_3$ temperature range (**Table 6(a)**) was affected to a lower extent, compared to the one of $CaCO_3$ from 0% up to 50% vol

CO_2/ N_2 environments. In the case of thermal decomposition of $MgCO_3$ in 75% and 100% vol CO_2/ N_2, the initial temperature was set 30 K higher and close to 20 K lower respectively, than in the low CO_2 concentration (15% and 50%) environments. Overall, at higher partial pressures of CO_2 the initial $MgCa(CO_3)_2$ thermal decomposition was performed at higher temperatures (**Table 6(b)**; **Table I; Appendix I**). This was realized even in studies as early as in 1958 by **Hyatt et al.** who noticed that the thermal decomposition of $CaCO_3$ was dependant on the CO_2 pressure on the reaction zone and on the temperature of the reactants ($CaCO_3$; gas mixture). In particular, it was shown that at higher partial pressures of CO_2 and at higher temperatures, the rate of the thermal decomposition of calcite is more rapid. **(Hyatt et al., 1958)**.

From the values of $T_{CaCO_3\,(i)}$ and $T_{CaCO_3\,(f)}$ **(Table 6(b))**, which stand for the initial and final temperatures during the calcinations that took place over the four repeated cycles, it became obvious that the higher the partial pressure of CO_2, the higher the temperatures ($T_{CaCO_3\,(i)}$) were at which the calcinations were initiated, and the shorter the temperature range ($T_{CaCO_3\,(i)}$ - $T_{CaCO_3\,(f)}$) was in which they were concluded. Over the repeated cycles of the low (5%, 15% CO_2/ N_2) and high (75%, 100% CO_2/ N_2) volumetric concentrations, the initial calcination temperature was higher than in the previous calcinations step. **McIntosh et al. (1990)** in their study of dolomite's thermal decomposition suggested that by increasing the CO_2 pressure the second peak of its decomposition that corresponds to the calcination of $CaCO_3$, was shifted to higher temperatures. This is established from the TGA dry runs in several % vol CO_2/ N_2 mixtures as seen in **Table 6(a)** and **(b)**. Similarly to **McIntosh**, the $MgCO_3$ decomposition temperature range (**Figure 7(b)- (f); Table 6(a)**) did not seem to be affected significantly by the pressure of CO_2 applied. Exception to the previously mentioned resulting rule was the run for the 4 calcinations in 50% vol CO_2/N_2.

The carbonations were realized during the low temperatures of the cooling-down and heating up steps (**Figures 7(b) to (f)**), which is a phenomenon exhibited in earlier work of thermal analysis of dolomite and calcite (**Chrissafis et al.[(a)], 2005; Chrissafis et al.[(b)], 2005**). The presence of CO_2 would initiate the CRB reaction regardless of the energy input in the system as long as the material itself

stores enough heat for the activation of such a reaction. In **Table 7** the initial and final temperatures of selected cooling-down and heating-up steps of carbonation are presented. The resulted wider temperature range, when the volumetric flowrate of CO_2 within N_2 was increased while heating at a rate of 10 K min^{-1}, allowed for greater residence times for the gaseous mixtures.

Table 7 Initial and final carbonation temperatures (in K) of fully calcined dolomite/ $CaCO_3$ (CaO) during 4 heating (h- subscript corresponding to the left hand side columns)/ cooling (c- subscript corresponding to the right hand side columns) cycles as presented in **Figure 7(b), (c)**

	5% CO_2		5% CO_2		15% CO_2		15% CO_2	
Carbonation	$T_{CaOcarb\ (i)c}$	$T_{CaOcarb\ (f)c}$	$T_{CaOcarb\ (i)h}$	$T_{CaOcarb\ (f)h}$	$T_{CaOcarb\ (i)c}$	$T_{CaOcarb\ (f)c}$	$T_{CaOcarb\ (i)h}$	$T_{CaOcarb\ (f)h}$
1	943	874	874	965	1038	882	882	1021
2	940	873	873	962	1038	882	882	1053
3	938	878	878	952	1038	877	877	1066
4	937	877	-	-	1038	891	-	-

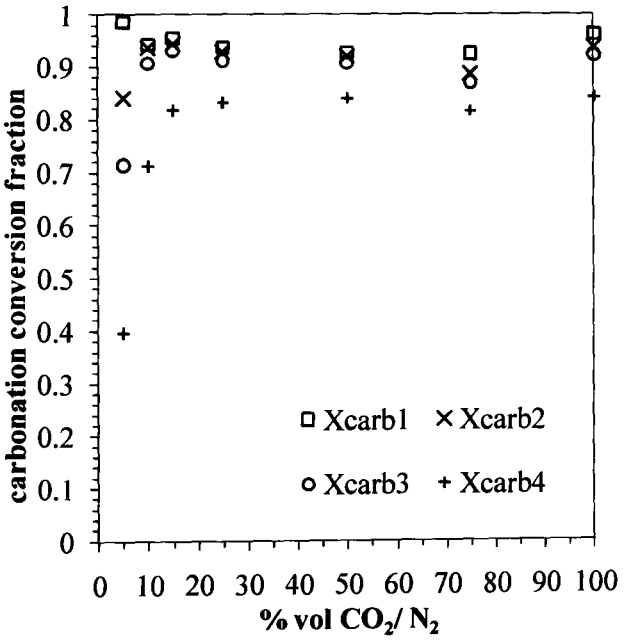

Figure 8 Extent of carbonation molar fractions conversions (α_{CaO}) in various CO_2/ N_2 (% vol) mixtures as studied on a micro- scale (TGA analysis, 10 mg)

A consequence of the latter described phenomenon was the enhancement of the carbonation conversion, as it is seen in the graph above (**Figure 8**) for the 4

carbonation cycles performed in the various CO_2/ N_2 mixtures, based on **Figure 7(b), (c), (d), (e), (f).**

A natural decay of the carbonation step (**CRB**) was noticed over the four cycles for all gaseous environments applied for the TGA study. The higher the presence of the CO_2 was in the supplied gas stream, the higher the conversions of CaO into $CaCO_3$ were. In the 5% vol CO_2/ N_2, the conversion achieved in the first cycle was $X_{carb1\,(5\%)} = 0.986$ whereas by the fourth, it had a final value of $X_{carb4\,(5\%)} = 0.396$. In the 100% CO_2 the respective values were 0.962 and 0.842. Therefore, the higher the CO_2 concentrations were, the final values of carbonation conversion were slightly reduced by the end of the first cycle resulting in a dip in the intermediate CO_2 concentration range (25%, 50% and 75% CO_2/ N_2) while over the repeated cycles, their performance was more consistent in achieving a higher yield of $CaCO_3$. Therefore, the fact that the carbonation steps did not reach full conversion was not due to the lack of reactants (CaO) as the thermal decompositions were complete, but due to the material's sintering and to the applied P_{CO_2}.

4.3.2 2nd experimental set: 3mg thermogravimetric analysis (TGA)

The mass that was used for the kinetic study of the sorbent was 3 mg, since the acquired data was applied on the reproduction of the kinetic models which were described in **paragraph 4.2**. The CaO produced by the thermal decomposition steps was regenerated to $CaCO_3$ in three CO_2 mixtures (5%, 10% and 15% vol CO_2/ N_2). For the production of the CO_2/ N_2 mixtures, the carbon dioxide (CO_2) volumetric flowrates were based on a N_2 volumetric flowrate of 50 mL min^{-1} (at 1 bar; 295 K (22°C)). Contrary to the 10 mg runs, the 3 mg sorbent TGA thermal decomposition steps were performed in an inert environment (100% vol N_2; 50 mL min^{-1}) for three cycles. In this way any carbonation of the available CaO molecules present from earlier calcinations, as indicated in the earlier TGA study of the Warmsworth dolomite (**paragraph 4.3.1**) would be avoided. Otherwise, the kinetic analysis of the involved thermal decomposition and carbonation reactions would not be possible to validate as the developed FORTRAN program based on the

improved iterative Coats- Redfern method (**paragraph 4.2)** is applicable only for non-isothermal data at a set heating rate.

Additionally, in terms of experiment chronology, C_1 and C_2 were separated by a non-reactive cooling phase under N_2 flow, followed by a thermal decomposition phase (TD2) under heating, and by a further non-reactive cooling phase.

The initial thermal decomposition of the fresh 3 mg that occurred in 100 % N_2 (**TD**) was realized within the temperature range of 849- 1050 K (576- 777°C), whereas the same reaction when 10 mg of fresh sorbent were used started at 879 and concluded at 1057 K (606- 784°C), compared to the 1155 K as reported by **McIntosh et al. (1990)**. Therefore, by applying the same heating rate and volumetric flowrate of the supplied gas while the initial mass of dolomite was larger, the initial ($(T_{MgCa(CO_3)_2\,(i)}$) and final temperature ($(T_{MgCa(CO_3)_2\,(f)}$) of $MgCa(CO_3)_2$ thermal decomposition were elevated by approximately 40 K. The temperature range of the three cycles of calcination and carbonation steps are summarized in **Table 8(a) and 8(b)** that follow.

Table 8 (a) Initial and final thermal decomposition temperatures (in K) of fresh dolomite (m_i= 3mg) and recarbonated CaO ($CaCO_3$) of 3 heating cycles (TGA analysis) in various 100% vol N_2

	after 5% CO_2/N_2 CRB		after 10% CO_2/N_2 CRB		after 15% CO_2/N_2 CRB	
Calcination	$T_{CaCO3(i)}$	$T_{CaCO3(f)}$	$T_{CaCO3(i)}$	$T_{CaCO3(f)}$	$T_{CaCO3(i)}$	$T_{CaCO3(f)}$
1	978	1023	997	1050	990	1041
2	963	986	958	1009	899	992
3	942	986	966	1010	890	990

Table 8 (b) Initial and final carbonation temperatures (in K) of fully calcined dolomite/ $CaCO_3$ (CaO) during 3 heating cycles

	5% CO_2		10% CO_2		15% CO_2	
Carbonation	$T_{CaO(i)}$	$T_{CaO(f)}$	$T_{CaO(i)}$	$T_{CaO(f)}$	$T_{CaO(i)}$	$T_{CaO(f)}$
1	428	784	518	816	497	826
2	602	889	558	893	557	913
3	639	910	564	907	612	909

The final conversions achieved during the repeated carbonations steps while the samples were heated- up (10 K min^{-1}) in 5% CO_2/N_2, 10% CO_2/N_2, 15% CO_2/N_2 are shown in **Figure 9**.

As the volumetric flowrate of CO_2 was increased, the carbonation conversions' fractions showed that reaction **CRB** could yield a more extensive conversion of CaO into $CaCO_3$, but as the $CaCO_3$ continued to be decomposed in the calcination steps that followed, the carbonations' efficiencies were limited. This verified the dolomite's deterioration as in the previous 10 mg study, over repeated thermal processing. The material's stability regarding reactions **TD_a- TD_b/ TD** and **CRB** will be further discussed in **paragraph 4.5** in micro-scale and **5.4** in macro-scale. Initial use of dolomite as a CO_2-sorbent therefore causes a significantly larger deterioration in carbonation capacity for the all CO_2 mixtures.

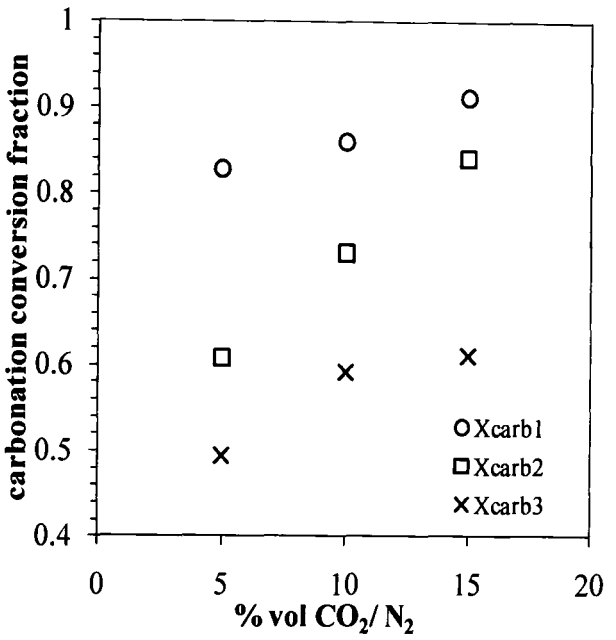

Figure 9 Extent of carbonation molar fractions conversions in various CO_2/ N_2 (% vol) mixtures as studied on a micro-scale (TGA analysis, 3 mg)

More importantly, the outcome of the 3 mg carbonations indicated that even when a smaller mass was applied, (under the same conditions of heating rate and gaseous mixtures flowrates as in the 10 mg of fresh dolomite runs), it resulted in lower extent of CaO conversion just in the first three cycles. This can be concluded by a simple comparison of **Figure 8** (**paragraph 4.3.1**) and **Figure 9** (**paragraph 4.3.2**).

Additionally, the temperature range of carbonations in the 10 mg runs were narrower and set at higher temperatures (**Table 6**; **paragraph 4.3.1**), whereas the one of the carbonation steps in the 3mg fresh dolomite runs occurred in a wider range. This is due to the fact that the carbonation steps were exclusively performed during the heating-up mode as any carbonation was avoided during the cooling

since the CO_2 feed was cut-off. Hence the carbonation steps were dependent on the total amount of energy supplied to them rather than the temperature range for which they might occur.

The residence time of CO_2 during the carbonation steps C_1 and C_2 increased by increasing its volumetric flowrate from 5 to 10% and from 10 to 15% over the TGA experiments. As long as there were only two carbonation steps (C_1) and (C_2) performed for every one of the previously mentioned gaseous mixtures, any comparison in the effect of residence time or else of the partial pressure chosen for each step was focused in these two cycles. It became definite that the effect the longer the residence time of CO_2 had in the fully calcined sample, was a higher final conversion of C_1 and C_2 (**Table 9**).

Table 9 Maximum molar conversions of 1st and 2nd thermal decomposition of recarbonated calcite ($CaCO_3$) in 100% N_2 (dry conditions) (50 mL min^{-1})- 1st and 2nd carbonation of calcite (CaO) in different CO_2- N_2 mixtures of TGA runs (dry conditions)

% vol CO_2/ N_2	max% C1	$CaCO_3$ mol $\times 10^{-5}$	max% TD2	CaO mol $\times 10^{-5}$	% C2	max mol $\times 10^{-5}$	$CaCO_3$ TD3	max% mol $\times 10^{-5}$	CaO
5	82.8	1.6	100.0	1.9	60.9	1.4	100.0	1.9	
10	89.9	1.7	100.0	1.9	73.1	1.4	100.0	1.9	
15	84.0	1.6	100.0	1.9	87.7	1.6	100.0	1.9	

4.4 Kinetic study of dolomite (micro-scale)

The previously discussed results signified the temperature range at which the sorbent's kinetic study experiments were conducted. The program that was discussed in **paragraph 4.2** was applied for the produced data of the 3 mg experimental sets giving useful kinetic data for reactions $\mathbf{TD_b}$ and **CRB**.

In particular the TGA kinetic study was focused in reactions $\mathbf{TD_b}$ (P_{CO_2}= 0 kPa; 100 kPa N_2) and **CRB** in P_{CO_2}= 5, 10 and 15 kPa in 100 kPa N_2. These CO_2 partial pressures were chosen for comparative reasons with the highest one being the most representative for the USR process as it was indicated in the methane and sunflower oil study (**Dupont et al., 2007; Dupont et al., 2008**).

4.4.1 Thermal decomposition kinetics discussion

In both cases of the 2nd and 3rd thermal decompositions of $CaCO_3$ (TD_2, TD_3) and carbonations (C_1, C_2), the need to split the conversion curve into two sections making up the full curve, resulting in two kinetic models for low T and high T that can be used, as performed before by **Sun et al. (2008)**.

The activation energy of the thermal decomposition (TD3) that follows the 2nd carbonation clearly indicates that it is set higher (**Table 10**) than in TD2, therefore more demanding to be initiated in terms of energy. This is so since the $T_{i(TD3)}$ was shifted to higher values as seen in **Table 8(a)**. Therefore, the thermal decompositions despite being performed in an inert environment (100% vol N_2) show that their kinetics were affected by the preceding carbonations which occurred in different % vol CO_2/ N_2 concentrations (**Table 10**).

The thermal decompositions were better described by the n^{th}- order reaction kinetic model. The reaction orders of the calcinations (**TD_b**) in the micro-scale study (TGA) are demonstrated in **Table 10**. The calcinations that followed the first and second carbonation steps denoted as TD_2 and TD_3 respectively for the lowest concentration in CO_2, are of order 1.3.

Higher order reactions occurred in the thermal decompositions following the carbonation steps in 10% vol CO_2/ N_2. Orders of thermal decomposition of n= 1.1 and 1.2 for TD_2 and TD_3 were found when they followed C_1 and C_2 in the higher % vol CO_2/ N_2 concentrations. In past study of **Dennis et al. (1987)** it was supported as well that the calcination of dolomite was controlled by a chemical reaction.

Table 10 Kinetic parameters under dry micro scale (TGA) conditions at different P_{CO_2} for CBR and in 100% N_2 for TD

Exp >	<--------lnA ± dlnA (A in s^{-1})-------><----------(E ± dE (kJ mol^{-1})----------><------r (corr. coeff.)-----><---no. of points----><---------- fitted α range----------														
P_{CO_2} (kPa)	5	10	15	5	10	15	5	10	15	5	10	15	5	10	15
C1	6.4±7.6 12.1±8.8	10.6±8.1 15.1±8.4	3.5±7.8	90.4±0.8	115.1± -1.6 122.7± -6.1	77.5± -2.5 142.1± -2.7	0.99	0.996 0.992	0.99 0.99	2627	925 430	565 820	0.06-0.82	0.02-0.39 0.41-0.82	0.07-0.25 0.26-0.97
C2	25.4±9 -5.4±7	29.1±9.4 -3.6±6.9	7.6±7.7	218±2 31.1±0.8	239.4± -5.5 40.0± -1.8	103.9± -0.6	0.99 0.97	0.99 0.99	0.99	717 928	640 720	2070	0.01-0.41 0.41-0.61	0.02-0.43 0.44-0.73	0.02-0.91
TD2	102±5 *n*=1.3	77.9±7.3 *n*= 1.2	40±1.6 *n*= 1.1	880±37	677.9±58.2	360.4±12.8	0.99 *n*= 1.3	0.99 *n*= 1.2	1 *n*= 1.1	292	430	630	0.03-0.99	0.03-0.99	0.03-0.99
TD3	107±12 *n*=1.3	113.7±14.8 *n*=1.6	66.7±4.7 *n*= 1.2	900±96	972.8±117.9	578.5±36.9	0.99 *n*= 1.3	0.99 *n*=1.6	0.99 *n*= 1.2	338	270	375	0.02-0.98	0.03-1	0.03-0.99

In the thermal decomposition curves that followed C_1 in 5 and 10% vol CO_2/ N_2, the exhibited temperature activities were close to each other. On the other hand, TD_2 following C_1 in 15% vol CO_2/ N_2 occurred at a higher temperature by 64 K (**Table 8(a)**), compared to those following the first carbonations at lower P_{CO_2}. This temperature difference could be explained by any residual physical adsorption of CO_2 during C_1 and the inert (100% vol N_2) cooling step. The higher partial pressure of CO_2 ($P_{CO_2} \approx$ 15 kPa) would have increased the diffusion of CO_2 in the material's pores resulting in an increased gradient when $P_{CO_2} \approx$ 0 kPa than when the pressure was lower (5 and 10 kPa).

The extent to which the model works for the calcination steps (TD_2) is exhibited in the graph of F_1 vs T^{-1} (**Figure 10**) as calculated based on the conversions (α) and temperatures, showing how closely their best linear fit follow each other. In **Figure 10** the conversions vs time and temperature under the TD_2 at the heating rate of 10 K min^{-1} in the TGA (dry conditions) agree very well with the model fit (reaction order equation). The degree the model fit is superimposed on the experimental curve of α defines the extent of excellence of the applied model; this is practically measured by the correlation coefficient, signifying an excellent fit when its value is equal to unity. These curves were produced by feeding back to the model the calculated kinetic parameters E and A.

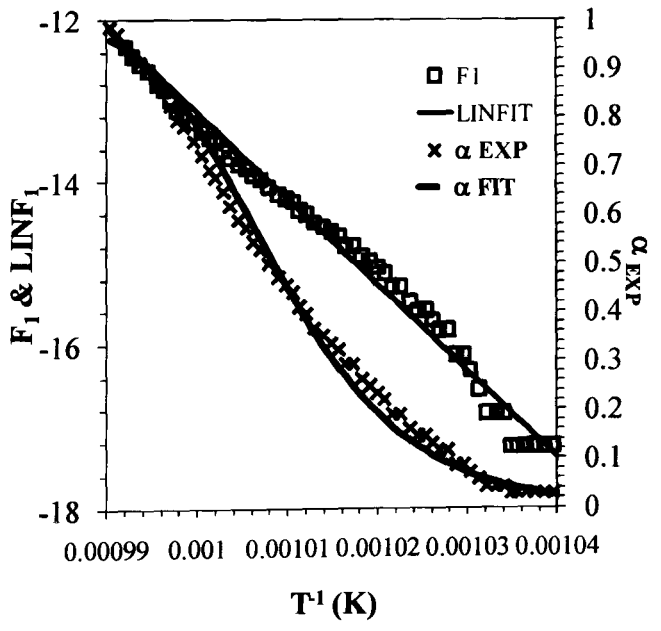

Figure 10 Small scale (TGA; m_i= 3 mg) thermal decomposition (TD) experimental conversions vs time superimposed by modelling fit curves

The activation energies of the thermal decompositions (TD) in the TGA (**Table 10**) for the ones that followed C_1 in the lowest applied P_{CO_2} indicated that there is potential repeatability in the cyclic thermal decomposition. This was not the case from TD_2 to TD_3 after the 1st and 2nd carbonations in 10% and 15% vol CO_2/ N_2 (**Table 10**), where the calculated activation energies (**Table 10**) indicated they were harder to initiate from cycle to cycle.

The kinetic parameters (**Table 10**) that were calculated for the TD_2 in the TGA were higher than E and ln$A$ (A in s^{-1}) presented in earlier works as in **Brailenau et al. (1996)** who calculated the first one at 190- 204 kJ mol^{-1} and the second at 11.4- 12.7 for the thermal decomposition of $CaCO_3$ in CO_2 and Bi_2O_3 based on the Coats- Redfern method. **Samtani et al. (2002)** studied the thermal decomposition of dolomite, calcite and magnesite in a DTG (differential thermal gravimetric) analyser at heating rates of 10 and 50 K min^{-1} in a inert environment (N_2) under vacuum; the activation energy of calcite's thermal decomposition was found to be 192.5 kJ mol^{-1} and its ln$A$ value was estimated at 16.62 based on the a zero-order reaction mechanism. In **Brailenau et al. (1996)**, the pre-exponential factor (A) was referred in s^{-1} and in **Samtani et al. (2002)**, it was reported in min^{-1}. **McIntosh et al. (1990)** found that the reaction mechanism was of zero order, whereas in the present study it was found that n=1.3.

4.4.2 Carbonation kinetics discussion

Carbonation steps (**CRB**) in the 1st and 2nd cycle (C_1 and C_2) were better explained in the TGA study, by the Jander diffusion equation (**Table 10**). For the 5% CO_2/N_2 experiments' calculated parameters (E: activation energy and ln$A$ (A: pre-exponential factor)), correlation coefficients, conversions' range at which the improved iterative Coats-Redfern method was applied and the number of points modeled are reported.

Regardless of the concentration (% vol) of CO_2 in the gaseous mixture, it was observed that during the second carbonations (C_2) higher activation energies were required (**Table 10**). It is interesting that at the highest CO_2 concentration (15% vol CO_2/N_2), the required activation energy in both the 1st (C_1) and 2nd (C_2) carbonation was set in the middle value scale than in the case of the 10% vol CO_2 and 5% vol

mixture. The same is noticed in the values of the natural logarithms of the pre-exponential factors ($\ln A$), with lower values noticed in the 15% vol CO_2/ N_2 runs.

From the final conversion (α) reached in C_1 and C_2 for the 5, 10 and 15% vol CO_2/ N_2, the sintering of the material became evident, despite of previous studies (**Li et al., 2005**) supporting the theory that the presence of MgO enhances dolomite against sintering.

As it was mentioned earlier, the carbonation steps were better described by the Jander (3D) diffusion equation (**paragraph 4.4.1, Table 10**). This was also the case in an old study of **Hyatt et al (1958).** It is interesting that in this work it was proposed that diffusion of CO_2 through $CaCO_3$ layers during recarbonation might occur. According to the same research, diffusion was not encountered as the rate controlling step of $CaCO_3$ decomposition in a CO_2 environment, which agrees with the reaction order that interprets the thermal decomposition steps in **paragraph 4.4.1**. **Jander** (1927) stated that in an exterior layer of a product formed by the reaction of a gas- solid system; (in this case of the $CaCO_3$ formation during carbonation), the gas (CO_2) that surrounds the solid is not allowed to penetrate the solid layer ($CaCO_3$) in order to react with the solid reactant (CaO). Similarly, **Chrissafis et al.[(b)] (2005)** mentioned that incomplete carbonations occurred due to the fact that CO_2 reacted close to the particle's (CaO) exterior surface, not allowing the CO_2 to reach the CaO closer to the particle centre. Therefore, the thicker the product ($CaCO_3$) layer grew, the slower the reaction became. The Jander diffusion mechanism is already well established in describing the kinetics and reaction mechanisms in gas–solid systems and lately in storage materials for hydrogen adsorption (**Cui et al., 2008; Lee et al., 2004**).

Between the first and second carbonations the curve produced by the 5% vol CO_2/ N_2 experimental conversions appeared slowed down at high temperatures which is verified by the calculated activation energies (**Table 10**). Similarly when the 15% vol CO_2/N_2 mixture was used in C_1 and C_2, more energy was required at high temperature conversions in C_1 as the values of E indicate, as well as the change in the slope of the curve compared to that of C_2.

L'vov et al. (2003) studied non-isothermally the decomposition of calcite ($CaCO_3$) samples of 9-14 mg in powder form under vacuum; the calculated

activation energies (E) varied from 266.5- 273.1 kJ mol^{-1} based on the third law method. **Lee et al. (2004)** supported that isothermal carbonations at low conversions were reaction controlled, whereas in high conversions they were diffusion controlled. In particular, the high and low temperature conversions were approached by a single line. Due to the fact that there were deviations from linearity at the intermediate temperatures of carbonation it was assumed that both the diffusion and reaction mechanisms occurred. The diffusion controlled regimes activation energies calculated in **Lee**'s **(2004)** work were found in the range of 102.5- 189.3 kJ mol^{-1} and the ln(A) was between 8.26 to 19.4. These values do not agree with the ones reported in **Table 10**.

The fact that between C_1 and C_2 the activation energies exhibited higher values regardless of the CO_2 concentration (% vol) (**Table 10**) indicated the deactivation of the material. The value of 90.4 kJ mol^{-1} for the C_1 in 5% vol CO_2/ N_2 cannot be directly related to the value of 26 kJ mol^{-1} (**Sun et al., 2008**) that was based on the power law. When modeling with the power law and the 3D diffusion equation, the carbonation activation energies produced are more than double between the first and second mechanism. Evidence for this was given by **Urbanovici et al.** (1999) who found that a ratio of 2.7 in the case of isothermal $Mg(OH)_2$ dehydration was obtained when the power law equation was applied compared to the 3D Jander diffusion equation.

When the power law was applied in the model described earlier (**paragraph 4.2.2**) for the experimental data of C_1 in 5% CO_2/ N_2, the fit curve over-predicted the high values of the experimental curve of conversion (α). Similarly to **Sun et al. (2008)**, the final conversions (α) of carbonation steps in 5 and 10% CO_2/ N_2 reached higher levels than in 15% CO_2/ N_2. **Sun et al. (2008)** also noted that for the carbonation of CaO in TGA at a pressure higher than 10 kPa (corresponding to the present study's 10% vol CO_2/ N_2 experiments), there was not an increase in the reaction rate, due to the formation of an intermediate $CaO.CO_2$ which saturated the sorbent's surface. The previous explanation agrees with the levels of final conversion (α) reached for the C_1 and C_2 runs in concentrations greater than 10% vol CO_2/ N_2.

4.5 3rd experimental set: stability study of dolomite (micro- scale)-. Discussion of effect of CO_2 partial pressure on sorbent's recyclability

The dolomite's stability study entails nine repetitive cycles of calcination-carbonation in a variety of % vol CO_2/ N_2 mixtures under non-isothermal conditions by applying a heating rate of 10 K min^{-1} to an initial mass of 10 mg.

The calcination steps were employed in an inert environment (100% vol N_2) at a volumetric flowrate of 50 mL min^{-1}, whereas for the carbonation ones gaseous mixtures of 5%, 10% and 15% vol CO_2/ N_2 were chosen. These conditions would enable the isolation of the carbonation steps in the different experimental environments in order to observe the effect of the applied CO_2 partial pressures. In **Figure 11** that follows the 9 carbonation steps are shown for the three different CO_2 environments.

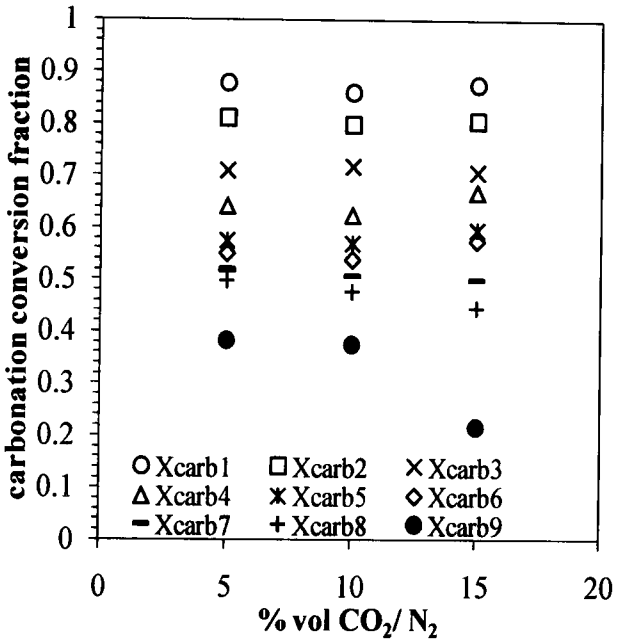

Figure 11 Extent of carbonation molar fractions conversions in various CO_2/ N_2 (% vol) mixtures as studied on a micro- scale (TGA analysis) (10 mg)

Prior to comparison of the performance of the repeated carbonation steps (**paragraph 4.3.1**), it is interesting to see the influence of the calcination steps in 100% vol N_2 that precede the first four carbonations in this stability study, (to those of the 10 mg runs in a CO_2 environment as in the preliminary dolomite study).

Despite of not achieving 100% conversion in the first of the 5 % vol CO_2/ N_2 carbonations steps (**Figure 9**) that were preceded by the inert calcination runs, the stability at the end of 4 cycles was better as it is apparent from the X_{carb_4}= 0.642.

On the other hand the carbonation conversion fraction in the last (4^{th}) cycle when the material was calcined in 5 % vol CO_2/ N_2 was in the vicinity of 0.4. The last value was achieved by the 9^{th} cycle of this stability study, when the material was fully calcined in 100% vol N_2. Dolomite was believed to resist sintering better, because of the presence of inert MgO in the material (**Li et al, 2005**), which increases the material's porosity. The carbonation steps in the stability study did not achieve the extent of the ones following calcinations in 10 and 15% vol CO_2/ N_2, when higher volumetric concentrations of CO_2 were used (**Figure 8**; **paragraph 4.3.1**). This is attributed to the fact that in the preliminary 10 mg dolomite study (**paragraph 4.3.1)** the thermal decomposition steps were realized in a CO_2 environment affecting on a secondary level the final carbonation conversions values and on a primary one the temperature range. This is so, since in the stability study the carbonations were isolated only during the heating-up mode, and to a smaller temperature range than in the preliminary study (3 mg) (**Table 7**; **paragraph 4.3.1**).

Similar to the dolomite's carbonations-calcinations in CO_2 mixtures in **paragraph 4.3.1 (Figure 8)**, the material's behaviour during carbonation in 10% vol CO_2/ N_2 in the stability study exhibited a dip in its final conversion values compared to the 5% and 15% vol CO_2/ N_2 runs. It was only in the case of the stability study that the 15% vol CO_2/ N_2 carbonation experiments fractional conversions were lower in value than the ones demonstrated in **Figure 8** (**paragraph 4.3.1**). This result is due to the different calcination environment, which was a 100% vol N_2 rather than 15% vol CO_2/ N_2, and the longer residence time of the 15% vol CO_2/ N_2 mixture during the carbonation runs in **paragraph 4.3.1**. More precisely, the fact that the calcinations occurred in a CO_2/ N_2 mixture broadened the temperature range during which carbonation took place either during heating or cooling. Therefore, for the same gaseous (CO_2/ N_2) environments the carbonation reaction can be said to be a function of the temperature of the reactants, hence the temperature range where they are active during reaction **CRB**. The latter conclusion was established as well by **Manovic et al. (2009)** while investigating the carbonation efficiency of CaO that was produced by the calcination of dolomite under different conditions of temperature and gaseous environment.

The lower conversion achieved in **Figures 9** (**paragraph 4.3.2**; 3 mg kinetic study) compared to the ones presented in **Figure 11** can be directly related to the larger mass (preliminary 10 mg experiments). Larger masses of sorbent can be linked to more available CaO sites during reaction CRB, and so, they can result to a higher yield of $CaCO_3$ than in the case of smaller employed masses while the same flowrate of CO_2/N_2 mixture is supplied. This is better explained by the Jander diffusion equation as described in **paragraph 4.4.2** and was confirmed by the kinetic study of the carbonation steps which were found to be limited by the diffusion mechanism.

Previous studies on the cyclic performance of dolomites mainly consisting of calcite **(Chrissafis et al., 2006)** showed that by the 9^{th} cycle these materials could recarbonate up to 80% under isothermal conditions, following earlier calcination. These higher carbonation conversions are directly related to the longer time and a constant heat supply for isothermal conditions conservation in the carbonation steps, whereas in the present experiments for the same steps the temperature range relates to the constant heating rate to achieve a pre-set temperature range, which resulted in smaller duration of the carbonations, hence giving lower conversions.

The natural decay in the CaO over repeated cycles is a well established fact of a fully calcined dolomite as proven by **Silaban et al. (1996), Chrissafis et al.[a] (2005), Chrissafis et al.[b] (2005), Chrissafis et al. (2006), Stendardo et al. (2009), Manovic et al. (2009).** Sintering has been discussed in the literature in the case of Ca-sorbents by CaO coalescence (**Li et al, 2005**) but also in terms of loss of microporosity (**Abanades et al, 2003**).

The results of this stability study clearly indicated the potentiality of the material's sintering. In **Chapter 5**, the preliminary study of the thermal stability of the sorbent for the application in the USR process is further discussed, and the case of the material's sintering is examined as the conditions of the macro-scale experiments are closer to the ones in the USR.

4.6 Summary of the micro- scale study of the sorbent

The mass of the dolomite used in the micro scale experiments (TGA) had an effect on the extent of conversion under carbonation and under calcination, as well as on the temperature regions over which these reactions operated. The gaseous environment in the micro- scale study had a more pronounced effect on both the TD and CRB steps for the larger mass tested (10 mg), which were performed in the presence of CO_2, compared to the 3 mg runs.

4.6.1 Mass effect on the calcination steps

- In the 10 mg experiments, the temperature region of thermal decomposition of the $MgCO_3$ in the dolomite (**Table 6(a)**) did not seem affected by the increase in concentration of CO_2 in the gaseous mixture.
- In the 10 mg experiments, the temperature range of thermal decomposition of the $CaCO_3$ in the dolomite varied significantly under the increased presence of CO_2. Even so, the repeated calcination steps had a small effect in shifting the temperature of initial thermal decomposition of $CaCO_3$ to lower values (**Table 6(b)**).
- In the 3mg experiments, a trend of decreasing initial calcination (thermal decomposition) of $CaCO_3$ temperatures following the CaO carbonations was noticed (**Table 8(a)**), denoting a calcination reaction increasingly easier to activate.
- Conversely, over repeated cycles the carbonations' initial temperature increased significantly compared to the first carbonation, denoting a carbonation reaction increasingly difficult to activate. The CO_2 concentration didn't seem to affect the initial temperature of the carbonation reaction (**Table8(b)**).
- When 3mg of dolomite were employed, any differences in the temperature range of the $CaCO_3$ calcinations (when an initial mass of the Warmsworth quarry dolomite was used) were attributed to the fact

that they were performed in an inert environment (100% vol N_2), rather than in the presence of CO_2, while the carbonations were limited in the heating- up mode.

4.6.2 Mass effect on the carbonation steps

- A broad range of carbonation temperatures was achieved in the 10 mg runs during cooling and heating when the same environment (% vol CO_2/ N_2) was used. The molar fractions of conversion during the carbonations, by the last cycle (4^{th}), were promoted when higher volumes of CO_2 were employed despite the lowest CO_2 mixture enhancing the first carbonation step (**Fig. 8**). The extent of conversion for the first carbonation reaction was the lowest when the CO_2 concentration was the higher.
- The different experimental set- up and the lower mass caused the carbonations with 3 mg to occur at a lower and broader temperature range (**Table 7** and **Table 8(b)**).
- Contrary to the 10 mg experiments, in the 3 mg runs the extent of conversion of CaO into $CaCO_3$ was higher when the % vol CO_2/ N_2 was higher (**Fig. 9**). Still, deterioration in the sorbent's efficiency in the carbonation steps was noticed as in the 10 mg runs. By the 3^{rd} cycle, the carbonation conversions were almost the same for all of the % vol CO_2/ N_2 tested (**Fig. 9**) except for the 5% vol CO_2/ N_2.

4.6.3 Kinetic and thermal stability study

- The thermal decompositions indicated that from cycle to cycle they became more energy intensive as the calculated activation energies showed, especially at the highest % vol CO_2/ N_2 (**Table 10**). The main effect of this would not be on the inert environment (100% vol N_2), in which the calcinations occurred, but rather on the different % vol CO_2/ N_2, in which the carbonations were performed. The model fits were verified based on the calculated conversions, while the excellence of

the applied model, which in this case was the reaction order, was confirmed by the calculated correlation coefficient.

- The carbonation steps were best interpreted by the Jander diffusion model. The activation energies' values for the 2nd carbonation appeared increased regardless of the % vol CO_2/ N_2. The latter observation actually confirmed the loss of the material's thermal stability (**Table 10**). The final conversion of the carbonations was not influenced to any great level by increasing the CO_2 content of the mixture, except for the second carbonation (C2; **Table 10**).
- The sorbent's stability study emphasised the loss of the thermal stability of the tested material (sorbent) (**Fig. 11**), which was not greatly affected by the performance of the intermediate carbonation steps at different % vol CO_2/ N_2.

Chapter 5
Study of CO_2 capture at the macro-scale for the USR (Unmixed Steam Reforming) process

In sorption enhanced steam reforming, the CO_2-sorbent is required to regenerate as quickly and completely as possible since it is the CaO amount present in the sorbent under steam reforming which determines the effectiveness of the chemisorption in delivering high H_2 purity, enhanced fuel conversion, and lower temperatures of operation than in the absence of sorbent. In the unmixed steam reforming process, this regeneration is carried out during the exothermic oxidation step of air feed over the reduced Ni catalyst. Operating in USR conditions creates specific environments for the carbonation and the thermal decomposition (calcination) of the sorbent. In this study, as a continuation of the sorbent's micro-scale performance (**chapter 4**) the behaviour of calcined dolomite in conditions that approach some of the USR and some sorption enhanced steam reforming environments, chiefly the use of the packed bed configuration, low CO_2 partial pressure and the presence of steam was investigated. Contrasting behaviours between macro and micro-scale are also discussed.

5.1 Methodology and experimental set- up

In the bench scale reactor experiments the mass of dolomite was packed on a stainless steel mesh at mid-depth of the reactor. The sorbent samples, of the same size as in the micro scale study (1000- 1400 μm), were sandwiched between beds of alumina oxide granules (4-8 mesh; SIGMA ALDRICH). The gases flowed from the bottom end of the reactor and exited at the top end. In the 2.5 g sample (dry and wet conditions) experiments, the flowrate of N_2 was at 750 mL min^{-1} (STP), with the relevant CO_2 flow added to it for the carbonation experiments. As in the micro scale experiments, thermal decomposition and carbonation under heating (10 K min^{-1}, up to 1073 K) were alternated with non-reactive cooling under N_2 flow, in order to produce data that will be useful in the calculation of kinetic parameters and

to enable comparison between behaviours at the micro and macro scales **(paragraph 4.4).**

The gases for the USR rig were regulated by using the MKS Instrument Type 247C controller with four channel readout while the resulting mixture could be further checked by a CSI 6000 Solid State calibration flowmeter. The partial pressures of CO_2 for the carbonation steps were at 5, 10 and 15 kPa, whereas the total pressure did not exceed atmospheric pressure (100 kPa).

During the 'wet' macro scale experiments in the USR reactor, the flows of the liquid deionised water used were 0.017, 0.045 0.073 mL min^{-1} for the 5, 10 and 15% vol CO_2/N_2 mixture flows. This resulted in H_2O vapour mole fractions of 0.028, 0.068 and 0.101 with partial pressures 2.8, 6.8 and 10.1 kPa respectively. The deionised water was pumped by a peristaltic pump (Watson Marlow 5058) and vapourised in a pre-heater situated beneath the reactor to 423 K (150°C). Therefore, the carbonation steps (**CRB**) in this case were performed in a 5-15% CO_2/2.9-11.5% H_2O/ N_2 by volume mixture. The step **TD2** (second thermal decomposition) in the wet macro scale experiments were performed in mixtures of 2.9, 7.4 and 11.5% vol H_2O/ N_2 based on the absence of CO_2 once the CO_2 supply was cut-off at the end of C1.

The start-up temperature of the reactor was also at 423 K (150°C) when steam was initially introduced. The 'wet' experiments were carried out in such a way that the same steam flow was present throughout the thermal decomposition, unreactive cooling (100% vol N_2) and carbonation experiments.

In all the cases of the macro scale experiments, the CO_2 content in the effluent gases was monitored online by an NDIR (non-dispersive infrared sensor) absorption gas analyzer (Uras 14 from ABB Advance Optima, ABB Automation Products), connected to a display and control unit. The smallest measurement range for CO_2 was 0-100ppm. In the absence of mass loss/gain measurement and unlike the TGA experiment, the on-line CO_2-measurement carried out every 5 seconds permitted the calculation of the sorbent conversion for the reaction under study **(Eqs 15-17 & 20; paragraph 5.1.1)** and the construction of smooth conversion vs. temperature curves.

Additionally the temperatures in the reactor were recorded every second with type K thermocouples at the bottom, centre and top of the reactor bed throughout the experiments. In the macro scale experiments, the temperature (T_{middle}) chosen in the modelling program was given by the thermocouple placed in the middle of the sorbent's bed. The linearity of temperature increase in the reactor, which was set at the heating rate of 10 K min^{-1}, was verified in the dolomite bed.

The steam, leaving the reactor was condensed, and left- over moisture was trapped downstream of the condenser using a silica gel trap. A second silica gel trap was used just upstream of the analyzer in order to avoid moisture entering it.

The stability tests (**paragraph 5.6**) in the macro scale experiments were performed for both calcination and carbonation steps at 10 kPa CO_2 during heating at a rate of 10 K min^{-1} and during natural cooling. The stability of the sorbent was studied for 9 cycles through the extent of calcinations and of carbonation, each cycle being comprised of a two-stage carbonation, one during the cooling period and another during the heating period, and by a single calcination step while heating.

5.1.1 Conversions' calculations for the USR rig experimental set

Based on elemental balances for the thermal decomposition of the sorbent (**TD**), the conversion for $MgCO_3$ is expressed as:

$$\%\alpha_{MgCO_3}^{TD_i} = 100 \cdot \left(\frac{\Delta N_{CO_2}}{N_{MgCO_3}}\right) \quad \text{for } \frac{\Delta N_{CO_2}}{N_{MgCO_3}} < 1, \qquad \textbf{Eq. 15}$$

and

$$\%\alpha_{MgCO_3}^{TD_i} = 100 \cdot \left(\frac{\Delta N_{CO_2} - N_{MgCO_3}}{N_{MgCO_3}}\right) \quad \text{for } \frac{\Delta N_{CO_2}}{N_{MgCO_3}} \geq 1. \qquad \textbf{Eq. 16}$$

where

ΔN_{CO_2} = net number of CO_2 moles that have evolved from the reactor during the i^{th} thermal decomposition (TD_i) step, and

N_{MgCO3} = number of $MgCO_3$ moles in the as-received fully carbonated dolomite.

The number of moles generated during each step, either thermal decomposition or carbonation is denoted by ΔN_{CO_2},while N_{MgCO_3} is the number of $MgCO_3$ moles present in a specific sample mass of fresh sorbent in the reactor's experiments.

The conversion ($\%\alpha^{i}_{CaCO_3}$) for the calcination of $CaCO_3$ as described by (**TD$_b$**), is,

$$\alpha^{i}_{CaCO_3}(\%) = 100 \cdot \frac{(\Delta N_{CO_2})}{N^{f,i-1}_{CaCO_3}} \qquad \text{for } i>1 \text{ and } (-1)^i <0.$$

Eq.17

The definition of the number of CO_2 moles produced, ΔN_{CO_2} is given by integrating the number of moles dN_{CO_2} that are evolved in the reactor over a time interval *dt*, which in this case is every 5 s,

$$\Delta N_{CO_2} = \int_{t_0}^{t} dN_{CO_2} = \int_{t_0}^{t} x_{CO_{2,out}} \cdot \dot{N}_{dry,out} dt \qquad \textbf{Eq.18}$$

The dry mole fraction of CO_2 is represented by x_{CO_2} as recorded by the gas analyzer every 5 s; t_o is the time when calcination starts and t is when it ends. $\dot{N}_{dry,out}$ is the total dry molar flow rate of the gases leaving the reactor (CO_2, N_2) and *dt* is the 5 s time interval preset on the online gas analyzer for the gas concentration (% vol) readings.

$\dot{N}_{dry,out}$ can be calculated from the following equation, according to the N_2 elemental balance,

$$\dot{N}_{dry,out} = \frac{\dot{N}_{N_2,in}}{(1-x_{CO_{2,out}})} \qquad \textbf{Eq.19}$$

with $\dot{N}_{N_2,in}$ being the molar flow rate of N_2 entering the reactor.

At the end of the thermal decomposition steps the moles of $CaCO_3$ ($N^{f,i}_{CaCO_3}$) and CaO ($N^{f,i}_{CaO}$) are calculated by equations **Eq.6** and **Eq.7**.

For the carbonation steps (**CRB**) the following equation for $(-1)^i>0$, was used for the calculation of the molar conversion ($\%\alpha^{i}_{CaO}$),

$$\alpha^{i}_{CaO}(\%) = 100 \cdot \frac{(\Delta N_{CO_2})}{N^{f,i-1}_{CaO}} \qquad \textbf{Eq.20}$$

During carbonation, the number of CO_2 moles consumed, ΔN_{CO_2} are calculated by the following integral,

$$\Delta N_{CO_2} = \int_{t_0}^{t} dN_{CO_2} = \int_{t_0}^{t} (\dot{N}_{CO_{2,in}} - x_{CO_{2,out}} \cdot \dot{N}_{dry,out}) dt \qquad \textbf{Eq.21}$$

where $\dot{N}_{CO_{2,in}}$ is the inlet molar flow rate of CO_2 during (**CRB**); $N_{CaO}^{f,i-1}$ and $N_{CaCO_3}^{f,i-1}$ are calculated based on equations **Eq. 9** and **Eq.10**.

5.2 Preliminary dolomite study: effect of mass and CO_2 partial pressure

Prior to the kinetic study of the dolomite on a bench scale, several parameters affecting the thermal decomposition and carbonation reactions (as discussed in the experimental results in **Chapter 4)** were tested in order to produce useful information when larger masses of the material were used and to utilize them in the dolomite reactor kinetic study. In **Table 11**, the effect of mass, the volumetric flow rate of the gaseous environment (TD in 100% N_2; CRB in 5% CO_2/ N_2) and the heating rate on the thermal decomposition (**TD**) of the fresh dolomite and the first carbonation step (**CRB**) is presented.

Table 11 Maximum conversions for TD1 step in 100% dry N_2 and for C1 (1^{st} CRB) step in dry 5%CO_2/ N_2 in the dry bench-scale USR conditions

Mass sample (g)	Flow (mL min^{-1})	max % TD1	Flow (mL min^{-1})	max % C1
5 (no heating rate)	500	100.0	526	64.0
5 (no heating rate)	2000	92.0	2105	55.4
2.5 (10 K min^{-1})	1000	85.3	1053	59.1
2.5 (20 K min^{-1})	750	80.4	1040	62.1
2.5 (10 K min^{-1})	750	84.0	1040	100.0

The slower volumetric flow rate applied to the larger mass (5 g) resulted in a higher conversion during the 1^{st} thermal decomposition and carbonation step (**Table 11**), while the heating rate during these two steps was arbitrary (no heating rate). When half of the mass was applied (2.5 g) two heating rates (10 and 20 K min^{-1}) and two volumetric flowrates (750 and 1000 mL min^{-1} of N_2) were used as the basis for the TD and carbonation reactions, as seen in **Table 11**. Similar values of final conversion of $MgCa(CO_3)_2$ into MgO.CaO were achieved when a higher

volumetric flow rate of N_2 was employed in the thermal decomposition steps at a heating rate of 10 K min^{-1}. For the same heating rate (10 K min^{-1}), the 1st carbonation step (C1) was more effective in terms of final value conversion when a lower partial pressure of CO_2 was chosen. On the other hand, a heating rate of 20 K min^{-1} for the thermal decomposition steps of the fresh dolomite in 750 mL min^{-1} N_2, resulted in poorer values of the final conversion than in the 10 K min^{-1} experiment. The same trend of poorer performance was observed in the non-isothermal 1st carbonation step (20 K min^{-1}) while the same CO_2 partial pressure was used as in the run of 10 K min^{-1} heating rate.

Therefore, in the macro scale experiments, the larger mass of 5 g at lower flowrates of gases enabled the thermal decomposition and carbonation of the material to reach higher final conversions even though there was not any fixed heating rate. Whereas, in the case of a high heating rate (20 K min^{-1}) with half the volume of the material (2.5 g), the performance of **TD** and **CRB** were poorer than for lower heating rates (10 K min^{-1}). It was concluded that the best performance of the dolomite in the macro scale experiments would be the combination of 2.5 g of fresh material, with a flow of 750 mL min^{-1} N_2 as the basis for the TD and carbonation steps, under a heating rate of 10 K min^{-1}.

From the micro scale (TGA) study of the dolomite, it was expected that the sorbent would be able to fully decompose, whereas in the bench scale full decomposition was attainable only in one of the experimental conditions (5g; 500 mL min^{-1} N_2; no heating rate). Despite dolomite having been extensively studied (as presented in **chapter 3; paragraph 3.3**) by earlier investigators, still its behavior at the macro-scale has not been examined compared to the micro-scale (TGA; DTGA) in regard to reactions **TD_b, TD** and **CRB**. In most of the small scale studies on dolomite and calcite where masses of the order of the mg were usually employed, the reactive gases mass transfer among the particles would be enabled either by isothermal or non-isothermal modes. Therefore, the necessary mass transfer of the reactive gas (CO_2) for the full thermal decomposition would be transferred in the volume of every particle, whereas in the case of packed volumes, as in the present macro scale (reactor) study, the mass of the reactive gas might not be effectively transferred to the total volume of a particle or from particle to particle. A parameter that may also have affected the latter phenomenon is the

volumetric flow rate of the carrier gas (N_2), which when set to the low value of 500 mL min^{-1}, resulted in the full calcinations of $MgCa(CO_3)_2$, hence an increased residence time. In theory, the velocity of the carrier gas around the particle increases, the boundary layer becomes thinner; hence the mass transfer rate increases.

5.3 Macro scale study

The fresh dolomite thermal decomposition steps of the macro scale study (dry) in an inert environment indicated that they were initiated at slightly higher temperatures than in micro-scale dry conditions. As mentioned previously, consecutive calcination experiments are termed 'TD*i*' for 'thermal decomposition', with TD_1 representing the first calcination conducted on the freshly mined, ground and sieved, fully carbonated dolomite. This may have been due to the larger mass used in the USR reactor, which, as described by **Bandi and Krapf (1976)** could result in the self-creation of a CO_2 atmosphere, as well as to the effect of packing of the material. The presence of CO_2, as indicated in the micro- scale study (**paragraph 4.3.1**), can initiate the thermal decomposition of the sorbent at elevated temperatures compared to the ones in an inert environment. The values for TD_1 assumed that all the $MgCO_3$ had decomposed. This was supported by observing a discontinuity in the rate of CO_2 release during the experiment which occurred at the same temperature as that of full $MgCO_3$ decomposition in the dry TGA experiments (with CO_2 present in the flow, **Dupont et al, 2007**).

In **Table 12** and **Table 13** the final number of sorbent moles and conversions at the end of C1, TD2, C2 are listed for the USR rig experiments. A very important aspect that arose from the macro-scale runs was the fact that the thermal decomposition of fresh dolomite or of recarbonated calcite, never reached full conversion ($\alpha << 1$), neither under dry or wet conditions.

Table 12 Maximum molar conversions for C1 & C2 in dry CO_2/N_2 mixtures and for TD2 in 100% dry N_2 (750 mL min^{-1}) in the macro scale experiments (2.5 g samples)

%vol CO_2/N_2	max% C1	$CaCO_3$ mol	max% TD2	CaO mol	max% C2	$CaCO_3$ mol
5	100.0	1.34×10^{-2}	90.4	1.21×10^{-2}	87.7	1.19×10^{-2}
10	72.0	1.09×10^{-2}	87.7	1.17×10^{-2}	59.6	9.10×10^{-3}
15	33.4	1.06×10^{-2}	80.9	1.14×10^{-2}	26.0	8.54×10^{-3}

Table 13 Maximum molar conversions for C1 & C2 in wet CO_2/N_2 mixtures, and for TD2 in 100% wet N_2 (750 mL min^{-1}) in the macro scale experiments (2.5 g samples)

% vol CO_2/ H_2O/ /N_2	max% C1	$CaCO_3$ mol	max% TD2	CaO mol	max% C2	$CaCO_3$ mol
5/ 3	97.9	1.32×10^{-2}	97.3	1.31×10^{-2}	91.5	1.20×10^{-2}
10/ 7	99.9	1.34×10^{-2}	85.4	1.15×10^{-2}	86.1	1.18×10^{-2}
15/ 12	90.2	1.28×10^{-2}	63.5	9.18×10^{-3}	59.6	1.01×10^{-2}

5.3.1 Experiments in the macro-scale (USR) reactor in the absence of steam

The maximum thermal conversion in the macro scale dry conditions seems to be affected in a positive way by the completeness of the previous carbonation run as the available amount of carbonate by the end of the 1st carbonation runs indicates. This is unlike the micro scale TGA experiments where TD2 was complete following from incomplete C1 (**Table 12**). Therefore larger scale experiments in dry conditions showed that both the carbonation and the calcination contributed to the decrease of the sorbent performance.

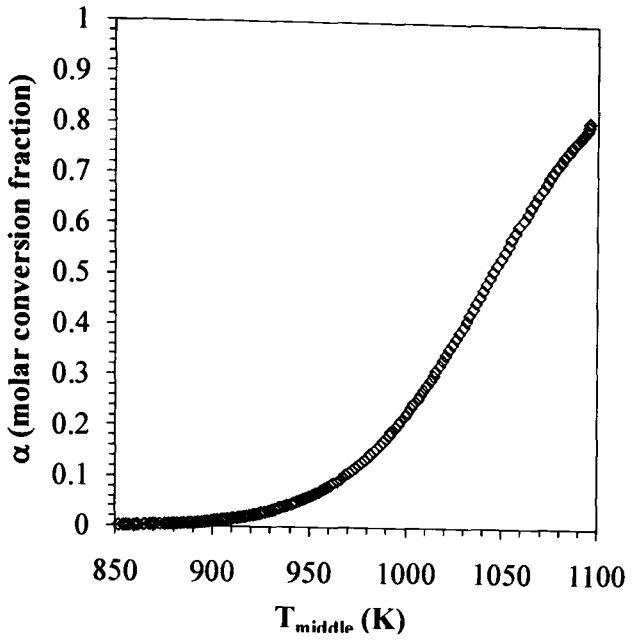

Figure 12 Experimental conversions (α) vs temperature (T) for TD2 in 100% N_2 (dry conditions; heating rate: 10 K min^{-1}) following C1 (5%CO_2/ N_2) in macro scale experiments

Figure 12 plots the curve of conversion 'α' vs. temperature 'T' for TD2 following from C1 in 5% CO_2/N_2, in dry macro scale conditions. It reveals a less active curve, with a small gradient. The full conversion is not shown, as the temperature programming did not go above 1100 K (827°C) in heating mode, however, under cooling conditions from 1100 K, the conversion reached a maximum of 90.4% which is the value reported in **Table 12**. Interestingly, the curve also shows that the onset of thermal decomposition was measured at as low as 900 K (627°C), followed by a very slow rate at higher temperatures.

The first carbonation steps (**Table 12**) at the same P_{CO_2} as the ones applied in the TGA (micro scale) study, showed that the higher the partial pressure of CO_2, the lower were the final values of the thermal decomposition (**TD**) conversions reached. The conversion reached by the end of the second carbonation for the lower CO_2 partial pressure (5 kPa) exhibited the higher drop in value to the one of the first carbonation (**Table 12**) compared to the other two partial pressures investigated (10 and 15 kPa). The decreasing trend of carbonation capacity of CaO from dolomite or calcite under dry conditions has been noted in numerous studies at the micro scale (**Silaban et al. (1996), Chrissafis et al.[(a)] (2005), Chrissafis et al.[(b)] (2005), Chrissafis et al. (2006), Stendardo et al. (2009), Manovic et al. (2009)**).

Specifically, in the micro scale (TGA) experiments, it was found that the final conversion at the end of the first carbonation in 5% vol CO_2/ N_2 was $\alpha_{f(C1),\ 5\%\ vol\ CO_2/\ N_2,\ TGA,\ dry}= 0.83$ and under the same conditions at the end of the second carbonation $\alpha_{f(C2),\ 5\%\ vol\ CO_2/\ N_2,\ TGA,\ dry}= 0.61$, contrary to the respective values at the macro scale in the USR reactor under dry conditions, which were much higher and did not show the same extent of deactivation ($\alpha_{f(C1),\ 5\%\ vol\ CO_2/\ N_2,\ USR,\ dry}= 0.99$; $\alpha_{f(C2),\ 5\%\ vol\ CO_2/\ N_2,\ USR,\ dry}= 0.89$). This showed that in the larger scale experiments, under 5% CO_2/ N_2, for C_1 and C_2, the final conversions exhibited higher values. Therefore, carbonations at low CO_2 concentrations performed better when a larger mass of material was present. This can be attributed to the fact that the packing of the material increased the residence time of the gas (CO_2) that participated in **CRB** in order to reach more active sites of CaO. In addition to this, the fact that the TD_1 in the reactor was incomplete prior to the C_1 did not result in the extent of carbonation of CaO that could have been achieved.

Higher conversions of the sorbent were not promoted at larger concentrations of CO_2 when larger mass was used (2.5 g). This is because there was insufficient time for the reaction between the solid (CaO) and the gas (CO_2) to reach the desired levels of conversion. Furthermore, it can be added to the previously discussed results that at higher CO_2 partial pressures the poorer performance of the carbonation reactions C_1 and C_2 are as well supported by **Sun et al. (2008)**, who noticed a better performance of carbonations when partial pressures of CO_2 smaller than 10 kPa were used, whereas for P_{CO_2} >10 kPa the respective performance was limited.

5.3.2 'Wet' experiments (in the presence of steam)

The presence of steam is an important aspect in the USR process and these experiments are a preliminary study of the effects of partial pressure of steam on the sorbent's performance. During the USR process, the sorbent in the form of carbonated CaO needs to be regenerated (thermally decomposed by calcination) quickly and to the possible maximum extent. This is so because during the steam

reforming the more available CaO sites, the better the CO_2 chemisorption is, in order to produce an exit stream of high H_2- purity.

Wet conditions (**paragraph 5.1**) in the macro scale experiments increased slightly the onset temperature of thermal decomposition. The effect of a variety of CO_2 partial pressures have on the thermal decomposition (DTA) of $MgCa(CO_3)_2$ has been extensively studied earlier and recently (**Samtani et al., 2001; Bandi and Krapf, 1976; Otsuka, 1986; Smith et al., 1974; García-Labiano et al., 2002**). Many of these studies (**McIntosh et al., 1990; Khan et al., 2001**) were focused on the thermal decomposition of $MgCO_3$ and how it was affected by the parameters such as the partial pressures, gases, the sample masses used and the heating rates. From these studies it can be concluded that the lower the heating rate, the lower was the temperature of the onset of decomposition ($T_{MgCO_3(i)}$), but eventually the final mass loss (%) or extent of conversion was the same.

The presence of steam did not influence significantly the final conversion (**Table 13**) of the dolomite's first calcination ($\alpha_{TD1,\ dry\ (average)} = 0.905$; $\alpha_{TD1,\ wet\ (average)} = 0.888$). Similarly, it did not affect much the final conversion of the second calcination($\alpha_{TD2,\ dry\ (average)} = 0.849$; $\alpha_{TD2,\ wet\ (average)} = 0.792$). The temperatures of **TD** did not seem affected either by the presence of steam ($T_{TD1,\ dry\ (average)}$= 836 K or 563°C; $T_{TD1,\ wet\ (average)}$ = 875 K or 602°C; $T_{TD2,\ wet\ (average)}$= 920 K or 647°C). Therefore the macro scale experiments, either under dry or wet conditions, showed a poorer performance of the sorbent compared to the dry micro-scale (TGA) study for the calcination reactions.

These results indicate that low partial pressures of H_2O may be beneficial to the final conversion (**Table 13**) during thermal decomposition (e.g. 3-7 kPa), but the effect is soon reversed for higher steam partial pressures P_{H_2O} (12 kPa). Steam's higher flow rate resulted in the better transport of the increased CO_2/ N_2 mixtures to the available CaO sites. Therefore, the final conversion during the carbonation (**CRB**) steps were enhanced. The thermal swing regeneration step of the dolomite used in a sorption enhanced or unmixed steam reforming process may therefore benefit from the presence of a little steam but that too much may prove counterproductive, and thus the safer approach would be to maintain dry conditions

for calcination if possible. This is unlike hydrotalcite sorbents whose regeneration under thermal swing generated by steam addition is recommended.

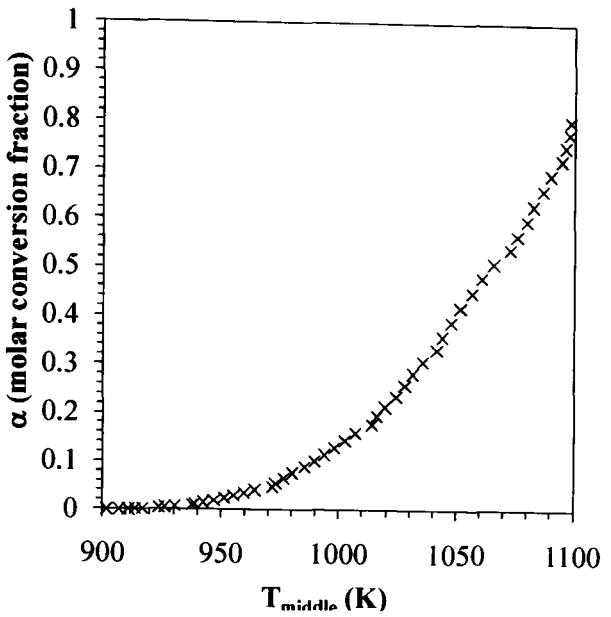

Figure 13 Experimental conversions (α) vs temperature (T) for TD2 in 2.9% H_2O/ N_2 (wet conditions) following C1 (5% CO_2/ N_2; heating rate: 10 K min^{-1}) in macro scale experiments

We can see in **Figure 13** the α vs. T profile for the 2.9% H_2O/N_2 TD2 following from C1 in 5%/ 2.9% vol CO_2/ H_2O/ N_2 wet macro scale conditions. It shows the onset of activity at 940 K (367°C), followed by a slow rise in activity. Unlike the C1 and C2 curves in wet conditions, which exhibited greater activity than their 'dry macro and micro' counterparts, the wet macro scale TD2 curve is the least active of the three conditions. A sharp increase in activity can be seen near 1100 K (827°C), which then followed by the cooling phase, reached the high 97.3% conversion reported in **Table 13**.

Therefore, there seems to be little benefit in carrying out thermal decompositions of dolomite in the presence of steam. These results seem to be in contradiction with the study of **McIntosh et al. (1990)** conducted at small scale, where the temperature for the 1st dry calcination was 1155 K (882°C) and lowered to 1148 K (875°C) in the presence of water vapour but overall these temperatures slightly exceed those found in the present study. However when looking closely at the high temperature of the TD2 curve in **Figure 13**, there is a sharp increase in activity just below 1100 K (827°C) suggesting that different kinetic regimes occur

below and above this temperature, which would bring this study's results closer to those of **McIntosh et al.** (1990) in this higher temperature range.

In the second set of experiments in the presence of steam at the macro scale, it was noticed that the temperatures at which the carbonations were initiated were lower than in the ones under dry conditions and at the micro scale (**paragraph 4.2.3**). The rate of reaction was enhanced by the presence of steam as illustrated by the temperature at which half the final conversion was reached ($T_{50\%}$). This value under wet conditions in 5% vol CO_2/ N_2 in C1 was 675-735 K (402-462°C) compared to 700-777 K (427-504°C) under dry conditions in the macro scale experiments. For the second carbonation (C2) experiment under the same dry conditions, it was 815- 820 K (542-547°C) whereas when wet it was 700-750 K (427-477°C). Therefore, the large scale experiment in the presence of steam achieved a measurable positive effect on the final experimental CO_2 capacity by increasing the carbonation reaction rate.

The temperature at which C1 started (T_i) for the lowest %vol CO_2 concentration under wet conditions was lower (456 K, 183°C) than in dry conditions (558 K, 285°C). The reverse occurred for C_2 in the presence of steam, where the initial temperature was higher (462 K, 189°C) than in dry conditions (357 K, 84°C). The same effect by steam was noticed in the first and second carbonations at the higher partial pressure of CO_2 of 15 kPa (522 K, 249°C) and ; (550 K, 277°C) respectively, compared to those in the absence of steam (430 K, 157°C and 436 K, 163°C). As mentioned previously, the carbonations' temperature range was chosen based on those identified from the micro-scale (TGA) study, and as the figures suggest, they were selected appropriately since the end of the conversion curve approached a plateau (**Figure 7; paragraph 4.3.1**).

It is worth noting that the temperatures where carbonations begin in this study are significantly lower than those reported in the literature. This may be due to the non-isothermal conditions of the experiments, which allow covering from ambient to high temperatures while generating kinetic data, as opposed to the kinetic studies so far carried out in isothermal conditions and at higher temperatures (minimum 850 K, 577°C).

The effect of steam in the carbonation steps, primarily in the 15% vol CO_2/N_2 mixture was strongest in its promotion of both C1 and C2, and slightly less for the 10% vol CO_2/ N_2 mixture. As it can be seen in **Table 13** and in **Figure 7 (paragraph 4.3.1)**, the final conversion achieved in 15% vol CO_2/N_2 by the end of C_1 was 0.33 and at completion of C2 it was 0.26, when by the end of C1 and C2 in wet conditions the respective values were much higher, at 0.90 and 0.60 respectively. The presence of steam improved the carbonation performance during the second cycle (C2) in 10% vol CO_2/ N_2 under dry conditions resulting in 0.86 in wet conditions compared to 0.60 (dry). Only the 5% vol CO_2/ N_2 carbonation runs seemed to be unaffected by the presence of steam based on the experimental conversions.

5.4 Kinetic study of carbonation and calcination of dolomite at the macro scale

The macro scale experiments in the USR reactor were aimed at investigating the sorbent material's ability to release (**TD**) and capture (**CRB**) carbon dioxide in dry and wet environment. This would enable the comparison of the final conversions reached in different gaseous mixtures and the repeatability of steps (**TD**) and (**CRB**) with those obtained at the micro-scale (TGA). The main parameters chosen for this comparison were the effect mass and steam and CO_2 partial pressure conditions would have on the sorbent's performance in terms of (i) efficiency (α) and (ii) of calculated kinetics parameters (E; ln$A$) and best model mechanism, using the improved iterative Coats-Redfern method (**paragraph 4.1.2**). The heating rate as well as the temperature range for the carbonation and thermal decomposition reactions was kept the same as in the micro scale (TGA) runs.

5.4.1 Kinetic study from the 'dry USR' experiments

In order to ascertain that experiments of carbonation were not mass transfer limited by lack of CO_2, the flow of CO_2 and mass of dolomite chosen was such that a large excess of CO_2 was always verified (see **Appendix II**).

In the kinetic study of the sorbent at the macro scale, 2.5 g of fresh dolomite were loaded in the USR reactor and the calcination (**TD**) and carbonation (C**RB**) reactions were examined. The same partial pressures of CO_2 as in the TGA study at the micro scale were used, only in this case a N_2 flow $\dot{V}_{N_2}$= 750 mL min^{-1} was used. Non-isothermal (+10 K min^{-1}) kinetic data and a best fit model were identified from the improved iterative Coats Redfern method, and these were then applied to re-construct the conversion vs. temperature curve via the best fit model. The resulting kinetic parameters from dry and wet (presence of steam) experiments could then be compared to those from the micro scale study. The produced kinetic parameters and identification of best fit model would enhance the understanding of the sorbent's behavior at the micro scale (in the USR reactor) in terms of the temperature range and final conversions achieved (**paragraph 5.3**).This was carried out for two consecutive TD and CRB reactions which are termed 'TD1- C1' and 'TD2- C2'.

5.4.1.1 Dry carbonation experiments

Kinetic modelling with the improved iterative Coats-Redfern method based on several mechanism models (different $g(\alpha)$ equations) enabled the prediction of conversions for each carbonation. In the case of carbonation, the best fit was obtained when using the 3D diffusion mechanism as described by Jander's equation model that assumes that the CO_2 reactant needs to diffuse through a carbonate product layer in order to react with the CaO inner core. The thicker the product layer grows, the slower the reaction becomes.

Under dry conditions (absence of steam) the higher activation energy (**Table 14**) for the 1st carbonation (C1) was observed for the lowest CO_2 concentration (5% vol) whereas in the second carbonation (C2) higher energy was needed for the reaction to initiate during the feed of 10% vol CO_2/ N_2. For the first carbonation (C1) the values of E (activation energy) can be explained by the extent of the thermal decomposition of $CaCO_3$ (α = 0.69) which was limited compared to the runs that preceded the 1st carbonations (C1) for the mixtures of 10% and 15% CO_2/ N_2 (α = 0.92 and 0.82 respectively).

The second carbonation step (C_2) started at a higher temperature in the 15% vol CO_2/ N_2 environment than in the 5% and 10% CO_2/ N_2. The higher partial pressure of CO_2 in the sorbent's environment therefore resulted in lower conversions which resulted in a low activation energy ($E_{C2(15\%\,CO_2/N_2)}$= 119 kJ mol^{-1}) as demonstrated in **Table 14.**

Table 14 Kinetic parameters under dry macro scale conditions at different P_{CO_2} for CBR and in 100% N_2 for TD

Exp >	<---------- lnA ± dlnA (A in s^{-1})----------><---------- (E ± dE (kJ mol^{-1})---------->						<----------r (corr. coeff.)-------><------no. of points----><----------fitted α range----------								
P_{CO_2}~ (kPa)	5	10	15	5	10	15	5	10	15	5	10	15	5	10	15
C1	13.5±8.7 13.3±8.3	6.0±7.7	10.1±8.2 9.4±7.8	144.6±-3.8 141.0±-2.2	95.2±-0.7	135.7±-2.1 164.2±-16.7	1 1	0.99	0.99 0.99	112 204	307	188 46	0.02-0.19 0.20-0.99	0.03-0.72	0.03-0.3(0.31-0.3<
C2	9.9±7.9	15.6±8.6 4.0±8.2	6.5±7.9	127.5±9.2	160.8±-3.1 89.7±-4.5	119.9±-0.9	0.99	1 0.99	0.99	330	138 105	282	0.03-0.86	0.02-0.30 0.30-0.60	0.01-0.26
TD1	143.4±39.0	115.6±15.6	138.5±24 .2	1341.3±327.1	1064.8±134.0	1269.7±207.0	1 *n*= 2.9	0.99 *n*= 1.2	0.99 *n*= 1.7	45	65	44	0.03-0.48	0.03-0.99 (normalised)	0.04-0.97 (normalisec
TD2	19.6±0.4	32.7±0.73	43.8±0.9	218.4±3.3	318.9±6.0	412.1±7.6	1 *n*= 1.8	1 *n*= 2.6	0.99 *n*= 1.5	213	165	175	0.02-0.81	0.03-0.84	0.03-0.99 (normalisec

During the first step (C1), the necessary energy to start the reaction between CO_2 and CaO active sites appeared to be increased at the macro scale when compared to the micro scale experiments, except in the case of 10% vol CO_2/ N_2. The activation energies for C2 at the macro scale in dry conditions (**Table 14**) were much lower than in the TGA experiments (**Table 12**), indicating that less energy needed to be supplied in order to initiate carbonation when more mass (m_i= 2.5 g) was used. This is because the initial temperatures of C2 in the TGA were higher (590 K, 317°C) than at the macro scale in dry conditions (357 K, 84°C).

The derived values of A and E were then fed back into the model to predict the conversions for given temperatures and re-build the α vs. T curves. In **Figure 14(a) and Figure 14(b)** the experimental conversions' α vs. temperature and the model fits for these curves can be seen.

For the first carbonations (C1) a single curve fitted the experimental data by applying the improved iterative Coats-Redfern method. The modelled curves that refer to the first carbonation step (C1; **Figure 14(a)**) are superimposable on the experimental curve for the whole range of conversions indicating an excellent model. The approach was excellent as the correlation coefficient suggests in **Table 14**.

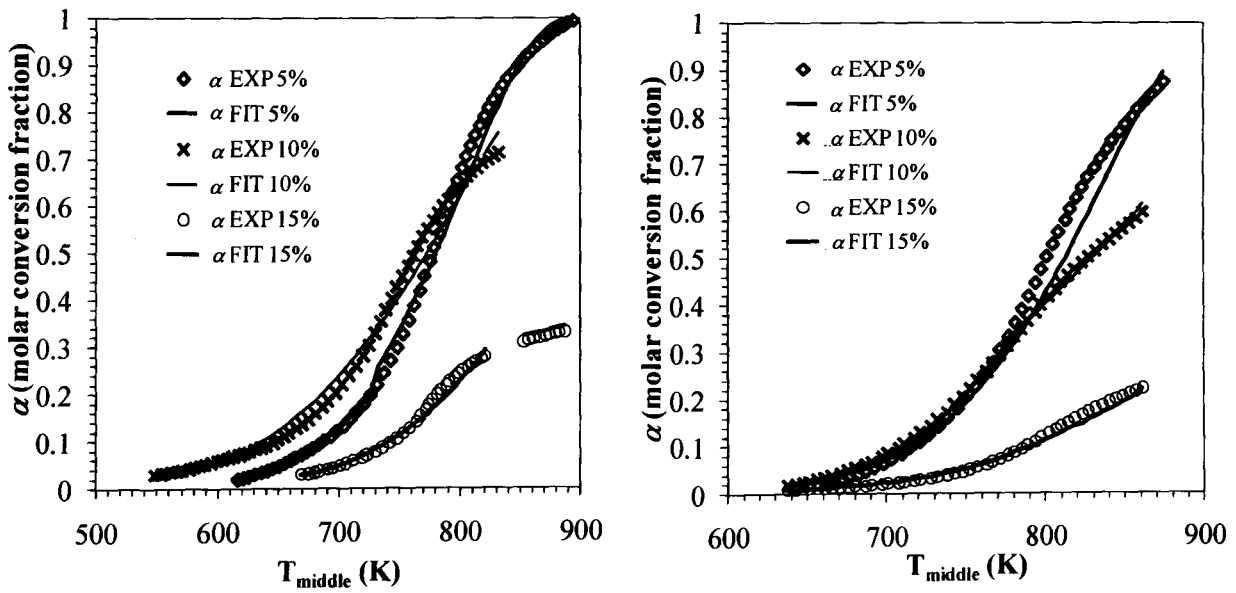

(a) First carbonation steps (C1) in 5, 10, 15% CO_2/N_2

(b) Second carbonation steps (C2) in 5, 10, 15% CO_2/ N_2

Figure 14 Experimental conversions ($\alpha_{EXP\ 5\%,10\%,15\%}$) and model fits ($\alpha_{FIT\ 5\%,10\%,15\%}$) vs temperature ($T_{middle}$ (K)) for the dry carbonation steps (C1 and C2) in macro scale

Similarly for the C_2, in various mixtures (5, 10, 15% vol CO_2/ N_2; **Figure 14(b)**) the experimental conversions data were simulated very well over the whole temperature. For the second carbonation step (C2) in 5% CO_2/ N_2 Figure 12(b) shows that between 50% and 85%, a slight divergence between the experimental and the modelled conversion curves, but the remainder of the conversions (10% and 15% CO_2/ N_2) were reproduced with excellent accuracy. In previous studies, as in the attempt of **Lee et al.** (2004) to model the experimental data of CaO carbonation, the model fit with a linear equation was limited into high and low temperature conversions and by very few data points compared to this study **(Tables 14 and 15)**.

5.4.1.2 Thermal decomposition in dry conditions

Despite using the same initial mass of fresh dolomite (2.5 g) over the three sets of tests in the macro scale study under dry conditions during the 1st thermal decompositions (TD) in 100% vol N_2 the activation energy values were different determining in this way the final conversion reached ($\alpha \ll 1$) which was reported in **paragraph 5.3 (Table 12 and Table 13)**. the E_{TD1} values, listed in **Table 14**, were higher than in those of TD2, due to the presence of $MgCO_3$ in the fresh dolomite. The activation energy (E_{TD2}) of the thermal decomposition of $CaCO_3$ was higher for lower concentrations of CO_2 (**Table 14**). For instance, it can be seen that the thermal decomposition TD2 in 100% vol N_2 that followed C1 in 5% CO_2/ N_2, yielded a lower activation energy than in the other two cases (10 and 15% CO_2/N_2), resulting also in a higher final conversion $\alpha = 0.90$, compared to $\alpha = 0.84$ following C1 in 10% vol CO_2/ N_2 and $\alpha = 0.81$ following C1 in 15% vol CO_2/ N_2.

The first thermal decomposition (**TD1**) of fresh dolomite (according to **TD**) under dry conditions exhibited different reaction orders for all three samples used, despite the activation energies being in the same range (**Table 14**). Following the 1st carbonation in the dry USR rig runs, the second thermal decomposition (TD2) of the $CaCO_3$ was best modeled with different reaction orders, with the highest being at n= 2.6 after C1 in 10% vol CO_2/ N_2.

Olszak-Humienik et al. (1999) reported activations energies (E) and pre-exponential factors (A) of the thermal decomposition of dolomite for 50 mg

samples at a heating rate of 5 K min^{-1} from 293 to 1273 K (ambient to 1000°C) in a static air atmosphere by using the Coats-Redfern method. In particular, for the first stage of decomposition, the activation energy and pre-exponential factor were calculated based on the 1D-diffusion equation, yielding the values of 219 kJ mol^{-1} and 1.52 × 10^9 s^{-1} ($\ln A$= 21.14) respectively. For the second stage of thermal decomposition the random nucleation model was chosen resulting in E= 390 kJ mol^{-1} and A= 3.98 × 10^{17} s^{-1} ($\ln A$= 40.53). These values are in close agreement with the E and $\ln A$ values presented in **Table 14** for TD2 after C1 in 15% CO_2/ N_2, which in this case were better interpreted by the reaction order equation for an order of n= 1.5.

5.4.2 Kinetic study in the presence of steam at the macro scale

In the past, in studies as in **McIntosh et al. (1990),** the effect of steam appeared to have an enhancing impact on Ca sorbents but not to the extent achieved in the present macro scale study. The presence of steam during carbonation appeared in other investigations was found to increase the kinetics and the carbonation capacity, as in the **Ochoa- Fernandez's (2007)** study on synthetic ceramic CO_2 sorbents (Li_2ZrO_2 and Na_2ZrO_2). **Ochoa- Fernandez (2007) posited** that the increase in the kinetics due to presence of steam was accredited to the increased ions' mobility. **Nikulshina et al.** (2007) introduced steam to enhance the kinetics of the carbonation reaction. The same authors modelled experimental data for adsorption of CO_2 from air with CaO in the presence and in the absence of water vapour using the Avrami model and the unreacted core (contracting volume) model respectively. They noticed that the presence of water vapour increased the rate of carbonation by a factor of 22. The effect of steam enhancing the kinetics of carbonation in Ca based sorbent is a known but poorly quantified phenomenon, and is generally attributed to increased CO_3^{2-} ions transport in the wet environment.

5.4.2.1 Kinetics of carbonation in wet conditions

Abanades et al. (2002) compared several CaO carbonation studies in which it was proposed/ found that at the latter stage of carbonation the reaction becomes

diffusion controlled. **Chrissafis et al.[(b)] (2005)** mentioned that the limitation of the CaO carbonation over repeated cycles might be due to the lack of sufficient diffusion of $CO_{2(g)}$ through the $CaO_{(s)}$ pores due to sintering.

Despite the higher activation energies (**Table 15**) in C1 and C2 in the large scale experiments under wet conditions, (which are directly linked to higher initiation temperatures (**paragraph 5.3.2**)), which were calculated based on the 3D Jander diffusion equation, the beneficial effect of steam at high P_{CO_2} was shown as these reactions were allowed to reach completeness. Full carbonation based on the theoretical available molecules of CaO present in the samples was reached with the steam enhancement (**Table 13**).

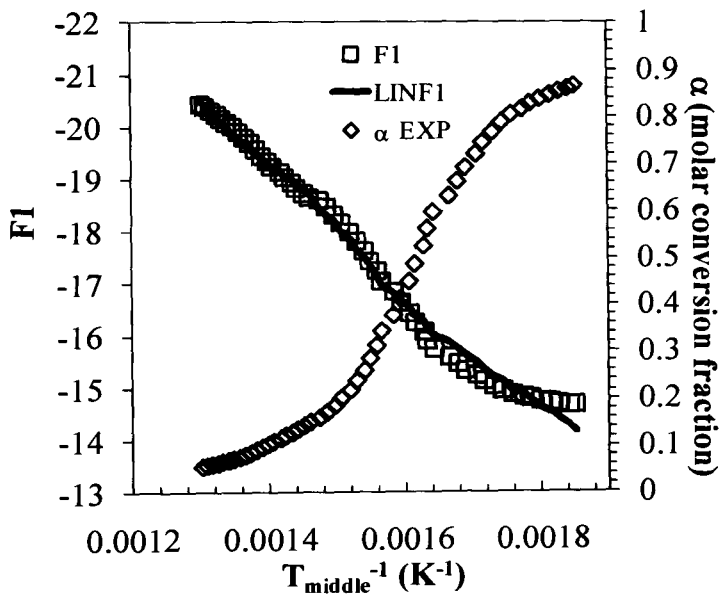

Figure 15 Experimental F1 (scatter points) and linear fit (line) (read on the primary y- axis) vs. T_{middle}^{-1} and experimental molar conversion fraction (α; read on the secondary y- axis) for C1 in 5% CO_2/N_2 mixture in 'wet macro-scale' conditions. Corresponding kinetic and goodness of fit parameters are listed in **Table 15**

The catalytic presence of steam activated more sites during the carbonation steps which led to a higher energy demand to complete the higher range of achieved conversions. Therefore, the higher activation energies in the 10 and 15% vol CO_2/ N_2 C1 can be directly linked to the higher final conversions reached. Hence the enhancement in the performance of reaction **CRB** due to the presence of steam is confirmed.

Table 15 Kinetic parameters in wet macro scale conditions at different P_{CO_2} for CRB and in 2.9, 7.4 and 11.5% vol H_2O/ N_2 f or TD

Exp	<----------lnA ± dlnA (A ins^{-1})---------->			<---------- (E ± dE (kJ mol^{-1})---------->			<-------r (corr. coeff.)----->			<------no. of points------->			<---------- fitted α range---------->		
P_{CO_2} ~ (kPa)	5	10	15	5	10	15	5	10	15	5	10	15	5	10	15
C1	8.3±7.6	8.75±7.9 4.50±7.7	25.6±8.7 -1.7±7.2	94.7±-0.4	97.6±-1.4 72.5±-2.2	206.8±-1.96 43±-3.1	0.98	0.99 1	1 0.99	425	175 129	196 103	0.02-0.98	0.05-0.60 0.06-1	0.03-0.7 0.7-0.9
C2	-0.47±7.5 13.43±8.2	29.89±8.8	17.1±8.4	59.3±-2.2 128.4±-2.1	237.4±-1.9	175.1±-1.2	0.99 0.99	0.99	1	112 165	251	265	0.05-0.15 0.15-0.87	0.01-0.819	0.03-0.6
TD1	7.5±0.2	3.30±-0.2	99.9±235.4 54.9±32.3	129.4±1	99.54±1.68	975±841.2 563.7±242.3	1 n= 0	1 n= 0	0.99 n= 2.9	275	389	13	0.01- 0.6	0.03-0.85	0.06-0.19
TD2	23.7±0.5	30.7±0.64	21.7±0.5	257.0±4.2	323.79±5.4	239.2±4.1	1 n= 1.8	1 n= 2.9	0.99 n= 1.2	197	191	21 175	0.02-0.83	0.02-0.69	0.2-0.40 0.03-1 (normalised)

In **Figure 15** the linear fits of factor F_1 vs T^{-1} are presented, as described in **paragraph 4.2.2** in accordance to the formulated FORTRAN program based on the C2 in 5% vol CO_2/ N_2 under wet conditions.

The wet USR linear fit (F1 vs. T_{middle}^{-1}) exhibited a shallow gradient at low temperatures followed by a steeper one at high temperature, which is usually attributed to reactions being controlled by diffusion and then progressing to surface kinetics regime.

The kinetic parameters emerging from the micro scale (TGA) and macro scale are directly comparable as both were best interpreted by the 3D diffusion model. Any increase in the activation energies in the dry and wet USR rig runs compared to the TGA (dry) is an issue that needs to be considered as it clearly indicates that in the macro scale more energy is required to initiate carbonations; this might be due to the packing of the material (2.5 g) compared to 3 mg in the small- scale, which in both cases used particles of the same size.

5.4.2.2 Thermal decomposition in the presence of steam

As discussed earlier, very low steam concentrations have been found to enhance the thermal decomposition performance, but the effect is reversed when the steam concentrations are increased. These results, at this early stage of the study, showed that the Warmsworth dolomite's regenerative capability is restricted to low steam partial pressures (P_{CO_2}) for the unmixed steam reforming process and that during calcinations, dry conditions are recommended.

From **Figure 16** where α vs T with the respective model curve are depicted, TD2 in the large scale study appears less active than at micro-scale. This is indicated by the smaller gradient of the model fit. In this figure, the full curve of TD2 at the macro scale is not shown, as TD2 reached its final conversion value during cooling. The final conversion reached during cooling of TD2 after the C1 in 5% vol CO_2/ N_2 was 0.90.

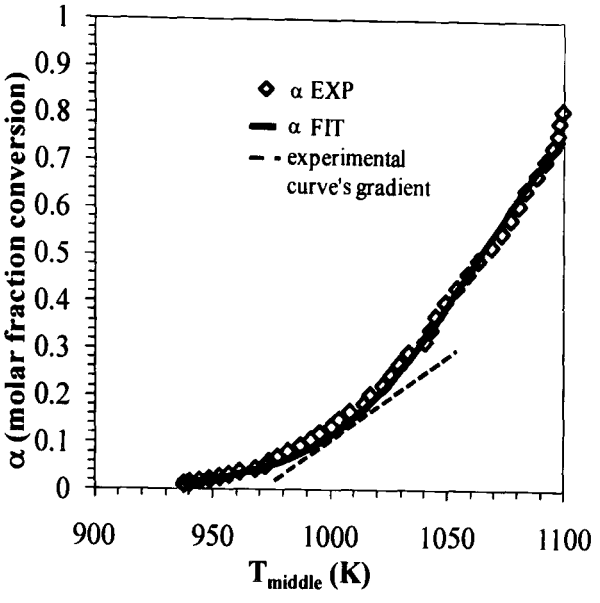

Figure 16 Experimental conversions ($\alpha_{1\,EXP}$) and model fits ($\alpha_{1\,FIT}$) vs temperature (T_{middle} (K)) for the macro-scale thermal decomposition (TD2) in wet conditions following C1 (5% CO_2/ N_2)

The model curve (**Figure 16**) indicated a low initial temperature (close to 950 K, 677°C), compared to TD2 in the TGA (dry) (978 K), at which **TD** started. it ended at slow rates of higher conversion than the curves presented. This early start resulted in a lower calculated activation energy (257 kJ mol^{-1}), compared to that in the micro scale (TGA) E_{TD2}= 880 kJ mol^{-1}.

The first thermal decomposition of the fresh sorbent (mainly $MgCa(CO_3)_2$) established lower *E* values for the fresh samples in the under wet conditions runs (**Table 15**), than when in the absence of steam (**Table 14**). This was to be expected, as **Beruto et al (2003)** verified higher reaction rates of the thermal half decomposition of dolomite ($MgCO_3$) in the presence of steam than under dry conditions. The activation energy values of the second decomposition runs (TD2) in the presence of steam following C1 in 5% and 10% vol CO_2/ N_2 were in the same range as those in dry conditions. The only exception was for the activation energy (E_{TD2}= 239.2 kJ mol^{-1}) of the calcination run (TD2) in 15% vol CO_2/ N_2 which was lower than in the corresponding run under dry conditions (323.8 kJ mol^{-1}).

The values of *E* and ln*A* for TD2 were calculated with a high precision as the correlation coefficients (0.99) instructs for the fit of F_1 vs T^{-1} (**Figure 17**) for conversions from 0.03 to 0.99 (**Table 15**). This high value of activation energy

clearly shows that this reaction (**TD**) is highly active in an inert environment (100% vol N_2), therefore it has a high energy demand to start ($T_{TD2,\ wet\ (i)}$).

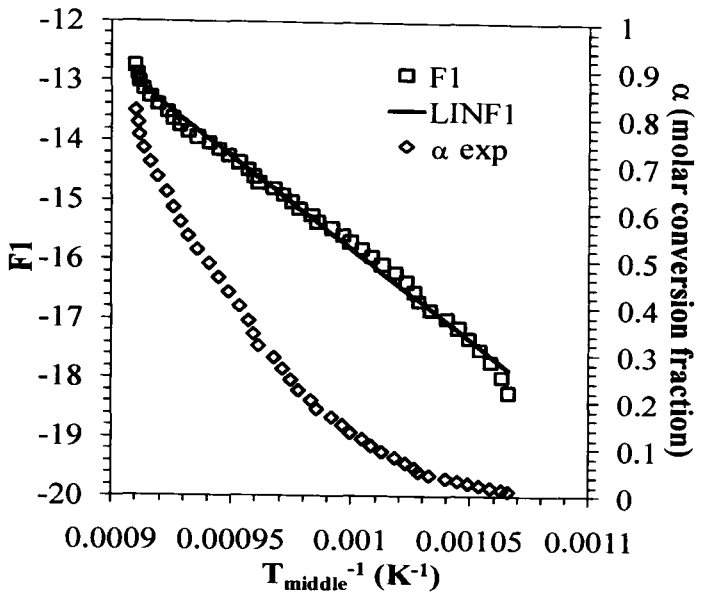

Figure 17 Experimental F1 (scatter points) and linear fit (line) vs. T_{middle}^{-1}, and experimental conversion fraction (α) for thermal decomposition (TD2) in 5% CO_2/N_2 mixture in wet macro scale conditions

The initial TD2 temperature under wet conditions (**Fig. 17**) following C1 in 5%vol CO_2/ N_2 under wet conditions, was 940 K (667°C) having a direct effect of increasing activity ($E_{TD2,\ USR,\ wet}$= 257.0 kJ mol^{-1}). This effect can be seen in the respective curve when it approaches 1100 K (827°C). In **Figure 17** where F1 vs T^{-1} is plotted, the fit of the model line over the experimental data shows the extent of accuracy of the *E* and ln*A* derived.

The thermal decompositions kinetic parameters in the macro scale (both dry and wet) experiments were calculated, as earlier referred, using the reaction order model; this means that diffusion was not the rate limiting step as the product layer of CaO at the outer surface of the sorbent's particles allowed further reaction TD. This might be assisted by the presence of MgO from the initial thermal decomposition of dolomite which enhanced the CO_2 mobility as it was produced on the particles interface.

The same effect as in the TD2 after the carbonation in the middle CO_2 concentration range was noticed under wet conditions as in the dry experiments, where the reaction order was the higher than in the calcinations that followed the carbonations (C1) in 10% vol CO_2/ N_2. The fresh sorbent's thermal decomposition

(wet) reaction order was higher (n= 2.9) in one out of the three samples tested; two samples exhibited a zeroth order of reaction (**Table 15**). The calculated E and ln$A$ for the thermal decompositions following C1 in the presence of steam were in the same range as in the dry experiment except in the TD2 that followed the second carbonation step in 15% vol CO_2/ N_2 (wet). The reaction was found to be of order 1.2, when n for the TD1 that preceded C2 in 15% vol CO_2/ N_2 (wet) was calculated to be equal to 2.9, linked to the highest ln$A$ value (**Table 15**).

L'vov et al. (2003) approached the activation energies calculation for 10-11 mg powder or crystal dolomite by the third law method under vacuum. The resulting values were in the range of 250 kJ mol^{-1} (244.8- 247.5 kJ mol^{-1}) when a heating rate of 10 K min^{-1} was applied from room temperature to 800 K (527°C) and from 800 K till full decomposition at 2 K min^{-1}. These values agree with those of TD2 after the C1 in 5% vol CO_2/ N_2 as presented in **Table 15** under wet conditions respectively. Despite noticing higher activity in the wet USR rig in the C1 and C2 as opposed to the respective experiments in dry macro- and micro-scale conditions, the thermal decomposition (TD2) followed C1 was found less active than the ones performed in dry micro- and macro-scale. As in the TD2 of dry USR rig runs, the experimental produced conversions at a heating rate of 10 K min^{-1} were better modelled when the reaction order model was used.

The significant finding that should be considered for the lower values of E and ln$A$ in the latter step, that is, TD2 following C1 in 15% vol CO_2/ N_2, should be the fact that C2 had a higher final conversion than under dry conditions. Therefore, more $CaCO_3$ molecules were available at the outer layers of the surface of the sorbent's particles present in the reactor which were ready to be thermally decomposed by a smaller energy supply. This is the most probable explanation rather that of the presence of steam, which did not seem to affect the rest of TD2 runs under wet conditions **(Table 15)**. The previous results come in contrast to the ones by **McIntosh et al. (1990)** who found that the presence of steam lowered the onset temperature of the calcite's small scale thermal decomposition from 1155 K (882°C) to 1148 K (875°C).

5.5 Stability study of dolomite under cyclic conditions at the macro- scale

The dolomite' stability, as measured by the final carbonation capacity and conversion by calcination, was verified over 9 repeated calcinations-carbonation cycles at a heating rate of 10 K min^{-1} and by employing N_2 as the gas carrier at a flowrate of 750 mL min^{-1}. The mass of the fresh material was chosen at 2.5 g (2500 mg) as determined in the macro scale kinetic study (**paragraph 5.4**). The macro scale set up promoted the study of dolomite under dry and wet conditions, while on the micro scale study (TGA) (**paragraphs 4.4, 4.5**) experimental information was gained only in dry conditions. Additionally, the aspect of cyclic repetition of thermal decomposition and carbonation steps was approached on a macro scale in order to be compared with the respective results produced on the micro scale sorbent's stability study (**paragraph 4.5**).

The wet stability study of the sorbent was performed in a steam to CO_2 ($S:CO_2$) ratio of ≈ 1 (0.77). This carbon content applied for the $S:CO_2$ ratio in the carbonation steps was calculated based on the $CO_{2(g)}$ mixed in the carrier gas ($N_{2(g)}$) at 1 atm and 20°C, while the deionised water (STP) was pumped by using a peristaltic pump (Watson Marlow 5058) to the steam generator, which produced steam at 423 K (150°C). The $CO_{2(g)}$ partial pressures (P_{CO_2}) employed in both the calcination and the carbonation steps for the stability runs in the absence of steam were 10 kPa while in the steam presence were 9.5 kPa. The wet thermal decompositions and carbonation steps were investigated in an environment of 10% vol CO_2/ 7.4 % vol H_2O/ N_2.

5.5.1 Discussion on dolomite's stability: effect of steam

In the first (TD1) thermal decomposition step full calcination of the dolomite was not achieved either under dry (steam absence) or wet (presence of steam) conditions (**Figure 18(a)**).

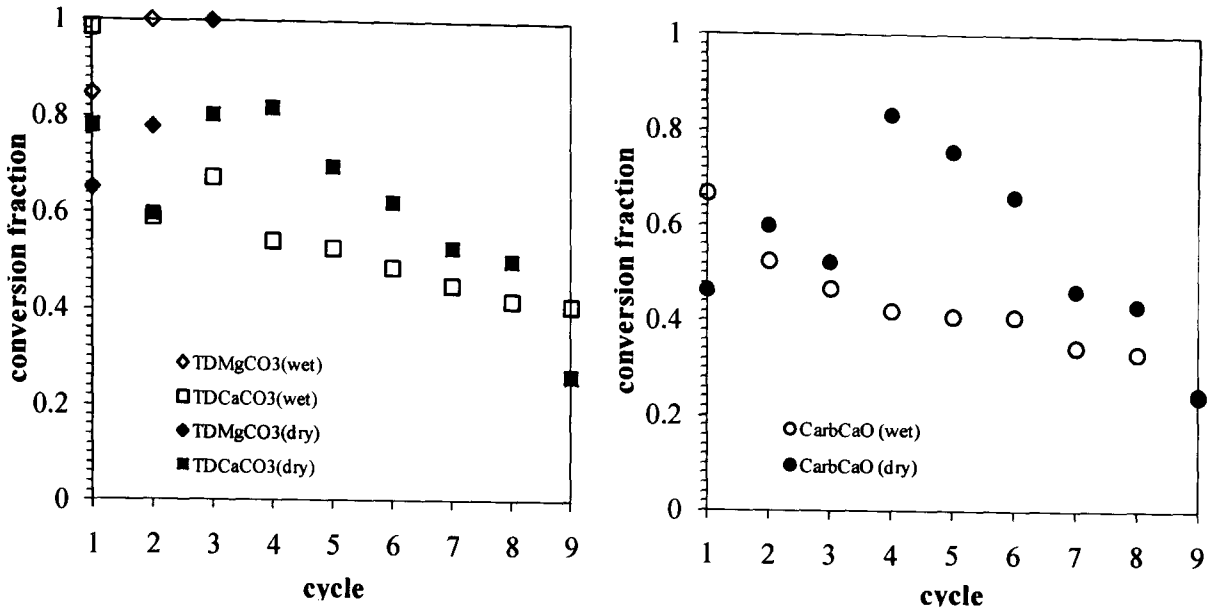

(a) Dry and wet thermal decomposition steps

(b) Dry and wet carbonation steps

Figure 18 Conversion of Warmsworth dolomite over nine (9) repeated thermal decomposition/ carbonation steps in CO_2/ N_2 under dry (10% vol CO_2/ N_2) and wet (10% vol CO_2/ 7.4 % vol H_2O/ N_2) macro scale conditions

Therefore, the presence of $CO_{2(g)}$ during the 1st calcination step did not affect the extent of the decomposition of $MgCa(CO_3)_2$ into MgO.CaO, something that had already been deduced in the absence of $CO_{2(g)}$ as in the bench scale kinetic study (**paragraph 5.3**). The same trend was followed by all thermal decomposition steps that succeeded the carbonation ones. In the presence of $CO_{2(g)}$ during the TD steps, it was possible to distinguish two $CO_{2(g)}$ peaks, over certain temperature intervals, each originating from the $MgCO_3$ and $CaCO_3$ decomposition respectively, based on the reaction equations TD_a and TD_b. This was realized with the help of the TGA experiments in regard to the thermal decomposition of the fresh dolomite in 10% vol CO_2/ N_2 as shown in **Figure 19(a)** and **(b).**

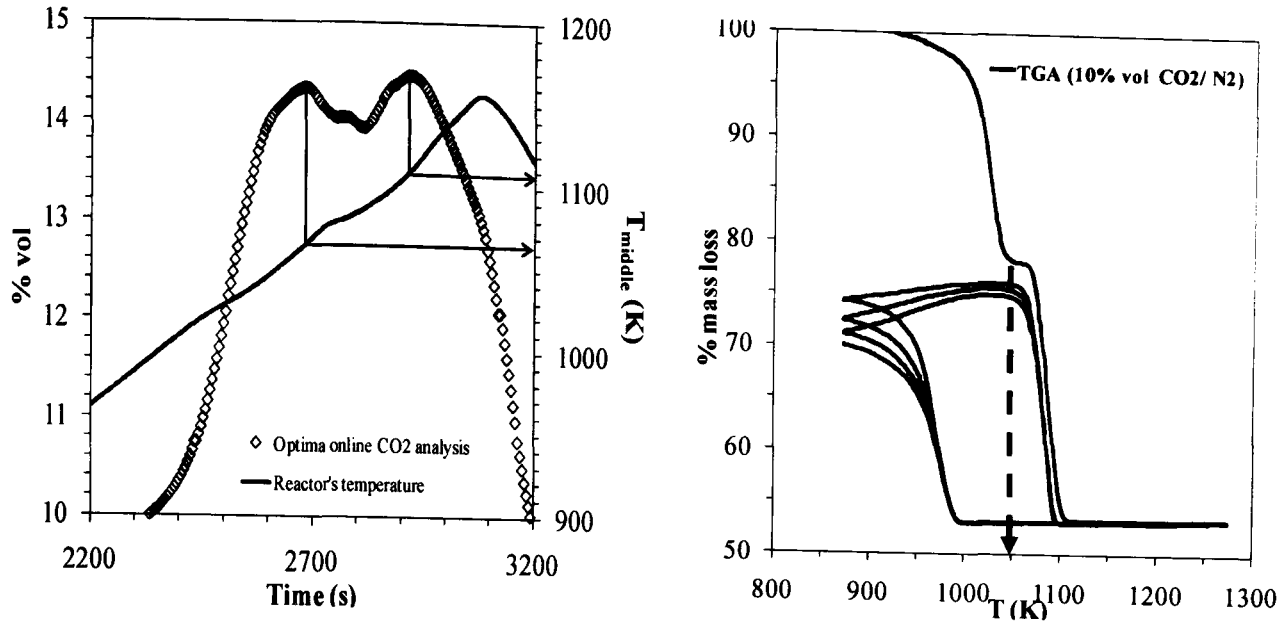

(a) First thermal decomposition step under dry conditions (USR rig)

(b) Thermal decomposition/ carbonation steps under dry conditions (TGA)

Figure 19 CO_2 concentration (scatter points) and bench scale reactor temperature (line) with time. First peak corresponds to $MgCO_3$ decomposition; second peak is $CaCO_3$ decomposition (symbols) in USR reactor (dry) for 10% CO_2/ N_2 mixture (b) TGA (same conditions) temperatures. (arrow indicates mass loss of sorbent based on its initial mass)

By comparing the temperature range for the mass loss curves of $MgCO_3$ and $CaCO_3$ decomposition in the TGA (**Figure 19 (b)**) with the temperatures at which the two peaks correspond for the macro scale experiment in **Figure 19(a),** it was possible to attribute the first peak to the decomposition of $MgCO_3$ and the second one to that of $CaCO_3$. This is because the thermal decomposition of $MgCO_3$ in the TGA in a 10% vol CO_2/ N_2, occurred between 916 and 1045 K (643-772°C) and the calcination of $CaCO_3$ started at 1055 K (782°C) and ended at 1101 K (828°C). Over the repeated calcination steps, these two peaks tended to merge, forming a single curve with a mere dip, which was used for detangling the temperature intervals of the two thermal decomposition reactions (**TD_a and TD_b**). Based on the previous observation it was possible to realize that the $MgCO_3$ that was initially present in the fresh dolomite was not fully decomposed by the first calcination in either dry or wet conditions. In particular, in the dry experiments, $MgCO_3$ was completely converted into MgO by the 3rd cycle, whereas in the presence of steam this was achieved by the 2nd cycle (**Figure 19(a)**). In a recent study of **Beruto et al. (2003)** on the first half thermal decomposition of dolomite, corresponding to the decomposition of $MgCO_3$ TD- it was mentioned that steam would accelerate its

rate, which is in agreement with this study. According to the Le Chatelier's principle, the CO_2 presence shifted the first half thermal decomposition of dolomite (TD of $MgCO_3$) to the left. The additional flow of $H_2O_{(g)}$ during the 'wet' experiments didn't allow the same residence time of the supplied and produced CO_2 as in the dry runs which allowed the TD of $MgCO_3$ to move further to the right, hence to the production of MgO and CO_2. In the wet reactor experiments, the initial temperature for $MgCO_3$ decomposition was found to be ca. 860 K (587°C) whereas for $CaCO_3$ the onset calcination temperature was in the range of 1000-1100 K (727-827°C).

Additionally the temperature range at which the carbonation occurred under dry conditions contributed to the incomplete decomposition of $MgCO_3$ up to the 3rd cycle, mainly due to the 10% vol CO_2/ N_2 conditions. **Bandi and Krapf (1976)** mentioned that the higher the partial pressure of CO_2, the lower the temperature at which the $MgCO_3$ started to decompose, as observed in the 10 mg micro-scale study (**paragraph 4.3.1**). The rate of calcination of $CaCO_3$ was found to slow down the overall rate of decomposition of dolomite rather than the $MgCO_3$ decomposition (**Otsuka, 1986**). On the other hand, by increasing the partial pressure of CO_2, it results in a higher temperature range of the $CaCO_3$ calcination (**Bandi and Krapf, 1976**).

From **Figure 19(a)** it can be seen that despite the incomplete thermal decompositions of $MgCO_3$ under dry and wet conditions, the extent of CaO carbonation is not affected in terms of final conversion fractions, even though it followed an expected descending trend over the repeated cycles as seen earlier in the dry TGA stability runs (**paragraph 4.5**). Earlier studies (**Chrissafis et al, 2005; García-Labiano et al., 2002**) supported that the presence of MgO was responsible for the high carbonation yield of MgO.CaO in CO_2 environments compared to calcite, whereas in the present study, it is shown that whether $MgCO_3$ is fully decomposed by the 1st thermal decomposition step (TGA stability study; **paragraph 4.5**) or not, as in the dry and wet runs on a bench scale, the extent of the final carbonation is not affected.

In particular, in the early carbonation steps under dry conditions, the final conversion fractions achieved were higher in value than the respective ones under wet conditions. After the complete decomposition of $MgCO_3$ under dry conditions

and while the $MgCO_3$ did not compete with the carbonation reaction at the low temperature range for the 3rd, 4th and 5th carbonations, the values were higher than in the first two regardless of the extent of the $CaCO_3$ calcinations, hence the higher availability of CaO. This phenomenon was not noticed under the wet conditions runs even when the $MgCO_3$ was fully decomposed. On the contrary, under the wet conditions (10% vol CO_2/ 7.4 % vol H_2O/ N_2), the carbonation efficiencies were more stable from cycle to cycle despite being lower in value up to the 8th cycle compared to carbonation cycles 1 to 8 under dry conditions. By the dry 9th carbonation cycle the conversion fraction was poorer than under the wet conditions. Therefore, despite the lower performance of the wet carbonations over the dry ones, the presence of steam actually enhanced the stability of the sorbent over the 9 cycles in terms of CO_2 adsorption.

5.5.2 Comparison between the micro and macro scale stability studies of dolomite: effect of mass, CO_2 partial pressure and steam

In the micro and macro scale studies, the carbonations under dry conditions exhibited a natural decay despite the full decomposition of $MgCO_3$ by the 3rd cycle in the 2500 mg experiments. This is based on the temperature ranges of $MgCO_3$ thermal decomposition and of the CaO carbonation. In particular the final temperatures of CaO carbonation reaction are close to the initial temperatures of the $MgCO_3$ thermal decomposition.

Particularly, the dry macro-scale carbonations from the 3rd till the 5th cycle performed better than the respective ones in the TGA. The large scale carbonations showed a sudden decrease in yield from the 6th to the 9th, an effect that did not coincide with the small scale findings.

The thermal decompositions as discussed earlier did not reach 100% conversion either through the mechanism of $\mathbf{TD_a}$ or $\mathbf{TD_b}$ and **CRB**, as it was expected from the micro-scale study (**paragraphs 4.3** and **4.5**). Despite this, the carbonation steps' efficiency was not affected by that of the decomposition steps. The fact that the material was packed in a bed during the thermal decomposition steps might have created internally an additional CO_2 environment through the reaction mechanisms of $\mathbf{TD_a}$ and $\mathbf{TD_b}$ (**Bandi and Krapf, 1976**). This would have

slowed down the decomposition of $MgCO_3$ making it start at higher temperatures in environments of > 10% vol CO_2/ N_2 (**paragraph 4.3.1; Table 6(a)**).

Khan et al. (2001), in an attempt to link the thermal decomposition exothermic peak of $MgCO_3$ in 100% N_2 (dry) and 50% CO_2/ N_2 (dry), realized that the $MgCO_3$ thermal decomposition started later in temperature when CO_2 was present. As a result of the larger sample mass, due to the material's packing, the effectiveness of the heat transfer might have contributed in the incomplete $MgCO_3$ and $CaCO_3$ thermal decomposition.

From the preliminary sorbent study on 10 mg fresh dolomite it was noticed that the thermal decomposition of $MgCa(CO_3)_2$ in an inert environment was shifted to a lower temperature range than in a CO_2/ N_2 mixture (**paragraph 4.3**) whereas the carbonations under the high range CO_2/ N_2 mixture resulted in a higher initiation temperature. This could explain the incomplete thermal decomposition of $MgCO_3$ by the 1st cycle in the 2500 mg runs under dry and wet conditions. Furthermore, the lower the CO_2 in the mixture, the closer in value the final carbonation temperature with the initial calcination temperature became. This meant that the lower the CO_2 concentration, the more competitive the reaction $\mathbf{TD_b}$ (TD of $CaCO_3$) became over CaO carbonation. The effect of steam in the macro scale stability experiments was to minimize the temperature gap between the end of carbonation and the start of calcination, resulting in the overlapping of the areas of the thermal decomposition of $MgCO_3$ and $CaCO_3$.

Additionally, the presence of steam did not promote the thermal decomposition of $CaCO_3$. This was established in the case of the $MgCO_3$ thermal decomposition under wet conditions compared to the dry experiments. The presence of steam, as well as the presence of CO_2, shifted the $MgCO_3$ and $CaCO_3$ decomposition to higher temperatures overall, hence their insufficient conversion according to $\mathbf{TD_a}$ and $\mathbf{TD_b}$. This resulted by comparing the bench scale kinetic study of the thermal decomposition steps in the absence of CO_2 (**paragraph 5.4**) to the ones of the stability study in the presence of CO_2. Furthermore, it was **Garcia-Labiano et al. (2002)** who noticed that under atmospheric conditions, the higher CO_2 concentrations present, the lower calcination's rate became.

According to **Wang et al. (1995)'s** findings, it was indicated that the calcinations in the presence of steam were enhanced, therefore the thermal decomposition of $MgCO_3$ became more competitive than that of $CaCO_3$. Hence $MgCO_3$ converted into MgO at earlier temperatures under wet conditions.

Therefore, the stability experiments at macro scale did not perform in accordance to the micro scale results, as the effect of larger mass created an internal CO_2 environment due to the packing, which in addition resulted to non-uniform temperature gradients among the mass of the sorbent.

5.6 SEM-EDX analysis of the sorbent from the micro- and macro-scale studies

In principle, the calcination of $CaCO_3$ in a CO_2 environment produces CaO whose pore sizes and volume allows complete recarbonation of CaO. This is prevented when the outer surface of the recarbonated material's pore volume becomes reduced therefore reducing the rate at which the CO_2 penetrates the surface of CaO to continue performing the **CRB** reaction (**Silaban et al., 1996**). The reason for the limited recarbonation of the CaO from the Warmsworth quarry dolomite was demonstrated by expressing its kinetic behavior under the **CRB** reaction by the Jander diffusion model as well (**paragraphs 4.4** and **5.4**). Later studies such as of **Stendardo et al. (2009)** investigated the mechanism of CaO reaction with CO_2 as described in **paragraph 4.4.2** based on the Jander diffusion model, which was established as early as in **1927 (Jander)**.

The SEM-EDX study of the previously presented micro- and macro- scale results (**chapter 4** and **paragraphs 5.2, 5.3, 5.4**) can give a qualitative outlook in the discussion made earlier based on the material morphology coupled with the local elemental composition.

The magnified surface of the thermally decomposed dolomite (TD1) in a 100% vol N_2 at a heating rate of 10 K min^{-1} under dry and wet conditions (**Figs 20(a-b)** is depicted for the macro scale experiment. The presence of fines in both samples indicates the evolution of CO_2 during both thermal decompositions under

dry and wet conditions which then resulted in the breaking down of the dolomite particles.

Additionally, in previous studies (**Manovic et al., 2009; Silaban et al., 1995**) it was noticed that the thermal decomposition step in an inert environment (100% vol N_2) would result in a more developed morphology, whereas in the presence of CO_2 (100 % vol CO_2) larger grains would be developed as larger pore diameters would be formed.

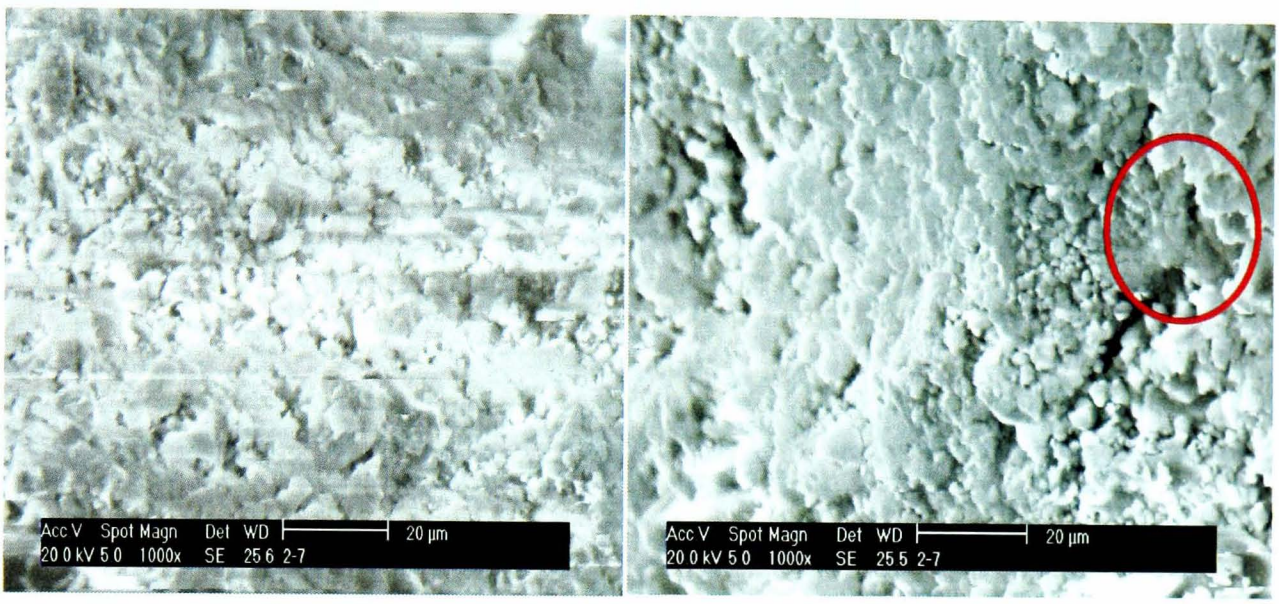

(a)after 1st TD in 100% vol N_2 (dry) (b) after 1st TD in 100% vol N_2 (wet)

Figure 20 Sorbent's particle SEM images of the sorbent from the macro-scale experiment

As mentioned earlier in **paragraph 5.3.3**, in the case of the first thermal decomposition (TD_1) at macro scale, a CO_2 environment during the thermal decomposition (**TD**) would be formed within the gaps formed between the packing of sorbent's particles. This would have resulted in a surface area of calcined dolomite closer to the one that would be thermally processed in a CO_2 mixture. The fact that no visible or clear pores (**Figure 20(a); Figure 20(b)**) could be seen after the 1st thermal decomposition of the Warmsworth quarry dolomite is an effect that is met among untreated dolomites (**Li et al., 2008**). In **Figure 19(b)**, the red cycle indicates fine bridges of sintering resulting soon after the 1st calcinations under wet conditions. This supports further that the presence of steam resulted in the poorer performance of the sorbent in the wet thermal stability study. Therefore the presence of steam had a significant effect on decreasing performance of the dolomite's thermal decomposition.

From the EDX analysis (**Figure 21(a)** and **(b)**), both samples of calcined dolomite after the TD1 bench scale step under dry and wet conditions did not show any significant changes. Only in the case of the sample when steam was present there were some impurities detected (Si, Al, Fe), which were known to be present in the fresh dolomite in the form of SiO_2, Fe_2O_3 and Al_2O_3 (**paragraph 4.1**). The influence of impurities on sintering of $CaCO_3$ in nitrogen atmosphere is in agreement with the loss of surface area and gain in activation energy (**Borgwardt, 1989**). The latter was demonstrated in **Table 15** (**paragraph 5.4.1.2**) of the kinetic data produced in the 1st TD under wet conditions compared to the ones under dry conditions (**Table 14, paragraph 5.4.2.2**).

(a) after 1st TD in 100% vol N_2 (dry)

Element	Weight%	Atomic%
C	10.84	16.59
O	56.28	64.69
Mg	12.21	9.24
Ca	20.67	9.48
Totals	100.00	

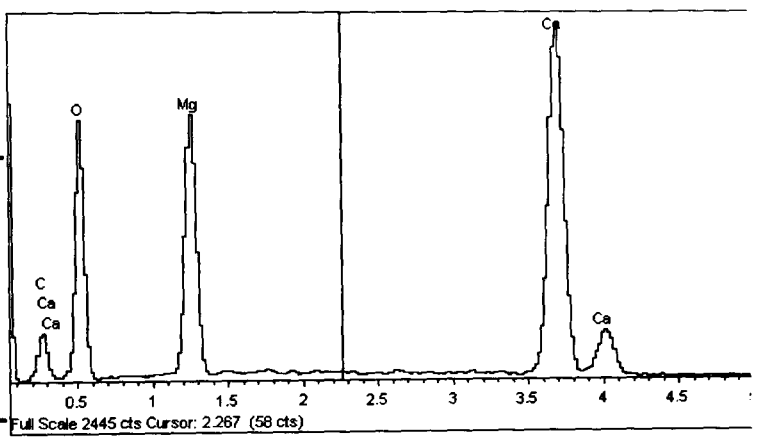

(b) after 1st TD in 100% vol N_2 (wet)

Element	Weight%	Atomic%
C	9.50	14.79
O	55.57	64.95
Mg	12.79	9.84
Al	0.12	0.08
Si	0.44	0.30
Ca	21.39	9.98
Fe	0.19	0.06
Totals	100.00	

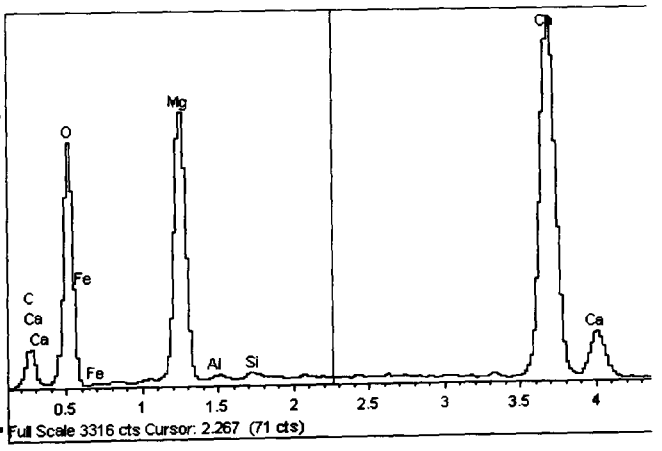

Figure 21 EDX analysis of sorbent's particles (macro scale experiments)

The effect of the material's sintering could affect both the calcination and the carbonation magnitude. According to the literature, the increase in the pores'

volume by the decomposition of $MgCO_3$ (**Silaban et al., 1995**) would result in superior performance of the dolomite during carbonation over calcite. Additionally, the carbonation reaction appeared to be rapid at the beginning while by the end it had slowed down, as seen earlier in the micro- and macro- scale kinetic study of the dolomite (**paragraph 4.4; paragraph 5.4**). The more rapid this transition in areas of higher to lower reactivity become, the higher is the change in the structural properties of the solid reactant which is supported by the literature (**Chrissafis et al., 2005**) and based on the work of **Bhatia et al., (1983)** who studied the effect of the carbonation product layer on the diffusivity of CO_2 on CaO. In **Figure 22(a1)** and **Figure 22(a2)** the surface of the sorbent after the 9^{th} carbonation at two magnifications (100 μm and 20μm) is shown where the sintering is obvious even in the smaller magnification (**Figure 22(a1)).** Additionally, in **Figure 22(a2)** the MgO.CaO- $CaCO_3$ particles seem solid and compact, which limits any further carbonation as CO_2 cannot diffuse through the surface. From the EDS analysis of the area it was not possible to quantify the change in the structure of the sorbent as the SEM and EDS depend on the particle and the selected area. This could be achieved by computer controlled SEM with automated image analysis (**Manovic et al., 2009**).

(a1) SEM analysis under 250× magnification

(a2) SEM analysis under 1000× magnification

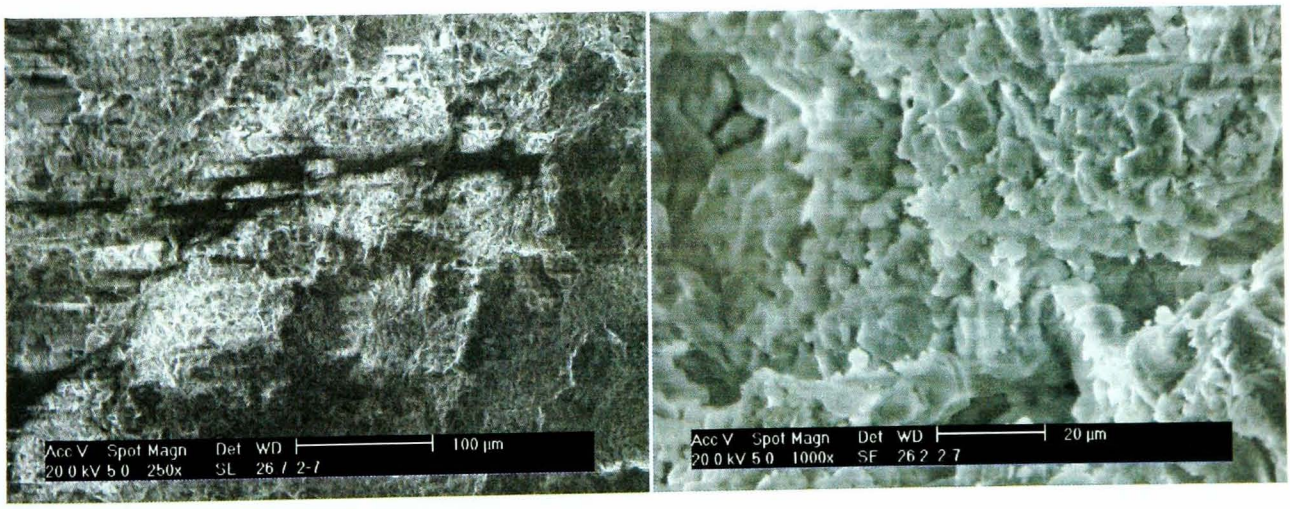

Figure 22 Sorbent's particle after 9^{th} cycle of carbonation in 10% vol CO_2/ N_2 from macro scale experiment under wet conditions

Element	Weight%	Atomic%
C	9.89	15.33
O	55.60	64.73
Mg	12.92	9.90
Ca	21.59	10.03
Totals	100.00	

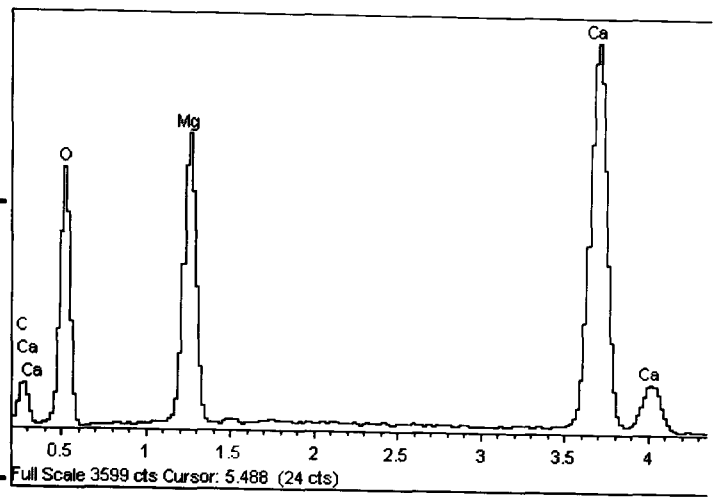

(b1) EDX analysis (b2) EDX spectrum

Figure 22 (b1)- (b2) Sorbent's particle after 9th cycle of carbonation in 10% vol CO_2/ N_2 (USR rig) under wet conditions

Furthermore, BET analysis can assist in the determination of the available surface area (m^2/g) that could react with CO_2. Mercury (Hg) porosimetry can quantify the mesoporous and macroporous volume (mL/ g) whereas the nitrogen gas adsorption isotherms can determine the micropores and mesopores volume. The application of porosimetry techniques can produce quantitative results that will further assist in the sorbent's study which, as presented in **chapters 4** and **5**, gave sufficient information on a preliminary level for its behaviour in the SEUSR (Sorption Enhanced Unmixed Steam Reforming) process (**Chapter 8**).

5.7 Summary on the macro- scale study of the sorbent

The effects of testing a larger mass of dolomite were examined in the macro-scale study of the sorbent and compared to those obtained from the micro- scale study (**chapter 4**). At the same time the larger sorbent's mass behaviour was assessed under dry and wet conditions and in non-isothermal conditions as previously in the micro- scale study in **chapter 4**. In the beginning of this chapter, the effect of different flow rates and sorbent masses on the sorbent's performance as well as their interaction was shown at macro- scale. It was proved that the lower flow rates of gases and the larger the masses were, the better the first calcination and carbonation steps became (**Table 11**). The macro scale study of the sorbent

was of great significance as it would reveal the sorbent's behaviour and compliance under the operating conditions when applied in the SEUSR (Sorption Enhanced Unmixed Steam Reforming) process.

5.7.1 Mass effect on macro- scale calcination steps under dry and wet conditions

- The main conclusion from the application of the sorbent's mass in the macro-scale experiments was that the sorbent mass was not fully decomposed in an inert environment (100% vol) under either dry and or conditions due to the packing effect, which created a CO_2 gaseous environment, which in turn worsened the gases' mass transfer on the sorbent's particles (**Table 12**; **Table 13**).

- The incomplete calcinations were an effect of the formed CO_2 environment within the packed bed of the sorbent.

- The final conversions of the calcination steps were not affected by the presence of steam in an inert environment (100% vol N_2) (**Table 12**; **Table 13**). This means that the extent of the sorbent's calcination was neither promoted nor restrained.

5.7.2 Mass effect on macro-scale carbonation steps under dry and wet conditions

The macro- scale carbonation steps performed in the kinetics study under dry or wet conditions were conducted in 5%, 10% and 15% vol CO_2/ N_2 mixtures.

- The 1st carbonation step in the low (5 and 10) % vol CO_2/ N_2 mixtures under dry micro and macro scale resulted in higher conversions than the high (15%) vol CO_2/ N_2. This came as a result of the formed $CaCO_3$ on the packed sorbent's particles outer surface which did not allow any further reactions between CO_2 and the remaining CaO. The latter effect came as a result of the particles' packing, which prevented the successful commencement of the carbonation step.

- The catalytic effect of steam was evident in both the 1st and 2nd carbonations in the wet macro scale set-up. The carbonations' rates were increased and the final conversions achieved by the end of the 1st carbonation step were doubled when using the low (5 and 10% vol) CO_2/ N_2 mixtures (**Table 12**; **Table 13**).

- The carbonation steps with low CO_2/ N_2 mixtures showed smaller deterioration from cycle 1 to cycle 2 compared to the respective micro-scale study. The lower the CO_2 content in the gaseous environment under which carbonation took place, the higher under both dry and wet macro- scale conditions was the extent of conversion.

- The carbonation temperatures were lower than in the ones found in the literature since in this study, the experiments were carried out in the dynamic conditions of non- isothermal experiments. The difference of the initial carbonation temperature between the dry and wet conditions was illustrated (**paragraph 5.3.2**).

5.7.3 Kinetic and thermal stability macro- scale study of the sorbent under dry and wet conditions

- The calcination steps were best interpreted by the reaction order model whereas the carbonation steps were best simulated by the Jander (3D) diffusion model. The order of the reaction order mechanisms was not affected for the 2nd calcination when steam was used (**Table 14**; **Table 15**).

- The lower the calculated activation energies based on the Coats-Redfern iterative method were, the lower the final conversions in the dry calcination runs were achieved (**Table 12**; **Table 14**).

- The commencement of the 1st dry carbonation step was more energy intensive as shown by the calculated activation energies, in the macro-scale than in the micro- scale study except in the 10% vol CO_2/ N_2 mixture (**Table 10**; **Table 12**).

- Lower activation energies were calculated for the dry 2nd carbonation steps when a 5 and 10% vol CO_2/ N_2 mixture was used than in the micro scale except in the 15% vol CO_2/ N_2 mixture.

- Despite the higher activation energies that were observed during the 1st carbonation step under wet conditions (**Table 15**), still the final conversions were higher (**Table 13**) than when under dry conditions were employed (**Table 12**- except for C1 (dry) in 5% vol CO_2/ N_2), as an effect of steam. Higher activation energies were calculated during the 2nd wet carbonations (**Table 15**) compared to the ones in the macro scale study under dry conditions (**Table 14**).

- The calcinations' final conversions did not benefit from the presence of steam (**Table 12; Table 13**). Lower activation energies were calculated for the 1st calcination under wet conditions (**Table 15**) than under dry conditions (**Table 14**) in the macro scale. Exception to this observation was the 2nd wet calcination in the 10% vol and 15% vol CO_2/ N_2 mixture where the calculated activation energies were slightly higher than under dry conditions.

- In the stability study, the sorbent's $MgCO_3$ part was fully converted in an earlier cycle (3rd) when wet conditions were used.

- In the cyclic macro- scale study of the sorbent, the presence of steam (wet conditions) resulted in a larger deterioration of the carbonation steps (**Fig 18(b)**) while by the 9th calcination step steam (**Fig. 18(a)**) didn't appear to promote the sorbent's performance.

- The SEM (Scanning Electron Microscopy) analysis of the sorbent's particles after the 1st calcination step on the dry and wet macro- scale study illustrated (**Fig. 20(a)** and **(b)**) the evolution of CO_2 that was earlier mentioned. This was confirmed by the large grains formed at the end of the thermal decomposition step.

- The poorer performance of the cyclic study of the sorbent in wet conditions was affirmed by the SEM analysis which showed that sintering was evident.

- By the 9th cycle of carbonation under dry and wet conditions of the sorbent's macro- scale study, the SEM study showed significant sintering on the particles' surface.
- The EDX (Energy Dispersive X-Ray) spectroscopy analysis results were qualitative rather than quantitative. Quantitative results can be generated by computer controlled SEM with automated image analysis.

Chapter 6
Liquids of waste biomass origin for the USR process

The current trend in hydrogen production is the investigation of liquids of biomass origin (vegetable oils and animal fats) as potential feedstock for biodiesel production. The main drawbacks of the direct use of these oils in diesel engines are their low volatility, low calorific value, high acidity and high viscosity. Biodiesel is currently produced from rapeseed, palm, soya bean and cotton seed oil. On the other hand, biodiesel production based on traditional methods (base catalysis) is not effective when fatty acids are contained in the primary material due to soap formation and thus pre-treatment is needed with a homogeneous acid catalyst i.e. sulphuric acid. Unfortunately, the aforementioned oils (rapeseed, soya bean and cotton seed oil) require large areas of farming land as they produce 0.40- 0.68 tonnes/hectare/year (**Janaun et al., 2010**) compared to palm oil which produces 3.62 ton/ha/year; (**Janaun et al., 2010**), adding to their high production cost (**Shu et al., 2010**). Based on the last remark, **Shu et al. (2010)** tried to produce biodiesel from waste vegetable oil although the carbon based acid catalyst was deactivated after 5 cycles.

Pyrolysis oils (or bio-oils) are under investigation as alternatives to fossil fuels. The source of pyrolysis bio-oils is found in biomass or biomass waste that is processed by either gasification or fast pyrolysis. During the latter process, the biomass is rapidly heated to high temperatures in the absence of oxygen; the product mainly consists of vapours, aerosols and some charcoal. High liquid yields are generated at high heating rates and short vapour residence times. The final product (bio-oil) is available after cooling and condensation. (**Bridgewater et al., 1999**).

During the unmixed steam reforming process the bio-oils can be potentially pyrolysed through evaporation when injected onto the hot catalyst bed as well as when vaporised by reacting with the steam. The complexity of the bio-oils composition (i.e. esters, ethers, ketones, aldehydes, phenols) in conjunction with their high content in oxygen unlike petroleum derived fuels, render them

challenging for unmixed steam reforming. Therefore, the preliminary study of these bio-oils through the determination of their composition (Gas Chromatography-Mass Spectroscopy 'GC-MS') and their thermal decomposition behaviour during pyrolysis in a dry inert environment (N_2) via thermogravimetric analysis, coupled with the qualitative assessment of the composition of the TGA products using FTIR (Fourier Transform Infrared) Spectroscopy can inform on the best conditions in which to conduct their steam reforming. The information gathered from such a preliminary study would provide better understanding of the chemicals that can potentially interact with the catalyst and help determine the best conditions for high yield of hydrogen from both the fuel and steam. Additionally this would assist in the design of a steam reforming process that avoids tar and coke formation. The latter is of particular significance as in the work of **Dupont et al. (2007)** the thermal decomposition of fresh sunflower oil resulted in coke formation during the H_2 production.

6.1 Preliminary study of liquids of biomass origin

The liquids of biomass origin considered for the unmixed steam reforming (USR) process were:

- Waste vegetable cooking oil (Houldsworth Building refectory, School of Process, Environmental and Materials Engineering (SPEME), Leeds University)
- Fast pyrolysis oils: of pine wood (BTG Biomass Technology Group BV, The Netherlands) and palm empty fruit bunch (EFB) (BTG via Genting Bio-oil Sdn. Bhd., Malaysia)

Fast pyrolysis is a more advantageous method of bio-oil production in terms of high liquid yields to the detriment of the gaseous and solids yields, and of generating a product that is readily stored and transported. The fast pyrolysis bio-oils are highly viscous fluids with a strong smoky odour; their elemental composition is closer to that of their biomass source than that of petroleum. They are corrosive when in contact with the skin, while their handling and storage needs to be considered as similar to hazardous material, and thus take place in a well

ventilated area. The fast pyrolysis oils are hydrolysed complex mixtures of hydrocarbons (**paragraphs 6.4** and **6.5**).

6.1.1 Analytical techniques for the elemental, chemical and thermogravimetric analysis of bio-oils from waste

Elemental (CHNS) analysis was carried out for the three oils derived from waste of biomass origin (cooking oil, pine oil and EFB oil). Such a test enables the mass and elemental balances of the thermochemical processes to which they are subjected, such as the USR process. The equipment that was used for the elemental analysis of the waste biomass origin oils was the FlashEA 1112 Series (CE Instrument; ThermoFisher Scientific) (**FlashEA1112 manual**). The organic elemental analysis was based on combustion analysis by burning the sample in the excess of oxygen while the gas products were collected and analysed by atomic spectroscopy. The samples were weighed in tin capsules and placed in the autosampler (MAS200 R). Their net weight varied from 2 to 5 mg depending on their density.

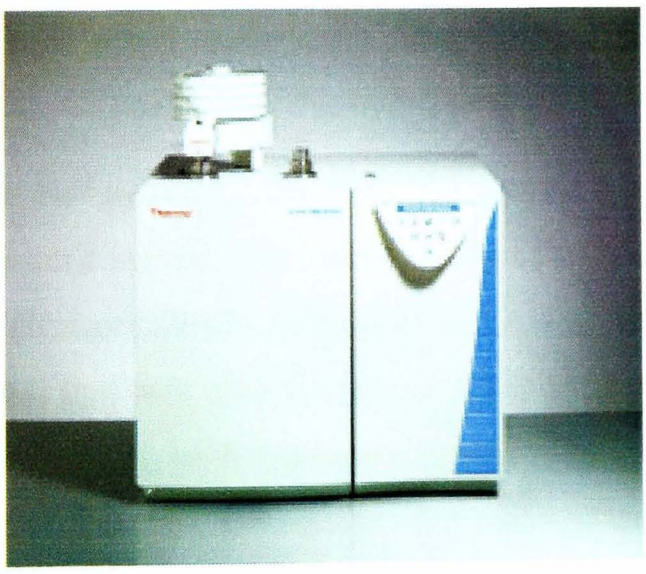

Figure 23 FlashEA 1112 Series (CE Instrument) (for organic elemental analysis)

Before placing the samples in the autosampler, they were immersed in ethanol and then dried in order to avoid any leakages from the tin capsules due to the volatile nature of the two fast pyrolysis bio-oils. Then, the samples were placed

in the furnace and kept at 1173 K (900°C) in an excess of oxygen while the oven's temperature was maintained at 333 K (60°C). The exothermic reactions elevated for some seconds the temperature within the reactor to 2073 K (1800°C). This high temperature allowed both organic and inorganic compounds to decompose into constituent gases (CO_2, N_2, H_2O, SO_2), which, when reduced were separated in a chromatographic column and then led by pure helium (He) to a highly sensitive thermal conductivity detector (TCD). These allowed quantification of the mass fractions in C, H, N and S in the samples, while the oxygen mass fraction was calculated by difference to 1. Knowledge of the C, H, N, S, O mass fractions in the fuels permits the conversion to a molar composition, and thus the knowledge of the potential global reactions that the fuels may undergo, as well as theoretical outputs such as maximum hydrogen yield, reactants' conversions, maximum products' selectivity, etc. Knowledge of the CHNSO content also allows carrying out mass and elemental balances on the experiments, which can then be compared to their theoretical counterparts, and yield the process efficiency. The CHNS analysis is therefore the most crucial analysis that needs to be carried out on the fuels prior to experiments of their thermochemical conversion such as the USR process.

Information on the calorific values (**paragraph 6.3**) was produced for all liquids of biomass origin as it will assist in the future thermodynamic equilibrium process calculations which will determine the viability of the USR for these fuels.

The biomass origin fast pyrolysis oils were also analysed by GC-MS in order to determine their main constituents. This method combines gas chromatography and mass spectroscopy (**Robert, 2007; Adlard et al., 2001**). The Shimadzu 2010 GC-MS testing equipment that was used for this analysis is comprised bof a Trace GC 2000 TOP (Thermo electron) with a splitless injector and a mass spectrometer Fisons MD800. In the gas chromatograph the properties of the column (25 m × 0.25 mm RESTEK RT) for the samples tested is one of the parameters of its utility. In particular, the sample is vaporised in order to be broken down to its main constituents which produce the distinctive peak every component gives in a spectrum range. The retention time, which is the time between injecting the sample in the GC column (Rfx 1701 60m) and the elution of its constituents, can enable the distinction of the different compounds.

Following a calibration step, the surface area of recorded peaks can be measured and indicate the compounds that are in greater proportion to the others. This means that when the sample starts to vaporise, every component reaches its peak based on its speed of vaporisation that depends on its physical and chemical properties as well as on its shape. The oven in which the samples were vaporised operated from 333 to 583 K (60-310°C) at a heating rate of 5 K min^{-1}. Another parameter that affects the retention time of each substance is the interaction between the different molecules as well as between molecules of the same compound with the column's walls. An inert carrier gas (He or N_2) promotes the transport of the produced gases to the detector. In this study helium (He) of 1 mL min^{-1} was used. Finally, the resulting spectrum of the eluting molecules is recorded.

Calibration of the equipment is essential for its best performance; it is normally carried out when a range of concentration of substances that are potentially contained in the sample is known. In this study, for the two biomass origin fast pyrolysis oils, several compounds were used for the calibration of the GC based on the suppliers' product information. In mass spectrometry, the chemical compounds are identified by electrically charging the molecules which are deflected by a magnetic field and then in order for them to be detected, they are broken down to electrically charged particles.

In addition, all oils were thermogravimetrically analysed (Stanton Redcroft TGA- TGH 1000) in order to determine their decomposition temperature limits in a dry N_2 environment. This was important information for their treatment in the USR process as the oils need to be vaporised prior to meeting with the steam reforming catalyst. Sample masses of approximately 20 mg were used in the TGA's crucible. Based on this experimental data, the prediction of the decomposition curve over increased temperatures at a constant heating rate was realised. In particular, the heating rates that were selected for the prediction of the thermal decomposition curve were: 3, 6 and 9 K min^{-1} for the fast pyrolysis oils and 3 K min^{-1} for the waste cooking oil, using a Shimadzu TGA- 50 (as described in **chapter 4)**. The use of these variable but low heating rates was to determine the dependence of derived kinetic parameters of the oils' thermal decomposition with the heat transfer rates.

The fast pyrolysis oil TGA tests were coupled with the FTIR technique in order to confirm the loss of gases such as CO_2 and acetic acid (CH_3COOH), which are the main constituents of fuels' complete or incomplete oxidation, made possible under the N_2 inert atmosphere due to the high oxygen content of the biomass pyrolysis oils. The vapours that were produced by the pyrolysis were carried through a stainless steel line into the gas cell for the IR absorption detection. In order to prevent condensation of the vapours, the transfer line and the gas cell were maintained at a temperature of 443 K (170°C) while the cells temperature was at 573 K (300°C), without excluding the probability of partial condensation of vapours with a high boiling point. The IR spectra were produced by using of Magna system 560 spectrometer with a resolution of 4 cm^{-1} with 32 scans per spectrum in the wave number range of 4000–400 cm^{-1} by using a DTGS (detector) KBr (beam- splitter) detector. The total data collection time depended on each heating rate, with the maximum being 4.5 hours and the minimum being 1.5 hours.

Table 16 Equations tested for the integral conversion function g(α) used to model the conversion curves (mass loss) vs. temperature from the TGA of the waste biomass pyrolysis oils

Reaction mechanism	**Mechanism's equation g(α)**
Avrami Eroveef	$[-\ln(1-\alpha)]^{1/n}$ for n=3/2
Contracting Surface	$2[1-(1-\alpha)^{\frac{1}{2}}]$
Contracting Volume	$3[1-(1-\alpha)^{\frac{1}{3}}]$
1D diffusion	α^2
3D (Jander) diffusion	$[1-(1-\alpha)^{\frac{1}{3}}]^2$
Power Law	$\alpha^{\frac{1}{m}}$, for m=1,2,3 and 4
n^{th} reaction order *special cases:* n=1/2: contracting surface n=2/3: contracting volume (shrinking core) n=0 power law (m=1)	$\frac{[1-(1-\alpha)^{1-n}]}{1-n}$ for n=1, $g(\alpha) = -\ln(1-\alpha)$

The thermal decomposition data of these three liquid hydrocarbon mixtures was used for predicting their conversion curves over increasing temperatures based on the improved iterative Coats-Redfern method (**paragraph 4.1.2**) for non-isothermal data for the kinetic parameters calculation. The mechanisms that were

tested for the TGA study of the three waste biomass origin oils are presented in **Table 16**.

6.2 Elemental analysis of waste vegetable cooking and fast pyrolysis oils

The elemental analysis of the fuels was based on the determination of the C, H, N, S weight percentage so that their empirical formula could be determined, while the oxygen content was calculated based on the sum of the weight percentage of carbon, hydrogen, nitrogen and sulphur. Then the molar fraction of the constituent elements of the bio-fuels could be calculated. These results are presented in **Table 17**,

Table 17 Elemental analysis (CHNS) of the bio-fuels considered for USR process

Average molar fraction	C	H	N	O	H:C	C:O
EFB oil	0.285	0.488	0.0046	0.222	1.710	1.285
Pine oil	0.257	0.494	0.0008	0.248	1.927	1.034
Waste vegetable Cooking Oil	0.316	0.645	0.0004	0.038	2.038	8.232

There was no sulphur measured at the detection levels of the CHNS apparatus in the palm empty fruit bunch (EFB), and the pine wood fast pyrolysis oils as well as in the waste vegetable cooking oil, indicating that sulphur poisoning of the catalyst during the USR process would be minimised.

Two other important parameters that were deduced by the elemental analysis of the oils as seen in **Table 17**, is the molar ratio of hydrogen to carbon (H:C) and the molar ratio of carbon to oxygen (C:O). These ratios are indicative of the oils' performance in the USR process. In both the pine and EFB fast pyrolysis oils the carbon content is high (1.927 and 1.710 respectively) indicating a high potentially carbon deposition on the nickel based catalyst. This may be attributed to the

process of fast pyrolysis that normally results in a product of high content in char. The H:C ratio is related to the theoretical amount of hydrogen that would be produced in the USR process and the performance of the oil is determined by the theoretical relative production of hydrogen to the carbon products by the decomposition of hydrocarbons. In the case of the EFB and pine fast pyrolysis oil the resulting H:C ratios showed that high efficiencies must be achieved in the USR process in order to achieve such a ratio in the end gaseous stream. The high content of water in the fast pyrolysis oil as an effect of their production process, which was confirmed by the significant mass loss of the oils' samples up to 373 K (100°C) in their TGA study (**paragraphs 6.4** and **6.5**) and would benefit the unmixed steam reforming process by reducing the amount of water to be supplied as steam.

Additionally, this information was useful in terms of the needs of the system in oxygen supply or the carbon to be burned (**R9**) during the oxidation step which in the case of the unmixed steam reforming process is the regeneration phase of the catalyst.

$$C + O_2 \leftrightarrow CO_2 \qquad \textbf{(R9)}$$

The H:C ratio is slightly higher in the waste vegetable cooking oil than in the two biomass origin pyrolysis oils, indicating a higher content of hydrogen over the carbonaceous content of all three fuels. The higher H:C ratio also implies that less steam ($H_2O_{(g)}$) would be necessary for the conversion of any carbon deposited on the catalyst to carbon dioxide (CO_2):

$$C + 2H_2O \leftrightarrow CO_2 + 2H_2 \qquad \textbf{(R19)}$$

The C:O ratio of the fast pyrolysis oils (Pinewood and EFB) was found to be much lower than the one of the waste cooking oil. Based on the previous discussion on the effect of C:O ratio, the two fast pyrolysis oils ratios (being in the range of 1.0-1.3, **Table 17**) signify potentially less carbon deposition on the Ni based catalyst in the USR process. The higher oxygen content in the two fast pyrolysis oils showed that the catalyst's capability to reduce during the FF (fuel feed) step (hydrogen production) will be reduced compared to the waste vegetable oil's use in the USR process.

In the literature, there are many studies on the thermogravimetric analysis of the pyrolysis of wood or palm wood for biomass fuels production (**Reina et al., 1998**; **Luangkiattikhun et al., 2008; Idris et al., 2010**), but there are very few studies on the decomposition analysis of pyrolysis oils (**Qiang et al., 2010; Dou et al., 2009[(b)]; Garcia–Perez et al., 2007**).

6.3 Waste biomass origin oils' calorific values

For the definition of the three biomass origin oils calorific values, a 6200 Oxygen Bomb calorimeter (Parr Instrument Co) (**Figure 24**) was used.

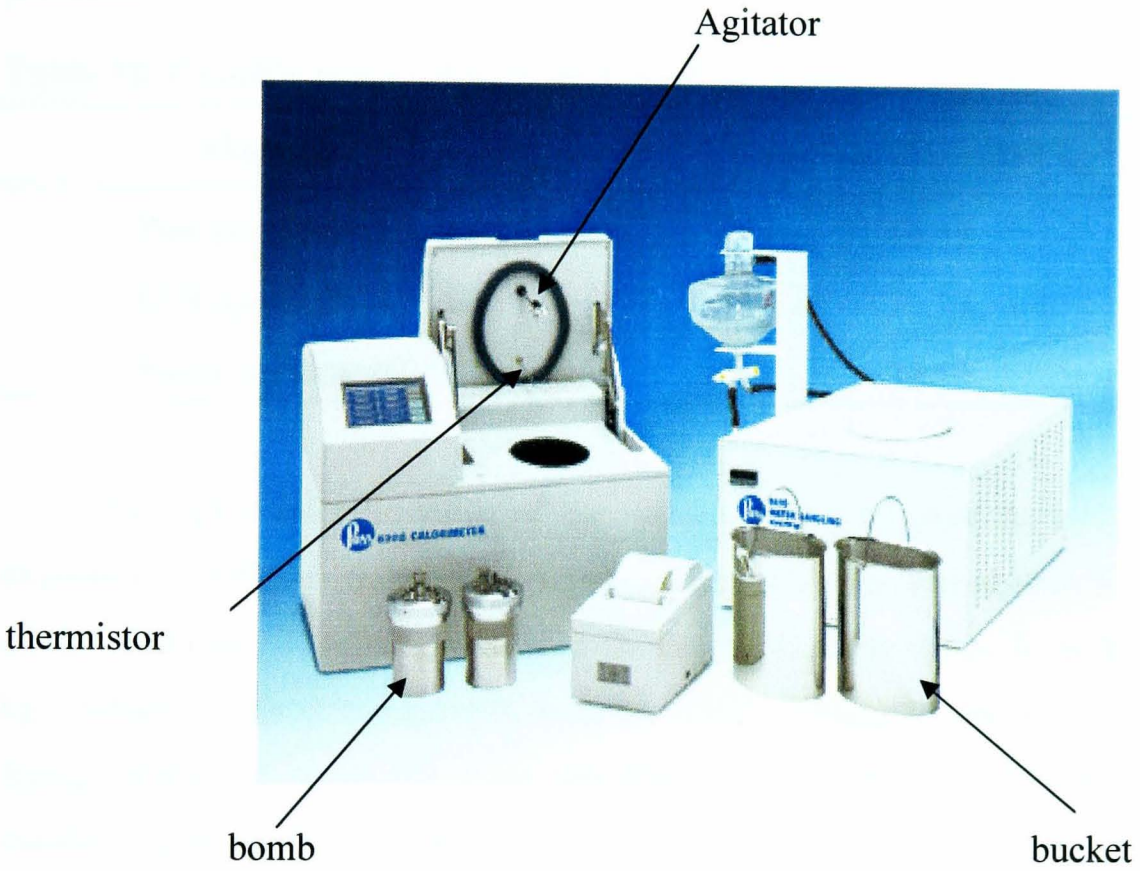

Figure 24 6200 Isoperibol Calorimeter (Parr Instrument Co.)

Initially, the thermistor and the jacket (bucket) were allowed to converge in temperature. The jacket (bucket) was filled with 2 L of deionised water. Water (cooling medium) was used in the jacket to take off the heat from the bomb, when combustion took place. During the run, an agitator in the water ensured uniform temperature distribution across the water, in order to be kept constant and take off any heat from the bomb efficiently.

A stainless steel crucible was placed in the bomb. A sample of 0.2- 0.5 g of bio-oils was placed in a syringe (which was weighed for every tested sample). The crucible was wrapped with cellulose tape so that when these volatile materials were tested, their evaporation would be minimised. This would ensure the prevention of any significant mass loss. Then, the cellulose film was pierced and the sample was injected in the crucible. The gross calorific value of the cellulose film had already been incorporated in the bomb calorimeter programme in order to calculate the bio-oils' gross calorific value. Once the bomb was enclosed in the calorimeter, the bomb was pressurised at 30 bar of oxygen.

The bio-oils were tested twice and in **Table 18** the average values are presented.

Table 18 Calorific values of pinewood, EFB and waste cooking oil

Material	Calorific value (MJ kg^{-1})
Pine pyrolysis oil	15.55
EFB pyrolysis oil	19.79
Waste cooking oil	39.50

The higher calorific value of the waste cooking oil over the two biofuels is expected since the elemental analysis of the three bio-oils (**paragraph 6.2**) is based on the H:O ratio. The fresh vegetable oil's calorific value varies from 39 to 48 MJ kg^{-1}, which by direct comparison with the waste cooking oil shows the effect that frying foods had on it. All three bio-oils are poorer in calorific value than the current liquid fuels (natural gas: 43 MJ kg^{-1}; diesel: 44.8 MJ kg^{-1}), whereas ethanol's respective value (29.7 MJ kg^{-1}) is poorer than the one of the waste cooking oil. In every case, the determining factor of the calorific value can be linked to the H:O and H:C ratios.

6.4 Pine wood pyrolysis oil GC-MS analysis, TGA-FTIR study, and kinetic modelling of its thermal decomposition

The qualitative analysis of the two fast pyrolysis oils of biomass origin was performed by using the GC-MS (Gas Chromatography-Mass Spectroscopy)

method. Several oxygenated compounds such as phenols, acids, aldehydes and ketones and a small percentage of polyaromatic hydrocarbons were detected in both pyrolysis bio-oils. The GC-MS spectrum (**Figure I; Appendix III**) based on the produced chromatogram formed by the peaks for the pine wood origin pyrolysis oil showed that the four major compounds were acetic acid (21.46%) 1-hydroxy-2-Propanone (15.37%), 5-methoxy-Phenol (5.04%) and tetrahydro-2,5-dimethoxy-Furans (4.48%). The estimated concentrations of the compounds of the tested samples can be seen in **Table I (Appendix III)**. It is worth noting that the method was semi-quantitative as many of the identified compounds had not been pre-calibrated with standards. Phenol compounds are toxic while acetic acid is ignitable at temperatures as low as 313 K (40°C). The presence of any significant amount of oxygenated compounds can be attributed to the presence of hemicellulose in the biomass sample (**Özbay et al., 2008**).

As it can be seen in **Figure 25**, the thermal decomposition of the pinewood fast pyrolysis origin oil at different heating rates showed that it was incomplete, as residual mass was left in the end product representing carbon residue and mineral matter (ash).

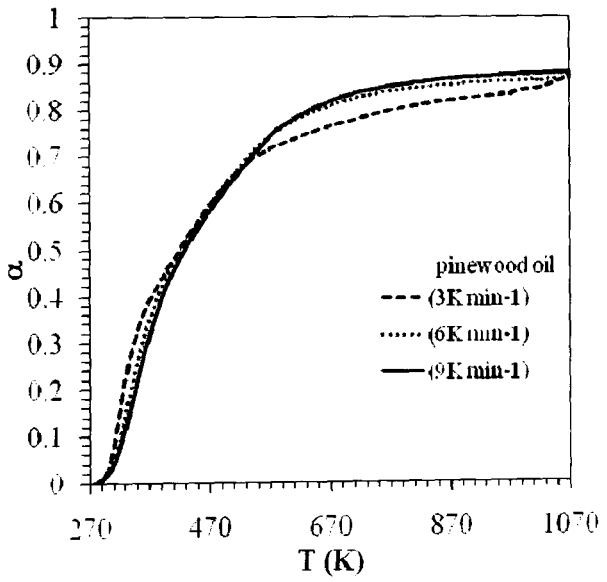

Figure 25 Mass loss conversion (α) of pinewood pyrolysis oil in a flow of 50 mL min^{-1} N_2 at different heating rates, up to 1073 K (800°C) (TGA)

This residual amount shows the theoretical solid residue of a likely pyrolysis process (**Galvagno et al., 2009**). The remaining solid matter for all the TGA runs, accounted for 11.79- 13.41% of the initial mass used. **Uzun et al. (2007)** noticed

the solid residue was higher by more than 7 times in the inert environment than in the oxidising environment for olive waste pyrolysis oil.

In **Table 19**, the reported mass losses (%) are based on the initial mass of each sample. The heating rate effect is evident from the temperatures at which the two different decomposition phases occurred. From **Figure 25** it can be seen that the produced curves' shapes were similar; the different heating rates seemed to affect slightly the temperature range at which mass losses occurred. The higher the heating rate, the higher the mass loss was at low temperature. From the same figure it became evident that the three mass loss curves that were produced at three different heating rates demonstrated two distinctive phases of decomposition, henceforth termed phase PH1 for the low temperature range, and phase PH2 for the high temperature range of thermal decompositions, as seen in **Table 19**.

Table 19 Thermal decomposition phases of pinewood pyrolysis oil in TGA, using 50 mL min^{-1} N_2, at different heating rates, up to 1073 K (800°C)

		Mass loss (%)		**T_i (K)**		**T_f (K)**	
	TD	1	2	1	2	1	2
Heating rates	3	44	36	279	396	396	779
	6	48	35	279	411	411	719
	9	42	45	281	398	398	896

No specific trend can be noticed with regard to mass loss and temperature ranges with heating rate. The medium heating rate used here (6 K min^{-1}) seemed to achieve to extend the temperature range of PH1 and shorten PH2. The compounds decomposed in the low temperature phase were water, acetic acid (boiling point= 118°C= 391 K) and n-propyl acetate (boiling point= 102°C= 375 K). The mass loss in the second pyrolysis phase (T_i= 349- 393 K; T_f= 534- 283 K) was attributed to substances such as phenols that are pyrolysed within this aforementioned temperature range. The final pyrolysis phase was concluded at different temperatures (**Table 19)** depending on the heating rate. The change in the curve's slope can be attributed to the kinetics that the different heating rates might cause.

The thermogravimetric analysis apparatus used in the thermal decomposition analysis of all bio oils was coupled with FTIR (Fourier Transform Infrared Spectroscopy). This was chosen due to the complexity of the bio-oil's composition and to assist the interpretation of the TGA runs. The results of this study will be

beneficial to the fast pyrolysis bio-oils application in the USR process. In the produced graphs (**Figure 26**) from the TGA-FTIR, the acetic acid (CH_3COOH) and the carbon dioxide (CO_2) relative intensity curves were plotted over the thermal decomposition curves of the two pyrolysis bio-oils, in order to relate the gaseous emissions of the decomposition of the complex mixtures of compounds comprising the prospective USR fuels to the respective thermal decomposition phases. It should be noted that the mass losses percentage is read on the left hand side y-axis (primary y-axis), whereas the temperature and the relative intensities of either CO_2 or CH_3COOH are on the right hand side y-axis (secondary y-axis).

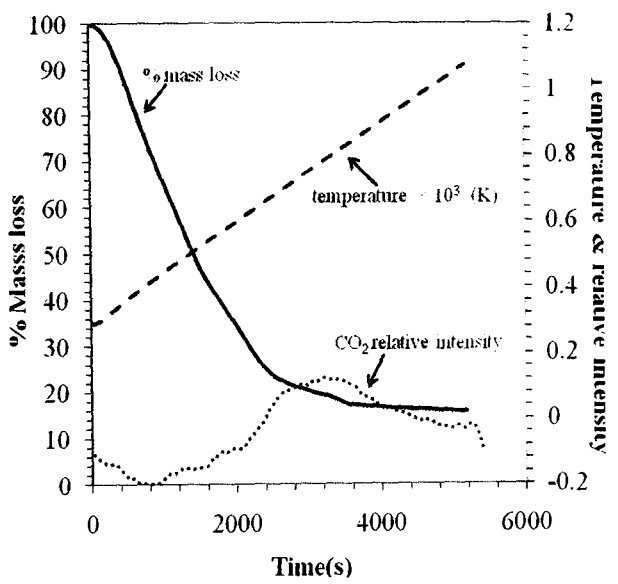

(a) TGA curve and relative intensity of CO_2 from the FTIR spectra

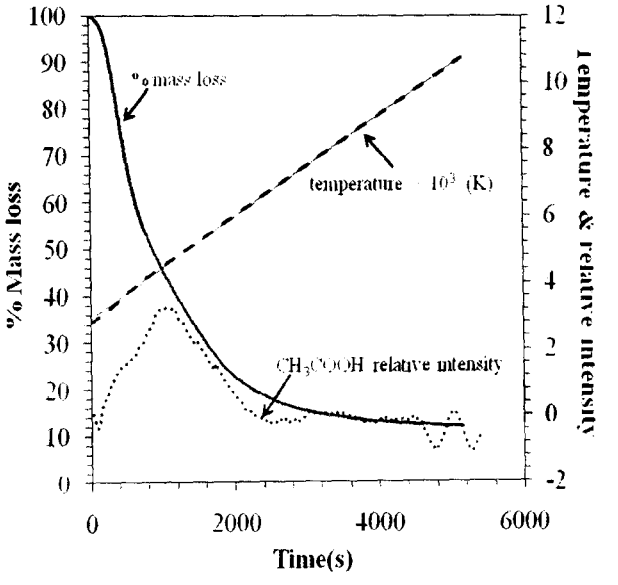

(b) TGA curve and relative intensity of ethanoic acid from the FTIR spectra

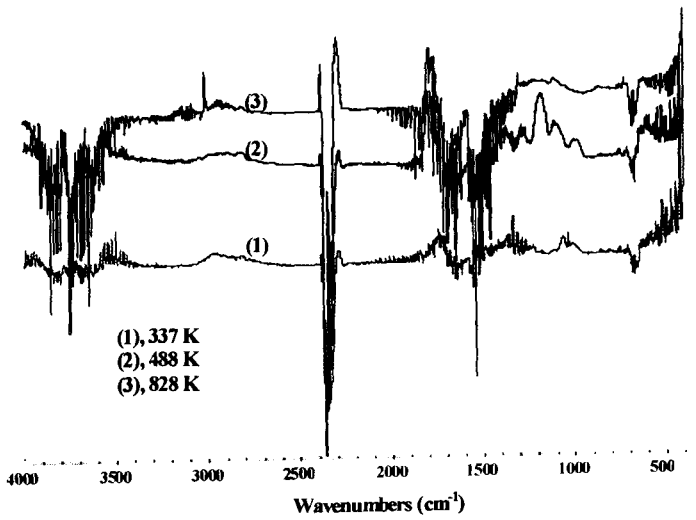

(c) FTIR spectra of the pyrolysis of pine oil 9 K min^{-1}

Figure 26 TGA- FTIR analysis of pinewood pyrolysis oil at 9 K min^{-1}

The presented graphs were selected because they had the most intense curves of CH_3COOH (spectra bands: 1600-1900 cm^{-1}) and CO_2 (spectra bands: 2360-2365 cm^{-1}) (**Figure 26(c)**) produced by these experiments. The spectral bands 3500-4000 cm^{-1} corresponded to the O-H stretch which is found in water, phenols and alcohols contained in the bio-oils. The spectra produced were similar regardless of the heating rate. Two strong carbonyl (C=O) stretches were produced (at 1777 and at 1800 cm^{-1}) associated with the acetic acid production. **Figure 26(b)** was produced from a heating rate of 9 K min^{-1} showing that CH_3COOH started to evolve at 377 K (104°C). The C-O stretching which occured at 2361.9 and 2349.3 cm^{-1} signified the release of CO_2 at 477 K (204°C) (**Figure 26(c)**). In **Figure 26(a)** it can be seen that the pyrolysis of the bio-oil is accompanied until the end of the test by the CO_2 release. From these two observations of the FTIR results it can be said that the CO_2 release occurring at temperatures above 477 K (204°C) is related to the pyrolysis of the pinewood oil while the mass loss of 50% (**Figure 25**) of the sample is attributed to the loss of CH_3COOH. The last conclusion was initially indicated by the GC-MS analysis of this bio-oil as seen in **Table 19**. Such results were common for all three heating rates (3, 6, 9 K min^{-1}) (**Figure 25**). Based on the FTIR spectra, it is noticed that the majority of the detected functional groups were oxygenated compounds. On the other hand, there was no detection of N- or S-containing compounds whereas gases such as H_2, N_2, and O_2 are not IR absorbing (**Yan et al., 2005**).

The TGA curves produced by the thermal decomposition study of the pinewood pyrolysis oil at the heating rate of 3, 6 and 9 K min^{-1} were split in two sections, as the intercepts of the linear fits dictate for their kinetic study (**Figure 25**). Each phase (PH1 and PH2), for conversions from 0.0 to 0.45 (low temperature conversions) and from 0.45 to 0.90 (high temperature conversions), was re-normalised between 0 and 1. Normalising a conversion curve over increasing temperatures meant that every section was treated as an autonomous mechanism of decomposition, starting from a conversion of 0.0 and ending at 1.0. The first section of conversions 0.0-0.45 was fed in the FORTRAN program (**paragraph 4.1.2**) as 0.0-1.0, and so was the section of 0.45-0.90 conversions. The models used in the improved iterative Coats-Redfern method for the thermal decomposition of the fast pyrolysis oils are shown in **Table 16.**

From the tested equations (**Table 16**) in the improved iterative Coats-Redfern method, the one giving the best interpretation of the thermal decomposition of the bio-oil was the reaction order model equation. This was concluded from the correlation coefficients produced from the Fortran program (**paragraph 4.1.2**). The correlation coefficients were ca. 0.99 and showed a very good fit of the modelled conversions compared to the experimental ones for the 3, 6 and 9K min^{-1} experiments (**Figure 23**).

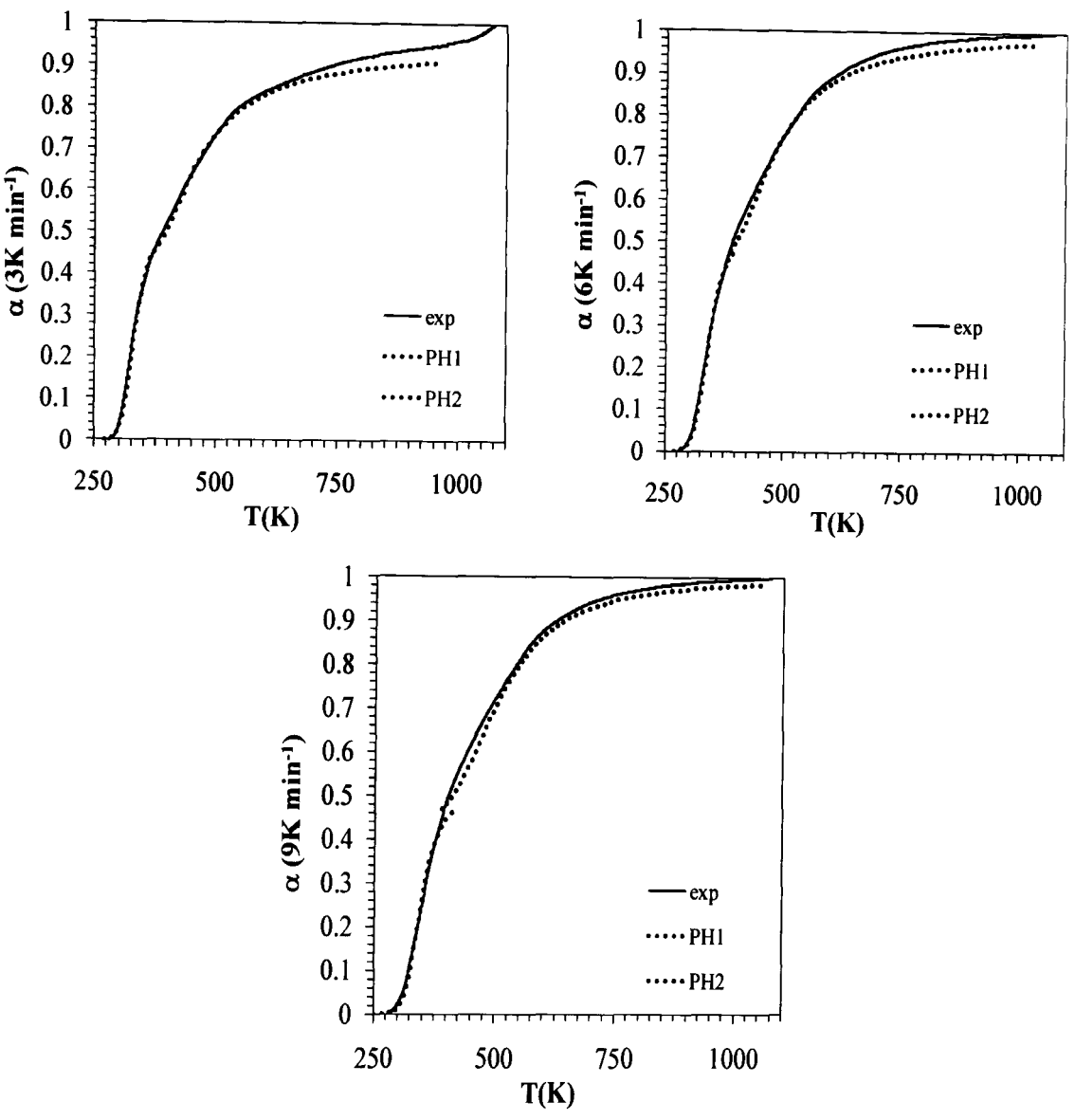

Figure 27 Experimental and modelled conversion curves for PH1 (α<0.45) and PH2 (α>0.45) using the reaction order model for the TGA experiments of pinewood pyrolysis oil at heating rates 3, 6, and 9 K min^{-1}

In **Table 20** the calculated kinetic parameters derived from the iterative Coats-Redfern modelling can be seen for both the PH1 and PH2 decomposition phases. For the lower heating rates, the order of the reaction was higher at the

higher temperature conversions, whereas for the highest heating rate (9 K min^{-1}) the respective values of the kinetic parameters were found to be smaller. The activation energies for higher heating rates were found to be lower in value, indicating that the higher heat supply enabled the mixture of hydrocarbons contained in the pinewood pyrolysis oil to decompose more easily. This outcome is confirmed by the temperature at which all heating rates reached a conversion of 0.90. When the heating rate was 3 K min^{-1}, 90% of the initial mass of the pyrolysis oil was thermally decomposed at 940 K; for the 6 K min^{-1} the same conversion was achieved at 640 K and for the 9 K min^{-1} at 636 K.

Table 20 Kinetic parameters for the TGA decomposition at heating rates of 3, 6 and 9K min^{-1} of pinewood pyrolysis oil based on the reaction order model $\boldsymbol{g(\alpha) = \frac{[1-(1-\alpha)^{1-n}]}{1-n}}$, the correlation coefficient values and the conversions (α) temperature range used for the model

PH1 (K min^{-1})	$E \pm dE$ (kJ mol^{-1})	$\ln A \pm d\ln A$ (A in s^{-1})	order	correlation coefficient	temperature fit range (K)
3	78.1±0.28	23.3 ± 0.10	2.9	0.995	282-362
6	63.8±0.31	17.6 ± 0.12	2.3	0.993	281-386
9	68.5±33.1	19.6 ± 0.12	3	0.985	283-390

PH2 (K min^{-1})	$E \pm dE$ (kJ mol^{-1})	$\ln A \pm d\ln A$ (A in s^{-1})	order	correlation coefficient	temperature fit range (K)
3	70.7±0.11	13.9±0.05	6.6	0.993	368-546
6	49.4 ±0.09	7.32 ±326	4.2	0.987	378-600
9	45.2 ± 0.16	6.13± 0.04	3.8	0.984	385-608

The kinetics of the thermal decomposition of the pinewood pyrolysis oil were better interpreted by the reaction order model in both the low and high temperature conversion sections (PH1 and PH2) (**Table 20**). The calculated activation energies (**Table 20**) indicated that they become lower in both PH1 and PH2 when higher heating rates are applied. These results confirm that the faster the thermal decomposition of the bio-oil is, the lower the temperatures at which their compounds react (**Figure 25**). This outcome is followed by the same trend in terms of reaction order as in the kinetic parameters. The evaporation of low temperature organic compounds (**Table I; Appendix III**) like the 2-cyclopenten-1-one with a boiling temperature of 337 K (64°C), furfural (328 K; 55°C), and n-propyl acetate

(375 K; 102°C) may have occurred at this phase. Ammonium acetate (melting point; 387 K; 114 °C) found by the GC- MS analysis of the pinewood bio-oil, decomposes to acetamide and water as shown in the reaction below within the temperature range of PH2 like the acetic acid (391 K; 118°C),

$$CH_3COONH_4 \rightarrow CH_3C(O)NH_2 + H_2O$$

6.5 EFB (Empty Fruit Bunch) pyrolysis oil GCMS analysis, TGA-FTIR study- kinetic modelling of the oil's thermal decomposition

Octadecanoic acid (stearic acid; $CH_3(CH_2)_{16}COOH$) (**Table II; Appendix III**) is one of the high percentage substances contained in the tested bio- oils. The large percentage of the mass loss at higher temperatures (**Figure 28**) can be attributed to the octadecanoic acid as its boiling point is 656 K (383°C). The similarities in the TGA-FTIR analysis of the EFB fast pyrolysis oil with the pinewood origin fuel (**Appendix III; Figure II**) also confirm the similar composition of both fuels based on organic groups such as acid, phenols, aldehyde and ketones (**Table II; Appendix III**). **Aho et al., (2008)** and **Abdullah and Gerhauser, (2008)** (who researched bio-oil production from pinewood and palm wood respectively) also reached the latter conclusion.

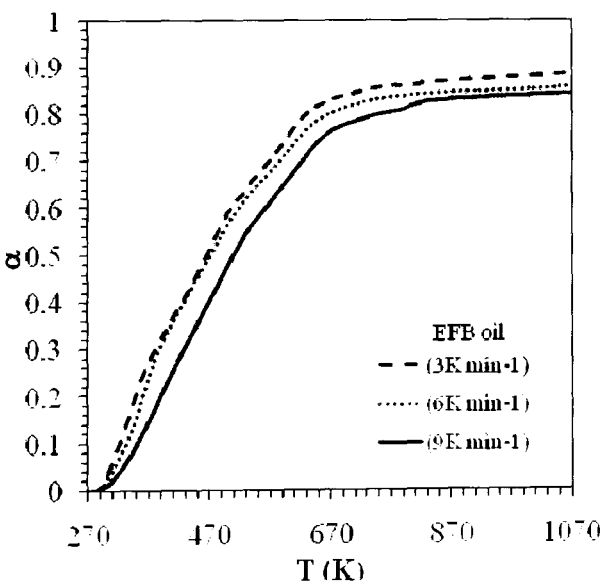

Figure 28 Mass loss conversion of EFB (Empty Fruit Bunch) pyrolysis oil in 50 mL min^{-1} N_2 at different heating rates, up to 1073 K (800°C) from the TGA experiments

Similarly to the present bio-oil (EFB), the palm wood derived bio-oil that was studied by **Abdullah et al. (2008)** exhibited a high water content (20- 30% wt). **Li et al. (2008)** also mentioned that the pyrolysis for different chemical bonds involved different energies that were required for breaking these bonds down, something that was ascertained by the kinetic study that followed.

The kinetic study of the TGA of the EFB (Empty Fruit Bunch) pyrolysis oil was based on the developed FORTRAN program as described in **paragraph 4.1.2**. The equations tested in this program in order to interpret in the best way the thermal decomposition of the bio-oil were derived from **Table 16** similarly to the pinewood bio-oil kinetic study. As previously found for the TGA pinewood oil study, the TGA curves produced by the thermal decomposition of the EFB pyrolysis oil at the heating rates of 3, 6 and 9 K min^{-1} were split in two sections or phases (PH1-2) for their kinetic study, as the curves' intercepts dictated (**Table III; Appendix III**). The 3D Jander diffusion equation was found to give the best fit on the experimental data of all heating rate thermal decompositions, except for the low temperature conversions section (PH1) at 3 K min^{-1} (**Appendix III; Table IV**). For the low conversions of the 6 and 9 K min^{-1}, correlation coefficients of 0.986 were produced while for the higher temperatures conversions (0.20- 0.90 and 0.30-0.90 respectively) correlation coefficients values close to 1 were achieved (0.998-0.996). For the 3 K min^{-1} run, a single curve was produced, as predicted by the improved iterative Coats-Redfern method based on the experimental data, resulting in the very high correlation coefficient of 0.996. These very good or excellent fits are confirmed by the closeness of the modelled conversion curves vs temperature to the experimental ones. The excellent agreement of the Jander diffusion model with the experimental data (**Appendix III; Table IV**) may be due to the gradual transition of the bio-oils decomposition where there is a diffusion gradient between the reactant and products phases (**Galway et al., 1990**) in the low and high temperatures conversion section (PH1 and PH2).

The fact that lower activation energies were calculated at higher heating rates (6, 9 K min^{-1}) can be attributed to changes in the reactivity of the bio-oil due to some components' boiling point such as dodecanoic acid (498 K), oleic acid (467 K) and tetradecanoic acid (523 K). In a previous study by **Dou et al. (2007)**, it was

shown that temperature is a key factor in thermal decomposition mechanisms and its gaseous products. In the cases of non-isothermal thermogravimetric analysis of the pyrolysis of synthetic materials (**Ahmaruzzaman et al., 2005**) it was realised that due to the complexity of their content, many consecutive and competing reactions occurred. **Zhang et al. (2007)** confirmed by using the liquid chromatography analysis, the variety of hydrocarbons contained in the bio-oils. This analysis showed that in the water phase there was a high content of acetic acid and hydroacetones, whereas in the oil phase there were less aliphatic and aromatic hydrocarbons and more polar components.

6.6 Waste cooking oil (WCO) TGA and kinetic modelling of the oil's thermal decomposition

There are many studies focused on the production of biofuels from sunflower cake followed by its chemical and calorific determination (**Gercel, 2002**) or the physical characteristics of biodiesel based on vegetable oil (**Ramadhas et al., 2003; Lang et al., 2001**). Moreover, even though quite a few studies were found for the hydrogen production from bio-oils (discussed in **chapter 7**), there were no preliminary kinetic studies for any bio-oils of vegetable origin.

The waste vegetable cooking oil thermal decomposition analysis was performed at 3 K min^{-1} in the Shimadzu TGA-50 thermogravimetric analyser as described in **paragraph 4.1**. The decomposition curve (**Figure 29**), based on the initial mass loss of sample (14.93 mg), determined two distinctive phases of decomposition which would define the oil's pre-treatment temperature prior to its use in the USR and SEUSR processes. The curves geometry, as interpreted by the kinetic study that follows, gave significant additional information for the reactions during the combustion and/or oxidation steps that would be involved in USR and SEUSR.

From the TGA mass loss curve (**Figure 29**) it can be seen that during heating, the sample started to lose mass from 541 K (268°C) and up to 875 K (602°C) (97.8% of its initial mass was thermally decomposed). From the same curve it was noticed that its thermal decomposition slope changed between 679- 736 K (406.4-

463°C). The sample's thermal decomposition got close to completion at 876 K (603°C), leaving a residual (ash and carbon) of 2.2% of the initial mass at the maximum temperature of 1173 K (900°C). The fact that 97.8% of the initial mass of the sample was decomposed by 876 K (603°C) illustrated the potential of the waste vegetable cooking oil to be able to be steam reformed in its most elemental materials in the USR process.

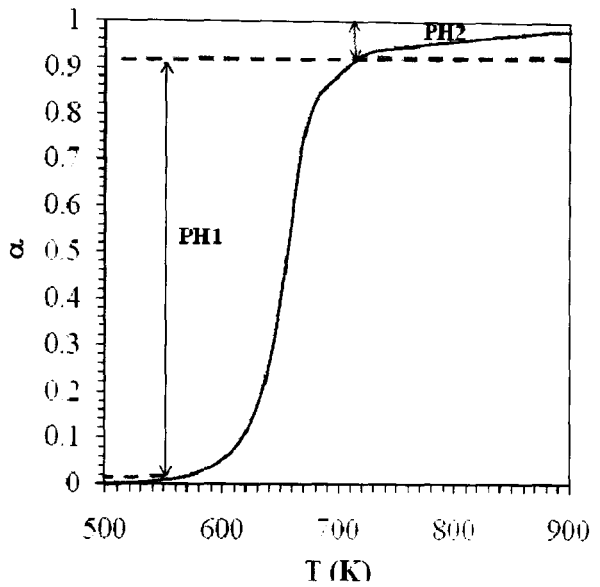

Figure 29 Mass loss conversion fraction vs. temperature of waste cooking oil (WCO) tested in TGA apparatus at a heating rate of 3 K min^{-1}

From the thermogravimetric analysis of the waste vegetable cooking oil, it was observed that the unreacted mass was much less than (with the same heating rate) that of the two biomass fast pyrolysis oils (**paragraphs 6.4** and **6.5**), despite the fact that the C:O ratio from the CHNS analysis exhibited a higher value than in the same analysis of the pinewood and EFB origin pyrolysis oils (**Table 17**). It should be noted that the same gas and gaseous flowrate was used (N_2 at 50 mL min^{-1}) in the TGA tests of the three oils. This result showed that the waste cooking oil had the potential to behave well in the unmixed steam reforming process (**chapter 7 and 8**) and was verified by the fact that any present hydrocarbons can be potentially decomposed when the temperature is about 876 K (603°C).

Based on the data from the conversion of the liquid mass to gases at the heating rate of 3 K min^{-1}, kinetic parameters (*E*: activation energy; *A*: pre-

exponential factor) were produced by applying the improved iterative Coats-Redfern method for non-isothermal data. The tested models were the Avrami-Eroveef ($g(\alpha)= [-\ln(1-\alpha)]^{1/n}$ for n=3/2), the contracting surface, the contracting volume, the 1D-diffusion, the 3D-diffusion and the power law. From the geometry of the decomposition conversion curve (**Figure 29**) the power law could potentially interpret the lower temperature conversions.

The best model for the experimental data produced, in the TGA, were by application of the 3D 'Jander' diffusion and the contacting volume equations, both for the range of conversions of 0.02-0.92. The experimental curves needed to split up in two sections (PH1 and PH2), in order to predict the model curves and the kinetic parameters for the decomposition of the waste cooking oil in an inert environment. This was illustrated by the correlation coefficient produced which for the conversions' range of 0.02 to 0.85 was 0.996 and for the range of 0.85-0.92 was 0.999 for both equations. The best linear fit of experimental data was achieved by the contracting volume equation as shown in the graph of F_1 vs T^{-1} (**Figure 30(b)**). Similarly from **Figure 30(a)** it can be seen that the best linear fit was achieved by the same equation.

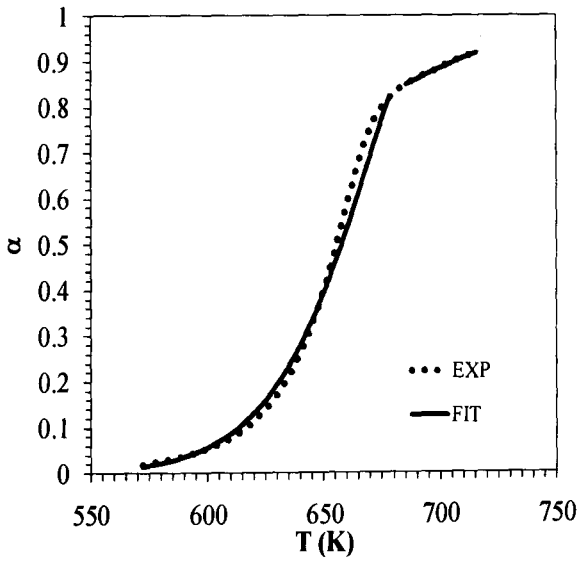

(a) Low and high temperature conversions model fits on experimental data

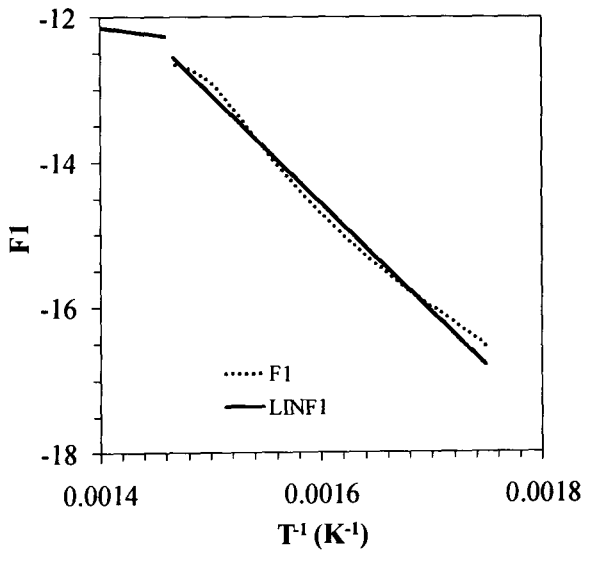

(b) Experimental F_1 vs. T^{-1} (scatter points) and linear fits LINF1(line)

Figure 30 Modelled and experimental conversion curves for low temperature and high temperature sections (PH1; PH2) using the contracting volume model for the TGA runs of WCO at 3 K min^{-1}

Shale oil is sourced in mineral rocks and in order to produce a fuel, it requires more processing than in the case of crude glycerol. It is worth mentioning that it is considered to be a synthetic form of glycerol. From oil shale studies, it was shown that the oxygen content was higher than in the CHNS analysis of the waste cooking oil, leading tolower activation energies (**Jaber et al., 2000**) than in the present study (**Table 21**).

Table 21 Kinetic parameters for the TGA decomposition of waste cooking oil at 3K min^{-1} based on the contracting volume equation ($\boldsymbol{g(\alpha) = 3[1-(1-\alpha)^{1/2}]}$, the correlation coefficient values and the conversions (α) temperature range used for the model

PH1	***E*±d*E***	**ln*A*±dln*A***	**correlation**	**temperature**
(K min^{-1})	**(kJ mol^{-1})**	**(A in s^{-1})**	**coefficient**	**fit range (K)**
3	124.88±-1.32	17.29±8.08	0.996	572-685
PH2	***E*±d*E***	**ln*A*±dln*A***	**correlation**	**temperature**
(K min^{-1})	**(kJ mol^{-1})**	**(A in s^{-1})**	**coefficient**	**fit range (K)**
3	16.51±-5.37	-3.56±6.71	0.999	686-716

Aboulkas et al. (2008)'s study on the non-isothermal decomposition of olivine found an activation energy of 165 kJ mol^{-1}, which is slightly larger than the one obtained using the contracting volume model in the present study of dolomite (**Table 21**).

The kinetic parameters (*E*, ln*A*) that were calculated based on the improved iterative Coats-Redfern method for non-isothermal data were found to be high (**Table 21**) in the low temperatures conversions section. This clearly indicated that the cracking of the waste cooking oil organic compounds is more difficult to initiate, compared to the pinewood and EFB pyrolysis oils. Therefore, a heating treatment is needed prior to the USR process while at the same time its mass loss by thermal decomposition should be minimised, based on **Figure 29**. For these reasons, the pre-heat temperature of the waste cooking oil for USR process was chosen to be at 573 K (300°C), when its mass loss does not exceed **2.2** % and according to the derived kinetic information in **Table 21**, less energy will be needed for its reforming. This result is directly related to fewer oxygenated compounds contained in the waste cooking oil compared to the two fast (pinewood and EFB) pyrolysis oils (**Table 19; paragraph 6.2**).

6.7 Summary on the preliminary study of the liquids of waste biomass origin

The results of the initial study of the waste biomass origin fuels WCO (Waste Cooking Oil), EFB (Empty Fruit Bunch) and pinewood origin fast pyrolysis oils;) could determine their potential as feedstocks for the USR and SEUSR processes. The major areas of their assessment were their elemental analysis, the determination of their calorific value and the kinetic study of their thermal decomposition which was conducted by TGA-FTIR (Thermogravimetric Analysis-Fourier Transform Infrared Analysis). The EFB (Empty Fruit Bunch) and pinewood origin fast pyrolysis oils were analysed by the GC-MS (Gas Chromatography- Mass Spectrometry) method in order to determine their main components.

6.7.1 Elemental analyses of the waste biomass origin liquids

The CHNS (Carbon, Hydrogen, Nitrogen, Sulphur) analysis of the potential fuels provided useful information with regard to the possible reactions they would be involved in the USR and SEUSR processes. The elemental balances of these potential fuels could be used in order to compare them to the theoretical mass balances they gave. These elemental balances can be used to indicate the processes' and hydrogen's maximum yield.

The main findings from the three waste biomass origin oils upon their application in the USR and SEUSR processes are:

- The catalyst's poisoning would be minimal as no sulphur was detected by the CHNS apparatus (**Table 17**). The S detection was possibly below a predetermined threshold.
- Because the H:C ratio of the WCO was smaller than the H:C ratios of the two fast pyrolysis oils, while the C:O was greater than the respective ratios of EFB and pinewood origin oils, there is the possibility of carbon deposition on the catalyst when the WCO is used in the USR and SEUSR processes (**Table 17**).

- The higher H:C ratio of the WCO compared to that of the two biomass pyrolysis oils showed that it was the fuel with the best potential hydrogen yield by the USR and SEUSR processes.
- The determined C:O ratios for all three waste biomass origin oils, can be used to determine the theoretical oxygen amount that would be necessary during the AF (Air Feed) steps during the USR and SEUSR processes in order to burn away any deposited carbon on the catalyst.
- The two fast pyrolysis oils will be reduced with more difficulty during the FF (Fuel Feed) steps in the USR process, as their content in oxygen is very high.

6.7.2 Calorific values of the waste biomass origin oils

The elemental analysis of all three waste biomass origin oils demonstrated that a higher calorific content could be expected from the WCO compared to the two fast biomass pyrolysis oils (H:C and C:O ratios; **Table 17**). This was confirmed by the calorimetric analysis (**Table 18**).

6.7.3 Waste biomass fast pyrolysis oils GC-MS analysis and waste biomass origin oils TGA- FTIR analysis and kinetics study

The GC-MS analysis of the two waste biomass fast pyrolysis oils gave a qualitative and a semi- quantitative analysis. Both oils consist of acids, phenols, ketones and aldehydes,

- The TGA- FTIR results of the two fast pyrolysis oils confirmed their similarities as indicated by their GC- MS analysis (**Appendix III; Figure I, Table I and II**). A residue of solid matter (**Figures 25, 28 and 29**) which was comprised by ash and carbon was left when both waste biomass origin fast pyrolysis oils were thermogravimetrically tested.

- Two different phases (PH1 and PH2) of thermal decomposition were noticed for the three heating rates (3, 6, 9 K min^{-1}) used in the thermogravimetric analysis of the EFB (**Fig. 28**) and pinewood fast pyrolysis (**Fig. 25**) oils. The higher heating rates allowed higher conversions of the pinewood but not of the EFB origin fast pyrolysis oil (**Fig. 25 and Fig. 28**) in the low temperature regions.

- No particular trend with respect to heating rates was noticed on the curves of the mass loss with temperature from the TGA experiments on the fast pyrolysis oils.

- The FTIR analysis coupled with the TGA analysis aided the understanding of the two fast pyrolysis oils. The intensity curves of acetic acid (CH_3COOH) and carbon dioxide (CO_2) were chosen to be plotted against the thermal decomposition curve which resulted from the thermogravimetric analysis.

- The semi- quantitative GC-MS analysis of both pyrolysis oils was confirmed by the TGA-FTIR tests which illustrated that 50% of the pyrolysis oils' mass loss was attributed to the amount of CH_3COOH they contained.

- The TGA mass loss curves were renormalized in order to apply them in the FORTRAN program, where models in the improved iterative Coats- Redfern method were employed. High correlation coefficients (0.99) of the reproduced conversion curves resulted when compared to the experimental conversion curves.

- Since the two fast pyrolysis oils already have a large quantity of water, as their TGA analysis confirmed, they would need less steam when used in the USR and SEUSR processes.

- It was the reaction order model which better interpreted the thermal decomposition curves of the waste pinewood origin fast pyrolysis oil (**Table 20**), while the Jander diffusion equation resulted in the best correlation coefficients in the TGA study of the EFB origin fast pyrolysis oil (**Appendix III, Table IV**).

- Higher activation energies were calculated for both the EFB (**Appendix III, Table IV**) and pinewood origin fast pyrolysis oil (except for the PH2 conversion curves) when higher heating rates were applied during the TGA runs. Therefore the higher the heat supply is, the easier the oil decomposes.

- Less residual matter was noticed in the TGA analysis of the WCO (**Fig. 29**) in comparison to the solid masses left by the end of the TGA analysis of the two waste biomass origin fast pyrolysis oils. This confirms the produced C:O (**Table 17**) ratios from the elemental analysis of all three oils.

- Since approximately 98% of the WCO mass was decomposed by 877 K, the application of this temperature should also be appropriate for the FF (Fuel Feed) steps of the USR process.

- The model that best reconstructed the experimental thermal decomposition curve of the WCO was the contracting volume model (**Table 21**).

- Higher activation energies were calculated for the low temperature conversions' region (PH1) in the WCO kinetic study (**Table 21**) than in the same region in the kinetic study of two waste biomass fast pyrolysis oils (**Table 21; Table IV in appendix III**). This clearly indicates that WCO thermal cracking can be more energy intensive to initiate when compared to the EFB and pinewood origin fast pyrolysis oils.

- From the last remark it is clearly evident that, unlike the two biomass pyrolysis oils, the WCO needs to be thermally pre-treated prior to its employment in the USR process while at the same time an appropriate temperature should be applied for its pre-treatment which would minimise the WCO's mass loss. This temperature was chosen to be 573 K because the TGA mass loss curve (**Fig. 29**) at this temperature showed that only 2.2% of the initial mass of WCO was lost.

Chapter 7
Unmixed Steam Reforming (USR) of waste cooking oil

Unmixed fuel processing and chemical looping have been described in **chapter 2** (**paragraph 2.3**). Both can produce sequestration ready CO_2 (chemical looping combustion), a N_2-free syngas product (unmixed steam reforming 'USR', *aka* chemical looping reforming 'CLR' in a packed bed), or ultimately, a pure H_2 reformate (sorption enhanced steam reforming 'SEUSR', also known *as* sorption enhanced chemical looping reforming 'SECLR' in a packed bed). Recall the difference in using the terms 'unmixed' or 'chemical looping' arose mainly from the type of reactor used: packed bed with alternated gas/vapour flows for 'unmixed', and dual recirculating fluidised beds with fixed gas flows and moving solids for 'chemical looping', although the expression 'CL in a packed bed' has recently increasingly been used in the literature in place of 'unmixed'. The thermogravimetric analysis of the waste cooking oil, henceforth shortened 'WCO', (**chapter 6, paragraph 6.6**) indicated its basic features, informing its need to be pre-heated in the USR (Unmixed Steam Reforming) process to 573 K(300°C).

Based on the results of these preliminary results, the effect of the mass of the catalyst on the process was to be examined on a recyclability study of six unmixed steam reforming cycles. The performance and stability for 80 and 40 g of fresh catalyst were investigated. The latter is of particular interest as it is the mass that was used for the following sorption enhanced unmixed steam reforming (SEUSR) experiments as discussed in **chapter 8**.

7.1 Materials, experimental set-up and equipment

In the paragraphs that follow, the materials that were employed in the USR and the chemical looping USR experiments as well as the experimental set-up and the equipment used, are discussed.

7.1.1 Materials

A commercial catalyst (Johnson Matthey) was chosen for the unmixed steam reforming process which consisted of 18% wt NiO supported on Al_2O_3 in the originally pellet form as received. Prior to loading in the reactor, the fresh catalyst was ground and sieved (mesh size of 10-20) resulting in particles whose size was distributed between 850 and 2000 μm. A mass of 80 g (as in the 1st USR experimental set; **paragraph 7.3**) or 40 g (as in the 2nd USR experimental set; **paragraph 7.4**) of fresh, as-received catalyst particles were used. Other solid species present in the reactor was the aluminum oxide (SIGMA- ALDRICH) spherical beads (4-8 mesh) which were placed at the bottom of the reactor. These were assumed to be inert.

The average elemental molar formula of the waste cooking oil is $C_{0.3164}H_{0.6448}O_{.038}$ (**Table 19; paragraph 6.2**), while the molar mass associated with this formula was calculated at 5.0695×10^{-3} kg mol^{-1}. The density of waste cooking oil was determined to be 920 kg m^{-3} (293 K; 20°C). It was assumed that all the liquid water and bio oil at the pumps were vaporized in the two pre-heaters (**Figure 2; paragraph 2.3**) and prior to entering the reformer reactor.

7.1.2 Experimental set- up

At the beginning of this study the unmixed steam reforming step was tested for the steam to carbon (S:C) ratios of 2.5: 1 and of 4:1 (excess of steam) at the temperatures of 973 K (700°C) and 873 K (600°C), in order to determine the best conditions of the SR step within the USR process including the optimum waste cooking oil and steam conversions to hydrogen. The mass of the fresh catalyst used was 80 g. For both S:C ratios, the first steam reforming step was performed on a pre-reduced catalyst (see **paragraph 7.1.2.1**) while those that followed were carried out on the oxidised catalyst produced by the preceding air flow feed.

The experiments took place in the unmixed steam reforming (USR) rig (bench scale; **Figure 2; paragraph 2.3**). The catalyst bed was heated to 973 K (700°C) or/ and at 873 K (600°C) in an inert environment by a volumetric flowrate of 600 mL min^{-1} N_2 until isothermal conditions were established. The presence of N_2 is of great importance as it ensures the avoidance of unnecessary reactions on

the catalyst during start-up and shut down but it additionally aids the closure of the elemental balances.

The reactor was heated for the reactive steps to commence as described below, using 1 kW maximum power of electrical input. When the desired temperature was reached, the steps of pre-reduction, SR, purge, and oxidation (AF) that followed occurred under set reactor temperature conditions by heating but not by cooling.

7.1.2.1 Pre-reduction step

The fresh catalyst was isothermally pre-reduced at 973 K (700°C) in a mixture of 25% vol H_2/N_2 which was produced by flows of 200 mL min^{-1} of H_2 and 600 mL min^{-1} of N_2 respectively. This step was performed at the beginning of every USR experiment (i.e. only cycle one of the cyclic USR experiments). This key-point was denoted in an earlier work by **Dupont et al. (2007)** who showed that both methane and sunflower oil, were observed to successfully reduce oxidised catalyst (NiO on alumina).

Moreover, the first steam reforming (SR) step carried out on a reduced catalyst provided the means of comparing the H_2-reduced to the oil-reduced catalyst as the oxygen transfer material or 'OTM' for subsequent SR (FF- fuel feed) runs. Therefore the capability of performing the next five FF steps on oxidised catalyst can be demonstrated, since the AF step precedes them.

7.1.2.2 Fuel feed (FF) step description

The FF (Fuel Feed) step was performed at either set temperatures of 973 K (700°C) and/ or 873 K (600°C) resulting in near isothermal conditions. The waste cooking oil was fed at a rate of 0.55 mL min^{-1} in the pre-heater (**Figure 2; paragraph 2.3**) and was heated to 573 K (300°C). The steam was produced in a separate pre-heater at a temperature of 423 K (150°C), by passing through the pre-heater deionised water at 1.42 mL min^{-1} and at 2.32 mL min^{-1} for reforming at a molar S:C ratio of 2.5:1 and of 4:1 respectively.

The steam temperature of 423 K (150°C) ensures that the phenomenon of film boiling is avoided, whilst the WCO set pre-heat temperature ensured the vaporization of the fuel, as well as preventing tar formation before entering the reactor. It was assumed that all the liquid water and bio oil at the pumps were vaporized in the two pre-heaters and entered the reactor.

Both fluids entered at the bottom of the reactor as opposed to the top, which was suggested by **Dupont et al (2007)** as a method for improving mixing of the steam and the fuel over the catalyst. The steam was supplied in the reactor by an injector placed at the entrance of the reactor (bottom end) while the vaporised fuel (WCO) entered the reactor from its main inlet around the steam injector.

7.1.2.3 Air Feed (AF) step description

The air feed steps during which the oxidation of the catalyst bed under isothermal conditions at 873 K (600°C) occurred for the preliminary USR study at S:C= 2.5:1 and 4:1. It needs to be noted that for the chemical looping experiments the AF steps were performed at the set temperature of 923 K (650°C). It has to be underlined that in all steps a flow of N_2 at 600 mL min^{-1} was supplied, except in the air feed (AF) step where only air was supplied.

The concept behind the air feed step, was to illustrate the performance of an oxidized catalyst as an oxygen transfer material (OTM) in the steam reforming step during its reduction by the produced hydrogen (H_2) and the advantages it presented during the oxidation step that followed (AF- air feed step).

7.1.2.4 Purge step description

In between each FF and AF step, the reactor was purged (**purge step**) with the same volumetric flowrate of N_2 (600 mL min^{-1}). This step would minimize chemical interactions from the different feeds when switching to different temperatures or gaseous mixtures. The average duration of the inert purge intervals was of 20 minutes.

It is worth noticing that the purge step may not be necessary or much reduced at industrial scale whereas at this experimental level (bench scale) it aided the study of the chemistry.

7.1.2.5 Chemical looping experimental set-up

In the chemical looping experiments of both 80 and 40 g of fresh catalyst (**paragraph 7.5**) every cycle is comprised of one FF and one AF step which yield one cycle of unmixed steam reforming experiment. A sequence of FF and AF steps was conducted. The first steam reforming step is performed on a H_2-reduced catalyst whereas the similar steps that follow are performed on an oxidized catalyst. The active solid species in the reactor are NiO, when the catalyst is oxidized (AF step) and $Ni_{(s)}$, when the catalyst is reduced (FF step).

7.1.3 Equipment

The flow of all gases (N_2, H_2, air (20.9% vol O_2/ N_2)) at the different steps of the USR process was regulated by three MKS Type 1179A Mass-Flo® Controllers. These were connected to an MKS Type 247C 4-channel readout panel. The readouts were volumetric flowrates at standard temperature and pressure (STP) in order to control any changes in temperature and/ or pressure in the mass flow of the reactant gases.

The deionised water and WCO were fed in the two pre-heaters (**Figure 2**) by two Watson Marlow 5058 peristaltic pumps. The temperatures of the thermocouples, which were inserted in the catalyst bed, were monitored and recorded for every 5 s by the use of the Picolog Software.

Excess steam was condensed and removed from the system by having placed at the exit of the reactor two condensers and a water trap, with a cooling medium circulated on its outer jacket while the rate of cooling was maintained by an Isotemp Bath circulator (Fisher Scientific 3016S). A silica gel trap was placed before the gas analyzer to further ensure that the gases entering it were dry.

Therefore, the dry product gases were at STP before entering the ABB Advance Optima analyzers set up described in **paragraph 2.3**.

Further to the online products analysis, the gaseous products were collected in Tedlar bags every 5 minutes. Their analysis took place with the aid of a GC/ FID (Varian 3380, Gas Chromatograph with Flame Ionisation Detector) when N_2 was applied as the column eluent that passed through a 2 m × 2 mm (length×diameter) column which was packed with 80-100 mesh Haysep material, in order to separate different gaseous mixtures, i.e. CH_4 and CO_2. The GC/ FID was set to detect hydrocarbons from C_1 to C_4 and confirmed that the only hydrocarbon present in the sample was methane (CH_4).

7.2 Unmixed steam reforming conservation of elements analysis

The elemental balances of the reactive steps which were involved in the USR process are based on the reactions presented in **paragraph 2.3**. If the following inputs are considered:

$\dot{V}_{C_nH_mO_k}$	volumetric flowrate of waste bio- oil entering the pre- heater ($m^3\ s^{-1}$)
$\dot{V}_{N_2}$	volume flowrate (STP) of nitrogen entering the reactor ($m^3\ s^{-1}$)
$\dot{V}_{H_2O}$	volume flowrate of liquid water prior to vaporisation ($m^3\ s^{-1}$)
$m_{i\ (fresh\ catalyst)}$	mass of catalyst (kg)
$wt\ \%\ Ni$	% of Ni present in the total mass of the catalyst (%)

The dry on-line molar fractions of the following species are represented by the symbols below:

Table 22 Dry molar fractions y_i of species 'i' identified by the on-line gas analysis

Species	**CH_4**	**CO**	**CO_2**	**O_2**	**H_2**
Dry mol fraction	y_{CH_4}	y_{CO}	y_{CO_2}	y_{O_2}	y_{H_2}

The dry molar fraction of N_2 (represented as y_{N_2}; **Table 22**), was not measured by the ABB online gas analysers, but could be derived by measuring all the other dry gases molar fractions by difference to 1.

The mass of the reactants that entered the reactor were conserved by the species that were accumulated and or consumed in the system with respect to the final products that left the system. Based on the mass conservation of the open reactor system it was possible to determine the conversion fractions of the bio-oil and the selectivity to the product gases in the unmixed steam reforming step (under fuel feed- FF step) and the conversion fraction of the catalyst's oxidation in the under air flow (AF) step.

7.2.1 Fuel Feed (FF) step

The molar fraction of N_2 was based on the dry molar fraction of the product gases during the steam reforming step,

$$y_{N_2} = 1 - (y_{CH_4} + y_{CO} + y_{CO_2} + y_{O_2} + y_{H_2})$$

Eq. 22

The elemental balance of N (conservation of N), shows that the total dry molar flowrate of the gases is the fraction of the dry inlet molar flowrate of nitrogen $\dot{n}_{N_2,in}$ over the molar fraction of nitrogen (y_{N_2}) at the outlet of the system:

$$\dot{n}_{out,dry} = \frac{\dot{n}_{N_2,in}}{y_{N_2}}$$

Eq. 23

The waste cooking oil's conversion X_{WCO} is derived from the carbon balance of the system (**Appendix IV**) and is expressed by equation 24 as a function of the dry molar fractions of the product gases,

$$X_{C_mH_nO_k} = X_{WCO} = \frac{\dot{n}_{WCO,in} - \dot{n}_{WCO,out}}{\dot{n}_{WCO,in}} = \frac{\dot{n}_{out,dry} \times (y_{CO} + y_{CO_2} + y_{CH_4})}{n \times \dot{n}_{WCO,in}}$$

Eq. 24

where the numerator can be replaced by the term $\sum \dot{n}_{C-produced}$ as the sum of the molar carbon rate of the product gases. In the previous expression for X_{WCO} the term that encountered any accumulated solid carbon and any other hydrocarbons other than CH_4 were not taken into account (**Appendix IV**). At the denominator of **Eq. 24**, n represents the mol fraction of carbon in the WCO, i.e. n = 0.3164 from **Table 17** in section **6.2**.

The selectivity to the gaseous products (CO, CH_4, CO_2) during the steam reforming step was estimated based on the total rate of carbon produced, from the carbon balance, by setting the $MgCa(CO_3)_2$ term to zero since the sorbent was absent in the USR process,

$$SEL_{CO\ or\ CH_4\ or\ CO_2} = 100 \times \frac{y_{CO}\ or\ y_{CH_4}\ or\ y_{CO_2}}{y_{CO} + y_{CH_4} + y_{CO_2}}$$

Eq. 25

From the hydrogen balance the steam conversion during the FF step is calculated based on equation 26,

$$X_{H_2O} = \frac{1}{2 \times \dot{n}_{H_2O}} \times \left[\dot{n}_{out,dry}\left(y_{CH_4} + 2y_{H_2}\right) - m(\dot{n}_{WCO,in}X_{WCO})\right]$$

Eq. 26

with m representing the moles of hydrogen in the WCO (m = 0.645), as determined in the elemental analysis presented in **paragraph 6.2 (Table 17)**.

The reduction rate of the NiO catalyst ($\dot{n}_{NiO\rightarrow Ni,FF}$) was instructed by the oxygen balance,

$$\dot{n}_{NiO\rightarrow Ni,FF} = \dot{n}_{out,dry}\left(y_{CO} + 2y_{CO_2} + 2y_{O_2}\right) - \left(\dot{n}_{H_2O}X_{H_2O}\right) - k(\dot{n}_{WCO,in}X_{WCO})$$

Eq. 27

where k (mole fraction of oxygen in the WCO)= 0.0385 (**Table 17**). By integrating the previous equation over time, the estimation of the number of NiO moles reduced during the FF step was possible, as well as the calculation of the percent conversion of NiO to Ni during the course of a FF step.

7.2.2 Air Feed (AF) step

The elemental balances outlined in the current paragraph are valid only after the reactor has been flushed of residual syngas as evidenced by the H_2 and CH_4 peaks which are present at the beginning of the AF step, as explained in **paragraph 7.5.1.2**. The nitrogen balance during the air feed step was used as the basis for the definition of the total gas molar flow rate ($\dot{n}_{out,dry}$) exiting the USR process system. The rate of oxidation ($\dot{n}_{c,oxidation}$) of the deposited carbon from the FF step, which would result in either CO or CO_2 depending on partial or complete oxidation respectively, was determined by the carbon balance in the duration of the air feed (AF),

$$\dot{n}_{c,oxidation} = \dot{n}_{out,dry} \times (y_{CO} + y_{CO_2})$$

Eq. 28

The rate of Ni oxidation into NiO ($\dot{n}_{Ni \rightarrow NiO}$) was based on the oxygen balance and was expressed by equation 29,

$$\dot{n}_{Ni \rightarrow NiO} = 2\dot{n}_{O_2,in} - \dot{n}_{out,dry} \times (2y_{O_2} + y_{CO} + 2y_{CO_2})$$

Eq. 29

By integrating the Ni oxidation rate over the duration of the AF step, it was possible to calculate the total number of moles of the produced NiO, and the % of Ni conversion.

The fraction of O_2 conversion (X_{O2}) was based on the known inlet molecular flowrate of O_2 ($\dot{n}_{O_2,in}$) present in the air feed and the recorded online O_2 molar fraction (y_{O_2}),

$$X_{O_2} = \frac{\dot{n}_{O_2,in} - \dot{n}_{out,dry} y_{O_2}}{\dot{n}_{O_2,in}}$$

Eq. 30

Since the main products of the air feed (AF) step were oxygenated compounds, the selectivity to the product gases calculation relied on equation 31,

$$SEL_{CO\ or\ CO_2\ or\ NiO}\ (\%) = 100 \times \frac{(y_{CO}\ or\ 2y_{CO_2}) \times \dot{n}_{out,dry} or\ \dot{n}_{Ni \rightarrow NiO}}{(y_{CO} + 2y_{CO_2}) \times \dot{n}_{out,dry} + \dot{n}_{Ni \rightarrow NiO}}$$

Eq. 31

The errors that may have occurred during the USR process of WCO were taken into account. These errors were caused by experimental inaccuracies in (i) gas flow rates measurements by the mass flow meters, (ii) liquid flow delivery by the peristaltic pumps (iii) dry gas volume concentrations by the online gas analysers for CO, CO_2, CH_4, H_2 and O_2. Such errors would have propagated to the molar flows of the gases produced, in particular those of the most significant species H_2 and CO_2. In addition, errors of time-on-stream would have been introduced by the different transfer times of the reactor products through the sampling path and their respective analyser. These errors were estimated and worked out by the formulae that can be found in **Appendix IV**.

7.3 Thermodynamic equilibrium calculations

Thermodynamic equilibrium calculations were performed by Dr Dupont (details can be found in **Pimenidou et al[(a)], 2010**) to allow comparisons of the experimental outputs with theoretical maxima, assuming an ideal composition for the waste cooking oil based on that of a common fresh rapeseed oil.

The thermodynamic equilibria were calculated for the steam reforming of individual compounds of rapeseed oil such as oleic, linoleic, linolenic, palmitic and stearic acids as well as for a representative mixture of these fatty acids that better describe fresh rapeseed oil. This assumption was based on the work of **Eder and Brandsch (2002),** who analysed common rapeseed oil and found that it contained an average composition consisting of 62.5 wt% oleic, 17.8 wt% linoleic, 9.13 wt% linolenic, 4.5 wt% palmitic and 1.74 wt% stearic acid.

The bio-oil's conversion, steam conversion and selectivity to carbon containing and hydrogen containing products were determined from the

equilibrium calculations (**Eqs. 22-31**). Their values did not deviate when small changes in the composition were applied, ensuring in this way that in a case of slightly different compositions of the current waste cooking oil the results would not be greatly affected. Moreover, the term of % H_2 purity yield was introduced,

$$\%\, H_2\, purity\, yield = 100 \times \frac{y_{H_2}\, corrected\, for\, zero\, (0) N_2}{equilibrium\, y_{H_2}\, corrected\, for\, zero\, (0) N_2}$$

Eq. 32

By using this term, the closeness between the experimental conditions and the optimum ones as expressed by the thermodynamic equilibrium calculations was assessed.

7.4 USR of waste cooking oil with 80 g of fresh catalyst: effect of steam to carbon ratio

The molar steam to carbon ratios were calculated based on the formula:

$$S{:}C = \frac{\dot{n}_{H_2O}}{\dot{n}_{WCO} \times m}$$

Eq. 33

where $\dot{n}_{H_2O}$ and $\dot{n}_{WCO}$ are the molar flowrates (mol min^{-1}) of the deionised water and waste cooking oil at standard temperature and pressure (STP) and m the molar carbon fraction in the fuel. The S:C of (i) 2.5:1 and of (i) 4:1 were achieved by supplying 0.55 mL min^{-1} of WCO and 1.42 mL min^{-1} deionised water resulting in an WHSV (weight hourly space velocity) of 1.967 h^{-1} and 0.55 mL min^{-1} of WCO and 2.32 mL min^{-1} of water giving a WHSV of 2.640 h^{-1} respectively when 80 g of fresh catalyst were initially employed. The WHSV (weight hourly space velocity) is defined as,

$$WHSV = \frac{total\, mass\, flow\, rate\, of\, reactants}{catalyst\, mass}\ (\text{units of } h^{-1})$$

Eq. 34

The WHSV allows a discussion of the residence time of the fluids in the reactor.

7.4.1.1 Steam reforming (FF) step of waste cooking oil at S:C= 2.5:1 and 4:1 on the H_2-reduced catalyst

Two different steam to carbon ratios were initially used in the USR rig experiments (S:C= 2.5:1 and 4:1) for the FF steps under isothermal conditions of 973 K (700°C) and 873 K (600°C). These four experiments would enable the determination of the efficiency of the steam reforming reactions of waste cooking oil at different steam feeds and at the high and low temperatures respectively, when a mass of 80 g of fresh catalyst was employed.

The dry gas analyses from the pre-reduction step and the extent of the H_2-reduction of the catalyst prior to the SR step at the S:C= 2.5:1 are referred to in **Appendix IV (Figure I)**. The end of the reduction step was confirmed by a plateau of the hydrogen curve corresponding to its volumetric concentration in the inert gas (N_2) feed.

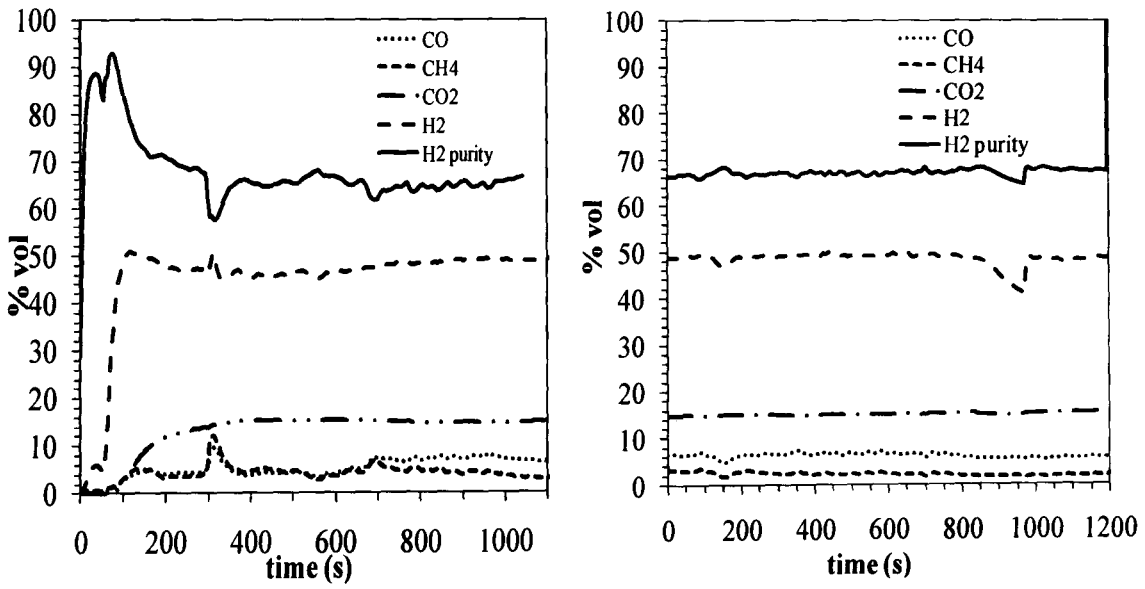

Figure 31 (a) Dry reformate analysis of the product gases during SR step on H_2- reduced catalyst at S:C = 2.5:1 at (T_{set}= 973 K, 700°C); (b) Dry reformate analysis on H_2-reduced catalyst for S:C = 2.5:1 at T_{set}= 873 K (600°C)

The FF step for the S:C ratio of 2.5:1 on the H_2-reduced catalyst was initially performed at 973 K (700°C) and then at 873 K (600°C), with a purge step in between the two FF steps in order to serve the scope described in **paragraph**

7.1.2.4. The steam reforming step at T_{set}= 973 K is presented in **Figure 31(a)** where the dry volumetric concentrations of the produced gases can be seen.

The purity of hydrogen ($\eta_{H_2\,purity}$) in the reactor's exit stream is defined as the volumetric concentration fraction of hydrogen over the total volumetric concentration fraction of the produced gases,

$$\eta_{H_2\,purity} = 100 \times measured\ dry\ volumetric\ fraction\ of\ H_2 corrected\ for\ zero\ N_2$$

$$= \left(\frac{\dot{v}_{H_2}}{\dot{v}_{H_2} + \dot{v}_{CO} + \dot{v}_{CO_2} + \dot{v}_{CH_4}}\right)_{measured}$$

Eq. 35

Another important parameter that is directly related to the waste cooking oil conversion is the consumption of steam, as described by the steam conversion equation (**Eq. 26**). The conversion of the bio-oil indicated the efficiency of the process under specific conditions (973 K, 700°C; 1 bar; reduced catalyst). For such a purpose the mass balances that were described in **paragraph 7.2** were used by considering the dry product gases, the carbon and nitrogen elemental balances in the calculation of the waste cooking oil conversion (**Eq. 24)** when a stable volumetric dry gas curve is produced as shown in **Figures 31(a)**. The fluctuations appearing in the dry reformate gas graph, may have been caused to the particles motion in the catalyst mass or the support material (alumina beads).

In studies of SR of CH_4 over a reduced nickel based catalyst (18% wt NiO/ αAl_2O_3; reduction temperature= 973 K= 700°C), a 24% and 12% of conversion of the hydrocarbon (CH_4) and steam was achieved (33% vol CH_4: 67% vol $H_2O_{(g)}$) (**Matsumura et al., 2004**), The same investigators clearly showed the advantage of the present S:C ratio on the employed catalyst. In the present study higher X_{WCO} and X_{H_2O} were achieved despite a more complex hydrocarbons mixture.

The feeds of the waste cooking oil and the steam were stopped when all the dry reformate gases showed a constant production rate (**Figure 31(a)**). Following the SR step at 973 K (700°C) the product gases were allowed to leave the system. Prior to cooling down to 873 K (600°C), the reactor was purged in 100% N_2. Once the temperature of 873 K was established within the system, the steam reforming started, by feeding the steam at 423 K (150°C) and the preheated waste cooking oil

at 573 K (300°C). The dry reformate gases analysis of the FF step for S:C = 2.5:1 at T_{set}= 873 K (600°C) is illustrated in **Figure 31(b)**.

Marquevich et al. (2000) studied sunflower oil's steam reforming on a commercial nickel catalyst for naphtha steam reforming. They tested several molar steam to carbon ratios (3, 6, 9) at temperatures varying from 823 K (550°C) to 1153 K (880°C) and at near the atmospheric pressure. It was noticed that at the lowest temperatures and S:C = 3:1, the oil was not fully converted. In the same study, at 873 K (600°C) for S:C= 3:1 the H_2 concentration was just above 50%, which is in close agreement to the H_2 value of the present study for a S:C= 2.5:1 at 873 K as shown in **Figure 31(b)**. This is confirmed by the bio-oil and steam conversion results as shown in **Table 23,** which in the case of the steam reforming temperature at 873 K were lower by 28.9% and 8.2% from the respective values in the 973 K experiment.

Table 23 WCO and steam fractional conversions experimental and calculated equilibrium values and molar production rates of CO, CO_2, CH_4 and H_2 obtained experimentally at steady state over (i) reduced and (ii) oxidised catalyst at a set reactor temperature of 973 K. Rates $\dot{n}_i$ are in **μmol s^{-1}**. For all experiments, the molar input rate of carbon was $\dot{n}_{C,in}$= 526 μmol s^{-1}

S:C	X_{WCO}	$X_{WCO_{th,eq.}}$	X_{H_2O}	$X_{H_2O_{eq.}}$	$\dot{n}_{CO,out}$	$\dot{n}_{CO_2,out}$	$\dot{n}_{CH_4,out}$	$\sum \dot{n}_{C-prod}$	$\dot{n}_{H_2,out}$
reduced catalyst									
2.5	0.863	1	0.357	0.530	126	251	76	454	829
4	0.999	1	0.279	0.376	117	376	33	526	1069
oxidised catalyst									
2.5	0.574	1	0.275	0.530	189	104	8	312	653
4	0.933	1	0.275	0.376	115	347	29	491	1035

The first steam reforming for the S:C = 4:1 on a pre-reduced catalyst with H_2 was initially performed isothermally at 973 K (700°C) (**Figure 32(a)**). In the same step the temperature was lowered to 873 K (600°C) in order to perform near-isothermally the FF step. The higher fuel and steam conversion under at 973 K and S:C = 4:1 than at the lower ratio of 2.5:1 emphasized the benefit of the higher steam ratio. The following dry reformate analysis for the steam reforming under near isothermal conditions (T_{set}= 873 K) is shown in **Figure 32(b)**.

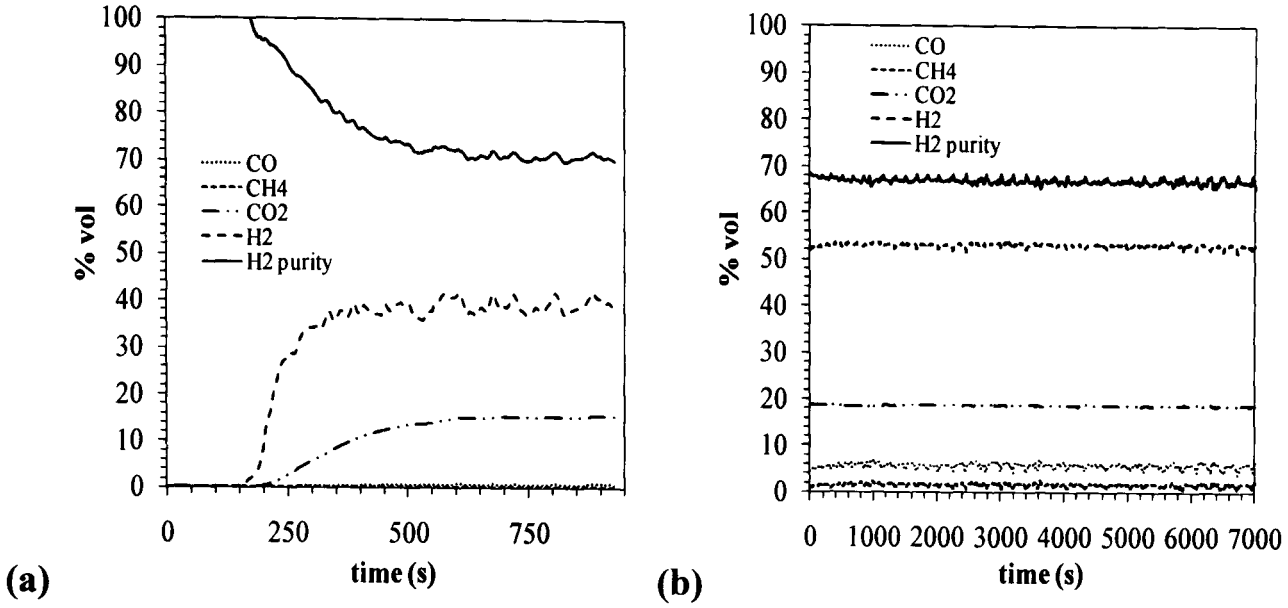

Figure 32 (a) Dry reformate analysis of the product gases during SR step on H_2-reduced catalyst at S:C= 4:1 at 973 K; (b) Dry reformate analysis on reduced catalyst for S:C= 4:1 at 873 K

The dry reformate analysis (**Figure 32(b)**) showed that the dry hydrogen content produced on the reduced catalyst at the set temperature of 873 K was 53.15% compared to the 38.97% of the set temperature of 973 K.

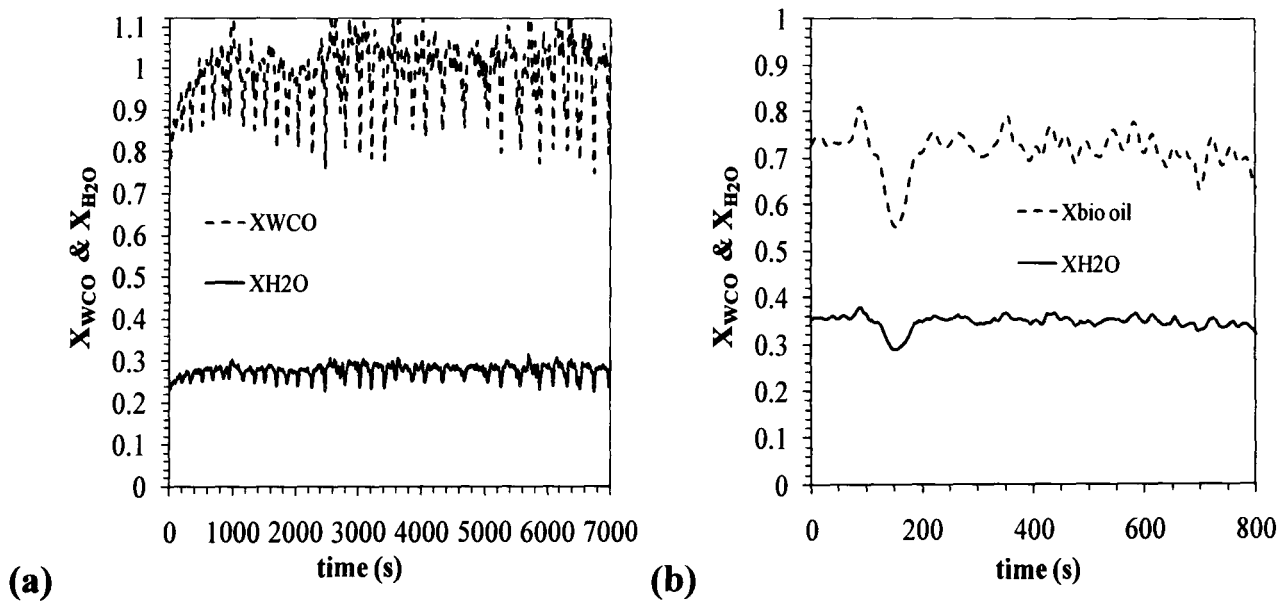

Figure 33 (a) WCO and steam conversion for S:C= 4:1 at T_{set}= 873 K; (b) WCO and steam conversion for S:C= 2.5:1 at T_{set}= 873 K

This can be confirmed by the waste cooking oil and steam conversions graph (**Figure 33(a)**). It can be clearly seen that for the first set of conditions' steam reforming step (T_{set}= 973 K; freshly H_2-reduced catalyst) the mean bio-oil

conversion (X_{WCO}) was 0.999 whereas for the second set of conditions (T_{set}= 873 K) the X_{WCO} was 0.990 (**Figure 33(b)**). Similarly the estimated steam conversions (X_{H_2O}) for the first (T_{set} = 973 K) and second (T_{set}= 873 K) steam reforming run were 0.279 and 0.277 respectively.

7.4.1.2 Steam reforming (SR) of waste cooking oil at S:C= 2.5:1 and 4:1 on oxidised catalyst

An air feed (AF) step was performed at the temperature of 873 K (600°C). The next steam reforming was conducted near isothermally on the oxidised catalyst first at 873 K (600°C) and then at 973 K (700°C) with purge steps in between.

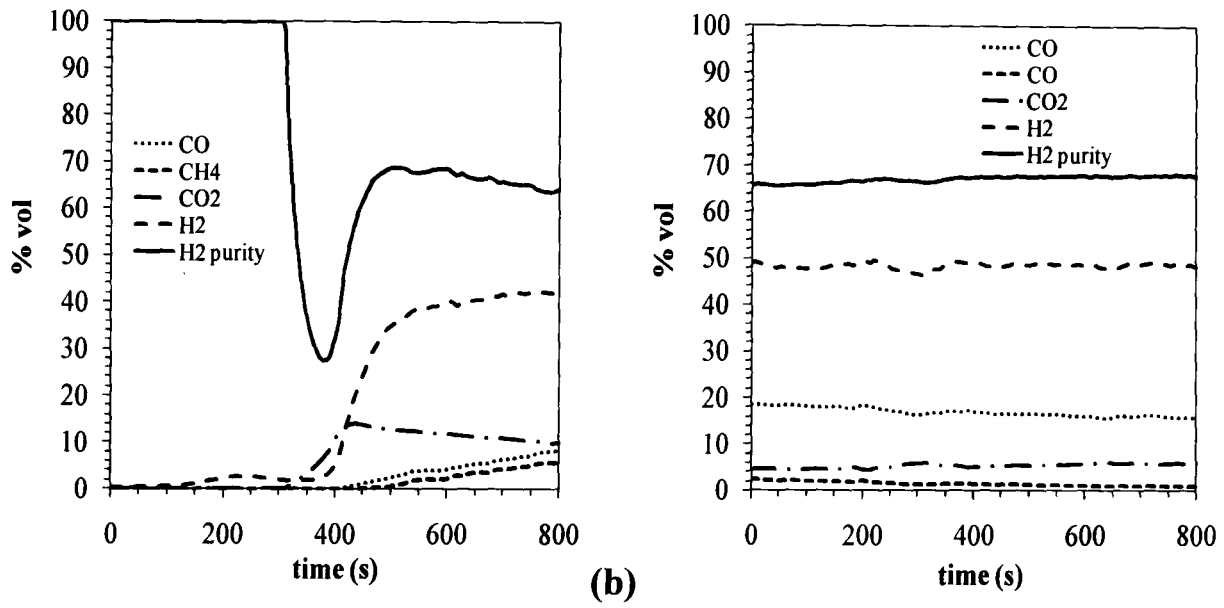

Figure 34 Dry reformate analysis on oxidised catalyst for S:C= 2.5:1 (a) at T_{set}= 873 K (600°C) and (b) at T_{set}= 973 K (700°C)

When isothermal conditions were achieved at 873 K, the steam reforming (S:C = 2.5:1) of the waste cooking was initiated and an oil mean conversion of 0.553 was obtained whereas the steam conversion was in average at 0.272. The CO and CO_2 % dry volumetric production indicated concentrations of 5.85 and 11.15 respectively, whereas the CH_4 exhibited a 3.69% when steady state conditions were established.

The SR step that followed was performed near isothermally at 973 K (700°C). The dry reformate gases analysis is shown in **Figure 34(b)**. The CO_2 dry volumetric concentration appears to decrease in favour of the respective ones for

CO and CH_4. This can be mainly attributed to the fact that the waste cooking oil's conversion was not achieved to the same extent as the H_2-reduced catalyst at the same temperature (**Table 23**).

From the same figure, it can be seen that the H_2 volumetric concentration, reached in average 47.67% for 973K, when on the oxidised catalyst at 873 K the average H_2 volumetric percentage was 41.38%. The average bio-oil conversion (X_{WCO}) during this step reached 0.574 and the average steam conversion was 0.275. Both conversions were at higher values than on the freshly oxidised catalyst at T_{set}= 873 K run (**Figure 34(a)**). The fact that the fuel's and steam's conversions did not reach the equilibrium values might possibly be due to the carbon deposition on the active catalyst sites. Additionally, the reverse water gas shift reaction might result in more CO than CO_2. This is supported by the values of $\dot{n}_{CO,out}$, $\dot{n}_{CO_2,out}$ and $\dot{n}_{CH_4,out}$ compared to the respective ones under the reduced catalyst run at T_{set}= 973 K (**Table 23**). The increased presence of CO in the end products' stream could result from the exothermic methanation reaction ($C + 2H_2 \rightarrow CH_4$). This would be possible since the conversion of WCO was incomplete in the previous FF step on the oxidized catalyst at 873 K and carbon deposition would occur on the catalyst's surface.

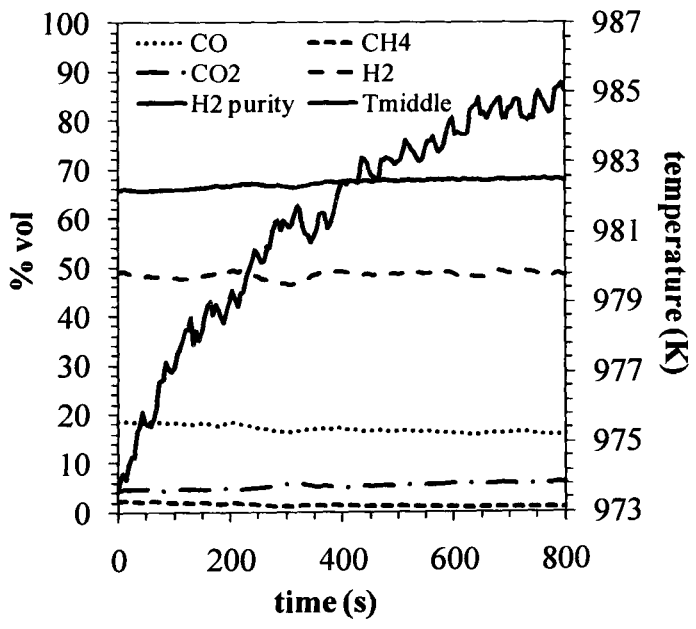

Figure 35 Dry reformate analysis of waste cooking oil steam reforming step on oxidized catalyst at S:C= 2.5:1 at 973 K (700°C)

The temperature increase of 15K from the set reactor temperature of 973 K was noticed (**Figure 35**) can be further attributed to H_2 production according to **R2**

$(C_nH_mO_k + (n-k)H_2O \rightarrow nCO + (n + \frac{m}{2} - k)H_2)$ since the OTM was sufficiently reduced. This reaction could be applied to C(s), CH_4, CO and H_2. Heat release would be expected to accompany **R2** around 973 K, in the case H_2 reacted with H_2O.

In **Figure 36** the first part of the steam reforming for a S:C = 4:1 on the oxidized catalyst at the set temperature of 973 K can be seen. The bio-oil conversion averaged in 0.933 (**Table 23**).

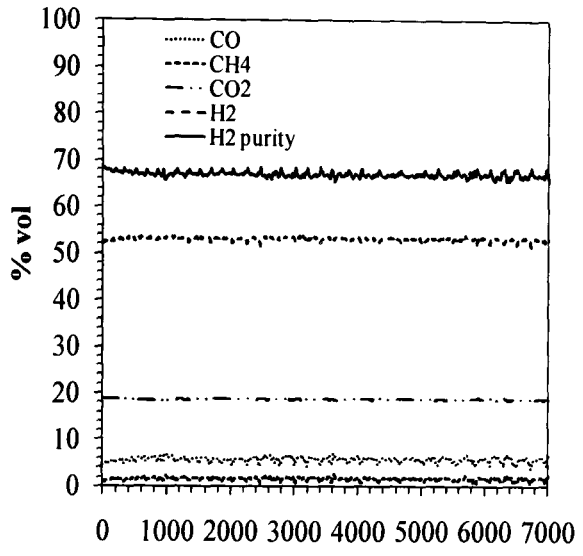

Figure 36 Dry reformate analysis of waste cooking oil steam reforming step on oxidized catalyst at S:C= 4:1 under isothermal conditions at T_{set}= 873 K

The temperature of the reactor's heating coil was then set at 873 K, after the feed of steam and fuel was stopped. The dry volumetric concentration of the product gases (**Figure 35**) showed that their values were close to those produced within the same FF step temperature range on the reduced catalyst (**Table 23**). The richer steam mixture allowed better yield of hydrogen and carbon dioxide at the lower temperature setting for the cases when the catalyst was reduced and oxidized. This partially agrees with the experiments of **Wang et al. (2007)** who steam reformed a crude biomass pyrolysis oil ($CH_{2.70}O_{0.50}{\cdot}0.79H_2O$) with a heat value of 17.42 MJ kg^{-1}, at different steam to carbon ratios over a wide temperature range (250- 750°C) by using C12A7-O^-/ x% Mg catalyst (% x weight percentage of magnesium in the prepared samples). The main conclusion was that the higher steam to carbon ratios at elevated temperatures increased the hydrogen yield. In

general, the higher steam to carbon ratio is expected to increase the hydrogen and carbon dioxide formation by shifting the equilibrium of the water gas shift reaction but temperatures above 600°C increasingly favour the reverse WGS, decreasing the H_2 yield.

The steady state results on the reduced and oxidized catalyst for the two different temperature settings of experiments in excess of steam at S:C= 4:1, showed no significant differences. The average WCO conversion within the range of 873 K on the partially oxidized catalyst was as equally effective (X_{WCO}= 0.934) while it was (X_{WCO}= 0.990) on the H_2-reduced catalyst. At T_{set}= 973 K on the reduced catalyst, the mean minimum bio-oil conversion was 0.999 while on the oxidized catalyst for the same temperature, the value attained was 0.993.

Therefore, regardless of the set temperature and the form of the catalyst (reduced or oxidised) the S:C of 4:1 exhibited a beneficial effect in the waste cooking oil's conversion which underlined the efficiency of the USR concept. The latter conclusion is of particular interest as the steam reforming of hydrocarbons on a NiO catalyst is known to be inactive, whereas in the present study it was shown to successfully steam reform the vaporized WCO resulting in steady gaseous production (H_2, CO_2, CO, CH_4) while it was being reduced by the fuel itself ('self-reduction'). The same parameters of X_{WCO} and of X_{H_2O}, for the lower S:C ratio (2.5:1), exhibited a large divergence in their value from the ones of SR on Ni or the initially oxidized Ni particles under the steam rich conditions (S:C= 4:1).

Czernik et al. (2007) performed steam reforming of a hardwood fast pyrolysis oil in a fluidized bed reactor using a catalyst of Ni, K, Ca and Mg at 1123 K (850°C) with a S:C = 5.8 resulting in a bio-oil conversion of 95% into H_2, CO_2, CO and CH_4. Therefore, the present commercial catalyst (18% wt of NiO on Al_2O_3) performed very well in its reduced and fully oxidised form for a moderate S:C ratio (4:1) and at a moderate temperature (T_{set}= 873 K, 600°C) in comparison to the previous studies (**Marquevich et al., 2000; Czernik et al., 2007**). Being able to operate at a lower temperature by 200°C and without H_2 pre-reduction must represent significant energy savings. This came as a result of using the USR process which alternates between FF and AF cycles and takes advantage of the benefits of the OTM (NiO) material. This will be further elaborated in **paragraph 7.5** in regard to the repeated cycles.

It is interesting to see that similar results of gaseous products concentrations (60% H_2, 10% CO, 20% CO_2, 10% CH_4) were produced by **Profeti et al. (2009)** who investigated steam reforming of ethanol for a water to ethanol ratio of 3:1 over Ni based catalysts promoted by noble metals ($NiPd/CeO_2–Al_2O_3$ and $NiPt/CeO_2–Al_2O_3$ respectively) at 873 K (600°C). The same investigators recorded the products composition was 55–60% H_2, 20% CO_2, 15–25% CO and 2–5% CH_4 when glycerol was steam reformed at 973 K (700°C). Therefore, the USR process can partially render a Ni catalyst as competitive as noble metals enhanced catalysts for the steam reforming of waste bio-oils.

Gornay et al. (2009) studied the steam reforming of a pre-treated mixture of vegetable oil and animal fat (from catering and food preparing) at 873 K (600°C) and at 1073 K (800°C) for a low steam to oil ratio (1.2:1) and at an average pressure of 1.12 bar. The oil, water, nitrogen or air were preheated at 573 K (300°C) and at the end, the product stream was composed of 45 mol% H_2, 14 mol% C1- C3 hydrocarbons for a steam to oil ratio of 1:2 and by 40 mol% H_2 and 27 mol% CH_4, ethylene and propylene for a steam to oil ratio of 1:1. Acetone tests for steam reforming at S:C= 5:1 and at 725 K (451.85°C) over Pt/ZrO_2 catalysts showed 100% conversion of the model bio-oil and of an approximately 67.5% average hydrogen yield after the first 40 min (**Takanebe et al., 2004**). As the results of the present study confirm the enhanced steam to carbon ratio can shift the steam reforming ratio (4:1) to lower temperatures (873 K) with an excellent conversion of the waste cooking oil with conversion into CO, CO_2 and CH_4, as the GC/FID on collected samples during the SR steps showed.

As expected, the higher steam to carbon ratio in the excess of steam, resulted in lower steam conversions. The best results in regard to the thermodynamic equilibrium were given by the experiments at the steam to carbon ratio of 4:1. These conditions were identified as the most appropriate for the chemical looping study.

7.4.2 Selectivity to the product gases in the FF steps on reduced and oxidised catalyst ($m_{i(fresh\ catalyst)}$= 80 g; S:C= 2.5:1 and 4:1)

The selectivity to the carbon containing products was also chosen as a parameter to underline the performance of the USR process during the fuel feed

step. The selectivity to the compounds formula in **paragraph 7.2.1** expresses the preference of the reactions involved in the FF step towards certain products (CO, CO_2 and CH_4). Based on this parameter the performance of the reactions during the steam reforming at a steam to carbon ratios (S:C) of 2.5:1 and 4:1 are evaluated.

7.4.2.1 Selectivity of the product gases in the FF steps ($m_{i(fresh\ catalyst)}$= 80 g; S:C= 2.5:1)

The selectivities of CO_2, CO and CH_4 in the S:C=2.5:1 at T_{set}= 973 K (700°C) over the H_2-reduced catalyst reached on an average of 60.0, 23.1 and 17.6 % respectively. During the steam reforming step at 873 K the average selectivity for CO_2 was 64.0 %, for CO was 26.6 % and for CH_4 it approached 10.0 % (**Figure 37(a)**).

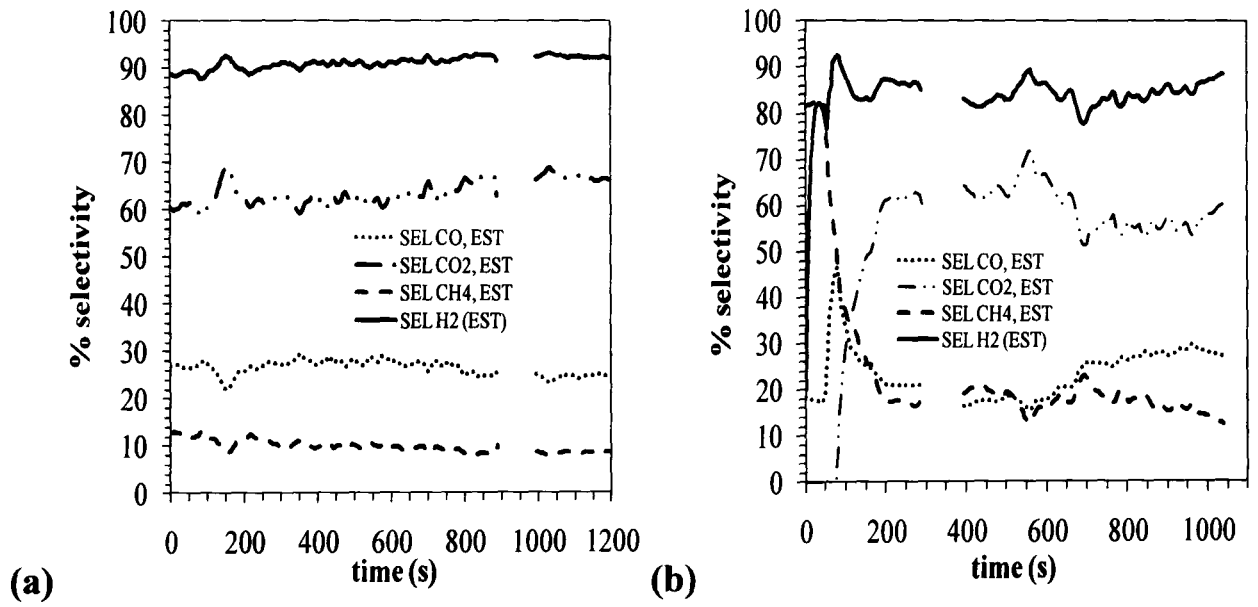

Figure 37 Selectivity to C-containing products CO, CH_4, CO_2 and H-containing products H_2, CH_4 (not shown) on H_2-reduced catalyst during steam reforming step in a S:C= 2.5:1 at (a) 873 K (600°C) and (b) 973 K (700°C)

For the S:C= 2.5:1 the higher temperature of 973 K showed that the FF step performance was enhanced, which is confirmed by the average bio-oil and steam conversions presented earlier in this **paragraph** (**7.4.1.1**). This was underlined by the selectivities of the produced gases (CO, CO_2, CH_4, H_2). In particular, the selectivity to hydrogen (H_2) from the H-containing products at 973 K was 85.2 and at 873 K it was 91.6 where the by-product was CH_4.

The selectivity to CO_2 during the steam reforming with the oxidised catalyst at the high temperature setting (973 K) was lower than that found at the lower temperatures, tested at 873 K. This is in agreement with the equilibrium of the water gas shift reaction, which, due to its exothermicity, is hindered at increasing temperatures.

The selectivity to hydrogen from the H-containing products (H_2 and CH_4) was 97.8% at T_{set}= 973 K on the oxidised catalyst , higher than that found at 873 K. The latter in conjunction by the lower selectivity to CH_4 (**Figure 37(b)**) compared to the reduced catalyst test indicated that the cracking of the hydrocarbons contained in the bio-oil was enhanced. On the other hand, the CO_2 selectivity was at a higher value on the H_2-reduced catalyst. This can be explained by the fact that the temperature during the first SR step on the H_2-reduced catalyst was within the range of 901- 943 K (average of 920 K or 647°C) due to the high energy demand of the organic compounds bonds breaking down, this might have enhanced the CO conversion into CO_2 via the water gas shift.

In general, the selectivity to gaseous products proved that the steam reforming of the waste cooking oil at the ratio of S:C of 2.5:1 on the reduced and oxidised catalyst performed more efficiently in the highest temperature setting (973 K, 700°C) in terms of bio-oil and steam conversions and of the selectivity to product gases.

7.4.2.2 Selectivity to the product gases in FF steps ($m_{i(fresh\ catalyst)}$= 80 g; S:C= 4:1)

The selectivity to C-containing products for the steam to carbon ratio of 4:1, on the H_2-reduced catalyst at 873 K (700°C) experiment were 95.4% for CO_2, 4.5% for CO, and 0.1% for CH_4, whereas the selectivity to the H-product H_2 was 99.9% (**Figure 38(a)**).

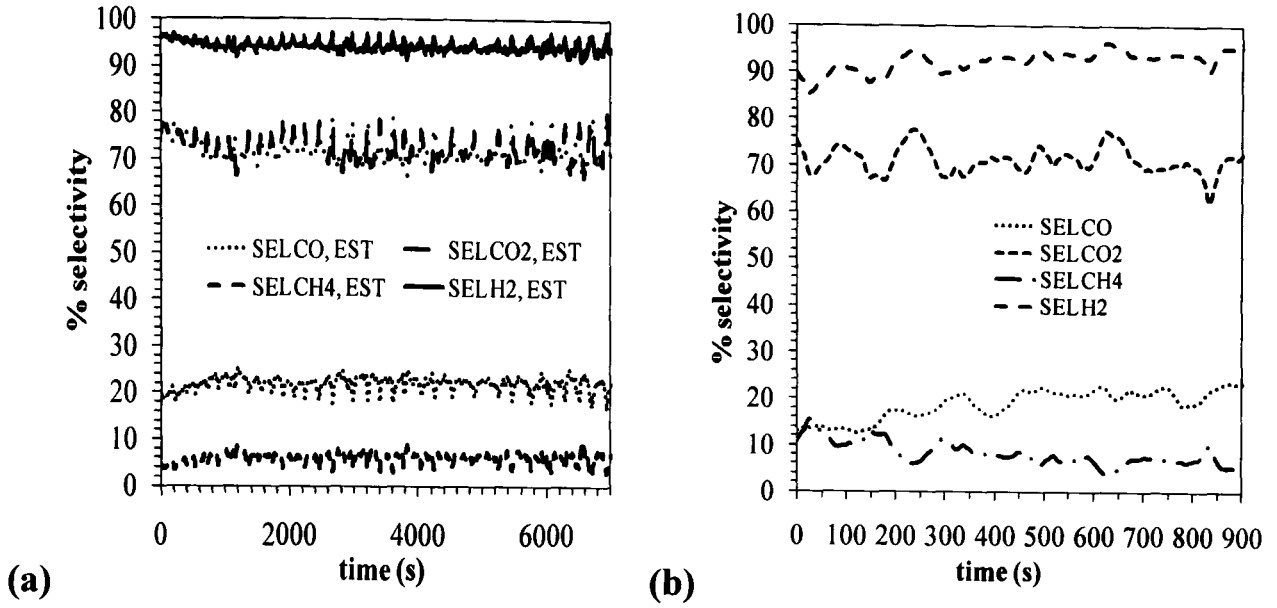

Figure 38 Selectivity to C-containing products (CO, CO_2, CH_4) and selectivity to H-product H_2 for FF step at 873 K (600°C) for S:C= 4:1, on (a) H_2-reduced and (b) oxidised catalyst

These results indicated that when the steam reforming step reached steady state, which is shown by the dry reformate analysis graph, it performed better at S:C of 4:1 under the same conditions of temperature and catalyst form than at 2.5:1.

At the initially oxidised catalyst SR run (T_{set}= 873 K; **Figure 38(b)**) for the same initial form of catalyst, the selectivities of the carbon containing gases were 72.0% for CO_2, 21.9% for CO, and 6.1% for CH_4, when for H_2 the selectivity of H-containing products was 94.38%. The initially oxidised catalyst favoured H_2 selectivity as the methane was further decomposed to CO_2. This may lead to the conclusion that the selectivity to CO_2 at the lower temperature was partly attributed to the decomposition of the hydrocarbons contained in the fuel as well as the CO_2 produced by the water gas shift reaction.

7.4.3 Oxidation (AF) steps following the FF steps at S:C= 2.5:1 and 4:1

In **Figure 39(a)** the volumetric concentration oxygen concentration is shown and the effect of the exothermicity of the nickel catalyst oxidation is reflected by the peak of temperature in the middle of the catalyst bed. The high flow of air (2000 mL min^{-1}) had the effect of flushing residual gases left by the previous FF

step. This occurred due to the pressure change in the reactor despite the previous purging step.

The temperature curve against time is drawn over the volumetric concentration of the recorded gases and can be read on the right hand side (y-) axis. The two peaks of the H_2 and CH_4 curves of the same shape, which appear for the same time interval, are due to the flushing of the previous FF step product gases. On the other hand, the CO and CO_2 curves geometry and duration are directly linked to the nickel and carbon oxidation reactions **R8, R9 and R10 (paragraph 2.3)**. The end of reactions during the air feed step was accompanied by the increase of oxygen from zero (0) to 21vol% as seen in **Figure 39(a),** where the primary y-axis indicates that the O_2 consumption has ended. The middle reactor temperature profile with time is drawn in **Figure 39(a)** as a red line which exceeded the set temperature of 873 K (600°C), due to the exothermicity of the oxidation reactions **R8-10**.

When the middle reactor temperature returned to the initial set temperature (873 K (600°C)) the termination of any reactivity between the oxygen and the nickel particles was confirmed.

During the catalyst's oxidation step, the CO_2 curve exhibited two distinctive sections. The first section (flushing section) (0 to 555 s) during which the reactor temperature was maintained close to 873 K (600°C), corresponded to carbon burning as carbonaceous residue deposited on the catalyst during the steam reforming of the waste cooking oil. The second section (chemical reaction section) (555 to 1125 s) is attributed to the catalyst's oxidation which was identified by the exothermic temperature curve that forms a peak of 400 K above the set temperature.

The gases analysis of the AF step that followed the FF step at S:C= 4:1 on the H_2-reduced catalyst, as recorded online, is shown in **Figure 39(b)**. Once again it was noticed that any initial oxygen consumption was due to carbon burning on the surface of the catalyst as in the described oxidation step succeeding the SR step at S:C of 2.5:1. This is clearly shown for the time interval from 0 to 455 s.

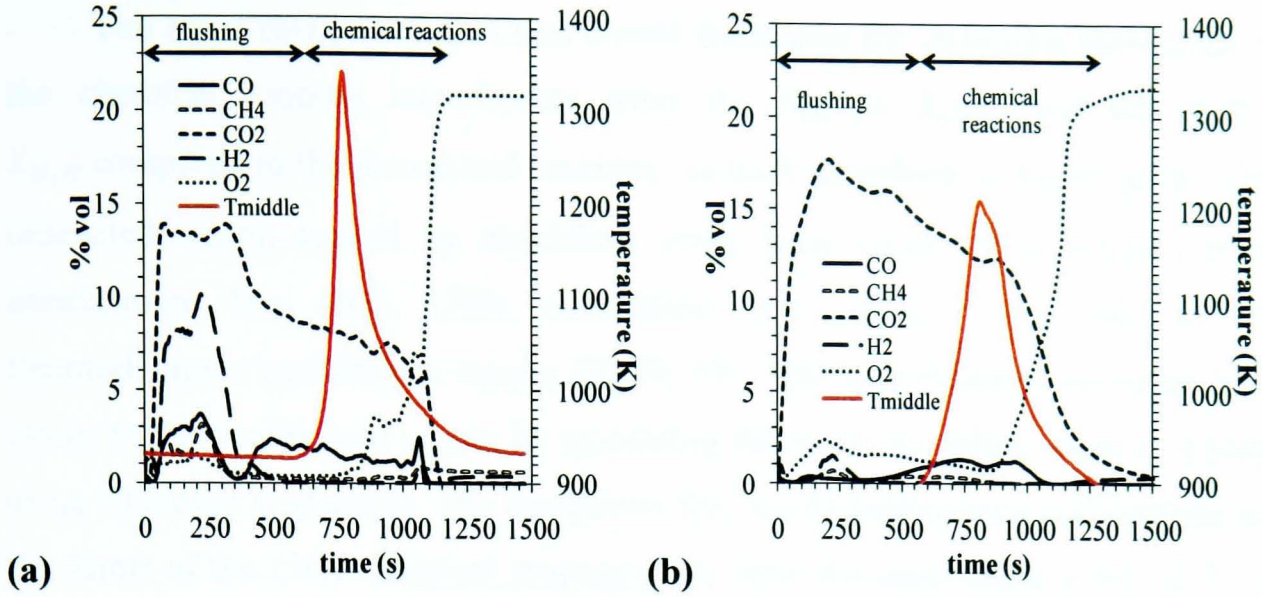

Figure 39 Products and reactor temperature profile under AF at T_{set}= 873 K (600°C) **(a)** following the S:C= 2.5:1 FF step; **(b)** following the S:C= 4:1 FF step. In both cases, the reactor's middle temperature (T_{middle}) is represented by the red line and read on the secondary y-axis

When the Ni particles started to oxidize, corresponding to the time period between 455 to 1310 s, the temperature in the middle section of the reactor reached a peak of an additional 316 K from the initially set temperature (873 K). During the oxidation of the catalyst, CO_2 was still being formed. This means that both the reactions of the Ni oxidation and of carbon burning occurred in parallel. The exothermic character of the nickel particles' oxidation reaction possibly helped with the activation of the carbon oxidation to CO_2 on the catalyst. Therefore the level of regeneration of the catalyst was further promoted.

It is counter-intuitive that the lower bio-oil conversions in the 2.5:1 FF step resulted in lower carbon depositions on the catalyst. These are expressed by the amounts of CO_2 and CO produced during the oxidation step chemical reactions' section compared to the respective AF step that followed the FF step at S:C of 4:1. The amount of CO_2 and CO evolved during the AF step via the reaction mechanisms (**R10**) and (**R9**) can be calculated by the integrating over time the rate of production of the respective gases ($\dot{n}_{CO_2,out}$; $\dot{n}_{CO,out}$). The maximum temperature during the AF step that follows the FF step at a S:C of 4:1 did not reach the peak value of the respective step that followed the steam reforming of the WCO at 2.5:1. This is directly related to the excess of steam that acts as a heat sink to the reactions exotherms.

The main two parameters that would determine the optimum conditions for the chemical looping experiments were the highest X_{WCO} and the highest X_{H_2O} compared to the theoretical maxima, as both contribute to the H_2 yield while unreacted steam, caused by conditions away from equilibrium, behaves as an unnecessary heat sink. This conclusion was further confirmed by the thermodynamic equilibrium results (**Table 23**). The experimental outcomes came closer to the equilibrium results by increasing the steam to carbon ratio, as a result of Le Chatelier's principle. The conditions that would better serve such criteria and the scope of the USR chemical looping study were the ones under a S:C of 4:1 at the set temperature of 873 K (600°C). The latter temperature was chosen as the most appropriate one from activity of the waster gas shift and with a view to future in-situ CO_2 capture.

In order to establish the promising results of the steam reforming step at 873 K (600°C) in a S:C environment of 4:1, a cyclic study for the unmixed steam reforming process was performed when 80 g of fresh catalyst was used over the course of one step of steam reforming on a fully H_2-reduced catalyst followed by five cycles on the subsequently oxidized catalyst under air flow feed (**paragraph 7.5**). In addition, a replicated stability study was performed by using half the mass of the fresh catalyst (40 g) by conserving the conditions and experimental set-up, as described in **paragraph 7.1**.

7.5 Effect of chemical looping of Ni-based catalyst for USR of waste cooking oil: effect of catalyst mass

Two sets of USR experiments were undertaken for the recyclability study; by using 80 g and 40 g of fresh catalyst. In the latter, by keeping the S:C= 4:1, the WHSV (Weight Hourly Space Velocity; **Eq. 34**) was at 5.28 h^{-1} compared to 2.64 h^{-1} for the 80 g of fresh catalyst runs. A repeatability study of 6 cycles for the unmixed steam reforming was performed for both cases of a fresh catalyst bed of 80 and 40 g. Furthermore, the experiments with 40 g catalyst allowed the optimisation of the unmixed steam reforming (USR) of WCO with sorption enhancement (featuring in-situ CO_2 capture), producing experiments of sorption

enhanced unmixed steam reforming (SEUSR) (**chapter 8**) where pure H_2 can be produced autothermally.

Six cycles of steam reforming and six oxidation steps were performed for this cyclic study in order to establish the initial results as discussed in **paragraph 7.4**. The chemical looping oxidation steps were performed at 923 K (650°C). Odd numbered steps (from 1 to 11) refer to the fuel feed (FF- WCO/ steam/ N_2) step and the even ones (from 2 to 12) refer to the air flow (AF) steps, i.e step 1 and step make up cycle 1, and steps 11 and 12 make up cycle 6. Purge N_2 steps were intermediate to the FF and AF steps. Due to small O_2 impurities in the N_2 flow which according to the manufacturer are 20 ppm, some small Ni oxidation might have occurred as described by reaction (**R8**). Additionally, the occurrence of Ni reduction and $C_{(s)}$ removal by reactions (**R10**) and (**R9**), was possible.

7.5.1 Effect of 80 g of NiO/ Al_2O_3 for 6 cycles of the USR at S:C of 4 and T_{set}= 873 K (600°C)

The initial step of the catalyst's reduction was performed under the same conditions (25% vol H_2/N_2; 873 K) as those mentioned in **paragraph 7.4**. The coupled steps of fuel feed and air feed that constitute a cycle of USR in the chemical looping experiments are separately discussed. The purpose of this discussion is to isolate the effect of the catalyst mass on the steam reforming reaction alone, separate from the potentially competing reduction reaction of the catalyst by the fuel.

7.5.1.1 Pre- reduction runs ($m_{i\,(fresh\ catalyst)}$= 80 g)

The dry reformate analysis of the catalyst's pre-reduction step is shown on the left hand side y-axis and the reactor's middle temperature is presented on the right hand side over time in **Figure 40.**

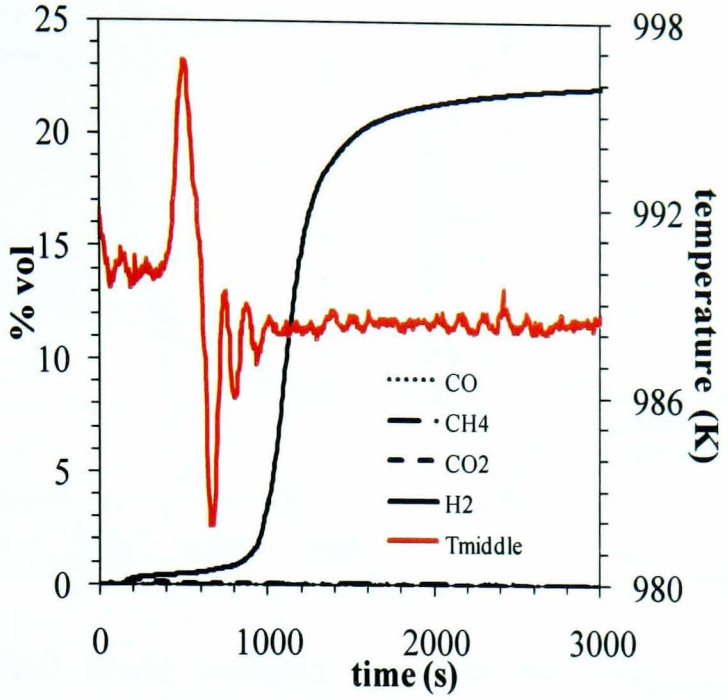

Figure 40 Dry gases analysis of fresh catalyst's ($m_{i\,(catalyst)}$= 80 g) reduction in 25% vol H_2/N_2 at 973 K (700°C)

Despite setting the temperature for the first reduction step at 973 K (700°C) a clear increase of up to 9 K between 265 to 725 s is shown in **Figure 40**. This exothermic effect may be attributed to steam ($H_2O_{(g)}$) production due to the reduction of the NiO molecules according to reaction **R6**. This is a main characteristic of the reduction of an oxygen transfer material (OTM) by hydrogen as mentioned by **Dupont et al. (2008)**,

$$NiO_{(s)} + H_{2\,(g)} \rightarrow Ni_{(s)} + H_2O_{(g)} \qquad [\Delta H < 0] \qquad \textbf{(R6)}$$

The extent of the fresh catalyst's reduction is represented by the rate of the NiO particles converted into Ni (**R6**). While the catalyst is reduced, $H_2O(g)$ molecules are formed. Based on this principle, the produced $H_2O_{(g)}$, not experimentally measured, can be calculated based on a hydrogen balance specifically for this pre-reduction step ,

$$\dot{n}_{H_2O,out\,(H_2,red)} = \dot{n}_{H_2,in} - \dot{n}_{H_2,out}. \quad \textbf{Eq. 36}$$

Therefore, the rate of reduction of the catalyst is as follows,

$$\dot{n}_{NiO\rightarrow Ni,red} = \frac{dNiO_{red}}{dt} = -\dot{n}_{H_2O,out\,(H_2,red)} \qquad \textbf{Eq. 37}$$

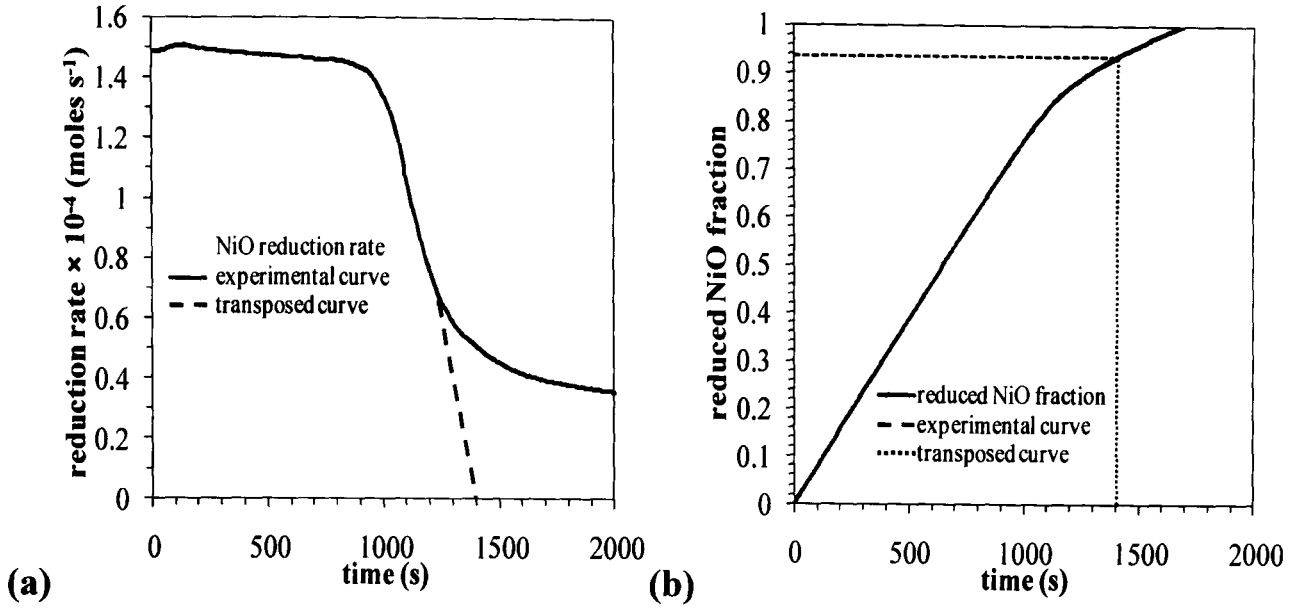

Figure 41 (a) NiO (fresh catalyst) reduction rate ($\dot{n}_{NiO \rightarrow Ni,red}$) in the duration of the reduction step (25% vol H_2/ N_2); (b) Molar fraction conversion of NiO to Ni ($X_{NiO \rightarrow Ni,red}$)

A transposed curve is used to determine the end-time of the catalyst's reduction when the curve's gradient decreases (**Figure 41(a)**) and then it would start to level off, which is represented as a dashed line of the same gradient as the original (experimental) molar reduction rate curve. This particular point in time (1500 s) is then applied in the experimental fraction of the NiO conversion curve (**Figure 41(a)**), in order to define the actual extent of the reduction of catalyst.

The area below the NiO reduction rate experimental curve, is given by integrating over time the rate of NiO reduction ($\dot{n}_{NiO \rightarrow Ni,red}$), which in turn yields the calculation of the fraction of the NiO particles' conversion,

$$X_{NiO \rightarrow Ni,red} = \frac{\int_0^t \dot{n}_{NiO \rightarrow Ni,red}}{n_{Ni}} = \frac{\int_0^t \frac{dNiO_{red}}{dt}}{n_{Ni}}$$

Eq. 38

The estimated time (t) the reduction was ceased, is indicated in **Figure 41(a)** by the transposed curve on the y- axis.

The $X_{NiO \rightarrow Ni,red}$ is presented in **Figure 41(b)** with respect to the elapsed time. It is evident that the calculated values above 1 are not realistic and can be attributed to the cumulative error in the oxygen balance arising from uncertainties in the experimental data (**Eq. 37**). By completion of the reduction step, the final fraction of NiO that was converted into Ni was 0.959.

7.5.1.2 Experiments under Fuel feed (FF) for $m_{i(fresh\ catalyst)}$ of 80 g

In **Table 24(a)** the mean conversion of the bio-oil and steam, the mean selectivity to carbon products (CO_2/CO/CH_4, and the vol % of H_2 in the syngas achieved at steady state, over the reduced and the upcoming oxidised catalyst are presented along with the reactor temperatures.

Table 24 (a) Chemical looping reforming outputs under FF (WCO/steam/N_2) step for an 80 g fresh catalyst load at S:C= 4:1 and WHSV of 2.64 hr^{-1}. H_2 concentration (%) is corrected for zero nitrogen (N_2)

							C-Selectivity		
catalyst (SR)	**cycle**	**step**	X_{WCO}	X_{H_2O}	T_{middle} **K**	**H_2 % vol**	**CO_2**	**CO**	**CH_4**
reduced	1	1	0.891	0.252	844	63.48	72.98	7.20	19.83
	2	3	0.737	0.197	833	63.71	76.71	5.45	17.84
	3	5	0.865	0.244	848	65.16	78.78	6.64	14.58
oxidised	4	7	0.794	0.205	825	64.08	79.24	6.45	14.32
	5	9	0.946	0.247	835	63.41	74.06	8.13	17.81
	6	11	1.030	0.269	839	63.48	72.72	9.70	17.59

(b) Thermodynamic equilibrium outputs under FF (WCO/$H_2O_{(g)}$/N_2) step for an 80 g fresh catalyst load at S:C= 4:1 and WHSV of 2.64 hr^{-1}

							C-Selectivity (%)		
catalyst (SR)	**cycle**	**step**	X_{WCO}	X_{H_2O}	**H_2 purity yield**	**H_2 purity**	**CO_2**	**CO**	**CH_4**
reduced	1	1	1	0.37	93.2	68.7	70	19	5.6
	2	3	1	0.36	93.7	68.0	70	17	5.4
	3	5	1	0.37	95.2	68.5	70	19	5.5
oxidised	4	7	1	0.36	95.1	67.4	69	16	5.4
	5	9	1	0.36	93.1	68.1	70	18	5.5
	6	11	1	0.37	92.4	68.7	70	19	5.6

Despite the variations in the conversions of the WCO (X_{WCO}) and steam (X_{H_2O}) from cycle to cycle, no worsening in the performance of the SR steps was shown in terms of the results achieved by the end of the 6th cycle. In particular, one can see from the second and third column respectively, that the reactants conversions X_{WCO} and X_{H_2O} increased from the 4th cycle to 6th cycle.

The selectivity of CH_4 is indicative of the extent of H_2 purity during the FF steps as long as it is the only hydrogen containing product among the carbonaceous ones. The minimisation of the CH_4 presence could be potentially achieved by maintaining the isothermal conditions at 873 K, hence a better control of the reactive system's temperature as addressed earlier. This could eventually push the experimental conditions towards equilibrium (**Table 24(b)**). The effect of the temperature drop in the catalyst bed during the steam reforming reactions was met by **Kumar et al (1999)** in their UMR (Unmixed Reforming) of methane study. They additionally mentioned the increase of CH_4 production and the decrease of that of CO in the product stream. In the present study the T_{middle} (**Table 24(a)**, 5th column) could not be maintained at the T_{set} (873 K) due to the highly endothermic reaction with the steam reforming of the bio-oil being predominant.

The oxidised catalyst at the beginning of the 2nd SR step (FF-step 2) was partially reduced in its duration as shown in **Figure 42(a)**. The extent of the catalyst's reduction during this second FF run in terms of the NiO particles rate (mol s^{-1}) is depicted in **Figure 42(b)**.

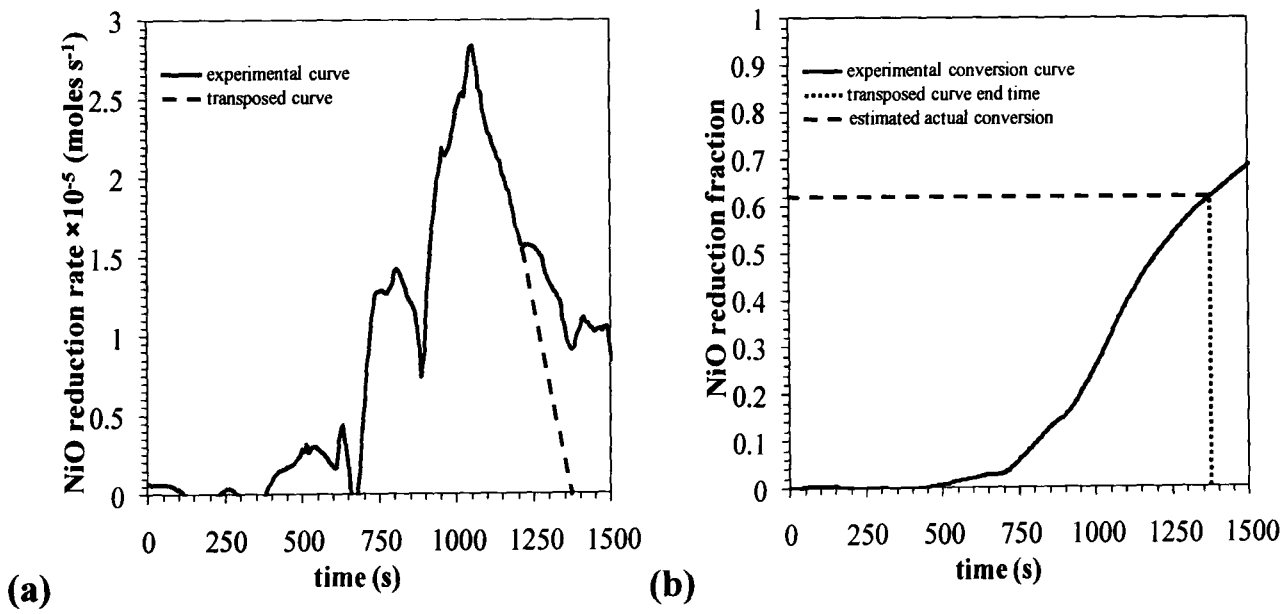

Figure 42 (a) Catalyst's reduction rate ($\dot{n}_{NiO\rightarrow Ni}$) and (b) fractional conversion of NiO to Ni ($X_{NiO\rightarrow Ni,FF}$) in the duration of the 2nd FF step ($WCO/H_2O_{(g)}/N_2$) under S:C= 4:1 for the $m_{i(catalyst)}$= 80 g chemical looping experimental set

7.5.1.3 Oxidation runs (AF) for $m_{i(catalyst)}$ of 80 g

Six oxidation steps (AF) were performed in the 80g catalyst chemical looping study. The rate of reduction of the catalyst and the NiO reduction conversion fraction during the SR step were determined as described in **paragraph 7.2**.

The AF step temperature was set at 923 K (650°C) hoping the latter would raise to temperatures which would promote the sorbent's regeneration step of calcination (as defined in **chapters 4 and 5**) in the SEUSR chemical looping experiments (**chapter 8**). Higher exotherms would be expected for the oxidation reactions **R8-R10** as they could potentially reach higher temperatures than 1123 K (850°C) as shown in the preliminary study (**paragraph 7.4.2**). It is of great significance to monitor the extent of the carbon burned during the catalyst's regeneration step (AF) as this is the key in sustaining its performance during the FF steps (**Kumar et al, 1999; Lyon et al, 2000**). Otherwise the carbon deposition can eventually deactivate and poison the catalyst.

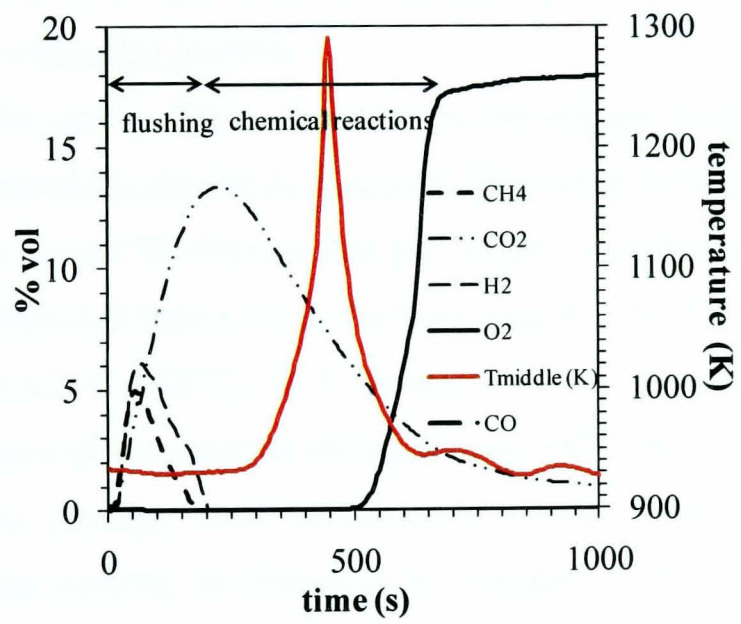

Figure 43 Dry gas analysis during a typical AF step (2nd cycle) following from the 1st $WCO/H_2O_{(g)}/N_2$ feed step for 80 g catalyst load and T_{set}= 973 K (650 °C). The middle-reactor temperature measurement includes the exotherm reaching 1290 K (1017°C) at 450 s

Figure 43 refers to the 1st oxidation step immediately following the second FF. The dry volumetric concentrations as recorded on-line during the oxidation step are presented coupled with the temperature in the middle of the catalyst bed. The

O_2 concentration measured was within the range of 0-18 vol%, rather than reaching the maximum value of 21 vol% in the air flow due to the residual CO_2.

At the beginning of this experimental section, three peaks of the dry gases concentration curves were formed. Two of them represented the H_2 and CH_4 curves which occurred solely due to the retention in the system of products from the preceding fuel feed step, whereas the third curve representing CO_2 was due to carbon deposited in the 1st SR being oxidised according to **R9**. During the time that the H_2, CH_4 and CO_2 curves (0-190 s) could be seen, the O_2 curve appeared to be at zero. This means that all the oxygen in the air that was supplied in the system was consumed. At the time of 240 s the CO_2 curve reached a peak, the middle catalyst mass temperature started to increase indicating that the oxidation of the catalyst was taking over (**R8**).

The previously described phenomena showed that the oxygen reacts first with the $C_{(s)}$ rather than with the Ni molecules. This is supported by the fact that the oxygen molecules are initially diffused on the catalyst's outer surface, as noticed by both **Haugrud (2003)** and **Mrowec et al. (2004)**. This makes the oxidation of nickel a diffusion controlled process.

Therefore, the carbon that is deposited on the catalyst's particles, due to the steam reforming reactions, has to be removed first via producing CO_2. Then there should be enough vacant Ni sites so that the catalyst's oxidation can be initiated. For a significant period of time (335 s) the temperature of the reactor was above the set temperature of 923 K (650°C) till it reached a maximum temperature of 1290 K (1017°C). In the case of the sorption enhanced unmixed steam reforming where the sorbent would be present, such temperatures would enable the regeneration (calcination) of the sorbent, as discussed in **chapter 8** and would decrease the effect of exothermicity of the Ni oxidation as the $CaCO_3$ thermal decomposition is an endothermic reaction (**chapter 4 and 5**).

The mol fraction of N_2 (y_{N_2}), based on the mol fractions of CO (y_{CO}), CO_2 (y_{CO_2}), O_2 (y_{O_2}) and CH_4 (y_{CH_4}) measured in the AF step (**Figure 43**) was calculated by using **Eq. 22** (**paragraph 7.2.2**). The total dry molar flowrate (mol s^{-1}) of the gases ($\dot{n}_{out,dry}$) that leave the reactor is calculated according to the N_2 balance that is based on the inlet N_2 molar flowrate ($\dot{n}_{N_2,in}$) (**Eq. 23**).

Generally, the molar rate of any product gas (i), can be calculated by,

$$\dot{n}_i = y_i \times \dot{n}_{out,dry}$$

Eq. 39

The aforementioned two separate phases (flushing and chemical reactions) during this step clearly enable the calculation of the catalyst's oxidation (chemical reactions section) as the rate of conversion ($\dot{n}_{Ni \rightarrow NiO}$) and the % Ni oxidation which are calculated by **Eq. 29 (paragraph 7.2.2)**.When the same equations are integrated over the time interval of the AF step, the total number of Ni moles that are oxidised to NiO and consequently the extent of Ni conversion to NiO, can be calculated,

$$X_{Ni \rightarrow NiO}\ (\%) = 100 \times \frac{n_{Ni,t}}{n_{Ni\ (i)}}$$

Eq. 40

where $n_{Ni,t}$ is the number of Ni moles that are converted to NiO at any time interval (t-0) and $n_{Ni\ (i)}$ is the total number of Ni moles in the catalyst. The rate of the carbon combustion under the mechanisms of carbon complete and partial oxidation is calculated by **Eq. 28**. The selectivity to the oxygen containing products of the AF step is given by **Eq. 31** with variations depending on the oxygen containing product.

In the figure that follows (**Figure 44**), the rate of the oxidation of Ni ($\dot{n}_{Ni \rightarrow NiO}$) and the extent of conversion ($X_{Ni \rightarrow NiO}\ (\%)$) of Ni under the same step are presented over time. These results correspond to the dry gases as presented earlier in **Figure 43**. The equations that were used to calculate the $\dot{n}_{Ni \rightarrow NiO}$ in the 2nd oxidation, took into account y_{O_2}, y_{CO} and y_{CO_2}after the initial flushing period (0-190 s). Therefore, in order to produce a complete Ni oxidation rate curve an extrapolation of this rate towards zero time should be performed. The linearity of the $\dot{n}_{Ni \rightarrow NiO}$ curve until its peak point, at 530 s, helped the interpolation between 190 to 530 s (from the end of the flushing period to the peak of the catalyst's oxidation rate time) and eventually the extrapolation to zero time.

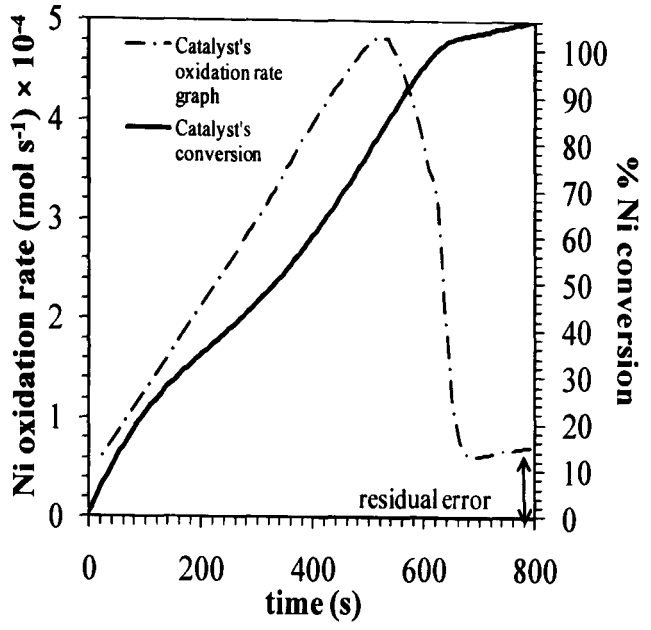

Figure 44 Rate of Ni oxidation to NiO ($\dot{n}_{Ni\rightarrow NiO}$) calculated with **Eq. 29** and extent of conversion of Ni to NiO (in %), for cycle 2 under air feed with an 80 g fresh catalyst load. Values for the rate prior to 190 s were linearly extrapolated to time zero, corresponding to syngas flushing period

The catalyst's conversion which reached a plateau at 100% would be expected from a fresh catalyst. A residual error (0.7×10^{-4} mol s^{-1}) was identified beyond the time of 680 s, as a result of cumulative errors in the O-balance. The error for the AF steps was smaller than the reduction rate of NiO moles for the FF steps as **Eq.29** for the $\dot{n}_{Ni\rightarrow NiO}$ carries fewer terms than the one used for the $\dot{n}_{NiO\rightarrow Ni,FF}$ calculations (**Eq.27**). The integration of the rate of Ni oxidation was limited to the time preceding the residual error, in order to determine the total number of the Ni moles converted to NiO. Therefore, the extent of the Ni particles' oxidation was limited to the time interval prior to the error. This means that the final conversion of Ni into NiO $X_{Ni\rightarrow NiO}$ was undervalued.

For the second AF step (3rd cycle), the $\%\,SEL_{CO}$ was at zero, while the $\%\,SEL_{CO_2}$ and $\%\,SEL_{NiO}$ started at 50% as soon as the flushing was resumed and finished at 11% and 89 % respectively. Therefore, the burning of the carbon deposits was complete and during the AF step CO_2 was produced which assisted the almost complete Ni oxidation. During this time, as the oxygen was under depletion, the conditions in the catalyst mass directed small amounts of $C_{(s)}$ towards incomplete oxidation which is identified by the low CO formation within the chemical reaction section. As the step proceeded, there was more available oxygen

due to the fewer remaining carbon on the catalyst particles which shifted the $C_{(s)}$ conversion to full oxidation.

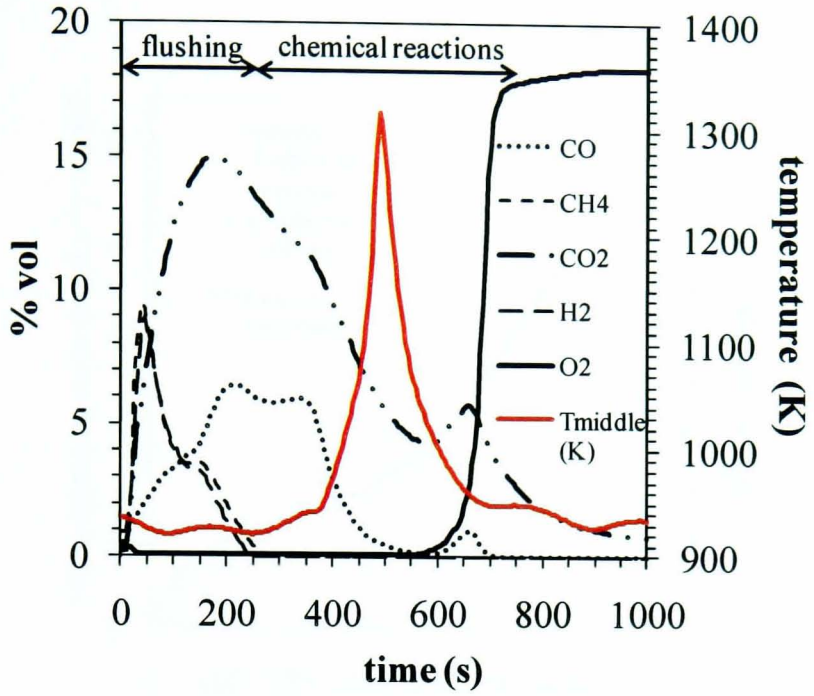

Figure 45 Dry gas molar concentrations during the 2nd air feed step (3rd cycle) following from the 3rd $WCO/H_2O_{(g)}/N_2$ feed step (with N_2 purge in between) for an 80 g fresh catalyst load and a set reactor temperature of 973 K (650 °C). The middle-reactor temperature measurement includes the exotherm of 1316 K at 490 s

In the second oxidation there was a considerable amount of CO produced. Indeed, the consumption of the supplied oxygen which aimed to burn the carbon deposits on the catalyst and to oxidise the Ni, created an environment of oxygen deprived conditions leading to the incomplete carbon oxidation which yielded the CO formation. As most of the $C_{(s)}$ was oxidised, more available O_2 molecules were present in the reactor in order for the full oxidation of carbon to be realised by producing CO_2, while the Ni oxidation became dominant because of the $C_{(s)}$ depletion.

It can be concluded that there is a primary preference of O_2 consumption for the solid carbon oxidation and a secondary one for the Ni particles' oxidation. This became well established during the catalyst's chemical looping performance.

The same methodology on producing the $\dot{n}_{Ni\rightarrow NiO}$ and Ni oxidation conversion curve over time as earlier was applied and resulted in **Figure 46**. It is clearly shown that the final Ni conversion reached 89.4 % when approaching

steady state instead of 100% compared to the 1st AF step, while the Ni oxidation rate (5.14×10^{-4} mol s^{-1}) reached a slightly higher value than the one in the 1st oxidation step (4.85×10^{-4} mol s^{-1}).

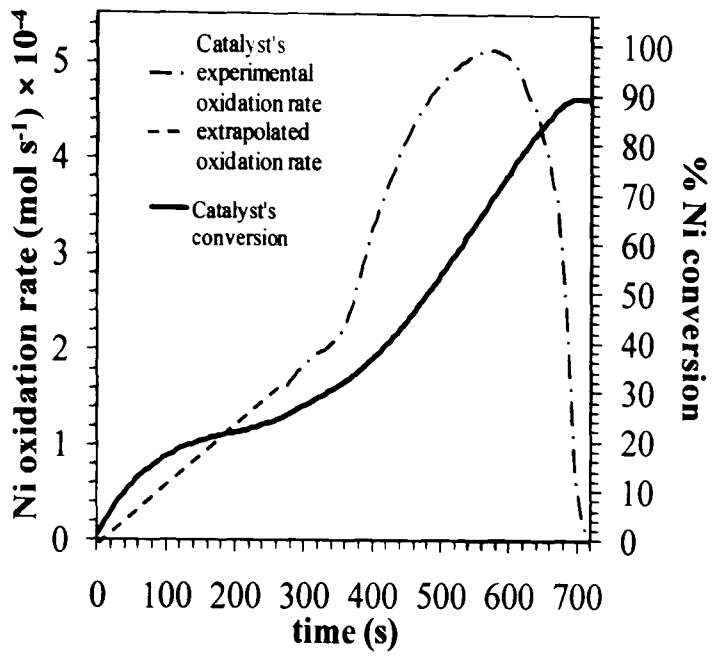

Figure 46 Rate of Ni oxidation to NiO ($\dot{n}_{Ni \to NiO}$ calculated with **Eq. 29**) and the extent of conversion of Ni to NiO (in %), for cycle 3 under air feed with 80 g fresh catalyst load. Values for the rate prior to 200 s were linearly extrapolated to time zero, corresponding to the syngas flushing period

The distinction of the flushing and chemical reactions interval within the 5 AF steps was evident except in the 6th oxidation step following the 6th FF step, due to the flushing period of the removal of the H_2 and CH_4, which lasted for the entire step. This made the application of **Eq. 29** impossible because the period of time for which it remains valid could not be isolated from the flushing period.

The NiO to Ni extent of conversions at the end of the FF steps were lower than the conversions of Ni to NiO at the end of the oxidation steps (**Figure 47**).

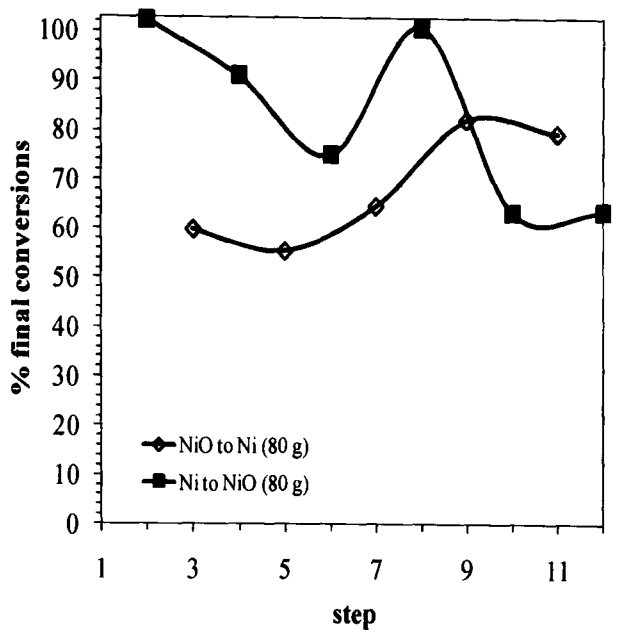

Figure 47 Extent of conversion of Ni to NiO during the air feed steps and extent of conversion of NiO to Ni during the $WCO/H_2O_{(g)}/N_2$ steps for the six cycles carried out with 80 g catalyst load

The Ni to NiO conversion in the 1st cycle was at 100% while in the 2nd and 3rd cycles it decreased to 91% and 76% respectively. It is interesting to see that by the 4th cycle it went back to 100% and eventually decreased to 64% by cycle 5. The extent of NiO conversion to Ni during the FF steps did not achieve the expected level as **Eq.27** carried larger errors.

Overall, the extent of conversion Ni↔NiO from the FF and AF steps over six cycles provided a credible picture in regard to the catalyst's performance as an oxygen transfer material. This is supported by the sequential curves of the reduced and oxidised catalyst's conversions which exhibited a mirror effect, which is in agreement with the concept of maintaining the catalyst's performance. The extent of the catalyst's reduction either at the pre-reduction ($\dot{n}_{NiO\rightarrow Ni,red}$) under H_2 flow, or during the FF steps ($\dot{n}_{NiO\rightarrow Ni,FF}$) carried errors as it is indicated from **Equations 37** and **27**. Despite this, the process and the methodology employed to assess its behaviour appear to be advantageous. Furthermore, the fact that the catalyst might have been reduced during the N_2 purge by direct reaction of C with NiO at the end of every FF run could contribute to eliminating the difference in the final conversions of NiO to Ni and Ni to NiO over the repeated cycles. This may be counteracted by some O_2 impurities in the N_2 carrier of up to 20 ppm. Thus the possibility of further reduction and oxidation of Ni from step to step exists.

Additionally, the NiO particles might be further reduced to Ni through the carbon surface eliminating reactions (**R10** and R9).

In total, the process may even yield an excellent performance if a better operation of the reactor's temperature was ensured for the FF steps, limiting the undesirable CH_4 by-product. This will potentially lead to equilibrium conditions for the steam reforming of WCO which will become more efficient as the residual CH_4 will be fully consumed. Additionally, less carbon would be deposited and eventually its oxidation during the AF steps and to a lesser extent during the N_2 purge steps would be eliminated. This would leave more available Ni sites to oxidise which will eventually increase the released rate of heat during the AF runs from which the USR and SEUSR can benefit.

7.5.2 Effect of 40 g of NiO/ Al_2O_3 for 6 cycles of the USR at S:C of 4:1, and T_{set}= 873 K (600°C)

A mass of 40 g of fresh catalyst was employed as a means of comparison for the 80 g runs as well as for the studied SEUSR (**chapter 8**) when the sorbent was present. Despite of these experiments' priority being the better understanding of the catalyst and sorbent performance when studying the SEUSR process, still it is interesting to identify the differences in performance of the catalyst in the USR process when the WHSV is doubled.

7.5.2.1 Pre-reduction step for $m_{(i)catalyst}$ of 40 g

At the end of the pre- reduction step the catalyst was fully reduced (**Figure 48**). The rate of reduction ($\dot{n}_{NiO\rightarrow Ni,red}$; **Eq. 37**) with half the initial mass of fresh catalyst, showed that it concluded within the same duration as the experiments with 80 g (**paragraph 7.4.1.1**).

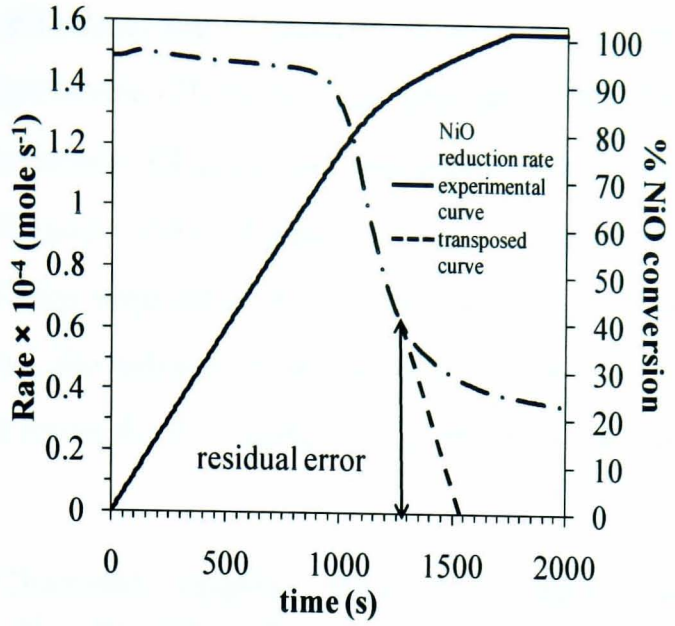

Figure 48 Rate of NiO reduction **to Ni ($\dot{n}_{NiO \rightarrow Ni,red}$) calculated** with **Eq. 37** and the extent of conversion of NiO to Ni (in %), for cycle 1 under hydrogen feed (25% vol H_2/ N_2) with 40 g fresh catalyst load

7.5.2.2 FF steps for $m_{(i)catalyst}$ of 40 g

The dry reformate analysis of the produced gases in the first SR on the pre-reduced catalyst, is presented in **Figure 49**,

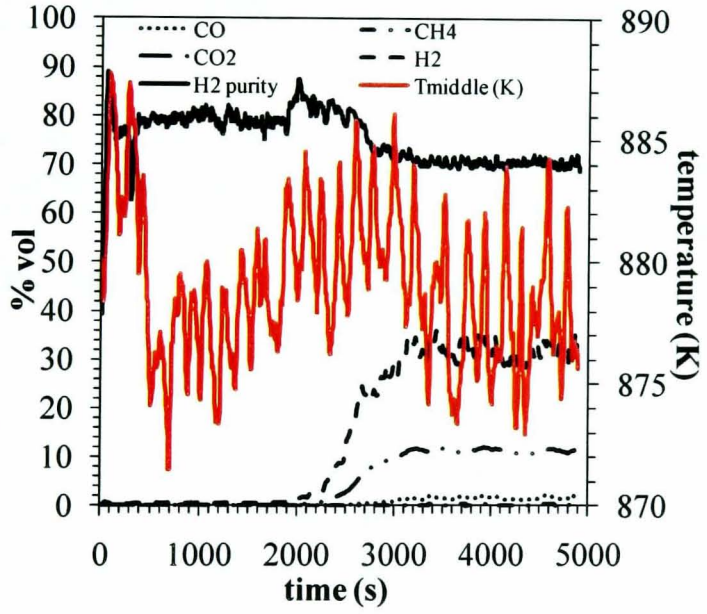

Figure 49 Dry reformate analysis of waste cooking oil steam reforming step on reduced catalyst and steam's conversion at S:C= 4:1 and WHSV of 5.28 hr^{-1} for 40 g at T_{set}= 873 K (600°C)

The dry gases % volumetric concentration clearly showed that they were lower than the respective ones in the 80 g experiments. The outcome of this direct comparison is due to the fact that the present gases were diluted in the same

flowrate of N_2. Nevertheless, the H_2 purity (%) when steady state was established, reached slightly higher levels (70.59 %) than with 80 g (64.12%).

The WCO conversion (X_{WCO}) and the steam conversion (X_{H_2O}) for the 1st cycle were at 0.194 and 0.067 (**Table 25 (a)**). These results showed that the efficiency of the FF step with 40 g of the fresh catalyst was much lower than with 80 g. During this step, the selectivity to the carbon containing products was higher for CO_2 and CO and lower for CH_4 compared to the 80 g runs for the 1st SR.

Table 25 (a) Chemical looping reforming outputs under the FF ($WCO/H_2O_{(g)}/N_2$) step for a 40 g fresh catalyst load at S:C= 4:1 and WHSV of 5.28 hr^{-1}. H_2 concentration (%) is corrected for zero nitrogen (N_2)

							Selectivity (%)			H_2
catalyst (SR)	**cycle**	**step**	X_{WCO}	X_{H_2O}	T_{middle} **K**	**H_2 % vol**	**CO_2**	**CO**	**CH_4**	**purity**
reduced	1	1	0.194	0.067	878	70.48	86.1	12.3	1.9	101.9
	2	3	0.213	0.066	858	68.93	80.3	16.1	3.6	99.1
	3	5	0.203	0.062	858	68.53	74.1	20.1	5.1	98.6
oxidised	4	7	0.200	0.058	860	67.28	69.7	23.0	7.5	96.6
	5	9	0.218	0.052	860	62.36	68.0	16.0	15.8	93.1
	6	11	0.205	0.066	866	68.79	69.0	23.0	7.4	98.6

(b) Thermodynamic equilibrium outputs under the FF ($WCO/H_2O_{(g)}/N_2$) step for 40 g fresh catalyst load at S:C= 4:1 and a WHSV of 5.28 hr^{-1}

						Selectivities (%)		
catalyst (SR)	**cycle**	**step**	X_{WCO}	X_{H_2O}	**H_2**	**CO_2**	**CO**	**CH_4**
reduced	1	1	1	0.37	69.2	70	21	5.6
	2	3	1	0.38	69.5	70	22	5.6
	3	5	1	0.38	69.5	70	22	5.6
oxidised	4	7	1	0.38	69.7	70	23	5.6
	5	9	1	0.38	69.6	70	22	5.6
	6	11	1	0.38	69.8	70	23	5.6

A temperature drop in the middle of the catalyst bed is noticed as in the 80 g runs. The magnitude was much smaller than in the experiments carried out with 80 g of fresh catalyst (**paragraph 7.4.1.1**) apparently due to the lower heat consumption involved in the steam reforming reaction. This can be seen from the lower conversions of the waste cooking oil and steam at 40 g than at 80 g. It is

interesting to note that in the study of **Marquevich et al. (2000)** for the steam reforming of sunflower oil, the catalyst bed reached a uniform temperature profile after 14 hours. Additionally, in the same study, any temperature drop in the reactor indicated the part of the catalyst bed where the conversion of the oil was close to completion due to the endothermicity of the involved reactions. Therefore, the temperature on the catalyst mass was not the limiting factor of the steam reforming of reactions' performance as expressed by X_{WCO} and X_{H_2O}, but it was the mass of the catalyst and consequently the WSHV which for these SR runs (**Table 25 (a)**) was halved compared to the 80 g runs.

7.5.2.3 AF steps for $m_{i(catalyst)}$ of 40 g

The dry gases composition of the air feed (AF) run following the 2nd SR, is shown in **Figure 50** where the two main reactive steps were noticed at an earlier point than in the 80 g study. The first curve indicates a flushing period for the gases produced in the second FF step and the following curve represents the onset of chemical reactions that incorporated the carbon and catalyst oxidations.

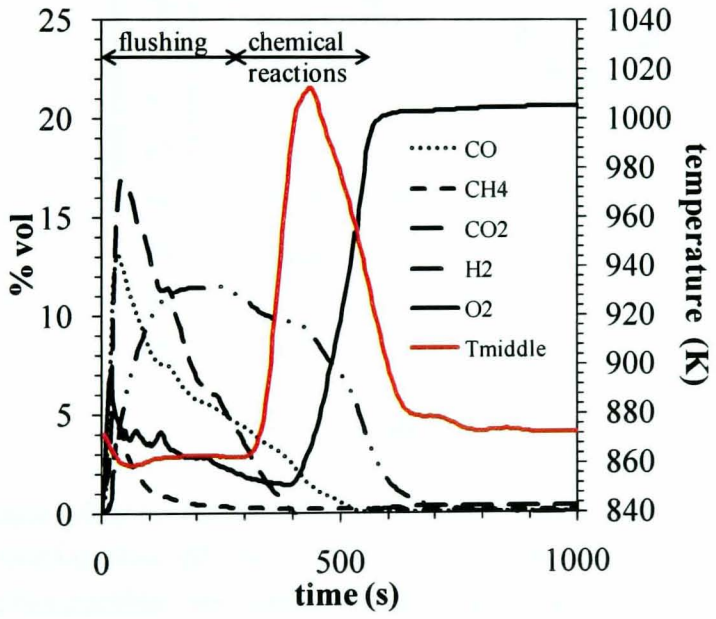

Figure 50 Dry gas molar concentrations during the 1st air feed step (2nd cycle) following from the 2nd $WCO/H_2O_{(g)}/N_2$ feed step (with N_2 purge in between) for a 40 g fresh catalyst load and $T_{set} = 923$ K (650°C). The middle- reactor temperature measurement includes the exotherm of 1010 K at 425 s

It is worth noticing that the O_2 curve exhibits an initial increase and then it appears to be more intensely consumed which was not noticed in the 80 g runs'

chemical looping AF steps. Additionally, the temperature during the AF steps did not reach the peak temperature of the 80 g runs that was above 1123 K (850°C) but a slightly lower one (**Figure 50**). This phenomenon can be further attributed to the fact that half of the mass of catalyst was employed, therefore the amount of the heat released during the highly exothermic Ni oxidation was less when less catalyst was present.

The AF steps ensured that any carbon deposited during the steam reforming step is removed primarily as CO_2 and secondarily as CO. The latter was outlined in the works of **Dupont et al. (2008)** and **Kumar et al. (1999)**. Hence the more active Ni sites were available at the end of the carbon burning phase the more Ni particles potentially would be able to react with the supplied O_2 via air. Therefore the extent of the oxidation of the Ni ($X_{Ni \rightarrow NiO}$ (%)) would determine the performance of the following SR of waste cooking oil steps.

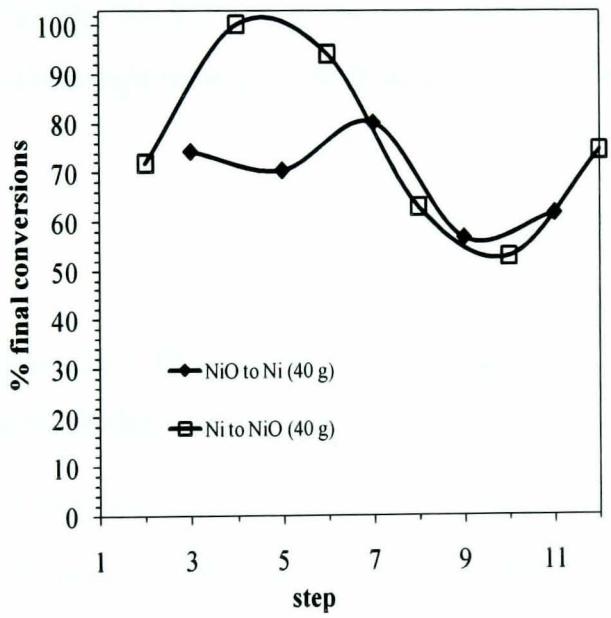

Figure 51 Extent of conversion of Ni to NiO during the air feed steps and extent of conversion of NiO to Ni during the WCO/$H_2O_{(g)}$/N_2 steps for the six cycles carried out with a 40 g fresh catalyst load at 600°C

The Ni particles during the 2nd, 4th and 6th steps, that correspond to the second, third and fourth cycle right after the 1st SR step on the reduced catalyst and the 2nd and 3rd SR steps on the oxidised catalyst, were oxidised to a large extent and resulted in conversions of the WCO in the range of 0.213 to 0.200 (**Table 25(a)**). On the other hand, the magnitude of the 4th and 5th oxidation steps which correspond to the 5th and 6th USR steps resulted in X_{WCO} of 0.218 and 0.205 (**Table**

25(a)). The final values of the Ni conversions to NiO signify the available OTM catalyst able to participate in the steam reforming steps (**Figure 51**). The NiO conversions to Ni (60- 80%) during the AF steps followed an oscillatory behaviour similar to the 80 g fresh catalyst chemical looping USR experiments. These oscillations express the compensating effect of the oxidative material's lower transfer from one cycle to higher transfer to the next USR cycle. Still this needs to be ascertained by powder XRD analysis (Rietveld refinement) at every cycle. Despite of the low fuel and steam conversions, the USR process appeared repeatable and sound.

Temperatures above 1100 K are of particular importance for the AF steps during the SEUSR since the sorbent is expected to be regenerated requiring high energy supply (highly endothermic reaction) and as the bench scale study indicated (**paragraph 5.4.2.2**). In a nutshell the performance of the USR process by applying half of the catalyst mass were far from equilibrium conditions as opposed to the experiments with 80 g for the FF step. This is attributed to the higher WHSV, which did not allow sufficient reaction time between the WCO and steam on the catalyst.

7.6 Summary of the WCO (Waste Cooking Oil) in the USR (Unmixed Steam Reforming) process

The WCO was preheated to 573 K (300°C) prior to entering the reactor, as decided from the conclusions of the oil's preliminary study in **chapter 6**. The USR of WCO was initially tested for two steam to carbon (S:C) ratios of 2.5:1 and 4:1. Both steam to carbon ratios conditions were tested for the FF (Fuel Feed) step on a pre- reduced and on a fully oxidised catalyst at 973 and 873 K (700 and 600°C). The best WCO and steam conversions were found for the S:C of 4:1 at 873 K (**paragraphs 7.4.1.1** and **7.4.1.2**). This temperature was the most appropriate for the successful operation of the sorbent (which will be discussed in **chapter 8)** and as corroborated by the conclusions of the macro-scale study under wet conditions (**chapter 5**), simulating the FF steps for the removal of the produced CO_2. The chemical looping reforming experiments of the WCO were performed for 6 cycles ; each cycle was comprised by a FF (Fuel Feed) and an AF (Air Feed) step. Two set-

ups for the USR chemical looping experiments of the WCO were tested; in the first one 80g of fresh catalyst was employed (**paragraph 7.5.1**), while in the second one half the mass (40 g) was used (**paragraph 7.5.2**). The first cycle's FF step was always performed on a pre- reduced catalyst in hydrogen flow, whereas the remaining five FF steps were done on an oxidised catalyst under the previous air flow. Thermodynamic equilibrium calculations were performed for the FF steps of the chemical looping experiments when 80 g (**paragraph 7.5.1.2**) and 40 g (**paragraph 7.5.2.2**) of fresh catalyst were used.

7.6.1 Effect of 80 g of fresh catalyst on the USR chemical looping experiments of WCO

The main findings from the 80g fresh catalyst chemical looping experiments at S:C of 4:1 are listed below,

- The FF steps (when the pre- reduced and oxidised catalyst was used) resulted in an almost complete conversion of the WCO (**Table 23**), which was very close to the calculated thermodynamic equilibrium value (**Table 24(a)** and **(b)**) in addition to the steam's conversions that were quite close to those indicated by the thermodynamic equilibrium study.
- By the end of the chemical looping experiments (by cycles 5 and 6) (**Table 24(a)**), an excellent conversion of the WCO was obtained
- Better temperature control of the catalyst's bed at the set reactor temperature can enhance the minimisation of the CH_4 and the CO produced. This can lead to conditions which are closer to equilibrium. Additionally, less solid carbon would be deposited on the catalyst which would leave more free Ni sites for oxidation during the AF step.
- The oxidation (AF) steps which occurred in between the FF steps were successfully concluded since they resulted in the carbon deposits' removal from the catalyst which was afterwards regenerated

to an OTM. Therefore, the mechanism of the catalyst's oxidation was implied to be diffusion controlled.

- In general, the estimated extent of conversion of Ni into NiO, during the AF steps was larger than that of NiO into Ni during the FF steps (**paragraph 7.5.1.3; Figure 47**). However the latter was most likely underestimated due to shortening the integration time for the rate of NiO reduction, due to a larger steady state error. In addition, there is the possibility of Ni reduction during the N_2 purge step which followed the FF steps via the reaction of $C_{(s)}$ with NiO. The performance of the catalyst as an OTM was confirmed as reliable, based on the mirror effect (**Fig. 47**) of the respective curves of Ni oxidation and NiO reduction

7.6.2 Effect of 40 g of fresh catalyst on the USR chemical looping experiments of WCO

- The conversions of the WCO during the FF steps on either a pre-reduced or oxidised catalyst, when 40 g was employed were much lower than in the 80g catalyst chemical looping experiments (**Figures 46** and **47**).
- The calculated WCO and steam conversions from cycle 1 to 6 were far from their thermodynamic equilibrium values (**Table 24(a)** and **(b)**). These results are attributed to the fact that the catalyst mass was halved.
- Higher selectivities of CO_2 and CO and lower selectivities of CH_4 were calculated during the FF steps than in the corresponding values of these compounds in the 80 g chemical looping experiments.
- Despite the temperature drop in the catalyst bed (**Fig. 49**) that was noticed, as in the 80 g catalyst mass tests, the limiting factor was found to be the catalyst mass and hence the WHSV which in this case was half than in the 80 g experiments.

- During the catalyst's regeneration (AF steps) the same mechanisms of oxidation via the full carbon oxidation, the partial carbon oxidation and the catalyst oxidation reactions (**Fig. 50**) were noticed as in the 80 g AF steps.

- The larger the extent of the catalyst's regeneration under AF was the better the yield of the following FF step was (**Fig. 51** and **Table 25(a)**).

- The cyclic behaviour of the 40 g of OTM between being reduced and regenerated states was very similar (**paragraph 7.5.2.3**; **Figure 51**) to that observed in the 80 g USR study (**Fig. 49**). Even though low WCO and steam conversions were achieved for40 g of OTM, the USR process appeared repeatable and reliable (**Fig. 51**). For the S:Cof 4:1 and when 80 g of catalyst were used, the chemical looping experiments for cycles 2-6 of USR confirmed the steady and consistent OTM's behaviour which was successfully reduced by the WCO during the FF steps at 873 K (600°C).

Chapter 8
Sorption Enhanced Unmixed Steam Reforming (SEUSR) of Waste Cooking Oil (WCO)

There is an intense interest at present in the chemical looping systems, which are mainly developed for the combustion industry and applied to the fluidized bed technology. Sorption enhanced steam reforming (SESR) is the process that incorporates sorption of CO_2 within the steam reforming process. In the present study, the metal oxide transfer of O_2 to the fuel (for the energy release associated with its combustion) and the in-situ capture of the resulting CO_2, as well as that produced by the water gas shift reaction, occur in a single fixed bed reactor. In practice, to achieve a continuous flow of hydrogen-rich syngas (>90 vol%), at least two reactors must be employed; one for the FF step to be realized with simultaneous adsorption of CO_2 while in the other the sorbent and the catalyst are regenerated. Using a single reactor results in an intermittent production of H_2. The advantage of the SEUSR process is that the oxidation step serves three roles: oxidizing the OTM (oxygen transfer material), removing the solid carbon present on the catalyst by burning it, and regenerating the sorbent by calcination, in order to produce its active part (MgO.CaO) ready for the CO_2 adsorption of the following FF step under reducing atmosphere.

Several researchers have worked on enhancing the steam reforming of CH_4 or bio-fuels in the presence of various sorbents. In their studies, they either used CaO-based or meta-based sorbents, and either in the presence of catalysts, or not, as well as various operating conditions. Their conclusions provided a basis for comparison with the results from the experimental work on the SEUSR of waste cooking oil, which is presented in this chapter.

Jakobsen et al. (2009) experimented on hydrogen production from methane for various operational modes of the reformer (i.e. as a fluidized bed reactor). It was deduced that when CaO was used as the sorbent compared to Li_2SiO_4 and Na_2ZrO_3, the CaO could cope with high flowrates of gases produced during the steam reforming for the CO_2 adsorption. From the same study it was also concluded that in order for the

CaO to perform desirably, the gases flowrates should be low or the reactor long enough to allow for a high yield hydrogen stream.

The biomass oil sorption enhanced steam reforming of phosphoric acid fuel cell (PAFC) was investigated in the study of **Iordanidis et al (2005)**. The bio-oil's main constituents were acetic acid, acetone, acetaldehyde, ethyl glycol, formic acid, formaldehyde and ethanol. The sorbent that was used was once again CaO which was applied at 923 K (650°C) and 10 atm, which were also the conditions of the steam reforming step. At atmospheric pressure and for a $H_2O_{(l)}$:C ratio of 4:1, the product gas consisted of 8-9% CO, 65-68% H_2, 22-23% CO_2 and 2-3 % CH_4. The processing of the product gas by CaO was presented in the temperature region of 923 K (650°C). The CaO performance was not presented over time while it was assumed that the CaO conversion after 10- 20 cycles dropped to 20% and remained stable.

Sorption enhanced steam methane steam reforming (SESP) was studied (**Solieman et al., 2009**) with CaO as the sorbent, at 600°C and 16 atm; while the steam to carbon ratio was 3 to 1. A simulation program for adsorption and desorption steps was applied by considering in the flowsheet a pre-reformer and a SERP (Sorption Enhanced steam Reforming Process) reactor in which both the sorbent and catalyst were present. The carbon capture ratio (CCR) was calculated to be 0.85. It was concluded that in order to achieve a CO_2 partial pressure of 0.0032 bar at 873 K (600°C), which was considered to be sufficient for improved CO_2 adsorption on CaO, the reforming pressure needed to be reduced to 4 bar or the S:C to be increased to 4.2.

It is worth mentioning that in all the above studies, the regeneration of the sorbent, i.e. the $CaCO_3$ conversion into CaO demanded additional heat in order to reach higher CO_2 desorption temperatures. In the SESR of the waste cooking oil, the temperature elevation was reached via the oxidation step due to the exothermicity of the nickel oxidation reaction, as it is confirmed in the following paragraphs (**paragraph 8.2.2**) and was indicated in **chapter 7** (**paragraph 7.5.1.3**).

Another study (**Johnsen et al., 2007**) on sorption enhanced steam methane reforming (SE-SMR) in a fluidizing environment was focused on the air jet attrition index (AJI) of dolomite when mixed with a commercial catalyst during the process.

Dolomite and limestone were tested together with a commercial catalyst using a gas air attrition apparatus. The results of these experiments showed that dolomite experienced the higher attrition with an AJI of 0.23 compared to that of limestone of 0.14. This meant that 23% of the initial sample fines were lost over a 5 h generation, rendering the dolomite less resistant than limestone over repeated cycles. This was attributed to the extra pore volume created by the decomposition of $MgCO_3$ present in the dolomite.

A dual fluidized bed reactors' system was built to work in parallel for the sorption enhanced steam reforming of methane (**Arstad et al., 2009**). Both reactors were loaded with a Norwegian natural dolomite powder and an alumina based nickel catalyst (NiO/ $NiAl_2O_4$) at a ratio of 80% to 20% vol. For the steam reforming, temperatures of 863- 873 K (590- 600°C) were applied while for the regeneration of sorbent those of 1183- 1193 K (910- 920°C) were used. All steps were performed at atmospheric pressure. The catalyst- dolomite mixture's initial weight was 135 g. During the process more mixture was introduced in the reactor due to attrition losses. From the regeneration step it was indicated that only 65% of the CO_2 produced during the steam reforming was actually adsorbed. These results came in contrast with the TGA study of this particular dolomite carried out by the same researchers who showed that for a specific contact time a particular CO_2 content would be adsorbed (**Arstad et al., 2009**).

Earlier **Hildenbrand et al (2006)** studied the CO_2 capture by CaO in a fluidized bed reactor for steam reforming of methane. They found that a high purity of hydrogen end product stream (up to 99% vol) resulted, which lasted for 8 min when methane was steam reformed at a S:C of 2:1 at a pressure of 5 bar and for isothermal conditions at 853 K (580°C).

In the work of **Dou et al. (2009)**, the sorption enhanced steam reforming of glycerol was studied. A S:C ratio of 3:1 produced a gas stream of H_2 purity of 68% at 873 K (600°C) in the absence of sorbent. When fully calcined, the naturally formed dolomite was used, mixed with a Ni catalyst at a ratio of 50:50 by mass, the product gas stream resulted in a H_2 purity of 97% vol at 773 K (500°C) for 3 $\frac{1}{2}$ hours while at 873 K (600°C) a product stream of 93% by vol of H_2 was produced for 4 hours.

In other studies (**Devi et al., 2005**) the enhanced catalytic activity of dolomite based catalysts was observed due to the porous matrix that the MgO.CaO could provide. **Basagiannis et al. (2007)** found that when Ni/Al_2O_3 catalysts were supported on MgO during the steam reforming of acetic acid, they exhibited a higher catalytic activity and a more stable behavior. Additionally, the alumina carrier (Al_2O_3) favours the carbon deposition while it retards the carbon deposition rate. Regardless of the Al_2O_3 behavior the addition of MgO in the Ni/Al_2O_3 reduced the carbon deposition.

The presence of either MgO or CaO in the structure of mineral oxide based catalysts enhanced the catalysts' performance as presented by other investigators (**Mastral et al., 2002; Myren et al., 2002**). It will be interesting to check whether in the present study this is also the case for the Ni catalyst's performance when in the presence of calcined dolomite.

8.1 Experimental set-up and analysis for the sorption Enhanced Unmixed Steam Reforming (SEUSR)

The SEUSR process performance was realised in the same reaction system as in the USR steps which were described in **chapter 2**. The major difference with the USR process is that a sorbent is also present among the catalyst particles in the reactor . Special attention was paid in the AF steps among the SESR (Sorption Enhanced Steam Reforming) cycles, which aimed not only to oxidise the OTM (Ni to NiO) in order to produce the heat necessary for the steam reforming of the WCO, but at the same time to regenerate the sorbent's active part for the CO_2 removal ($CaCO_3$ to CaO).

The results of the experimental runs in **paragraph 7.3** provided the most suitable conditions for the FF and AF steps in sorption enhanced unmixed steam reforming (SEUSR). In terms of the FF step, a S:C ratio of 4:1 exhibited the higher conversions for the bio-fuel (WCO) and for the steam, which agreed closely with the thermodynamic equilibrium calculations. When the AF step was performed under a high volumetric flow of air (2000 mL min^{-1}) at a temperature set at 923 K (650°C), the temperatures reached during the oxidation of the catalyst and its carbon deposits were

also expected to assist in the calcination of the sorbent. As discussed in **chapter 5** for the bench scale study of the sorbent, regeneration temperatures of the sorbent under dry and wet conditions were found to be above 930 K (657°C) (**paragraphs 5.3.1** and **5.3.2**) and were not concluded below 1090 K (817°C) under a 10 K min^{-1} heating rate when a flow of nitrogen at 750 mL min^{-1} was fed on the sorbent's bed.

8.1.1 Materials and scope of SEUSR

For the experiments presented in this chapter, 40 g of freshly ground catalyst (18% wt NiO/ Al_2O_3) and 40 g of fully calcined ground dolomite (MgO.CaO) were evenly mixed and loaded in the reactor. The particles sizes for the catalyst and the sorbent were the same as the corresponding ones in the USR runs (**chapter 7**) and the bench scale sorbent's study (**chapter 5**). The same sequence of fresh catalyst's pre-reduction in H_2 flow- FF- AF steps were followed as in the chemical looping USR experiments with the same flows of reactants (WCO, water and air), as well as the same pre-heat temperatures of the FF steps reactants, and at the set temperatures of 973 K (700°C)- 873 K (600°C)- 923 K (650°C) for the pre- reduction, FF and AF steps respectively. The three type K thermocouples were placed at the very top, middle and bottom positions as in the USR experiments (**chapter 7**).

Six full SEUSR cycles were performed in order to:

- Determine and realise the effectiveness of this chemical looping process.
- Assess the effect of the presence of the sorbent on the performance of the catalyst as compared to the 40 g of fresh catalyst experiments without sorbent (**paragraph 7.4**).

8.1.2 SEUSR calculations analysis

The description analysis through the mass balances relevant to the USR (**paragraph 7.2**) process needed to be revised, due to the additional reactions introduced by the sorbent's presence in the SEUSR process. Therefore, for the FF (fuel feed) step, the oxygen and carbon mass balances were altered for the additional

reaction of carbonation of the sorbent. The produced CO_2 from the SR reactions of the WCO was absorbed by the CaO particles which were intermixed with the catalyst. Similarly, for the AF step elemental balances, the rate of desorption of CO_2 from the sorbent's thermal decomposition should be incorporated.

The online dry gases analysis of the SESR (Sorption Enhanced Steam Reforming) steps indicated three sections of activity. The first one was related to the period of time the steam reforming reactions occurred while at the same time the produced CO_2 was fully adsorbed on the calcined dolomite. This first period correspond to CO_2 pre-breakthrough conditions (**PB**). In the second period, the sorbent appeared to become saturated, which covers the time when the CO_2 was recorded in significant concentration for the first time until it reaches a maximum, corresponding to the breakthrough period (BT). The third reactive section of the SESR (Sorption Enhanced Steam Reforming) step is going to be referred to as the steady state (SS) section as it is the one that refers to the SESR part when the carbon containing products (CO_2, CO, CH_4) concentrations reached steady state.

The division of the SESR steps into the PB (pre- breakthrough), BT (breakthrough) and SS (steady state) described sections was necessary for the application of the elemental balances during the time that the sorbent was active (PB). As there was no detection of CO_2 due to its capture on the dolomite (MgO.CaO), the direct calculation of the rate of carbonation ($\dot{n}_{CO_2,carb}$) was not feasible, nor as the determination of the WCO conversion for this time interval (PB). However, the WCO conversion could be calculated during steady state, as the carbon products were fully accounted for in the reformate gas, after sorbent saturation. (**Figure 52**). In this figure, the 'BT' and 'SS' periods have been compounded together into a single'post' breakthrough period.

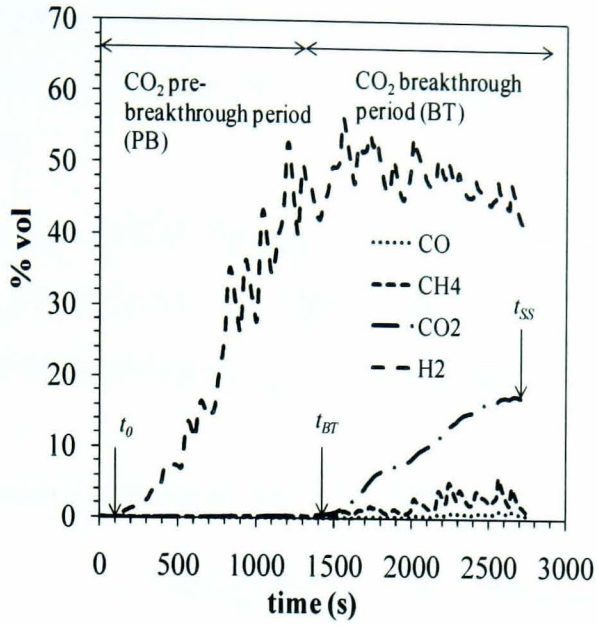

Figure 52 Division of the dry reformate gas analysis of the 1st SESR (Sorption Enhanced Steam Reforming) step (intermixed $m_{i(catalyst)}$ = 40 g and $m_{i(sorbent)}$= 40 g) to pre- breakthrough (t_{BT} - t_0) and post- breakthrough periods (t_{SS} - t_{BT}) depending on the sorbent's activity

During the breakthrough time interval (BT), the sorbent was still active but did not operate in its full capacity as some CO_2 was detected. As mentioned earlier, the bio-oil's (WCO) conversion calculation was possible once in the steady state (SS) period and is given in Eq. 41,

$$X_{WCO,SS} = \frac{\dot{n}_{WCO,in} - \dot{n}_{WCO,out}}{\dot{n}_{WCO,in}} = \frac{\frac{\dot{n}_{N_2,in}}{y_{N_2,SS}}(y_{CH_4} + y_{CO} + y_{CO_2})_{SS}}{n \times \dot{n}_{WCO,in}}$$

Eq. 41

The calculation of $X_{WCO,SS}$ is realised through the elemental balances of nitrogen and carbon as in the case of the USR process (**paragraph 7.2**). It was assumed that the minimum WCO conversion in pre-breakthrough and during the breakthrough time (BT) is the same as in the steady state period, yielding Eq. 42,

$$X_{WCO,PB} = X_{WCO,BT} \approx X_{WCO,SS}$$

Eq.42

Equation 42 neglects any enhancement effect that may have occurred during CO_2 sorption of the PB and BT periods, hence it is a minimum estimate for the conversion for these two periods.

Once the $X_{WCO,PB}$, hence $X_{WCO,BT}$, and the molar production rates of CO and CH_4 ($\dot{n}_{CO_2}$ and $\dot{n}_{CH_4}$) are known, the calculation of the molar production rate of CO_2 and hence the rate of carbonation ($\dot{n}_{CO_2,carb}$) is possible, as laid out in Eq. 43.

$$\dot{n}_{CO_2,carb} = X_{WCO,PB\ or\ BT} \times n \times \dot{n}_{WCO,in} - \left(\frac{\dot{n}_{N_2,in}}{y_{N_2,PB\ or\ BT}}\right) \times (y_{CH_4} + y_{CO} + y_{CO_2})_{PB\ or\ BT}$$

Eq.43

By integrating this equation over the whole carbonation period including the breakthrough period until steady state was reached (t_{SS}), a minimum estimate for the carbonation efficiency ($\alpha\%$) was calculated, and expressed as the ratio of the chemisorbed number of moles of CO_2 over the theoretical maximum molar CO_2 capacity of the sorbent, according to Eq. 44.

$$\alpha = 100 \times \frac{\int_0^{t_{SS}} \dot{n}_{CO_2,ads}\, dt}{n_{CO_2,max}}$$

Eq.44

The performance of the sorbent over the repeated chemical looping reforming cycles could be assessed, based on the calculated parameter α from **Eq. 44**.

Based on the same principle of the WCO conversion ($X_{WCO,SS}$; **Eq. 41**) calculation, an estimation of the steam conversion during the (PB) and (BT) periods was possible according to the hydrogen elemental balance,

$$X_{H_2O,PB} \approx \frac{1}{2\dot{n}_{H_2O,in}} \times \left[\frac{\dot{n}_{N_2,in}}{H_{SS}}\left(4y_{CH_4} + 2y_{H_2}\right) - m(\dot{n}_{WCO,in}X_{WCO,SS})\right]$$

Eq.45

The selectivity to the carbon containing product gases is given by **Eq.46**,

$$SEL_{CO\ or\ CH_4\ or\ CO_2} = 100 \times \frac{y_{CO}\ or\ y_{CH_4}\ or\ y_{CO_2}}{y_{CO} + y_{CH_4} + y_{CO_2}}$$

Eq.46

8.2 H_2 production by SEUSR of waste cooking oil

The SEUSR chemical looping experiments are discussed based on the sorption enhanced fuel feed steps and the air feed steps. The sorbent's participation in CO_2 removal can be used to discuss the promoted WCO and steam conversions and the overall performance of the process.

8.2.1 FF steps

The 1st SESR (Sorption Enhanced Steam Reforming) step was performed on a pre-reduced catalyst under H_2/N_2 flow. The dry volumetric concentration of the product gases as recorded by the Advance Optima (AO2000 Series) gas analyser are presented in **Figure 53**.

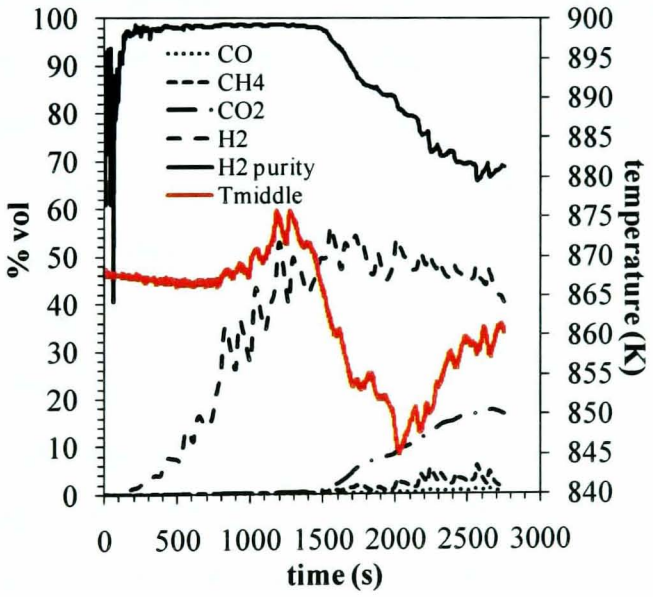

Figure 53 Dry reformate gases concentrations with time on stream of the 1st SESR (Sorption Enhanced Steam Reforming) step at $\boldsymbol{T_{set}}$= 873 K and S:C= 4:1 with intermixed $\boldsymbol{m_{i\ (catalyst)}}$= 40 g and $\boldsymbol{m_{i\ (sorbent)}}$= 40 g. The graph includes the H_2 purity and middle reactor's bed temperature ($\boldsymbol{T_{middle}}$; read on the secondary y-axis)

The purity of hydrogen ($\eta_{H_2 purity}$) in respect to the product gases, as defined by **Eq.35 (paragraph 7.4.1.1; chapter 7)** reached 98.6% for 255 s when the steam reforming of the reactants reached steady state. The CO_2 volumetric concentration (% vol) in the product stream was at zero until 1435 s from the start of the run as shown in **Figure 53**.

The increase of the measured mid-reactor temperature $\boldsymbol{T_{middle}}$ from the set temperature $\boldsymbol{T_{set}}$ (secondary (right hand side) y- axis) prior to the CO_2 - curve breakthrough at 710 s was caused by the chemisorption of the CO_2 from the SR reactions. The sorbent started to become saturated at 1435 s, which signified the onset of breakthrough (BT) point and reached saturation by 2800 s. The breakthrough (BT) interval began when the CO_2 curve was initiated. The CO_2 breakthrough was accompanied by a sharp drop in temperature which continued through the entire breakthrough period. It is worth noticing that the temperature drop in the present reactive system (SESR) was larger than in the 40 g fresh catalyst experiments without sorbent (**paragraph 7.5.2**). This observation confirms the enhanced WCO and steam conversions which are presented later (**Table 29; paragraph 8.3**) as the highly endothermic SR reaction (**SR**) demands a large power consumption which was not observed in the 40 g fresh catalyst chemical looping experiments. Nevertheless, when the sorbent was deactivated, the H_2 purity curve returned to the values of 68% as in the 40 g fresh catalyst runs when the sorbent was absent (**paragraph 7.5.2.2**). The reactor bed's temperature ($\boldsymbol{T_{middle}}$) started to recover by the middle of the breakthrough period. When a steady state CO_2 curve was established, $\boldsymbol{T_{middle}}$ returned to the vicinity of 873 K, with the lowest at 846 K, as in the 40 g only catalyst runs when steady state was reached (**paragraph 7.5.2.2**).

A very important aspect of the SEUSR step was derived from the previous graph (**Figure 53**). It was not only that any produced CO_2 was adsorbed, but additionally no CO and CH_4 were observed which is indicated by the CO and CH_4 curves. This was expected from Le Chatelier's principle, where the suppression of the CO_2 product from the gas stream promoted the water gas shift and, from the resulting decrease in CO, also the promotion of the steam reforming reactions, with as a result, the disappearance of all the carbon-containing gases from the product. Once the sorbent reaches its

saturation limits (breakthrough point; t_{PB} in **Figure 52**) all the carbonaceous products from the WCO steam reforming reactions started to be recorded on-line.

The extent of the WCO and steam conversions was based on **Equations 41**, **42** and **45**. These equations were applied from the point that the sorbent starts to become saturated (t_{BT}) and the exothermic reaction related to the CaO conversion to $CaCO_3$ (**CB**), as indicated by the T_{middle} recordings (**Figure 53**), was stopped. The sorbent's saturation starts when any CO_2 appears in the dry gases graph whereas hydrogen production has already begun.

During the SEUSR experiments, the % power input to the reactor system was logged in among the three reactor's bed (sorbent- catalyst) temperatures. The maximum power input to the heating element surrounding the reactor was 1 kW. Therefore the % of the recorded power input expresses the percentage of its maximum value (1 kW).

The % power ratio is an expression based on the % maximum power per unit time (s) ($\%\max power$) input during the run that can be supplied to the reactive bed (sorbent-catalyst) in order to maintain the set temperature (T_{set}) through the reactor walls,

$$\%\, power = \frac{\%\, power_{\,(t)}}{\%\max power} \times 100$$

Eq. 47

where $\%\, power_{\,(t)}$ is the % power input per unit time (s).

The following graph (**Figure 54**) corresponds to the % power ratio with respect to the exothermicity of the CO_2 adsorption as indicated by the reactor's middle temperature (T_{middle}) during the 1st SESR step.

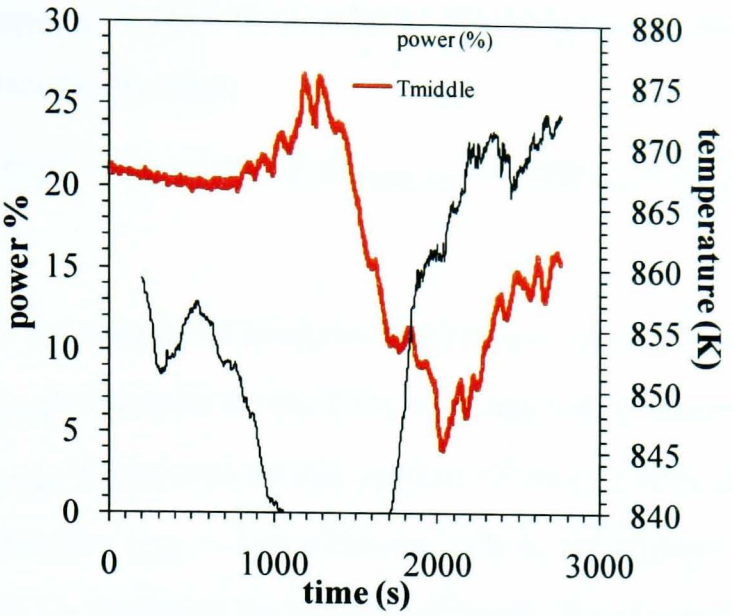

Figure 54 Percentage input in the reactive system (% power) based on a maximum of 1 kW coupled with the middle reactor's bed temperature (T_{middle}) in the duration of the 1st SESR (Sorption Enhanced Steam Reforming)

The % power ratio was used to quantify the power (kW) that was supplied to the reactive bed in order to relate the power requirements of the system when exothermic reactions are involved in the course of this step. There was indeed evidence that there was no power supply during the chemisorption of the CO_2 on the sorbent (**Figure 54**). This observation was a clear indication of the ability of the system to support itself in terms of energy, for the implementation of the steam reforming on the hot catalyst bed. This was valid before the sorbent began to saturate ($(t_{BT} - t_0)$= 650 s; **Figure 52**).

The carbon products and hydrogen selectivities were calculated once the breakthrough CO_2 curve started to appear for the same reason as mentioned earlier for the X_{WCO} and X_{steam}. This was due to the fact that during the steam reforming step CO_2 was produced and at the same time, captured by the sorbent via the carbonation reaction. The difference in time between the onset of the H_2 curve which is when the steam reforming reactions commence and the onset of the CO_2 curve which appears after t_{BT} in **Figure 52,** is expressed by the term $dt_{100\%\,CO_2}$,

$$dt_{100\%\,CO_2} = t_{SS} - t_{BT}$$

Eq.48

The term $dt_{100\%\,CO_2}$ is applied in order to determine the sorbent's capacity when the CO_2 curve reaches steady state,

$$\%\ sorbent's\ capacity\ at\ dt_{100\%\,CO_2} = 100 \times \frac{n_{CO_2\ captured}}{n_{CaO\ (i)}}$$

Eq. 49

with $n_{CaO\ (i)}$= the amount of available CaO mol in the sorbent to capture CO_2 and $n_{CO_2\ captured}$= the term for the CO_2 mol captured by the sorbent.

The $n_{CO_2\ captured}$ is the sum of the number of mol of CO_2 captured during the pre-breakthrough time (for $(t_{BT} - t_0)$; when the CO_2 % vol appears to be zero) and the number of moles of CO_2 produced during breakthrough (for $(t_{SS} - t_{BT})$),

$$n_{CO_2-captured\ (total)} = n_{CO_2\ pre-breaktrhough} + n_{CO_2\ breakthrough}$$

Eq.50

The same effect of the sorbent's presence was noticed in all 6 SESR steps.

The efficiency of the sorbent as described in **paragraph 8.1.2** and represented by **Eq. 44** was divided into pre-CO_2 breakthrough and a post-CO_2 breakthrough period (where the latter includes breakthrough and steady state) as seen in **Figure 52**. The sorbent's performance for the pre-breakthrough time from t_0 to t_{BT} is defined as α_{PB}. The term α_{BT} was introduced for the carbonation efficiency between the time of CO_2 breakthrough (t_{BT}) and the time the sorbent reached its full capacity (t_{SS}) which was when steady state conditions were achieved. Therefore, the overall efficiency of the sorbent during the SESR step is determined by the following equation,

$$\alpha = \alpha_{PB} + \alpha_{BT}$$

$$= 100 \times \frac{\left(X_{WCO,PB} \times n \times \dot{n}_{WCO,in} \times (t_{BT} - t_0)\right) + \int_{t_{BT}}^{t_{SS}} n_{CO_2,ads,BT}\, dt}{n_{CO_2,max}}$$

Eq. 51

Since there was no production of CO, CH_4 and CO_2 in the pre-CO_2 breakthrough period, the sorbent efficiency is presented in its simplified form **Eq.51**. The sorbent was fully pre-calcined natural dolomite ($MgCa(CO_3)_2$; Warmsworth quarry) and was employed in its active form of MgO.CaO for the 1st SESR step. Since the sorbent's (MgO.CaO) mass was weighed to be 40g and the CaO mass fraction in the natural

dolomite to be known as 0.307, it was possible to calculate its maximum CO_2 adsorbing capacity ($n_{CO_2,max}$= 0.417 mol) based on the carbonation reaction (**CB**).

The main interest in distinguishing the sorbent's efficiency behaviour into pre- and during CO_2 breakthrough periods relies on the fact that in the first period, the H_2 purity was at 100%, whereas in the second period, the H_2 purity steadily decreases. Finally it reaches steady state conditions identical to those of the SR steps in the absence of the sorbent (**paragraph 7.5.2.2**).

In the PEMFC (Proton Exchange Membrane Fuel Cell), hydrogen purity is an important parameter since any CO presence in the H_2 reformate may poison the fuel cells while any large CO_2 content drops their efficiency. Furthermore, as the fuel cells initiate the reverse water gas shift reaction (**RWGS**) more CO is produced. Therefore, by elongating the time (t_{BT} - t_0) for a rich H_2 reformate production, the absence of CO can be attained. Consequently, hydrogen of high purity would be available for a longer period with regard to lack of CO_2 compared to the PSA (Pressure Swing Adsorption) system (**Majlan et al., 2009**). In the SOFC (Solid Oxide Fuel Cell) or the MCFC (Molten Carbonate Fuel Cell) the presence of CO is not a critical parameter for their good performance (**Sugiura et al., 2003**).

In the table that follows (**Table 26**), the sorbent's efficiencies α_{PB} and α_{BT} for the respective time intervals ($t_{BT} - t_{0)}$ and ($t_{SS} - t_{BT}$), as well as the overall sorbent's efficiency (α) are presented.

Table 26 Time at which SESR started (t_0), pre-breakthrough period ($t_{BT} - t_0$) and breakthrough period ($t_{SS} - t_{BT}$);). Rate of CO_2 adsorption on the sorbent pre- breakthrough ($\dot{n}_{CO_2,ads,PB}$), pre-breakthrough efficiency of the adsorbent (α_{PB}), adsorbent's efficiency during breakthrough (α_{BT}) and total adsorbent's efficiency (α; **Eq. 51**) for the SESR step

Cycle	t_0 (s)	$t_{BT} - t_0$ (s)	$t_{SS} - t_{BT}$ (s)	$\dot{n}_{CO_2,ads,PB}$ (mol s^{-1})	α_{PB} (%)	α_{BT} (%)	α (%)
1	230	1270	990	2.42×10^{-4}	73.7	27.3	101
2	400	750	550	1.59×10^{-4}	34.2	12.0	46.2
3	2290	1105	555	1.61×10^{-4}	42.6	12.6	55.2
4	1700	1000	725	1.70×10^{-4}	40.7	20.2	60.9
5	1500	1025	890	1.22×10^{-4}	17.3	35.9	53.2
6	1800	1480	545	1.42×10^{-4}	50.3	13.8	64.1

Summarizing the presented results in **Table 26, Figure 55** was produced, where the pre-CO_2 breakthrough (α_{PB}) and the total efficiency (α) are presented for the 6 SEUSR cycles,

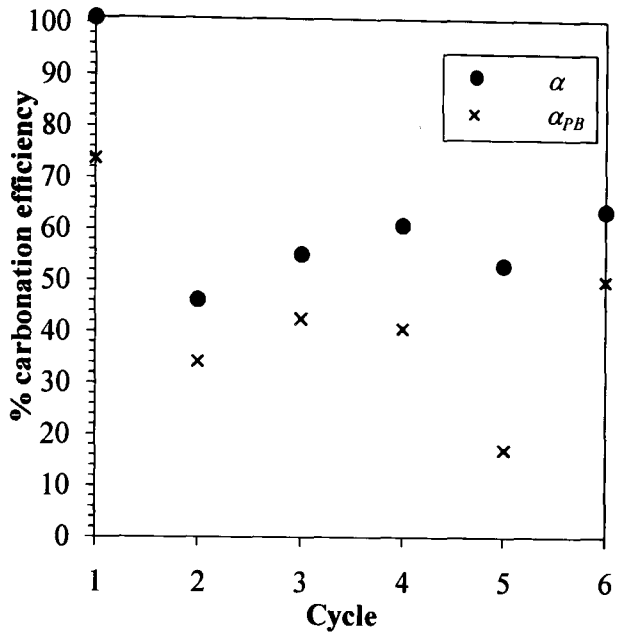

Figure 55 Sorbent's efficiencies for the pre-breakthrough period (α_{PB}) and for the entire FF step (α) of the SEUSR chemical looping (6 cycles)

It is worth mentioning that the total efficiency (% α) for cycle 1 was estimated to be close to 100 % even with the errors that **Eq.51** carries for the calculation of α. The decreasing trend of the final values of the sorbent's conversion (α) was expected in naturally formed dolomites and by the micro- and macro studies of the Warmsworth dolomite discussed in **chapters 4 and 5**. From the present work on the sorbent's macro scale study (**paragraph 5.3**), it was shown that under wet conditions the first carbonation did not reach full regenerative levels, which was attributed to the fact that the dolomite had not been fully calcined during the 1st thermal decomposition step. It needs as well to be noted that for the first carbonation in 15% vol CO_2/ N_2, the lowest efficiency was achieved among the lower % vol CO_2/ N_2 tested. This is an important observation, since in the 1st SESR step (**Figure 52**), when steady state conditions were reached the dry % vol CO_2 was in the range of 17 for the time t_{SS} and still the total carbonation efficiency α reached 100 %. An abrupt decrease from cycle one to cycle two was noticed as shown in curve of the total carbonation efficiencies (% α) vs.

cycles (**Figure 55**). From cycle 2 to 6 the efficiency of the sorbent appeared to be stable and consistent in the vicinity of 55.9%. The decrease in the carbonation CO_2 capacity performance of this sorbent was to be expected and attributed to sintering, as indicated by the stability study performed at micro and macro- scale (**chapter 4: paragraphs 4.3.1, 4.3.2 and 4.5; chapter 5: paragraph 5.5**). The difference in the TGA and process performance of CaO based sorbent is noticed in the H_2 production process when fluidised bed reactors technology is employed (**Arstad et al., 2009**). In general, this behaviour is met in un-pretreated CaO sorbents from natural mineral sources.

The efficiency of the sorbent in the pre-breakthrough time interval (% α_{PB}) followed the same trend over the 6 cycles (like the % α value), except for the 5th cycle. A final value of α_{PB}= 74 % for the 1st SESR step was calculated when by the 5th cycle it had reached the value of 17.30% which did not comply with the trend formed by the respective cycle value of % α (**Figure 55**). There are two parameters behind this abnormality:

- The fuel conversion $X_{WCO,PB}$, which contributed in the rate of CO_2 production; hence the extent of carbonation of the sorbent;
- the pre-breakthrough time interval ($t_{BT} - t_0$) over which the rate of CO_2 adsorption was integrated.

From **Table 27**, it becomes evident that the duration of the pre-breakthrough interval was not the main reason behind the low value of α_{PB} (%) by the 5th cycle, since its value ($t_{PB} - t_0$) was the same as in cycles 3 to 4. It was actually the low value of $X_{WCO,PB}$ (=0.232) (**Table 28; paragraph 8.3**), which was the lowest one achieved among the 6 repeated cycles. This phenomenon in effect would not imply that the rate of the fuel conversion is a rate limiting step for the sorbent's chemisorption (**CB**) process, but the low yield of the reactions (**SR- WGS- RM**). The longer post-CO_2 breakthrough period ($t_{SS} - t_{BT}$) in cycle 5 (**Table 26**) led to a final total yield of carbonation (% α) within the same range as in the rest of the five cycles. It needs to be underlined that during the 5th SESR step, there was not any interruption in the feed of the reactants, either of the fuel or the steam.

8.2.2 AF steps in SEUSR chemical looping

The AF steps in the SEUSR chemical looping experiments were not only used to clean-up the catalyst by burning the carbon deposits, but also used to regenerate the sorbent. The temperature profiles of the AF steps indicated a higher range in contrast to those of 40 g of catalyst without sorbent. In **Table 27**, the peak temperatures of the AF steps performed on the 40 g sorbent-40 g catalyst and the corresponding AF steps peak temperatures on the 40 g catalyst only are shown. The expected AF temperatures from the experiments with the catalyst alone were promising for the sorbent's regeneration. The maximum AF steps temperatures when the sorbent was present were higher than in the experiments with just 40 g catalyst.

Table 27 Peak temperatures in the top and middle of the reactive bed in the AF steps of USR (T_{middle} and T_{bottom} catalyst only) and SEUSR chemical looping (T_{middle} and T_{bottom} sorbent- catalyst)

	SEUSR	USR	SEUSR	USR
AF step	T_{middle} (K)	T_{middle}(K)	T_{bottom} (K)	T_{bottom} (K)
1	1098	1012	1124	926
2	1089	987	1117	925
3	1126	1012	1092	926
4	1130	1024	1155	930
5	1126	1032	1165	942
6	1131	1078	1130	968

Moreover, the temperature probe inserted at the top of the sorbent-catalyst bed recorded higher temperatures during the AF steps compared to those recorded at the same position in the corresponding steps of the experiments with just 40 g catalyst. Keeping in mind that the Ni oxidation is an exothermic reaction whereas the $CaCO_3$ thermal decomposition is an endothermic one, the further temperature increase in the sorbent-catalyst AF steps could be due to the increased Ni conversion to NiO. This might be due to the fact that some carbon ($C_{(s)}$) was deposited on the sorbent during the FF steps leaving less carbon on the Ni particles' surface. Such a shift in the solid carbon deposition preference in the FF steps could enable the carbon burning on the

catalyst surface to a greater extent in the AF steps. Consequently, there were more free active Ni sites to react with the O_2 content of the supplied air and a higher conversion into NiO which led to a higher heat release.

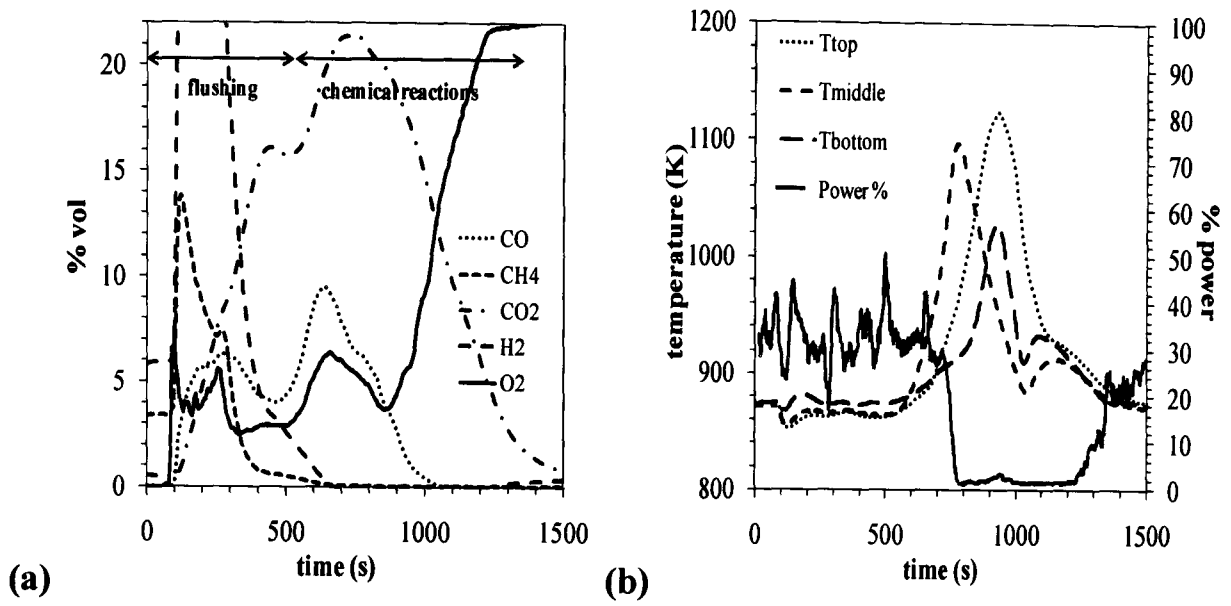

Figure 56 **(a)** Dry gases concentrations with time on stream over the course of the 1st AF step in the chemical looping of SEUSR, exhibiting distinct flushing and chemical reactions intervals; **(b)** Reactive bed's top, middle and bottom temperatures coupled with the % power used over the course of the 1st AF step in the chemical looping of SEUSR

In **Figure 56(a)**, two distinctive phases for the CO_2 production in the AF (1st) step can be seen, as in the experiments with just catalyst (**paragraphs 7.4.3, 7.5.1.3 and 7.5.2.3**). The first CO_2 curve peak was formed in the first 200 s and was indicative of the flushing of the remaining CO_2 from the previous FF step due to the pressure difference effect as described earlier in **paragraphs 7.5.1.3** and **7.5.2.3**. Similarly, the H_2 and CH_4 curves that appeared during the flushing period could only be sourced in the SR step. Along with the flushing CO_2, some CO was recorded. The CO_2 curves formation delay was due to its counterinfluence with the reactive bed (sorbent-catalyst).

As in the 40 g catalyst only experiments (**paragraph 7.5.2.3**), the second CO_2 peak corresponded to the carbon burning. During this time interval, Ni oxidation occurred, which increased the temperature in the reactive system. The CO_2 concentration (% vol) (**Figure 56(a)**) increased between 300 and 500 s when at the

same time the CO % vol concentration decreased, due to the restoration of the oxidative (O_2) flow, hence the enhancement of the complete oxidation of the deposited carbon present on the reactor's bed. In **paragraph 7.5.2.3**, it was shown that during the complete and incomplete carbon oxidation reactions (**R10**; **R9**) the Ni particles were oxidized. Furthermore, it was concluded that the dominant reaction during the chemical reactions time interval in the oxidation step, was the oxidation of the catalyst (**R8**), which monopolized the oxygen consumption. It was the temperature profile for the same time interval of the oxidation step (**Figure 56(b)**) that gave a better insight of the type of reactions that were involved in an AF step. The calcination of the sorbent (**TD of calcite**; **Figures 56(a) and 56(b)**) became recognisable based on the well established AF step temperature range (873- 1010 K ; **paragraph 7.5.2.3**).

From the sorbent's study (**chapters 4 and 5**), it was expected that at temperatures greater than 1023 K (750°C), the $CaCO_3$, which was formed in the SESR steps, would be thermally decomposed. From the experimental results of the AF steps during the SEUSR chemical looping experiments, it was indicated, as shown in **Figures 56(a)** and **56(b)**, that higher temperature gradients within the reactor's bed could initiate the decarbonation of the sorbent at lower temperatures than the aforementioned one.

By combining the two previous figures (**Figures 56(a) and 56(b)**), the top and middle temperatures of the reactor and the rate of CO and CO_2 evolution, **Figure 57** results. The moment the reactor temperatures (T_{top}, T_{middle}) exceeded 873 K, which was the set temperature (T_{set}) for the AF steps, the power was cut off from the system. For the following 400 s the system could conserve enough energy (**Figure 56(b)**) and proceed with the participating reactions as the Ni oxidation is highly exothermic. The power input cut-off recording implied the potential for autothermal behaviour in the SEUSR process. This can be verified by future work by performing energy balances.

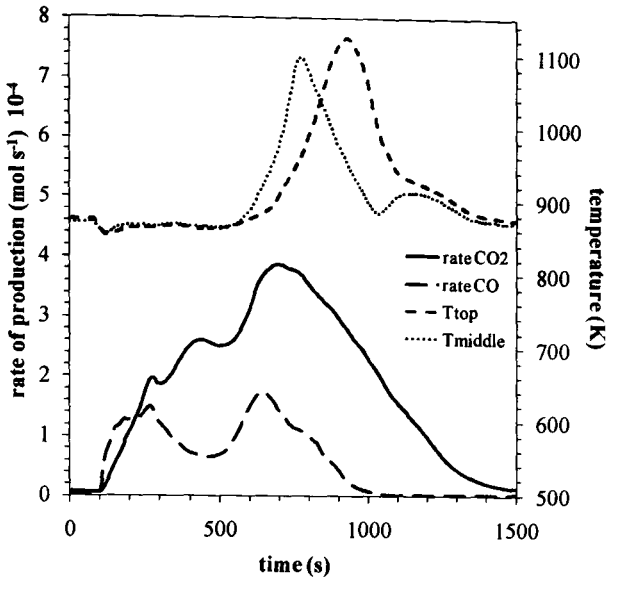

Figure 57 Molar rate of CO_2 and CO production (mol s^{-1}) coupled with the top and middle temperature of the reactive (reduced catalyst-partially saturated sorbent) over the duration of the 1st AF step of the SEUSR chemical looping

By the end of the AF step, the sorbent's capacity was expected to be at 29% of the initially available number of CaO moles. This was established by the integration of the CO_2 curve over time between 400 and 1500 s (**Figure 56(a)**). On the other hand in **Table 26** it is presented that the sorbent was saturated up to 46% by the end of the 2nd SESR step, indicating that in the previous AF step, a longer thermal decomposition period of the sorbent took place.

The sorbent's regeneration during the AF step in the chemical looping of the SEUSR process confirmed the fact that it was incomplete at bench (macro) scale as it was shown for the sorbent alone study under wet conditions in **chapter 5**. In particular, from the bench scale sorbent's study in the presence of steam, the regeneration fractional extent was calculated from 0.79 to 0.50 over cycles 1 to 6. Additionally, it should be noted that in the dry micro- scale (TGA) study, the efficiency of the sorbent's thermal decomposition (TD) reached 1 (full calcination).

8.3 Recyclability of the Ni-based catalyst for SEUSR of waste cooking oil: effect of sorbent

One of the aims of the SEUSR was to observe whether the catalyst's performance was enhanced, by the presence of the sorbent in terms of WCO and steam conversions. This should take place while the sorbent was active; that is during the time period that any produced CO_2 by the steam reforming reactions was adsorbed (**paragraph 8.2**).

It was found that both conversions of WCO and steam for the time interval that no CO_2 was detected, were enhanced compared to the 40 g catalyst runs in the absence of sorbent (**paragraphs 7.5.2.2** and **7.5.2.3**), based on the conversion calculations after saturation of the sorbent. It is worth mentioning that the internal volume of the reactor did not allow a mass of more than 80 g to be loaded, therefore limiting the cases of different sorbent to catalyst ratios to be employed; thus a ratio of 60 g catalyst:40 g sorbent was not possible. Based on the experiments with just 40 g catalyst (USR), the conversions of WCO and steam in the FF steps of SEUSR chemical looping experiments and after CO_2 sorption were not expected to exceed the range of 0.20 and 0.09 respectively (**Table 25(a); paragraph 7.5.2.2**). The findings of the 6 SESR runs are presented in **Table 28**, where the values of X_{WCO} and X_{H_2O} during the CO_2 post-breakthrough, steady state period (SS; $t > t_{SS}$) are listed.

Table 28 40 g catalyst- 40 g sorbent chemical looping SESR steps including $\Delta T_{middle,max}$= pre-breakthrough maximum temperature difference from set temperature (T_{set}= 873 K)

cycle	average $X_{WCO,SS}$	average $X_{H_2O,SS}$	max % H_2 purity(SS)	SEL_S s CO	SEL_{SS} CO_2 %	SEL_{SS} CH_4 %	$\Delta T_{middle,\,max}$ (K)	$T_{middle,BT}$ (K)	$t_{PB} - t_0$ (s)	m % purit
1	0.460	0.191	69.7	4.0	81.0	15.0	2	872	1330	9
2	0.301	0.110	71.3	9.8	89.3	1.0	6	880	950	9
3	0.303	0.101	70.5	9.9	89.0	1.0	3	883	1315	9
4	0.324	0.117	70.1	11.0	86.0	3.0	2	877	1200	9
5	0.232	0.082	70.6	11.5	85.2	3.3	8	881	1160	9
6	0.270	0.114	72.3	6.0	78.1	15.9	18	891	1600	9

Recall that we also assumed that the conversions in pre-breakthrough (PB, ($t_0 < t < t_{BT}$) would at least match the values at steady state. This way, the effect of the sorbent's presence in the overall activity of the Ni catalyst can be highlighted by the enhanced WCO and steam conversions.

The first cycle of SESR exhibited the highest WCO and steam conversions at steady state. For the FF steps that followed from cycle 2 to 4 it was shown that the sorbent's carbonation capacity decreased as expected from the wet bench (macro) scale stability study of the dolomite (**paragraph 5.5**; **chapter 5**). This conclusion is further strengthened by the % H_2 purity values at steady state greater than 68% (as presented in **Table 28**).These can also be compared to the maximum theoretical H_2 % purity of 74.3% in absence of CO_2 sorption for this fuel, given by ($100 \times (2n+0.5m-k)/(3n+0.5m-k)$), not taking into account equilibrium limitations. The margin of the % vol of H_2 purity is chosen as a comparative parameter of the SESR steps' performance to the average ones achieved in the USR chemical looping experiments (**chapter 7**, **paragraph 7.5.2.2**). The average values of $X_{WCO,SS}$ and $X_{H_2O,SS}$ in the steady state (SS; $t > t_{SS}$) over the chemical looping of SEUSR were 0.312 and 0.121 respectively (**Table 28**). The $X_{WCO,SS}$ and $X_{H_2O,SS}$ values over cycles 2 to 4 and 6 were maintained close to the average, except in cycle 5 where these values were well below average.

The good performance of the 1st SESR cycle, in terms of the X_{WCO} and X_{H_2O}, can be further supported on this step's highly endothermic conditions caused by the steam reforming reaction (**SR)** as reflected in the temperature in the middle of the sorbent-catalyst bed ($T_{middle,PB}$) (**Table 28**). A side effect of the highly endothermic SR reaction involved in this step was the higher selectivity of CH_4 over CO. As the energy demand to steam reform the WCO over the repeated cycles was decreased (which was reflected in the $X_{WCO,\ PB}$ values), so did $T_{middle,BT}$ remain closer to the set temperature T_{set}= 873 K = 600°C. This could be mainly linked to the decreased performance of the sorbent over the repeated cycles (whose presence in any case promoted the efficiency of the FF steps) and to the adsorption of any produced CO_2 which supplied less energy to the system than when working in full capacity (**Table**

26; paragraph 8.2.1). The selectivity to CO_2, CH_4 and CO in steady state (for $(t_{SS} - t_{PB})$) (**Table 28**) indicated that the conditions must have been favorable to CO_2 sorption for the duration of the pre-breakthrough $(t_{BT} - t_0)$ period.

By the 6th SESR step, the selectivity (%) range to CH_4 and CO indicated similar conditions to those in the 1st cycle, in spite of $T_{middle,BT}$ (**Table 28**) being close to the set temperature during the 6th cycle. The latter can be associated to the smaller activity of the steam reforming reaction (**SR**) via the values of ($X_{WCO,SS}$; $X_{H_2O,SS}$, **Table 28**). On the other hand, at this stage, the hydrogen purity (%) had the second higher value throughout the 6 cycles, due to the prolonged pre- breakthrough time ($t_{BT} - t_0$= 1480 s; **Table 26**) which was while the sorbent was highly active.

The steady state period was chosen not only for estimating $X_{WCO,\ SS}$ and $X_{H_2O,\ SS}$, but to estimate the molar rate of NiO reduction ($\dot{n}_{NiO\rightarrow Ni,\ SS}$). Therefore, it was possible to verify whether the catalyst was reduced and the extent of its reduction at the same time the WCO was steam reformed and the sorbent was carbonated. The performed oxygen balance for the post- CO_2 breakthrough time is presented below,

$$\dot{n}_{NiO\rightarrow Ni,SS} = \dot{n}_{out,dry,SS}(y_{CO} + 2y_{CO_2})_{SS} + 2\dot{n}_{CO_2,carb} + \dot{n}_{H_2O,in}X_{H_2O,\ SS} - k(\dot{n}_{WCO,in}X_{WCO,\ SS})$$

Eq.52

By the estimates of the terms $\dot{n}_{CO_2,carb}$, $X_{H_2O,SS}$ and $X_{WCO,SS}$ in **paragraph 8.1.2** (**Eq.43, 45, 41** and **42** respectively), the approximation of the rate of NiO reduction becomes,

$$\dot{n}_{NiO\rightarrow Ni,SS} = \boxed{\dot{n}_{WCO,in}\,X_{WCO,SS}(2n + 0.5m - k)} - \boxed{y_{H_2,SS}\frac{\dot{n}_{N_2,in}}{(1 - y_{H_2,SS})}}$$

term A **term B** **Eq.53**

The rate of the NiO reduction from the previous equation corresponds to its maximum value when the only gaseous product was hydrogen, as reflected in term A, by subtracting the molar rate of the produced hydrogen (term B). The latter term is based on the NiO reduction reaction (**NiRed; R1**) where 1 mol of H_2 is necessary to reduce 1 mol of NiO to Ni by formation of H_2O.

In the following figure (**Figure 58**) the $\dot{n}_{NiO\rightarrow Ni,SS}$ and the steady state $X_{WCO,\ SS,}$ are depicted over the 6 repeated cycles.

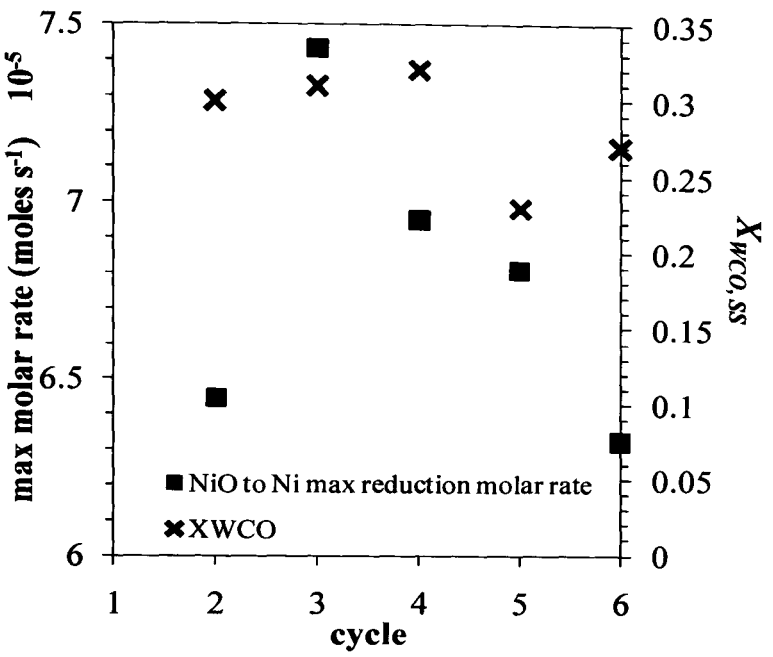

Figure 58 Maximum rate of NiO reduction ($\dot{n}_{NiO\rightarrow Ni,SS}$) and WCO conversion ($X_{WCO,SS}$) in the post- breakthrough period during the FF steps in the SEUSR chemical looping process

Despite the fact that the WCO conversions ($X_{WCO,SS}$) from cycle to cycle are within the same range, in the calculation of the $\dot{n}_{NiO\rightarrow Ni,SS}$, the involvement of the $y_{H_2,SS}\frac{\dot{n}_{N_2,in}}{(1-y_{H_2,SS})}$ term resulted into a discontinuity of the produced values of $\dot{n}_{NiO\rightarrow Ni,SS}$ (**Figure 58**).

The time needed for the full reduction of the catalyst during the SESR steps was derived by integrating **Eq. 53**. The product of this integration is defined as the necessary time (t_{FR}) to fully reduce the catalyst,

$$t_{FR} = \frac{n_{Ni}}{\dot{n}_{NiO\rightarrow Ni,SS}}$$

Eq. 54

For the 4th SESR cycle, the catalyst was fully reduced within the pre-CO_2 breakthrough time while for the 3rd SESR cycle the catalyst was fully reduced, at the beginning of the CO_2 breakthrough time. On the other hand, in the 3rd and 6th SESR steps, t_{FR} was achieved by the 3rd and 5th minute of the CO_2- breakthrough time. These

results are useful since they showed that in the SESR steps, the steam reforming of the fuel, the carbonation of the sorbent and the NiO reduction occurred simultaneously. By comparing directly $\dot{n}_{NiO\rightarrow Ni,SS}$ and $X_{WCO,SS}$, it becomes evident that the SR reaction is responsible for the extent of the H_2 produced as expressed by its purity (**Table 29(a)**), as the first term represents the NiO reduction by unmixed combustion (**UC**) and steam reforming (**SR**).

It is important to remember that the available NiO moles during the chemical looping experiments with just 40 g catalyst would have been fully reduced if X_{WCO} reached its maximum of 1 at 63 s, through the unmixed combustion reaction (**SR**). During the SESR steps, it was not easy to distinguish whether any reduction of the NiO particles occurred during $(t_{BT} - t_0)$ due to the presence of the sorbent and non-closure of the carbon balance. The FF steps of the USR chemical looping (**paragraph 7.5.2.2**) were considered to establish the possibility of a period of time where only NiO reduction occurred.

Another parameter that is of particular significance is the % of the ratio of the NiO reduction rate in every cycle over the maximum reduction rate for the same cycle (R_{red}),

$$R_{red} = 100 \times \frac{\dot{n}_{NiO\rightarrow Ni,PB}}{\dot{n}_{WCO,in} X_{WCO,SS} (2n + 0.5m - k)}$$

Eq.55

One can realize based on the above equation (**Eq.55**) which of the two fuel consuming reactions (**UC**; **SR**) was the most dominant during the pre-CO_2 breakthrough period. The maximum value of R_{red} could only be reached if no steam reforming took place. From **Figure 59** that follows, the R_{red} is plotted against the repeated 5 cycles of FF step in SESR which began with the oxidized catalyst.

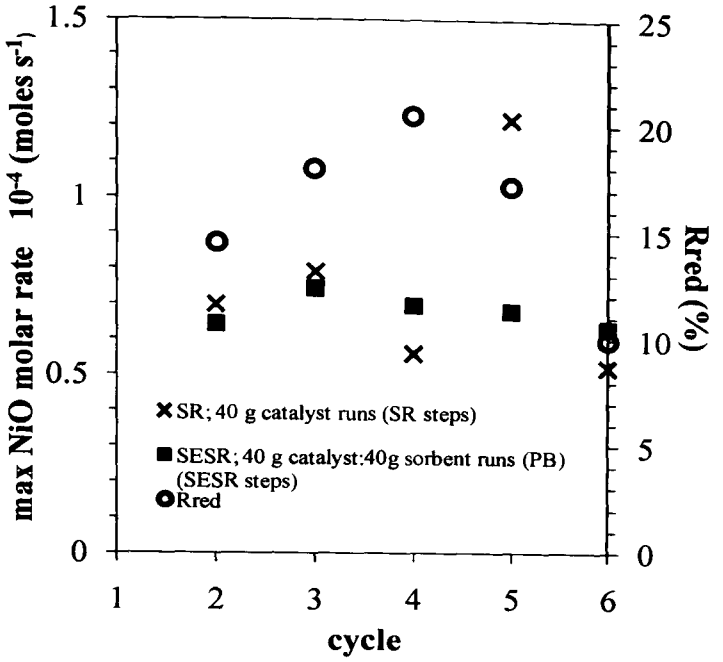

Figure 59 Maximum molar rate of NiO particles reduction to Ni over the chemical looping of USR ($\dot{n}_{NiO \rightarrow Ni}$; SR steps) and SEUSR ($\dot{n}_{NiO \rightarrow Ni,SS}$; SESR steps) processes

It is evident that as the R_{red} values were below 20%, the larger proportion of the fuel was consumed in the steam reforming reaction (**SR**) rather than in the NiO reduction (**R6**). Any uncertainties about the percentage of the catalyst reduction may be expected at the early stages of the experimental data recording where there was a time lag between the moment the reactants were fed until H_2 started to be recorded (**Figure 53**). The fact that there was no recording of any dry gases by the analyzer by the initial time (t_0) can be attributed to two factors. The first one is the necessary time for the fuel and steam to be transferred by the pipe work to the reactive system and eventually for the products to be transferred to the analyzer. The second one accounts for the time when steam reforming occurs (**SR**) with CO_2 being trapped by the sorbent, which resulted in no dry gases detection. Additionally, any other gaseous products, such as CO and CH_4, were absent from the reformate This is an effect which is based on the Le Chatelier's principle; according to this, the equilibrium of the unmixed combustion (**UC**) and the water gas shift reactions (**WGS**) are shifted to the right by the capture of the WGS product CO_2, which then decreased the WGS reaction's CO reactant, but also simultaneously the SR reaction's CO product, which in turns decreased the hydrocarbon fuels (WCO and CH_4 intermediate) . Whether **UC** (unmixed combustion reaction) occurred before the SR reaction would have been

indicated by large volumes of produced CO_2, before any H_2 was produced. Furthermore, a negative steam conversion would have been calculated from the elemental balances accompanied by a high NiO reduction rate. Such an observation was not noted in the chemical looping experiments with just 40 g catalyst **Table 25(a)** (**paragraph 7.5.2.2**). On the contrary, steam reforming was the primary reaction during the FF steps (2 to 6). Therefore, the catalyst's reduction was delayed in the presence of the sorbent by the steam reforming and carbonation reactions and eventually performed progressively. This conclusion serves in building up expertise for this process by indicating that the H_2 production was not delayed by the NiO reduction (**R6**). Moreover, this outcome clearly emphasizes the OTM's ability to perform the SR reaction and the additional benefit of coupling the SEUSR process with the waste cooking oil.

8.4 Comparison between SEUSR and USR of waste cooking oil cycling effect on the process's performance

The effect of the sorbent's presence in the 6 consecutive SEUSR cycles with respect to the 6 cycles of USR (**paragraph 7.5.2**) when the same mass of catalyst was applied, will be discussed in this paragraph.

The effect of sorption enhancement can be quantified by the comparison of the hydrogen yield efficiency with and without the presence of the sorbent, in particular in proven conditions of CO_2 sorption, i.e. in the CO_2 pre-breakthrough period. The fractional H_2 yield efficiency is defined as the ratio of the molar production rate of H_2 to the maximum molar production rate of H_2 as per the complete SR and WGS reactions following the equation 56 below:

$$\eta_{H_2,eff} = \frac{\dot{n}_{H_2,out}}{(\dot{n}_{H_2} \text{ max from WCO and steam})} = \frac{y_{N_2} \times \dot{n}_{out,dry}}{(2n + 0.5m - k) \times \dot{n}_{WCO,in}}$$

Eq. 56

The figure below shows for cycle 1 the H_2 yield efficiencies with (SEUSR) and without sorbent (USR).

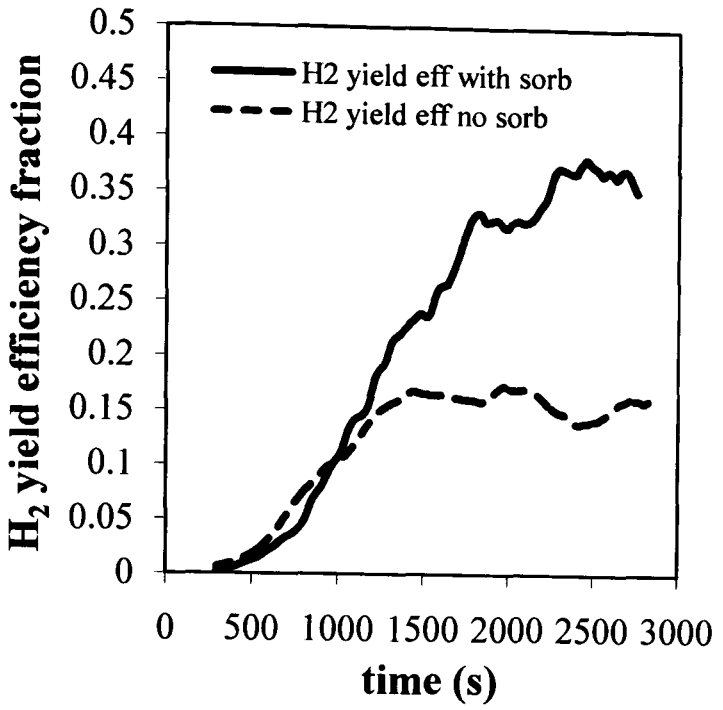

Figure 60 H_2 yield efficiency with time on stream for cycle 1 with and without sorbent

It is evident from **Fig. 60** that the H_2 yield efficiency was more than doubled by the presence of the calcined dolomite sorbent in the first cycle. This enhanced yield, together with the enhanced H_2 concentration in the syngas product (> 90 vol%) accounts for the full sorption enhancement effect.

Table 29 Maximum H_2 yields efficiency for the 6 cycles in SEUSR and USR

	max H_2 yields efficiency					
	1	**2**	**3**	**4**	**5**	**6**
SEUSR	0.44	0.30	0.34	0.37	0.22	0.27
USR	0.20	0.22	0.19	0.19	0.14	0.21

Table 29 indicates that the sorption enhancement was maintained throughout the chemical looping of SEUSR, although its effects decreased following the decrease in the sorbent' carbonation capacity with the increasing cycles. This decrease was mainly attributed to the sorbent's limited capability to carbonate and regenerate as it was

earlier illustrated in the sorbent's macro-scale study under wet conditions (**paragraph 5.5** and **5.6**). However by cycle 6, the sorption enhancement effect could still be quantified by an increase in 29% in H_2 yield, compared to the same process without sorbent.

Other side effects of the presence of the sorbent after CO_2-breakthrough, and thus in the absence of CO_2 sorption are explored in the following section.

From the USR **Tables 25(a)** and **(b)** and the SEUSR **Tables 29(a)** and **(b)** (**paragraphs 7.5.2.2** and **8.3** respectively) it becomes apparent that the sorbent's presence enhanced the process performance in regard to the conversions of the waste cooking oil and steam, the selectivity to the carbon products and the hydrogen purity even at steady state, post-CO_2 breakthrough. The average values of X_{WCO} and X_{H_2O} in the 6 repetitive runs of the USR process (sorbent's absence) was 0.20 and 0.06 respectively. On the other hand the post- CO_2 breakthrough values of X_{WCO} and X_{H_2O} in the SEUSR process (**paragraph 8.3**) were averaged in the range of 0.31 and 0.12 which were attributed to the sorbent's presence. The carbon containing products that were produced by the steam reforming reaction (**SR**) in both processes (USR and SEUSR) are further evaluated based on their selectivity. In the case without sorbent, the SEL % CH_4 was always lower than that of CO, implying the deficiency of the process in steam reforming the waste cooking oil, which was mainly reflected in the low values of X_{WCO} and X_{H_2O}. Since there were not enough available NiO (for the first cycle) or Ni (for cycle two to six) particles/ sites, the process was not as endothermic as in the case where 80 g of catalyst was employed. The temperatures in the middle of the reactor bed (**Table 25(b)**; **paragraph 7.5.2.2**) for the 6 cycles of USR appeared to be lower than in the case of the SEUSR (**Table 29(b)** ; **paragraph 8.3**), due to the power input control point in the reactive system. In the USR experiments the power input was controlled by an external coil around the reactor, whereas in the case of the SEUSR experiments the system's power was controlled by the measured reactor bed temperature. The latter configuration of power input control was chosen in order to better maintain isothermal conditions under the FF step, which are not easy to achieve due to the high endothermicity that accompanies the steam reforming reaction (**SR**) (**chapter 7**).

It becomes obvious that the slower rate of H_2 production resulted in higher rates of the NiO reduction, which was in the case of the USR experiments. This was expected since X_{WCO} was lower over the repeated cycles for the USR process. Therefore, less NiO particles were present for the steam reforming of WCO in the absence of sorbent and more when the sorbent was present due to the lower NiO reduction rates. Hence the more available OTM material, the more extensive is the conversion of WCO by steam. This might be due to the resulting larger volume within the reactor by the sorbent addition, which allowed longer residence time for the steam reforming reaction (**SR**). A secondary parameter responsible for this effect was the carbonation reaction which mainly removed CO_2, but on top of this, it removed any CO and CH_4 through Le Chatelier's principle from the product stream (**Figure 53, paragraph 8.2**).

In conclusion, the sorbent's presence in the steam reforming steps promoted the SEUSR process in the areas below:

- mainly in CO_2 capture and removal of CO and CH_4 by their enhanced conversion to CO_2, yielding a high purity H_2 product stream ($95.2 \leq \%\ H_2\ purity \leq 98.6$),
- the hydrogen yield efficiency was more than doubled by the presence of the sorbent in cycle 1, and on an average more than a factor of 1.5 in the following cycles.
- it was possible that the increased H_2 production allowed sufficient reduction of the OTM before the breakthrough point, which enhanced the WCO conversion even beyond the breakthrough period. The in-situ coupling of the endothermic steam reforming with the exothermic carbonation decreased the energy demand of the FF step therefore allowing a better temperature control in the reactor and more heat to be available for the steam reforming of the WCO.

In the SEUSR process's experiments, the AF steps were performed to regenerate both the catalyst and the sorbent. In both cases of USR and SESR AF steps, the common parameters used to compare their performance were the rate and the total

number of moles of CO ($\dot{n}_{CO,\ prod,\ AF}$) and of CO_2 evolved ($\dot{n}_{CO_2,\ prod,\ AF}$) from the reactor, along with the temperature variations in the reactive bed. In the following graph, these parameters for 1st AF step of the USR and SEUSR process are presented.

The peak temperatures range was reached when the Ni particles were oxidised in both AF steps following the SR steps in the absence (**Figure 61**) and presence of the sorbent (**Figure 57**). In the AF step that followed the 1st SESR step, the sorbent was considered to regenerate once the temperatures were higher than 1023 K (750°C) resulting in a second peak in the rate of CO_2 evolution.

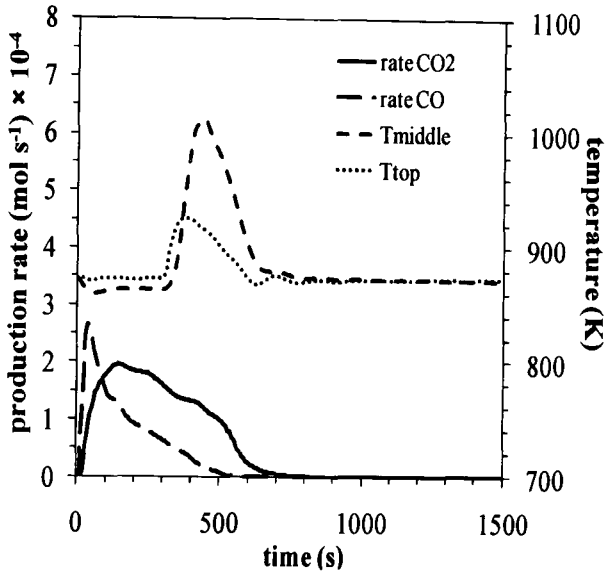

Figure 61 Molar rate of CO_2 and CO production (mol s^{-1}) coupled with the top and middle temperature of the reactive (reduced catalyst- partially saturated sorbent) over the duration of the 1st AF step of the USR chemical looping

One of the interesting differences observed in the USR and SEUSR chemical looping AF steps in the absence and in the presence of the sorbent was that the temperature distribution in the different sections of the reactor bed was more uniform in the presence of the sorbent (T_{top}, $T_{\ middle}$ in **Figure 58** and **Figure 61**). Whether the sorbent's presence enhanced the Ni oxidation conversion to NiO, as expressed by the $\dot{n}_{Ni \rightarrow NiO}$ term, could be difficult to quantify during the SEUSR chemical looping, as the elemental balances could not be realised. This was unless the origin of the evolved CO_2 molecules could be attributed to either the $CaCO_3$ thermal decomposition, or to any further carbon burning while the catalyst was regenerated via complete (**R9**) and

incomplete (**R10**) oxidation. The latter CO_2 molar rate curve for the catalyst regeneration section was accompanied by a second peak of the molar rate of CO curve (**Figure 57**). Any incomplete solid carbon oxidation that led to CO formation in the time interval of Ni oxidation, was produced due to the lack of oxygen caused by the highly competitive nickel oxidation reaction (**R8**). The temperatures ($T_{top,max}$= 926 K; $T_{middle,max}$= 1012 K) in the AF steps of USR process (**Figure 50; paragraph 7.5.2.3**) appear to be lower than those in the case where there was sorbent (**Figure 57**) ($T_{top,max}$= 1124 K; $T_{middle,max}$= 1098 K). These values hinted at the promotion of the Ni oxidation in the sorbent's presence. Despite the endothermicity of the $CaCO_3$ thermal decomposition, the Ni oxidation reaction (**R8**) gave rise to the T_{top} and T_{middle} by + 198 K and + 85 K when compared to the respective temperatures in the sorbent's absence (**Figure 59**). Based on this observation it can be assumed that a larger amount of the reduced catalyst was oxygenated. Additional support to this conclusion gives the duration of the temperatures greater than the T_{set}= 923 K in the cases where the sorbent was absent and present. In the sorbent's presence, the duration was at 944 s (**Figure 57**) when in its absence it was 417 s (**Figure 50**; **paragraph 7.5.2.3**).

Overall, the WCO exhibited a very good behaviour in reducing the OTM over 6 cycles of the chemical looping experiments of the SEUSR process while its performance was enhanced compared to the USR chemical looping (**chapter 7**). The sorbent's performance was ascertained over the final 5 cycles with an operating capacity of around 56% based on its optimum (theoretical) capacity. The sorbent and catalyst were able to regenerate during the AF steps and resulted in a repeatable trend which underlines the reliability of the process.

8.5 Summary of the SEUSR (Sorption Enhanced Unmixed Steam Reforming) of WCO (Waste Cooking Oil)

The influence of the sorbent's presence in the SEUSR process was studied with comparison to the USR chemical looping experiments with the 40 g catalyst which

was studied in **chapter 7** (**paragraph 7.5.2**). It needs to be noted, that the sorbent material was employed in the SEUSR process in its fully calcined form, which was MgO.CaO. The overall sorbent's efficiency under the FF steps can be compared to the macro- scale stability study of the sorbent as discussed in **chapter 5** (**paragraph 5.5**).

8.5.1 Process outputs performance during the SEUSR chemical looping experiments of WCO

The SEUSR process's chemical looping findings during the FF (Fuel Feed) and AF (Air Feed) steps are summarised below.

- The sorption enhancement effect was quantified by more than doubling the H_2 yield in cycle 1 compared to the process without sorbent, but this went down to a more modest 30% increase in H_2 yield by cycle 6 (**Table 29**), due to the decrease in carbonation efficiency of the sorbent (**Table 26**), as was expected from the micro- and macro-scale studies as well as the literature on the poor stability of CaO based CO_2 sorbents under cyclic operation.
- Even when saturated, the sorbent's presence improved the process performance throughout the 6 cycles of the SEUSR chemical looping study. This can be seen in **Table 28** (**paragraph 8.3**) where the steady state WCO and steam conversions were on average 0.31 and 0.12 respectively, compared to those of the USR chemical looping experiments conducted in the absence of sorbent (**Table 25(a)**; **paragraph 7.5.2.2**), (0.20 and 0.06 respectively).
- Hydrogen of 97% purity was obtained for more than 700 s during cycle 1 (**Fig. 53**), while purities were maintained above 90% for the time period of 800-1400 s for all cycles. Together with the increased H_2 yield, the purity of the H_2 near 100% completed the full observation of the expected sorption enhancement effect on the steam reforming process.

- The sorbent did not only successfully chemisorb CO_2, but additionally, it performed sorption enhancement by further converting CO and CH_4 into CO_2 (**Table 28**), thus eliminating them from the end-product.
- The reactor's bed temperature was closer to the set reactor temperature (T_{set}) as the sorbent's capacity to chemisorb CO_2 over repeated cycles produced additional heat in the system, which led to a more successful fuel conversion.
- When steady state conditions were achieved, the H_2 purity values became similar (70.2%; **Table 28**) to the theoretical maximum (74.3%; **Table 25(b)**) corresponding to conditions without sorbent notwithstanding the thermodynamic limitations, which are mainly attributed to the reverse water gas shift reaction.
- The selectivity to CO_2 (**Table 28**) calculated in the post-breakthrough period, showed the excellent conditions for the sorption enhancement which took place during the pre-breakthrough, active sorption period. The calculated pre-breakthrough estimation of '**%** R_{red}' (% of the ratio of the NiO reduction rate to its ideal maximum) (**Figure 59**; **paragraph 8.3**) showed that the dominant reaction during the FF steps was the steam reforming, while the unmixed combustion (UC was less significant from fuel consumption point of view.

Overall, the combination of the fuel (WCO) with the sorption enhanced chemical looping reforming process assisted the Ni catalyst to be active in the hydrogen production through steam reforming (**R2**) and water gas shift (**R3**) reactions without being fully reduced or without requiring the full conversion of the fuel.

Qualitative results emerged from the AF steps, as it was difficult to differentiate between the occurrence of either the complete carbon oxidation reaction (**R9**) or the sorbent's calcination (**TD** of calcite) which both produced CO_2. Therefore, the

elemental carbon and oxygen balances were not sufficient to solve the rates of Ni oxidation, carbon oxidation and the sorbent's calcination.

- A similar flushing period at the beginning of the AF step from the previous FF step product gases was identified compared to the 40g only dry gas analysis graphs (**paragraph 7.5.1.3**).
- The sorbent's calcination would start at 1023 K (750°C) without excluding the possibility that larger temperature gradients within the sorbent-catalyst mass would further promote the sorbent's regeneration.
- The AF steps' peak temperatures slightly exceeded 1073 K (800°C). This temperature was higher (**Table 27**) than the respective values obtained in the AF steps of the 40 g catalyst chemical looping experiments as the sorbent's decarbonation occurred, which is an endothermic process.
- During the AF steps autothermality was achieved (**Figure 56(b)**; **paragraph 8.2.2**).

In general, the AF steps contributed to the avoidance of carbon deposition, since in these steps, the sorbent's regeneration and the catalyst's oxidation, which produced an OTM, were combined.

8.5.2 Sorbent's stability performance in the SEUSR chemical looping experiments of WCO

The sorbent's performance over 6 cycles of SEUSR was investigated by studying the process outputs between the pre-breakthrough ($t_{BT} - t_0$), its breakthrough (t_{SS}-t_{BT}), and steady state period ($t > t_{SS}$), as well as its respective carbonation efficiencies during these periods (α_{PB}, α_{BT}) and its overall efficiency (α) in every cycle (**Table 26**; **paragraph 8.2.1**).

- The sorbent was fully carbonated during the first SEUSR cycle as α was calculated to be close to 100%. The sorbent's capability to adsorb CO_2 was rapidly decreased in cycle 2 (**Table 26**) while its capacity to be carbonated was stabilised for the rest of the cycles on an average of

α= 56%. This was expected as shown by **Pimenidou et al.** (2009) where the macro-scale sorbent's stability study was discussed.

- The pre-breakthrough carbonation efficiency (a_{PB}) followed the same trend as the overall efficiency (α) from cycle to cycle. The parameter that influenced the values of a_{PB} in every FF step was the WCO conversion and the duration of the pre-breakthrough period.

The SEUSR chemical looping experiments on the whole illustrated the SEUSR's capability to perform very well with a waste organic fuel (WCO). At the same time, the complexity of the reaction mechanisms in the AF steps demonstrated their difficulty to be studied, as the effects of the individual reactions could not always be isolated due to the chosen methodology, which could not allow clearly distinguishing the source of CO_2 from either combustion of carbon, or decarbonation of the sorbent.

Chapter 9
Conclusions

The main conclusions of this work are discussed in this chapter. This includes those from the characterization work on the waste cooking oil and the two fast pyrolysis oils (Empty Fruit Brunch and pinewood), the studies at the micro- and macro-scale of the dolomite CO_2 sorbent, and finally the Unmixed Steam Reforming (USR) and Sorption Enhanced Unmixed Steam Reforming (SEUSR) of Waste Cooking Oil under chemical looping conditions.

From the preliminary study of the sorbent (**paragraphs 4.3** and **4.5**; **chapter 4**), its limitations as a reversible material became apparent since, a reduced carbonation performance was observed upon repeated use. The presence of steam boosted the extent of decomposition in the macro scale reactor study (**paragraph 5.3; chapter 5**) but did not affect significantly the sorbent's thermal decomposition kinetics **(Pimenidou et al., 2009).** The presence of steam enhanced the performance of the sorbent carbonation steps (macro-scale study), as evidenced by the higher extent of carbonation reached over repeated cycles compared to those without steam. This was also reflected in the higher kinetic rates during cyclic carbonations, caused by larger pre-exponential factors ($\ln A$) - but similar activation energies- obtained for the 10 and 15% steam concentrations in the gas flow. **(paragraphs 5.4.1.1** and **5.4.2.1)**

The effect of multiple cycles of thermal decomposition and carbonation in micro- (**paragraph 4.5**) and bench scale conditions (**paragraph 5.5**) indicated deactivation of the material. Even though the sorbent in the first carbonation steps in the micro- scale experiments did not experience the same deterioration as in the macro scale experiments, under both dry and wet conditions, by the final cycle the sorbent exhibited the same extent of CO_2 capture for all set- ups and conditions.

The sorbent's participation in the FF (Fuel Feed) step in the SEUSR process led to full conversion of the WCO into H_2 by promoting the conversion of produced CO and CH_4 further into CO_2 and H_2, in addition to capturing CO_2. This behaviour of the sorbent could be further studied using SEM (Scanning Electron

Microscopy) and TEM (Transmission Electron Microscopy) in order to examine the composition of the sorbent after its application in the fuel feed step, as well as any possible carbon deposition on the sorbent. These analyses will also further benefit the understanding of the limitations of regenerating the sorbent by CO_2 consumption and of its calcination. This information could be used in assisting the design of an artificially CaO-based material which will serve the same scope as the sorbent employed in the present study. It needs to be noted that the alternative CaO based sorbent should operate at high capacity under the same conditions as in the fuel feed step and the air feed step in the SEUSR process.

The elemental analysis of all waste biomass origin oils (waste vegetable cooking oil, pinewood and EFB fast pyrolysis oils,) verified the lack of sulphur above the levels of detection of the CHNS-O analyser (**paragraph 6.2**) thus minimizing catalyst poisoning when they are employed in the USR and SEUSR processes. The C:O and H:C ratios could be used as indicative factors of the waste bio-oils performance in the USR and SEUSR processes. The carbon content was lower in the two fast pyrolysis oils than in the WCO, which showed a higher potential of carbon deposition on the catalyst when employed in the USR and SEUSR processes. Moreover, the H:C ratio was higher in the WCO oil than in the two fast pyrolysis oils.s. Finally, the waste vegetable cooking oil's calorific value was higher than the pinewood and EFB pyrolysis oils which can be attributed to the H:C ratio values.

All thermogravimetric analysis of the waste biomass origin oils left a residual (coke and ash) (**paragraph 6.4, 6.5** and **6.6**) which was not thermally decomposed. It is worth noticing that the higher heating rates promoted the thermal decomposition of the pinewood fast pyrolysis oil, whereas this effect was reversed in the case of the EFB pyrolysis oil.

The waste cooking oil in particular exhibited less carbon residues than the pinewood and EFB origin pyrolysis oils during the thermogravimetric analysis (TGA) experiments at the 3K min^{-1} heating rate. This is expected to have contributed to its good performance in the USR chemical looping, where the carbon deposits were removed cyclically under air feed, and resulted into a sufficiently good overall performance of the Ni based catalyst. The catalyst's

carbon deposits are expected to be more significant and thus more difficult to remove when the EFB and pinewood fast pyrolysis oils will be used in the USR and SEUSR processes. This conclusion can be derived from the thermogravimetric analysis of the EFB and pinewood fast pyrolysis oils under 3, 6 and 9 K min^{-1} heating rates, which demonstrated a carbon and ash residue as high as 11- 18% and 11.79- 13.41% of the initial respective masses. Despite this, an oxidative environment, as during the AF (Air Feed) steps, can benefit less solid residuals according to **Uzun et al. (2007)**. Therefore, the presence of the OTM (Oxygen Transfer Material) in the USR and SEUSR processes can mitigate solid products formation on the catalyst during the FF steps.

The activation energy for the thermal decomposition of WCO (**paragraph 6.6**) within the temperature range of 570- 700K indicated that its cracking was more difficult to start compared to the two fast pyrolysis oils (pinewood and EFB origin). This was reflected in the two fast pyrolysis oils' calculated activation energies (**paragraph 6.4** and **6.5**), which showed that these bio oils may not require thermal pre-treatment prior to their use in the USR and SEUSR processes, unlike the WCO. However, the two fast pyrolysis oils' activation energies at the high temperature range of conversion (PH2) indicated that more energy is needed for their decomposition. Therefore, their steam reforming may end being more energy intensive than for the waste cooking oil.

The present study of the WCO used in the USR and SEUSR processes confirmed that a high yield H_2 product can be produced (**paragraph 8.4**). The potential application of the two complex biomass origin fast pyrolysis oils (EFB and pinewood origin) could be advanced by the mechanisms of the USR process since the same process promoted the FF steps performance of the waste cooking oil.

The USR process which was based on the unmixed combustion, steam reforming and chemical looping principles was shown to cause no deterioration to the oxygen transfer catalyst material (OTM). The presence of the sorbent significantly enhanced the performance of the steam reforming process in USR conditions (**paragraph 8.3**). Unlike when applying CLC (chemical looping combustion) to fluidised bed reactors, where the OTM is continuously transferred between the air and fuel reactor (**Mattisson et al., 2006; Lyngfelt et al., 2001**), the

USR can be applied to two fixed bed reactors which alternate between the air feed (AF) and fuel feed (FF) steps. This allows the catalyst and the sorbent to be regenerated as of the integral parts of the SEUSR process.

The Ni based catalyst performed very well during the chemical looping of the USR and SEUSR experiments with waste cooking oil during both the FF and AF steps, as presented in **chapters 7 and 8.**

Even more surprisingly, with the lowest S:C (2.5:1) ratio and at the low steam reforming temperature (T_{set}= 873.15K), the waste vegetable origin oil still performed very well, underlining the effectiveness of the process compared to the conventional SR (Steam Reforming) process when non-waste fuels (**Marquevich et al., 2000**) or pure gases (CH_4) (**Matsumura et al., 2004**) were employed.

The effectiveness of the USR process was evident as the fuel (WCO) could successfully reduce the OTM over repeated of FF steps, which was confirmed by the fuel's and steam's conversions that were close to the thermodynamic equilibrium (**paragraph 7.5.1**). The advantages of the OTM were emphasized when this complicated hydrocarbon mixture was fully steam reformed at a moderate S:C (4:1) and at the low temperature of 873.15K (600°C) (**Pimenidou et al.[(a)], 2010**). Such performance accentuates the superiority of the USR process when it is employed for waste origin fuels, over the steam reforming process when simpler hydrocarbons are chosen (**Gornay et al., 2009; Czernik et al., 2007; Matsumura et al., 2004; Marquevich et al., 2000**).

The steam to carbon ratio of 4:1 proved to be suitable for the chemical looping conditions as the catalyst, starting from a hydrogen reduced OTM,. The OTM then maintained its ability to oxidise and reduce under the air and the WCO's feeds in subsequent cycles; This allowed the process to exhibit very good and similar fuel and steam conversions at steady state under the repeated FF step (**Pimenidou et al.[(a)], 2010**). The performance of the waste cooking oil under the FF step during the USR process at a set temperature of 873K (600°C) and at atmospheric pressure was shown to significantly lower the energy consumption when compared to the conventional steam reforming process. This is because lower temperatures of operation is made possible by the cyclic regeneration of the OTM

catalyst (**paragraph 7.5.1.3** and **7.5.2.3**) and the good coupling between the exothermic and endothermic reactions of the process under both fuel and air feeds.

The presence of the OTM shifted the steam reforming (FF) steps towards the reduction of the selectivity to the gaseous carbon containing products. The prevention of the reverse water gas shift reaction, for further promotion of the H_2 and CO_2 production, eliminates any future need of downstream water gas shift reactors. SEUSR used with waste cooking oil fuel is thus demonstrating its potential for very significant process integration.

It is recommended that the extent of oxygen transfer during the air feed and the fuel feed steps be further explored with the aid of powder XRD (X-Ray Diffraction) analysis to verify the amounts derived from the elemental balances.

The fluctuations in the OTM's performance under chemical looping conditions of USR still show the process's potential, as seen in **figure 47** (**paragraph 7.5.1.3**) and in **figure 51** (**paragraph 7.5.2.3**). Better temperature control of the reactor will ensure minimisation of the CH_4 presence and bring he process closer to equilibrium.

During the pre-reduction step under hydrogen flow, gas film transfer and gas pore diffusion processes might have occurred when an initial mass of 80g of catalyst was applied. These phenomena may prevent the reactant gases movement through the inner openings of Ni particles during the reduction step (**Szekely et al., 1996).**

Hidayat et al., (2008) noticed that the lower H_2/ N_2 mixtures at lower temperatures created a more porous structure than at higher temperatures. In a similar manner, the catalyst's morphology may affect the extent and the yield of the intermediate oxidation steps during USR. Overall, the conditions of the reduction-oxidation steps can potentially influence the microstructure of the catalyst's surface and its performance in every subsequent step. These can be verified by TEM (Transmission Electron Microscopy) analysis.

In order to reach thermodynamic equilibrium throughout the reactive system, a sufficient surface area of active sites of the catalyst is required. Therefore, adequate residence time of the reactants needs to be allowed within the catalyst mass. This can be achieved by either decreasing the flowrate of the diluting N_2 gas

stream (< 600 mL min^{-1}) or by employing the catalyst mass in a longer and smaller in diameter reactor. By choosing such geometry for the reactor, the flow supply of the reactive gases (WCO and steam) can be manipulated and allow a better mixing while at the same time a better distribution of the supplied heat can be achieved which will assist the maintenance of a more stable temperature throughout the catalyst bed.

The effect of the prevention of the catalyst's degradation in the present study was validated by the successful AF steps which ensured the removal of the carbon deposited on the catalyst. Nevertheless, it needs to be underlined that a study which will contain a higher number of USR cycles may demonstrate a better outlook on the possibility of the Ni-based catalyst's deactivation, even though the conducted effective oxidation steps were already quite beneficial to the Ni catalyst's performance.

The O_2 consumption by the reduced catalyst is a diffusion-controlled phenomenon and only after sufficient carbon removal from the Ni particles external layers, and the oxidation of the Ni particles can be realised. The residence time of the supplied O_2 in the catalyst bed was longer in the case of the 80g experiments, where higher rates of carbon oxidations were noticed, and which resulted in a greater extent of the OTM's regeneration. During the 40g runs, the only product of the carbon burning reactions was CO_2 which indicated that any carbon deposits' oxidation was complete.

The sorbent's presence confirmed the enhancement of the process's hydrogen yield as shown in the SEUSR chemical looping experiments by manipulating the WGS (Water Gas Shift) reaction **(Pimenidou et al.[(b)], 2010)**. The sorbent's regeneration and the prevention of the OTM's deactivation by alternating the reduction and the oxidation steps was ensured. The prevention of deactivation of both the catalyst and sorbent is the key factor in sustaining a constant high hydrogen yield. Another parameter that ensures the latter is the maintenance of the carbon products selectivity close to their thermodynamic equilibrium under the specific applied operating conditions of the S:C ratio and temperature.

The steam conversion (X_{H_2O}) was enhanced on average by 49.08% when the purity of the product stream reached a maximum of 98.6% in H_2 while its average

value was 96.7% (**paragraph 8.3**). The promotion of the fuel and steam conversion can be better attributed to the sorbent's reactive role, which did not just remove the CO_2 from the product syngas, but also almost fully allowed the conversion of the CO and CH_4 according to Le Chatelier's principle. Eventually the use of a CO_2 sorbent increased the cracking activity of the catalyst and the catalyst's resistance to coking. The selectivity to CO_2 confirmed the aforementioned results.

Longer calcination periods of the sorbent were evidenced in the SEUSR process than those of carbonation from cycle to cycle. Uncertainties on the latter arose from temperature measurement limitations, as the thermocouples could only pick up the bulk solid temperature, while larger heat amounts/ temperature gradients within the solids of the reactor bed were expected to be present **(Pimenidou et al.[(b)], 2010)**.

During the fuel feed step of the SEUSR process and while the sorbent was active and adsorbed the produced CO_2, high levels of energy were produced which compensated the needs of the steam reforming reaction, so that the system did not need any external energy supply. This was a clear indication of the process's capability to run autothermally, i.e. without requiring external heating, for long periods of time within each cycle.

In general, the WCO SEUSR based on a Ni-Al_2O_3 catalyst is a vigorous process as the catalyst is active to produce H_2 by steam reforming and water gas shift without needing to be fully reduced or under complete fuel conversion.

The WCO was involved in complex reactions during the fuel feed steps (in the SEUSR), which need to be quantified and isolated for analysis in the future. Additionally, these mechanisms and their interaction with the OTM catalyst and the sorbent would benefit from further study while their behaviour is monitored online. The OTM and the sorbent were studied for a limited number of cycles. The present study has to be extended to a larger number of chemical looping experiments in order to determine the catalyst's durability. In addition, an alternative CaO based sorbent's with high durability while maintaining high kinetics of CO_2 sorption and capacity would be required to overcome the shortcomings of the natural sorbent dolomite.

In conclusion, when the USR process was used to treat waste vegetable cooking oil (WCO) with 80 g of catalyst, it proved to be the most beneficial as the fuel's conversion was closer to the theoretical thermodynamic equilibrium conversion. This was further verified by the USR chemical looping experiments (**Pimenidou et al.[(a)], 2010**). In the SEUSR chemical looping experiments, the WCO conversion was greatly enhanced by the sorbent's presence compared to the 40g chemical looping USR experiments (**Pimenidou et al.[(b)], 2010**). At the same time the sorbent's presence in the fuel feed steps of the SEUSR runs showed that the process can potentially be operated autothermally while the sorbent is active (**Pimenidou et al.[(b)], 2010**). Therefore, the USR and SEUSR processes clearly exhibited their competence for treating liquids of waste biomass origin as fuels.

Appendices

Table I Initial and final thermal decomposition temperatures (in K) of fresh dolomite and recarbonated CaO ($CaCO_3$) for 4 heating cycles as presented in Figures 7 (e) and (f) (TGA analysis) in 75 and 100% vol CO_2/ N_2 mixtures

75% CO_2		100% CO_2	
$T_{CaCO3\ (i)}$	$T_{CaCO3\ (f)}$	$T_{CaCO3\ (i)}$	$T_{CaCO3\ (f)}$
1173.45	1204.45	1181.55	1226.45
1171.25	1203.45	1173.15	1224.55
1167.15	1203.45	1168.15	1224.55
1164.95	1203.45	1180.15	1224.55

Appendix II

CO_2 excess verification in the sorbent's macro- scale study

In the bench scale reactor experiments, during the carbonation steps CO_2 was consumed as expressed by the reaction equation (**R18** or **CRB**). For these steps the excess of CO_2 was verified by calculation of the maximum volume of CO_2 which would be required for the full carbonation of the maximum theoretical CaO moles ($n_{\max\ (CaO)}$) from the fully calcined 2500mg (=$m_{i\ (MgCa(CO_3)_2)}$) of the fresh sorbent ($MgCa(CO_3)_2$).

$$n_{\max\ (CaO)} = \frac{\%\ theoretical\ mass\ fraction\ of CaO}{\bar{W}_{CaO}} \times \frac{m_{i\ (MgCa(CO_3)_2)}}{100}$$

where the % theoretical mass fraction of CaO is equal to 30.7 (**Table 4**; **paragraph 4.1**; **chapter 4**) and

$\bar{W}_{CaO}$ is the molar mass of CaO which is equal to 56.08.

Therefore, the $n_{\max\ (CaO)}$ value should be equal to 0.0137 moles.

According to reaction **R18**, 1 mole of CaO consumes 1 mole of CO_2 in order to be fully carbonated and result in 1 mole of $CaCO_3$. Therefore, the theoretical CO_2 moles (n_{CO_2}) which would be required for the full carbonation of 0.0137 CaO moles would be 0.0137 moles.

It needs to be reminded that the CO_2 was diluted in 750 mL min^{-1} N_2 flows for the carbonation steps. For the full carbonation when the lower volumetric concentration was applied (5% vol CO_2/ N_2) the volumetric flowrate of CO_2 at STP was 50 mL min^{-1}. This CO_2 volumetric flowrate corresponds to the following molar flowrate,

$$\dot{n}_{CO2} = \frac{P\dot{V}_{CO_2}}{RT} = \frac{(101.325\ kPa) \times (0.05\ L\ min^{-1})}{(8.314\ L\ kPa\ K^{-1}\ mol^{-1}\ 293K)} = 0.021\ moles\ min^{-1}$$

which is sufficient for the $n_{\max\ (CaO)}$= 0.0137 moles.

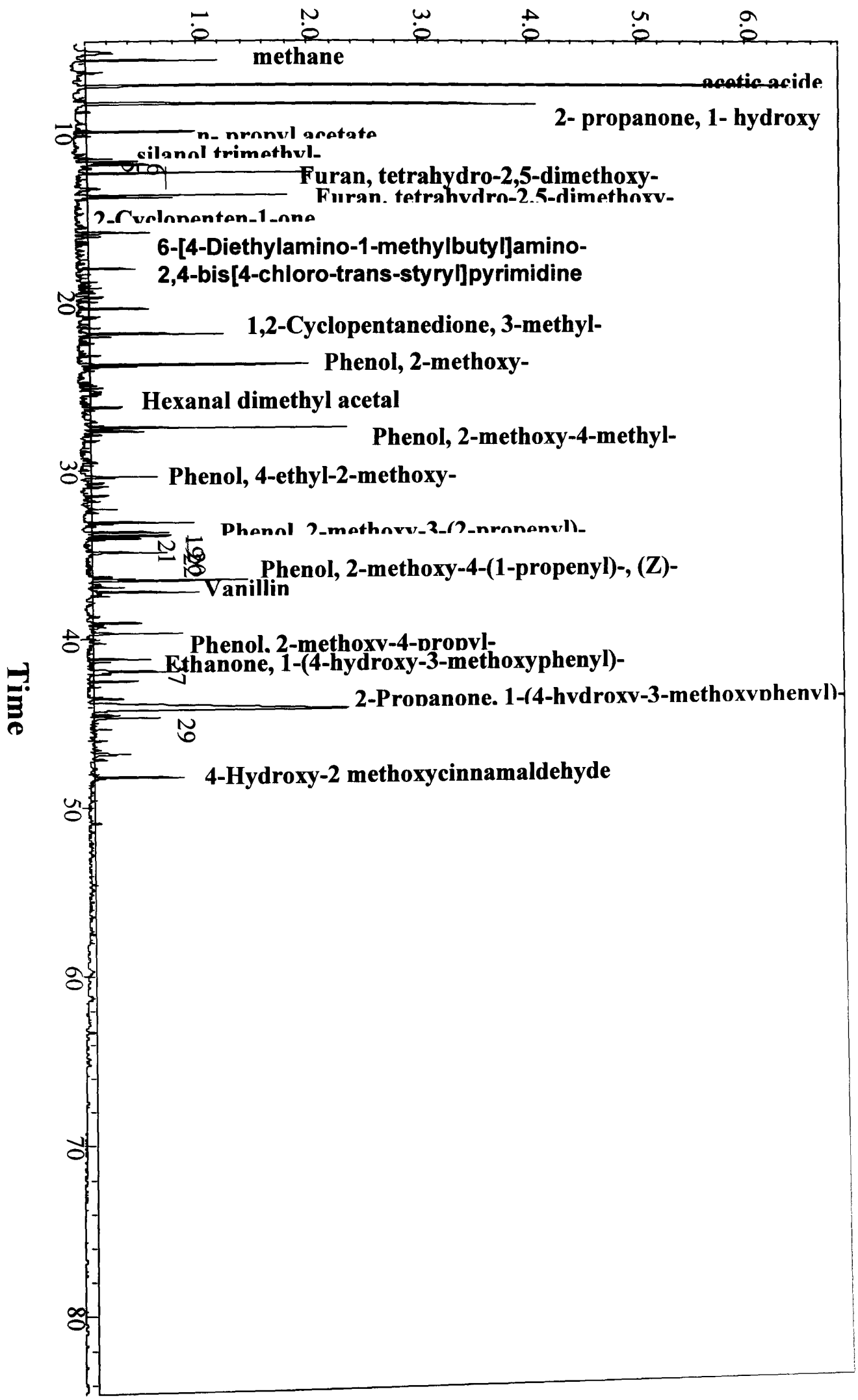

Appendix III; Figure I Pinewood fast pyrolysis oil GC-MS graph

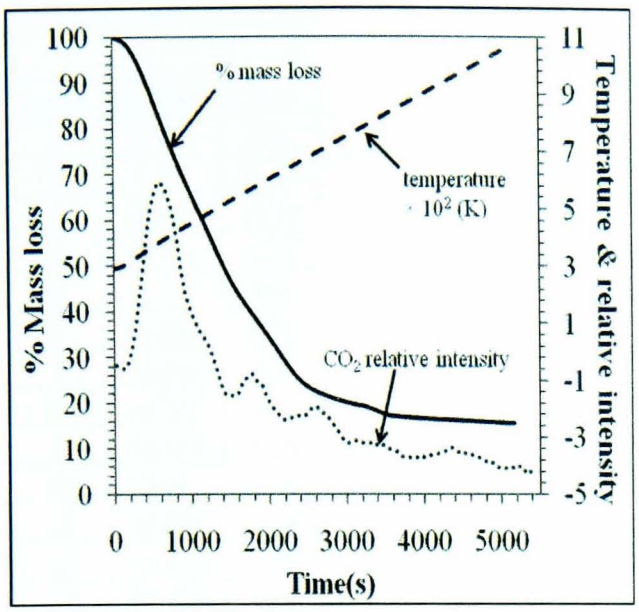

(a) TGA curve and relative intensity of CO_2 from the FTIR spectra

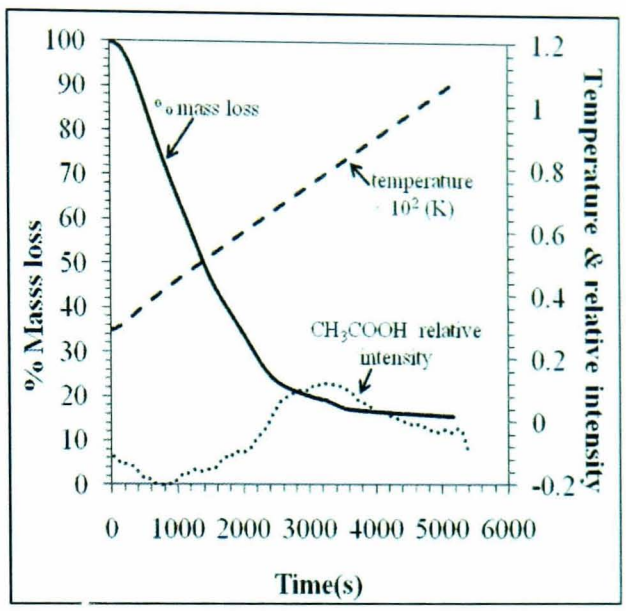

(b) TGA curve and relative intensity of ethanoic acid from the FTIR spectra

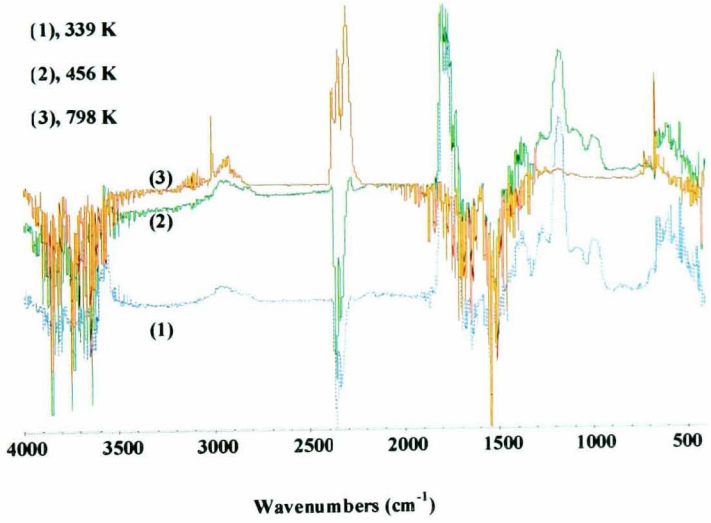

(c) FTIR spectra of the pyrolysis of EFB oil 9K min^{-1}

Figure II TGA- FTIR analysis of EFB pyrolysis oil at 9K min^{-1}

Table I GS- MS data on pine wood fast pyrolysis oil

Peak#	Ret.Time	Conc.	Name
1	5.982	2.51	Methane, (methylsulfinyl)(methylthio)-
2	7.431	21.46	Acetic Acid
3	8.546	15.37	2-Propanone, 1-hydroxy
4	10.144	2.49	n-Propyl acetate
5	11.717	0.44	Ammonium acetate
6	11.892	1.94	Cobalt, nonacarbonyl[.mu.3-(oxophenylethylidyne)]tri-, triangulo
7	12.066	1.25	Silanol, trimethyl-
8	12.552	4.5	Furan, tetrahydro-2,5-dimethoxy-
9	13.864	4.48	Furan, tetrahydro-2,5-dimethoxy-
10	13.933	1.24	2-Cyclopenten-1-one
11	14.005	1.87	Furfural
12	16.048	1.04	6-[4-Diethylamino-1-methylbutyl]amino-2,4-bis[4-chloro-trans-styryl]pyrimidine
13	22.025	4.63	1,2-Cyclopentanedione, 3-methyl-
14	23.823	5.04	Phenol, 2-methoxy-
15	23.94	1.14	Hexanal dimethyl acetal
16	27.55	7.1	Phenol, 2-methoxy-4-methyl-
17	30.404	1.25	Phenol, 4-ethyl-2-methoxy-
18	33.108	2.25	Phenol, 2-methoxy-3-(2-propenyl)-
19	33.704	1.74	2-Furancarboxaldehyde, 5-(hydroxymethyl)-
20	33.894	1.7	1,2-Benzenediol
21	34.049	1.03	Phenol, 2,6-dimethoxy-
22	34.877	1.65	Phenol, 2-methoxy-4-(1-propenyl)-
23	36.533	2.9	Phenol, 2-methoxy-4-(1-propenyl)-, (Z)-
24	37.235	2.43	Vanillin
25	39.055	1	Phenol, 2-methoxy-4-propyl-
26	39.683	1.85	Ethanone, 1-(4-hydroxy-3-methoxyphenyl)-
27	41.201	1.32	2-Propanone, 1-(4-hydroxy-3-methoxyphenyl)-
28	42.496	0.93	2-Propanone, 1-(4-hydroxy-3-methoxyphenyl)-
29	44.67	1.5	Methyl-(2-hydoxy-3-ethoxy-benzyl)ether
30	48.176	1.96	4-Hydroxy-2-methoxycinnamaldehyde

Table II GS- MS data on EFB (Empty Fruit Bunch) fast pyrolysis oil

Peak#	Ret.Time	Conc.	Name
1	7.405	25.84	Acetic acid
2	8.497	9.15	Octadecanoic acid, 9,10,18-tris[(trimethylsilyl)oxy]-, methyl ester
3	11.715	1.03	1-Hydroxy-2-butanone
4	16.055	1.83	2-Propanone, 1-(acetyloxy)-
5	16.291	1	1,2-Ethanediol, monoacetate
6	19.862	0.69	2-Cyclopenten-1-one, 3-methyl-
7	22.033	1.4	2-Cyclopenten-1-one, 2-hydroxy-3-methyl-
8	22.123	1.5	1,2-Cyclopentanedione, 3-methyl-
9	23.355	11.41	Phenol
10	23.838	1.66	Phenol, 2-methoxy-
11	25.051	1.06	Phenol, 2-methyl-
12	25.251	1.01	2-Cyclopenten-1-one, 3-ethyl-2-hydroxy-
13	26.324	0.81	Phenol, 4-methyl-
14	26.405	0.67	Phenol, 3-methyl-
15	27.742	0.82	1H-4-Azacycloprop[cd]indene, octahydro-4-methyl-
16	33.931	1.54	1,2-Benzenediol
17	34.1	3.62	Phenol, 2,6-dimethoxy-
18	36.533	0.77	Phenol, 2-methoxy-4-(1-propenyl)-, (Z)-
19	36.95	0.76	1,2,4-Trimethoxybenzene
20	37.468	0.61	Hydroquinone
21	39.769	3.79	Dodecanoic acid
22	41.402	0.76	Phenol, 2,6-dimethoxy-4-(2-propenyl)-
23	44.517	1.29	Phenol, 2,6-dimethoxy-4-(2-propenyl)-
24	44.854	1.33	Tetradecanoic acid
25	46.276	1.48	Hexadecanoic acid, methyl ester
26	49.763	14.7	n-Hexadecanoic acid
27	50.637	1.07	9-Octadecenoic acid, methyl ester
28	53.865	5.54	Oleic Acid
29	53.993	2.25	9,12-Octadecadienoic acid (Z,Z)-
30	55.764	0.6	Hexadecanoic acid, 2-hydroxy-1-(hydroxymethyl)ethyl ester

Appendix III

Table III Thermal decomposition phases of EFB origin fast pyrolysis oil in TGA, using 50 mL min^{-1} N_2, at different heating rates, up to 1073K (800°C)

		Mass loss (%)		T_i (K)		T_f (K)	
	TD phases	**end of PH1**	**end of PH2**	**PH1**	**PH2**	**PH1**	**PH2**
Heating rates	3	30.04	90.05	303.75	368.10	368.10	628.06
	6	29.01	90.07	299.14	372.44	372.44	636.16
	9	19.53	90.01	306.90	376.53	376.53	666.66

Table IV Kinetic parameters for the TGA decomposition of EFB origin fast pyrolysis oil based on the reaction order model $g(\alpha) = \frac{[1-(1-\alpha)^{1-n}]}{1-n}$ and the Jander diffusion equation $g(\alpha) = [1-(1-\alpha)^{\frac{1}{3}}]^2$, the correlation coefficient values and the conversions (α) temperature range of the applied model

PH1 ($K\ min^{-1}$)	**E±dE ($kJ\ mol^{-1}$)**	**lnA±dlnA ($A\ in\ s^{-1}$)**	**order**	**correlation coefficient**	**temperature (K)**
3	26.9±0.57	1.5±0.22	2.9	0.989	303- 367
6	56.6±1.04	11150.6±1640.03	-	0.986	299-375
9	55.4±1.40	2619.3±1816.6	-	0.989	307-378

PH1 ($K\ min^{-1}$)	**E±dE ($kJ\ mol^{-1}$)**	**lnA±dlnA ($A\ in\ s^{-1}$)**	**order**	**correlation coefficient**	**temperature (K)**
6	15.4±0.18	0.06±322.9	-	0.998	375-636
9	20.3±-0.21	0.02±428.1	-	0.996	378-667

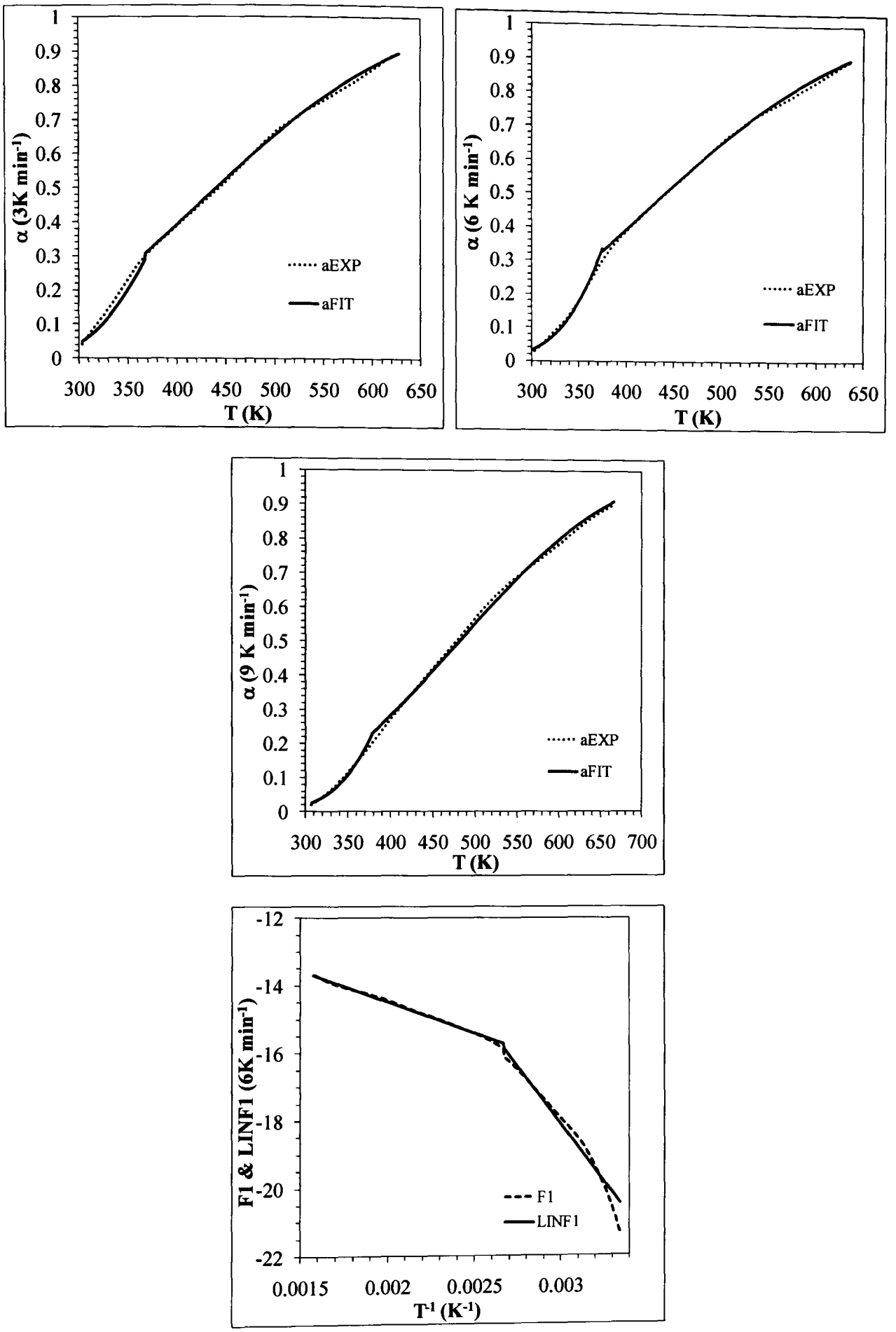

Figure III Predicted conversion curves for phases 1 and 2 (as seen in the above table; **Table III**) (α PH1; α PH2) based on the improved Coats-Redfern method program for the reaction order model over the experimental conversion curves (α exp) for the TGA runs of EFB (Empty Fruit Brunch) origin fast pyrolysis oil at 3 different heating rates (3, 6, 9 K min^{-1})

Appendix IV

Carbon balance for the FF step in USR

Any carbon species which enter the reactor in time *dt* originate only from waste cooking oil feed. The system balances by carbon leaving in the form of the produced dry gases (CO, CO_2 and CH_4) as well as other carbon products such as (i) carbon accumulated by coking and other C-containing hydrocarbons jointly called ($dn_{C,HC}$), as well as (ii) by capture on the CO_2 sorbent (dn_{CO2}), and (iii) unreacted fuel.

The carbon balance in this closed system according to the above description, is given by the following equation,

$$n \times \dot{n}_{C_nH_mO_k,in} = n \times \dot{n}_{C_nH_mO_k,out} + \frac{dn_{C,HC}}{dt} + \frac{dn_{CO_2}}{dt} + \dot{n}_{out,dry} \times (P + M + N)$$

$$= \frac{dn_{C,HC}}{dt} + \frac{dn_{CO_2}}{dt} + F_1 \times \dot{n}_{out,dry}$$

(Eq. I)

with $F_1 = P + M + N$.

On a molar rate basis, by keeping the unknowns on the left, and the known values on the right:

$$n \times \dot{n}_{C_nH_mO_k,out} + \frac{dn_{C,HC}}{dt} + \frac{dn_{CO_2}}{dt} = n \times \dot{n}_{C_nH_mO_k,in} - F_1 \times \dot{n}_{out,dry}$$

(Eq. II)

By keeping waste cooking oil conversion (in moles s^{-1}) on the right hand side of the **Eq. II**:

$$\frac{1}{n} \times \left(\frac{dn_{C,HC}}{dt} + \frac{dn_{CO_2}}{dt} + F_1 \times \dot{n}_{out,dry} \right) = \dot{n}_{C_nH_mO_k,in} - \dot{n}_{C_nH_mO_k,out}$$

(Eq. III)

Since there is no sorbent present during the unmixed steam reforming, contrary to the sorption enhanced steam reforming, **Eq. III** can be written as:

$$\frac{dn_{C,HC}}{dt} + \frac{dn_{CO_2}}{dt} + n \times \dot{n}_{C_nH_mO_k,out} = \left(n \times \dot{n}_{C_nH_mO_k,in}\right) - \left(F_1 \times \dot{n}_{out,dry}\right)$$

When the bio-oil conversion (in moles s^{-1}) is kept on the left hand side:

$$\dot{n}_{C_nH_mO_k,in} - \dot{n}_{C_nH_mO_k,out} = \frac{1}{n} \times \left(\left(F_1 \times \dot{n}_{out,dry}\right) + \frac{dn_{C,HC}}{dt}\right)$$

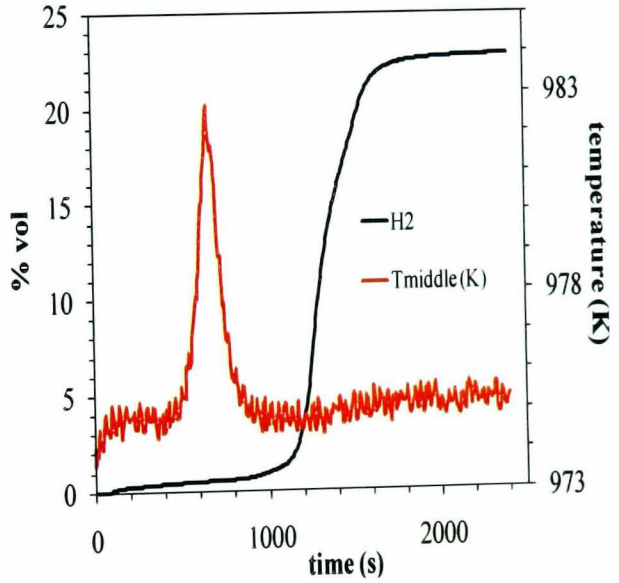

Figure I Fresh catalyst's ($m_{i(catalyst)}$= 80g) pre- reduction for the 1st FF step at S:C= 2.5:1

(i) Inaccuracies in gas flowrates' measurements by the mass flowmeters

By the beginning of the USR experiments the H_2, air and N_2 gases flowrate was calibrated in order to avoid any inaccuracies on the rig's control panel (**Fig. 2**) display. Thus any errors that could be propagated and be carried forward were reduced. This was realised by using (a) a bubble column which was used for calibrating the H_2 and air mass flow controllers and (b) gas flow meter which reading was converted for the N_2 mass flow controller.

(a) Bubble column

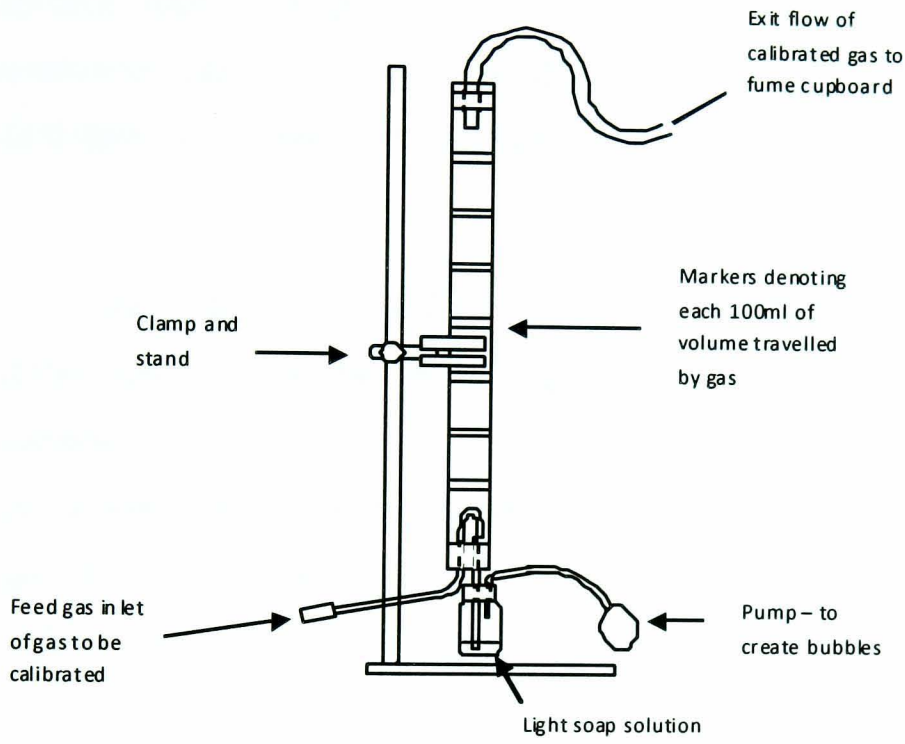

Figure II Bubble Column

The bubble column that was used was marked to indicate increments of 100ml of volume and a rising bubble which was formed by a pumped light soap solution. The bubble indicated the flow and level of the gas entering the column. The duration of this bubble to travel through a set volume would determine the gas's volumetric flowrate as follows,

$$\dot{V}_{i} = \frac{volume\ of\ gas\ passing\ through\ the\ column}{time\ taken\ for\ above\ volume\ to\ pass\ through\ the\ column}$$

where i denotes either the H_2 or air. The H_2 and air mass flow controllers' display was then adjusted to the calculated value of each gas's flowrate.

(b) Gas flow meter

A reading of the N_2 volumetric flow rate using an Agilent ADM1000 gas flow meter was taken and then was converted to a value which took into account the actual room temperature and pressure.

The measured flowrates of H_2, air and N_2 by the above methods had to correspond to standard temperature and pressure (STP) since this was required by the mass flow analysers used, MKS Type 1179A Mass-Flo® Controller, which in turn were connected up to a MKS Type 247C 4-channel readout panel. The channel readout panel necessitated the volume flow rates in STP so that each mass flow controller could control the amount of a reactant gas that was fed in to the reactor as if there was a change in temperature and/or pressure.

The MKS Type 1179A Mass-Flo® Controller operates by sensing the differential heat transfer between the temperature sensing heater elements that are connected to the sensor tube. This device senses the thermal mass movement across the sensor tube, which is converted to mass flow via the specific heat, Cp, of the gas (MKS Instruments: 1999). A schematic of the mass flow controller and the location of the sensor tube follow.

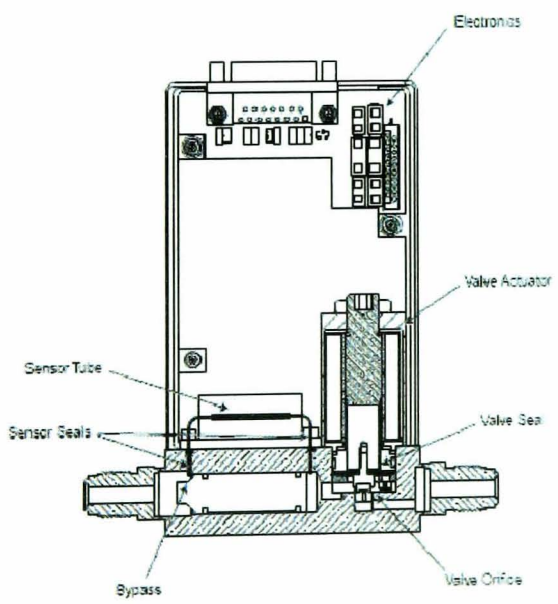

Figure III Cross section diagram of a Type 1179 Mass-Flo Controller (MKS Instruments: 2006)

The volume flow rates obtained at room temperature and pressure needed to be converted in to a volume flow rate at standard temperature and pressure. This was achieved by application of the following equation:

$$\dot{V}_{st} = \frac{P_{measured}}{P_{ST}} \times \dot{V}_{measured} \times \frac{T_{ST}}{T_{measured}}$$

where, $\dot{V}_{st}$= volume flow rate at STP

$P_{measured}$= measured pressure

P_{ST}= standard pressure= 101.325kPa

$T_{measured}$= measured temperature

T_{ST}= standard temperature= 298.15K

$\dot{V}_{measured}$= measured volume flow rate

The measured values of room temperature and pressure were taken from the Analytical Laboratory (located on the ground floor of the Houldsworth Building), from a barometer (mmHg) and thermometer (^{o}C). The pressure's reading was converted from mmHg to kPa as the following conversion was used:

$$P_{meas} = \frac{\rho_{Hg} \times h_{Hg} \times g}{1000}$$

where,

ρ_{Hg}= density of mercury= 13580 kg.m^{-3}

h_{Hg}= height of mercury

g = gravitational constant= 9.81 m.s^{-2}

(ii) Calculation of errors in dry gas volume concentrations by the online gas analysers

The errors' calculations are based on a function '*f*' which is the product or ratio of two or more variables e.g, '*u*', 'v', '*w*'. For instance $f = \frac{u \times v}{w}$ *or* $\frac{1}{u \times w \times v}$ etc.

Then, the relative error on *f*, 'R_f' follows:

$$R_f = (R_u^2 + R_v^2 + R_w^2)^{\frac{1}{2}} \qquad \textbf{Eq.IV}$$

where R_u , R_v and R_w are the relative errors on *u*, *v*, and *w*.

And if a function '*g*' is the sum or difference of two or more variables eg. '*u*', 'v', '*w*'. For instance $g = u - v - w$ or $g = u - v - w$ then the absolute error on *g*, Δg is given by:

$$\Delta g = (\Delta u^2 + \Delta v^2 + \Delta w^2)^{\frac{1}{2}} \quad \textbf{Eq.V}$$

This theory is applied to the assessment of errors on, as an example, the molar production rate of hydrogen ($\dot{n}_{H_2}$),

$$\dot{n}_{H_2} = y_{H_2} \times \dot{n}_{out,dry} \qquad \textbf{Eq.VI}$$

where

$$\dot{n}_{out,dry} = \frac{\dot{n}_{N_2,in}}{y_{N_2}} \qquad \textbf{Eq.VII}$$

$$\text{And } y_{N_2} = 1 - (y_{CH_4} + y_{CO} + y_{CO_2} + y_{O_2} + y_{H_2}) \qquad \textbf{Eq.VIII}$$

The following nomenclature is used:

'R_i' are the relative errors, 'AB_i' are the absolute errors.

Then, **Eq. IV** applies to **Eq. VI** and **V**

$$R_{\dot{n}_{H_2}} = (R_{y_{H_2}}^2 + R_{\dot{n}_{out,dry}}^2)^{\frac{1}{2}} \qquad \textbf{Eq.IX}$$

where

$$R_{\dot{n}_{out,dry}} = (R_{y_{N_2}}^2 + R_{\dot{n}_{N_2,in}}^2)^{\frac{1}{2}} \qquad \textbf{Eq.X}$$

And

$$R_{\dot{n}_{H_2}} = \frac{\Delta y_{N_2}}{y_{N_2}}$$

with $\Delta_{y_{N_2}} = (\Delta_{y_{CO_2}}{}^2 + \Delta_{y_{H_2}}{}^2 + \Delta_{y_{CO}}{}^2 + \Delta_{y_{CH_4}}{}^2)^{\frac{1}{2}}$

and for H_2, CO_2, CO, CH_4 and O_2, $\Delta y = R_y \times y$

The following assumptions are made in the following example:

(i) all the relative errors on the measurements are equal to ±0.02 (±2%).

(ii) From cycle 1, $m_{i\,(fresh\ catalyst)}$= 80g, S:C =4, T=600 °C, steady state values of:

y_{CO_2}=0.198, y_{H_2} =0.483, y_{CH_4}=0.055, y_{CO}=0.019

Thus, $\Delta_{y_{N_2}} = (\Delta_{y_{CO_2}}{}^2 + \Delta_{y_{H_2}}{}^2 + \Delta_{y_{CO}}{}^2 + \Delta_{y_{CH_4}}{}^2)^{\frac{1}{2}}$=0.0105

With y_{N_2}= 1- (0.198 + 0.483 + 0.055 + 0.019) = 0.246,

$$\boxed{R_{y_{N_2}} = \frac{0.0105}{0.246} = 0.043}$$

Therefore, the relative error on the N_2 concentration is ±4.3%.

Based on equation X, the error on the outgoing total dry gas molar flow rate is given by,

$$R_{\dot{n}_{out,dry}} = (R_{y_{N_2}}^2 + R_{\dot{n}_{N_2,in}}^2)^{\frac{1}{2}} = (0.043^2 + 0.02^2)^{0.5} = 0.047$$

Therefore, the relative error on the outgoing total dry gas molar flow rate is ±4.7%.

And finally, from

$$R_{\dot{n}_{H_2}} = (R_{y_{H_2}}^2 + R_{\dot{n}_{out,dry}}^2)^{\frac{1}{2}} = (0.02^2 + 0.047^2)^{0.5} = 0.051$$

the relative uncertainty on the molar rate of production of hydrogen is calculated to be ±5.1%.

This translates as a molar production rate of hydrogen of

$$8.2 \times 10^{-4} \pm \mathbf{4.2 \times 10^{-5}} \text{ mol s}^{-1}.$$

carbon dioxide: $\dot{n}_{CO_2} = 3.371 \times 10^{-4} \pm \mathbf{1.7 \times 10^{-5}}$ mol s^{-1}

-carbon monoxide: $\dot{n}_{CO} = 3.32 \times 10^{-5} \pm \mathbf{2 \times 10^{-6}}$ mol s^{-1}

-methane: $\dot{n}_{CH_4} = 9.5 \times 10^{-5} \pm \mathbf{5 \times 10^{-6}}$ mol s^{-1}

Using the same theory to estimate the uncertainty on the fuel conversion:

$$X_{WCO} = \frac{(y_{CO_2} + y_{CO} + y_{CH_4}) \times \dot{n}_{out,dry}}{n \times \dot{n}_{WCO,in}}$$

And assuming 2% relative errors on n, the molar fraction of carbon in the oil, and on $\dot{n}_{WCO,in}$ the molar input flow rate of oil to the reactor, then the relative error on the waste cooking oil conversion is calculated to be **5.7%**, which translates into, X_{WCO}=0.89 **±0.05**.

Missing pages are unavailable

Abanades J. C., Alonso M. and N. Rodriguez. 2010. Experimental validation of in-situ CO_2 capture with CaO during the low temperature combustion of biomass in a fluidised bed reactor. *International Journal of Greenhouse Control.* Article in Press

Abanades J.C.. 2002. The maximum capture efficiency of CO_2 using a carbonation/ calcination cycle of CaO/ $CaCO_3$. *Chemical Engineering Journal.* **90**(3), pp.303- 306.

Abanades J.C., Rubin E.S. and E. J. Anthony. 2004. Sorbent cost and performance in CO_2 capture systems. *Industrial and Engineering Chemistry Research.* **42**(13), pp.3462- 3466.

Abanades, J.C. and Alvarez, D.. 2003. The Conversion Limits in the Reaction of CO_2 with Lime. *Energy and Fuels.* **17**(2), pp. 308-315.

Abdullah, N. and Gerhauser, H. 2008. Bio-oil derived from empty fruit bunches. *Fuel.* **87**(12), pp.2606-2613.

Aboulkas A., El Harfi, K. & El Bouadili, A.. 2008. Non-isothermal kinetic studies on co-processing of olive residue and polypropylene. *Energy Conversion and Management.* **49**(12), pp.3666-3671.

Abu- Zahra M. R. M., Feron P.H.M., Jansens P. J., Goetheer E. L. V.. 2009. New process concepts for CO_2 post- combustion capture process integrated with co- production of hydrogen. *International Journal of Hydrogen Energy.* **34**(9), pp.3992- 4004.

Adlard, E. R.; Handley, Alan J. (2001). Gas chromatographic techniques and applications. London: Sheffield Academic. ISBN 0-8493-0521-7.

Adris A.M., Lim C.J. and J.R. Grace. 1997. The fluidised bed membrane reactor for steam methane reforming: model verification and parametric study. *Chemical Engineering Science.* **52**(10) pp. 1609- 1622.

Ahmaruzzaman M. and Sharma D.K. 2005. Non-isothermal kinetic studies on co-processing of vacuum residue, plastics, coal and petrocrop.

Journal of Analytical and Applied Pyrolysis. **73**(2), pp.263-275.

Aihara M., Nagai T., Matsushita J., Negishi Y. and H. Ohya. 2001. Development of porous solid reactant for thermal-energy storage and temperature upgrade using carbonation/decarbonation reaction. *Applied Energy*. **69**(3), pp.225-238.

Aki H., Yamamoto S., Kondoh J., Maeda T., Yamaguchi H., Murata A. and I. Ishii. 2006. Fuel cells and energy networks of electricity, heat and hydrogen in residential areas. *International Journal of Hydrogen Energy*. **31**(3), pp.967-980.

Alpern B. and M.J. Lemos de Sousa. 2002. Documented international enquiry on solid sedimentary fossil fuels; coal: definitions, classifications, reserves- resources, and energy potential. *International Journal of Coal Geology*. **50**, pp.3- 41.

Diego Alvarez and Carlos Abanades. 2005. Pore- size and shape effects on the recarbonation performance of calcium oxide submitted to repeated calcination/ recarbonation cycles. *Energy and Fuels*. **19**(1), pp.270- 278.

Andujar J.M. and S. Segura. 2009. Fuel cells: History and updating. A walk along two centuries. *Renewable and Sustainable Energy Reviews*. **13**(9), pp.2309- 2322.

Arstad B., Blom R., Bakken E., Dahl E., Jakobsen J.P. and P. Rokke. 2009. Sorption enhanced methane steam reforming in a circulating fluidized bed reactor system. *Energy Procedia*. **1**(1), pp.715- 720.

Asadullah M., Zhang S., Min Z., Yimsiri P. and C.-Z. Li. 2010. Effect of biomass structure on its gasification reactivity. *Bioresource Technology*. **101**(20), pp.7935- 7943.

DeAza A.H., Rodriguez M.A., Rodriguez J. L., de Aza S., Pena P., P. Convert, T. Hansen and X. Turrilas. 2002. Decomposition of dolomite monitored by neutral thermodiffractometry. *Journal of American Ceramic Society*, **85**(4), pp.881- 888.

Balasubramanian B., A. Lopez Ortiz, S. Kayatakoglou and D. P. Harrison.

1999. Hydrogen from methane in a single step process. *Chemical Engineering Science*. **54**(15), p.3543.

Bandi W. R. and G.Krapf. 1976. The effect of CO_2 pressure and alkali salt on the mechanism of decomposition of dolomite. *Thermochimica Acta*. **14**, pp.221- 243.

Barker R.. 1973. The reversibility of the reaction $CaCO_3$ □ $CaO+CO_2$. *Journal of Applied Chemistry and Biotechnology*. **23**(10), pp.711- 779.

Basagiannis, A and X.E. Verykios. 2006. Reforming reactions of acetic acid on nickel catalysts over a wide temperature range. *Journal of Applied Catalysis A: General*. **308**, pp.182-193.

Basagiannis A.C. and X.E. Verykios. 2007. Catalytic steam reforming of acetic acid for hydrogen production. *International Journal of Hydrogen Energy*. **32** (15), pp.3343- 3355.

Basagiannis, A. C and X. E. Verykios. 2007. Steam Reforming of the aqueous fraction of bio-oil over structured $Ru/MgO/Al_2O_3$ catalysts. *Catalysis Today*. **127**(1- 4), pp.256–264.

Belmabkhout Y. and A. Sayari. 2009. Adsorption of CO_2 from dry gases on MCM-41 silica at ambient temperature and high pressure. 2: Adsorption of CO_2/N_2, CO_2/CH_4 and CO_2/H_2 binary mixtures. *Chemical Engineering Science*. **64**(17), pp. 3729-3735.

Beruto D. T., Vecchiattini R. and M. Giordani. 2003(a). Effect of mixtures of H_2O (g) and CO_2 (g) on the thermal half decomposition of dolomite natural stone in high CO_2 pressure regime. *Thermochimica Acta*. **404**(1-2), pp.25-33.

Beruto D. T., Vecchiattini R. and M. Giordani. 2003(b). Solid products and rate limiting step in the thermal half- decomposition of natural dolomite in CO_2 (g) atmosphere. *Thermochimica Acta*. **405**(2), pp.183- 194.

Bhatia S.K. and D.D. Perlmutter. 1983. Effect of the product layer on kinetics of the CO_2—lime reaction. *A.I.Ch.E. Journal*. **29**(1), pp.79–86.

Blamey J., Anthony E.J., Wang J. and P.S. Fennell. 2010. The calcium looping cycle for large-scale CO_2 capture. *Progress in Energy and Combustion*

Science. **36**(2), pp. 260-279.

B. Bilinski, E. Stefaniak and P. Staszczuk. 1992. The influence of thermal activation on the surface properties of dolomite. *Powder Technology.* **73**(3), pp.261- 266.

Bing J., Zhenqing S. and L. Meiqin. 2010. China's energy development strategy under the low-carbon economy. *Energy.* In Press, Corrected Proof.

Bogahawatta VTL., Abdul-Jaleel A. and Behbehani M. 2004. The heat treatment and particle size effects in the thermal decomposition of dolomite for separation of constituents. *Transactions of the institution of mining and metallurgy, Section C- Mineral Processing and extractive Metallurgy.* (2), pp.111-117.

Bonjour J., Chalfen J. B. and F. Meunier. 2002. Temperature Swing Adsorption Process with Indirect Cooling and Heating. *Industrial and Engineering Chemistry Research.* **41**(23), pp 5802–5811.

Borgwardt R.H.. 1989. Calcium oxide sintering in atmospheres containing water and carbon dioxide. *Industrial and Engineering Chemistry Research.* **28**(4), pp.493- 500

Braileanau A., M. Zaharescu, D. Crisan, D. Fatu, E. Segal and C. Danciulescu. 1996. Kinetics of the decomposition of calcium carbonate in the presence of Bi_2O_3, The Journal of Thermal Analysis, **47**(2), pp.569- 575.

Bridgewater A.V., Maier D. and D. Radlein. 1999. An Overview of Fast Pyrolysis of Biomass. Organic Geochemistry. **30**(12), pp.1479- 1493.

Bridgwater A.V.. 1999. Principle and practice of biomass pyrolysis process for liquid. *Journal of Analytical and Applied Pyrolysis.* **5**, pp.3- 22.

Caceres P.G., E.K. Attiogbe. 1997. Thermal decomposition of dolomite and the extraction of its constituents. *Minerals Engineering.* **10**(10), pp. 1165-1176

Cailot T., Gelin P., Dailly J., Gaultier G., Cayron C. and J. Laurencin. 2007. Catalytic reforming of methane over $La_{0.8}Sr_{0.2}CrO_3$ based Ru catalysts.

Catalysis Today. **128** (3-4) 264- 268

Chaffee A.L., Knowles G.P., Liang Z., Zhang J., Xiao P. and P. A. Webley. 2007. CO_2 capture by adsorption: Materials and process development. *International Journal of Greenhouse Gas Control*. **1**(1), pp. 11-18

Chen C.- T. A. and A. V. Borges. 2009. Reconciling opposing views on carbon cycling in the coastal ocean: Continental shelves as sinks and near-shore ecosystems as sources of atmospheric CO_2. *Deep Sea Research Part II: Topical Studies in Oceanography*. **56**(8-10), pp.578-590

Chen L., Hong Q., Lin J. and F.M. Dautzenberg. 2007. Hydrogen Production by coupled catalytic partial oxidation and steam methane reforming at elevated pressure and temperature. Journal of Power Sources. **164**(2), pp.803-808

Chiu C. L. and T.-H. Chang. 2009. What proportion of renewable energy supplies is needed to initially mitigate CO_2 emissions in OECD member countries?. *Renewable and Sustainable Energy Reviews*. **13**(6-7), pp.1669-1674

V.R Choudary, S.G.Pataskar, M.Y.Pandit and V.G.Gunjikar. 1991. Thermal analysis of basic magnesium carbonate containing different alkali metal carbonates. *Thermochimica Acta*. 180, pp.69- 80.

V.R Choudary, S.G.Pataskar, V.G.Gunjikar and G.B. Zope. 1994. Influence of preparation conditions of basic magnesium carbonate on its thermal analysis. *Thermochimica Acta*. **232**(1), pp.95- 110.

Chrissafis K.[(a)], C. Dagounaki, K. M. Paraskevopoulos. 2005. The effect of sintering on the maximum capture efficiency of CO_2 using a carbonation/calcination cycle of carbonate rocks. *Journal of Thermal Analysis and Calorimetry*. **81**(1-2) (2005), pp.463- 468.

Chrissafis K., 2006, Multicyclic study on the carbonation of CaO using different limestones. *Journal of Thermal Analysis and Calorimetry*. **89**(2), pp.525-529

Chiu C. L. and T.-H. Chang. 2009. What proportion of renewable energy

supplies is needed to initially mitigate CO_2 emissions in OECD member countries?. *Renewable and Sustainable Energy Reviews*. **13**(6-7), pp.1669-1674

Corbo P and F. Migliardini. 2007. Hydrogen production by catalytic partial oxidation f methane and propane on Ni and Pt catalysts. *International Journal of Hydrogen Energy*. **32**(1), pp.55- 66

Cranston G. R. and G.P. Hammond. 2009. North and south: Regional footprints on the transition pathway towards a low carbon, global economy. *Applied Energy*. In Press, Corrected Proof

J. M. Criado, M.J. Dianez. 2004. Influence on the mechanical treatment on the structure and the thermal stability of alkaline- earth carbonates. *Journal of Material Sciences*. **39**(16-17), pp. 5189- 5193

Cui X.Y., Li Q., Chou K.-C., Chen S.-H., Lin G.- W., Xu K.- D., A. 2008. comparative study on the hydriding kinetics of Zr-based AB2 hydrogen storage alloys. Intermetallics. **16**(5), pp. 662- 667.

Curran G.P., Fink C. and E. Gorin. 1967. The CO_2 acceptor gasification process, American Chemical Society, Division of Fuel Chemistry, 8, pp.128-146.

Czernik S., French R., Feik C. And E. Chornet. 1999. Hydrogen from biomass via fast pyrolysis/catalytic steam reforming process. *Proceedings of the 1999 U.S Department Of Energy Hydrogen Program Review*.

Czernik S., Evans R. and R. French. 2007. Hydrogen from biomass-production by steam reforming of biomass pyrolysis oil. *Catalysis Today*. **129**(3-4), pp.265- 268.

Czernik, S and A.V. Bridgwater. 2004. Overview of Applications of Biomass Fast Pyrolysis Oil. *Energy Fuels*.**18**(2), pp.590–598

Dagoumas A.S. and T.S. Barker. 2010. Pathways to a low-carbon economy for the UK with the macro-econometric E3MG model. *Energy Policy*. In Press, Corrected Proof.

de Levie R., The electrolysis of water. 1999. Journal of Electroanalytical

Chemistry. 1999. **456**(1), pp.92- 93

Dennis J.S. and A.N. Hayhurst. 1987. The effect of CO_2 on the kinetics and extent of calcination of limestone and dolomite particles in fluidised beds. *Chemical Engineering Science*. **42**(10), pp.2361-2372.

Devi L., Ptasinski K. J., Janssen F.J.J. G., van Paasen S.V.B., Bergman P.C.A. and J.H.A. Kiel. 2005. Catalytic decomposition of biomass tars: use of dolomite and untreated olivine. *Renewable Energy*. **30**(4), pp.565- 587.

Ding Y. and E. Alpay. 2001. High temperature recovery of CO_2 from flue gases using hydrotalcite adsorbent. *TransIChemE*. **79**(1), pp. 45- 51.

Diskin A. M., Cunningham R. H. And R. M. Ormerod. 1998. The oxidative chemistry of methane over supported nickel catalysts. *Catalysis Today*. **46**(2-3), pp. 147- 158.

Dou B., Park S., Lim S., Yu T. U., Hwang J.. 2007. Pyrolysis characteristics of refuse derived fuel in a pilot- scale unit. *Energy and Fuels*. **21**(6), pp.3730- 3734.

Dou B., Dupont V., Rickett R., Blakeman N., Williams P.T., Chen H., Ding Y. and M. Ghadiri. 2009. Hydrogen production by sorption-enhanced steam reforming of glycerol. *Bioresource Technology*. **100**(14), pp.3540–3547

Dou B., Rickett G.L., Dupont V., Williams P.T. , Chen H., Ding Y. and M. Ghadiri. 2010. Steam reforming of crude glycerol with in situ CO_2 sorption, *Bioresource Technology*. **101**(7) , pp. 2436-2442

Dou B., Dupont V., Williams P. T., Chen, and Y. Ding. 2009. Thermogravimetric kinetics of crude glycerol. *Bioresource Technology*. **100**(90), pp. 2613-2620

Dubey P.K., A.S.K. Sinha, S. Talapatra, N. Koratkar, P.M. Ajayan and O.N. Srivastava. 2010. Hydrogen generation by water electrolysis using carbon nanotube anode. *International Journal of Hydrogen Energy*. **35**(9), pp.3945-3950

Dupont V. A., Ross A.B., Hanley I. and M. V. Twigg. 2007. Unmixed

steam reforming of methane and sunflower oil: a single reactor process for H_2-rich gas. *International Journal of Hydrogen Energy*. **32**(1), pp. 67- 79

Dupont V., Ross A.B., Hanley I. and M.V. Twigg. 2008. Production of hydrogen by unmixed steam reforming of methane. *Chemical Engineering Science*. **63**(11), pp.2066- 2079.

Eide L. I., Anheden M., LyngfeltA., Abanades C., Younes M., Clodic D., Bill A.A., Feron P.H.M., Rojey A. and F. Giroudiere, Novel Capture Processes, Oil & Gas Science and Technology, Vol. 60 (2005) No. 3, 497- 508

Eder K. and C. Brandsch. 2002. The effect of fatty acid composition of rapeseed oil on plasma lipids and oxidative stability of low-density lipoproteins in cholesterol-fed hamsters. *European Journal of Lipid Science and Technology*. **104**(1), pp.3-13.

Feng B., An H. And E. Tan. 2007. Screening of CO_2 adsorbing materials for zero emission power generation system. *Energy and Fuels*. **21**, pp. 123- 137.

Figueora J.D, Fout T., Plasynski S., McIlvried H. And R. D. Srivastava. 2008. Advances in CO_2 capture technology- The U.S. Department of energy's carbon sequestration program. *International Journal of Greenhouse Gas Control*. **2**(1), pp. 9-20.

Florin N. H. and A.T. Harris. 2007. Hydrogen production from biomass coupled with carbon dioxide capture: The implications of thermodynamic equilibrium. *International Journal of Hydrogen Energy*. **32**(17), pp. 4119-4134

Florin N. H. and A.T. Harris. 2008. Review- Enhanced hydrogen production from biomass with in situ carbon dioxide capture using calcium oxide sorbents. *Chemical Engineering Science*. **63**(2), pp.287- 316.

Ford report on the business impact of climate change: http://media.ford.com/downloads/05_climate.pdf

Foy K. and J. McGroven, Comparison of Ion Transport Membranes. 2- 5 May 2005. Conference Proceedings, 4rth Annual Conference of Carbon Capture and Sequestration DOE/ NETL (Department of Energy (U,S.)/ National

Energy Technology Laboratory).

Gallucci K., Stendardo S. and P.U. Foscolo. 2008. CO_2 capture by means of dolomite in hydrogen production from syngas. *International Journal of Hydrogen Energy*. **33**(12), pp. 3049-3055

Galvagno S., Casciaro G., Casu S., Martino M., Migazzini C., Russo A., Portofino S.. 2009. Steam gasification of tyre waste, poplar and refuse –derived fuel: A comparative analysis. *Waste Management*. **29**(2), pp.678- 689.

Garcia-Labiano, A. Abad, L.F.d Diego, P. Gayan and J. Adanez, 2002. Calcination of calcium based sorbents at pressure in a broad range of CO_2 concentrations. *Chemical Engineering Science*. **57**(13), pp. 2381–2393

Garcia-Perez M., Chaala A., H. Pakdel, D. Kretschmer, C. Roy. 2007. Characterization of bio-oils in chemical families, Biomass and Bioenergy. **31**(4), pp. 222-242

Gercel H. F.. 2002. The production and evaluation of bio-oils from the pyrolysis of sunflower oil- cake. *Biomass and Bioenergy*. **23**(4), pp.307- 314.

Gielen D. and T. Kra. 17-18 September, 1998. The Role of Non-CO_2 Greenhouse Gases in Meeting Kyoto Targets, "Climate Change and Economic Modelling: Background Analysis for the Kyoto Protocol" workshop. OECD Headquarters, Paris.

Gomi K., Shimada K. and Y. Matsuoka. 2009. A low-carbon scenario creation method for a local-scale economy and its application in Kyoto city Energy Policy, **38**(9), pp. 4783- 4796.

Gornay J., Coniglio L., Billaud F. and G. Wild. 2009. Steam cracking and steam reforming of waste cooking oil in a tubular stainless steel reactor with wall effects. *Energy and Fuels*. **23**(11), pp.5663- 5676.

Gemma S. Grasa and J. Carlos Abanades. 2006. CO_2 capture capacity of CaO in long series of carbonation/ calcination cycles. *Industrial and Engineering Chemistry Process Design*. **45**(26), pp.8846- 8851.

Grigoriev S.A., P. Millet, S.V. Korobtsev, V.I. Porembkiy, M.Pepic, C. Etievant, C. Puyenchet and V. N. Fateev. 2009. Hydrogen safety aspects related

to high- pressure polymer electrolyte membrane water electrolysis. *International Journal of Hydrogen Energy*. **34**(14), pp.5986- 5991

Gupta H. and Fan L.-S. 2002. Carbonation–Calcination Cycle Using High Reactivity Calcium Oxide for Carbon Dioxide Separation from Flue Gas. *Industrial and Engineering Chemistry Research*. **41**(16), pp 4035–4042

Guo H., Smallwood G.J., O.L. Gulder. 2007. The effect of reformate gas enrichment on extinction limits and NO_x formation in counterflow CH_4/ air premixed flames. Proceedings of the Combustion Institute. **31**(1), pp.1197-1204

Guo L.J., Zhao L., Jing D.W., Lu Y.J., Yang H.H., Bai B.F., Zhang X.M., Ma L.J. and X.M. Wu. Solar Hydrogen production and its development in China. *Energy*. **34**(9), pp.1073- 1090.

Hammons T.J. 2006. Impact of electric power generation on green house gas emissions in Europe: Russia, Greece, Italy and views of the EU Power Plant Supply Industry – a critical analysis. *Electrical Power and Energy Systems*. **28**(8) pp. 548–564

Han, C. and Harrison, D.. 1994. Simultaneous shift reaction and carbon dioxide separation for the direct production of hydrogen. *Chemical Engineering Science*. **49**(24B), pp.5875–5883.

Hao S., Xiao Q., Yang H., Zhong Y., Pepe F. and W. Zhu. 2010. Synthesis and CO_2 adsorption property of amino- functionalized silica nano-spheres with centro symmetric radial mesopores. *Microporous and Mesoporous Materials*. In press.

Haugsrud R. 2003. On the high- temperature oxidation of nickel. *Corrosion Science*. **45**(1), pp.211- 235.

Hartman M., O. Trnka, V. Vesely, K. Svoboda. 1996. Predicting the rate of thermal decomposition of dolomite. *Chemical Engineering Science*. **51**(23), pp. 5229-5232

Hauserman, W. B. 1994. High-yield hydrogen production by catalytic

gasification of coal or biomass. *International Journal of Hydrogen Energy* **19**(5) pp. 413-419.

Hendriksa C., de Vissera E., Jansenb D., Carbob M.. Ruijgb G. J. and J. Davisonc. 2009. Capture of CO_2 from Medium-scale Emission Sources. *Energy Procedia.* **1**(1) pp.1497- 1504.

Herzog H. 2001. What future for carbon capture and sequestration?. *Environmental Science and Technology.* **35**(7), pp.148A- 153A.

Hidayat T., Rhamdhani M.A., Jak E. and P.C. Hayes. 2008. The characterisation of metal pore structures and the measurement of intrinsic reaction rate during the reduction of nickel oxide in H_2- N_2 and H_2- H_2O atmospheres. Minerals Engineering. **21**(2), pp.157- 166.

Hildenbrand N., Readman J., Dahl I. M. and R. Blom. 2006. Sorbent enhanced steam reforming (SESR) of methane using dolomite as internal carbon dioxide absorbent: Limitations due to $Ca(OH)_2$ formation. *Applied Catalysis A: General.* **303**(1), pp.131-137

Hisschemöller M., Bode R. and M. Van de Kerkhof. 2006. What governs the transition to a sustainable hydrogen economy? Articulating the relationship between technologies and political institutions. Energy Policy. **34**, pp.1227-1235

Holladay J. D., Hu J., King D.L. and Y. Wang. 2009. An overview of hydrogen production technologies. Catalysis Today. **139**, pp.244- 260.

Hufton J., S. Mayorga, S. Nataraj, S. Sircar. 1999. Sorption-enhanced reaction process for the hydrogen production. *American Institute of Chemical Engineers Journal.* **45**(2) pp. 248–256.

Hughes R. W., Lu D., Anthony E. J. And Y. Wu. 2004. Improved long-term conversion of limestone- derived sorbents for in- situ capture of CO_2 in a fluidized bed combustor, Industrial and Engineering Chemical Research. **43**, pp.5529- 5539

Hyatt, E. P., Cutler, I. B., Wadsworth, M. E.. 1958. Calcium Carbonate

Decomposition in Carbon Dioxide Atmosphere. *Journal of American Ceramic Society*. **41**, pp.70- 74

Idem R.O. and N. N. Bakhshi. 1996. Kinetic modeling of the production of hydrogen from the methanol-steam reforming process over Mn-promoted coprecipitated Cu-Al catalyst. *Chemical Engineering Science*. **51**(14), pp.3697-3708

Idris S.-S., Rahman N.-A., Ismail K., Azil Bahari Alias, Zulkifli Abd Rashid, Mohd Jindra Aris. 2010. Investigation on thermochemical behaviour of low rank Malaysian coal, oil palm biomass and their blends during pyrolysis via thermogravimetric analysis (TGA). *Bioresource Technology*. **101**(12), pp. 4584-4592.

IEA (International Environmental Agency), 2007, Renewables in Global Energy Supply: An IEA fact sheet

IEA (InternationalEnvironmental Agency , "CO2 emissions from fuel combustion 2009- Highlights" (free publications papers)) website (http://www.iea.org/co2highlights/co2highlights.pdf)

Inui T. and S. B. Pu. 1995. Separation of 2,6-dimethylnaphthalene from a mixture of its isomers using lithium-incorporated zeolite Y synthesized by rapid crystallization method. *Separations Technology*. **5**(4), pp.229-237.

Iordanidis A., Kechagiopoulos P.N., Voutetakis S.S., Lemonidou A.A. and I.A. Vasalos. 2006. Autothermal sorption-enhanced steam reforming of bio-oil/biogas mixture and energy generation by fuel cells: Concept analysis and process simulation. *International Journal of Hydrogen Energy*. **31**(8), pp.1058 – 1065

Ishida, M., Zheng, D., Akehata, T. 1987. Evaluation of a chemical-looping combustion power-generation system by graphic exergy analysis. *Energy*. **12** (2), pp.147–154.

K. Iwafuchi, C. Watanabe, R. Otsuka. 1983. Thermal decomposition of ferromanganoan dolomite. Thermochimica Acta. **66**, pp.105- 125

Jakobsen J.P. and E. Halmoy. 2009. Reactor Modeling of Sorption enhanced Steam Methane Reforming. *Energy Procedia.* **1**(1), pp.725- 132

Janaun J. And N. Ellis. 2010. Perspectives on biodiesel as a sustainable fuel. *Renewable and Sustainable Energy Reviews.* **141**, pp.1312- 1320

Johnsen, K., Ryu, H.J., Grace, J.R., Lim, C.J. 2006. Sorption-enhanced steam reforming of methane in fluidized bed reactor with dolomite as CO_2-acceptor. *Chemical Engineering Science.* **61**, pp.1195–1202.

Johnsen K. and J.R. Grace. 2007. High temperature attrition of sorbents and a catalyst for sorption- enhanced steam methane reforming in a fluidized bed environment. (Short Communication) *Powder Technology.* **173**(3) 200- 202

Kazim, A and T.N. Veziroglou. 2001. Utilization of solar-hydrogen energy in the UAE to maintain its share in the world energy market for the 21st century. *Journal of Renewable Energy.* **24**, pp.259-274.

Kelly N. A., Gibson T.L. and D. B. Ouwerkerk. 2008. A solar- powered high efficiency hydrogen fueling system using high- pressure electrolysis of water: Design and initial results. *International Journal of Hydrogen Energy.* **30**, pp.2747- 2764

Khan N., D. Dollimore, K. Alexander, F.W. Willburn. 2001. The origin of the exothermic peak in the thermal decomposition of basic magnesium carbonate. *Thermochimica Acta.* **367- 368**, pp.321- 333.

Kirubakaran V., Sivaramakrishnan V., Nalini R., Sekar T., Premalatha M., and P. Subramanian. 2009. A review on gasification of biomass. *Renewable and Sustainable Energy Reviews.* **13**, pp.179- 186

Koh A.C.W., Chen L., Leong W.K., Johnson B.F.G., Khimyak T. and J. Lin. 2007. Hydrogen or synthesis gas production via the partial oxidation of methane over supported nickel- cobalt catalysts. *International Journal of Hydrogen.* **32**, pp.725- 730

Koppatz S., Pfeifer C., Rauch R., Hofbauer H., Marquard- Moellenstedt T. and M. Specht. 2009. H_2 rich product gas by steam gasification of biomass with insitu CO_2 adsorption in a dual fluidized bed system of 8MW fuel input.

Fuel Processing Technology. **90**, pp.914- 921.

Kumar Saha P., Saha S., Koner S. 2003. Chromotropism of Cr (salen) moiety in zeolite matrix: synthesis, characterization and catalytic activity study of Cr(salen)-NaY hybrid catalyst. *Journal of Molecular Catalysis A: Chemical*. **203**, (1-2), pp.173-178.

Kumar, R., Moorefield, C., Kulkarni, P., Eiteneer, B., Reinker, J., Zamansky, V., Manning, M. 1999. Unmixed Reforming: An advanced Steam Reforming Process. Fuel Division. In: Preprints of Symposia, 218th ACS National Meeting, August 22–26, New Orleans, LA, **44**(4), pp. 894–898

L'vov B.V., L. K. Polzik and V. L. Ugolkov. 2002. Decomposition kinetics of calcite: a new approach to the old problem. Thermochimica Acta. **390**, pp.5- 19

L'vov B.V. and V. L. Ugolkov. 2003. Kinetics of free-surface decomposition of dolomite single crystals and powders analyzed thermogravimetrically by the third-law method. Thermochimica Acta. **401**, pp.139-147

Lang X., Dalai A.K., Bakhshi N.N., Reaney M.J. and P.B. Hertz. 2001. Preparation and characterisation of bio- diesels from various bio- oils. *Biosource Technology*. **80**, pp. 53- 62.

Lee D.K., Baek I.H. and W.L. Yoon. 2004. Modeling and simulation for the methane steam reforming enhanced by in- situ CO_2 removal utilizing the CaO carbonation for H_2 production. Chemical Engineering Science. **59**, pp.931-942.

Lee D.K. 2004. An apparent kinetic model for the carbonation of calcium oxide by carbon dioxide. Chemical Engineering Journal. **100**, pp.71 -77.

Li D., Atake I., Shishido T., Oumi Y., Sano T. and K. Takehira. 2007. Self- regenerative activity of N/ Mg(Al)O catalysts with trace Ru during daily start- up and shut- down operation of CH_4 steam reforming. *Journal of Catalysis*. **250**, pp. 299- 312.

Li S.- D., C.-C. Wang and C.-Y. Chen. 2010. Water electrolysis for H_2

production using a novel bipolar membrane in low salt concentration. *Journal of Membrane Science*. **330**(1-2) pp. 334- 340.

Li X. T., Grace J. R., Lim C. J., Watkinson A. P., Chen H. P. and J. R. Kim. 2004. Biomass gasification in a circulating fluidised bed. *Biomass and Bioenergy*. **26**, pp.171- 193

Li Y., Zhao C., Duan L., Liang C., Li Q., Zhou W. And H. Chen. 2008. Cyclic calcination/carbonation looping of dolomite modified with acetic acid for CO_2 capture. *Fuel Processing Technology*. **89**(12), pp.1461-1469

Li Z. and N. Cai. 2007. Modeling of Multiple Cycles for Sorption-Enhanced Steam Methane Reforming and Sorbent Regeneration in Fixed Bed Reactor. *Energy Fuels*. **21**(5), pp 2909–2918

Li, Z., Zhao, W., Meng, B., Liu, C., Zhu, Q. & Zhao, G. 2008. Kinetic study of corn straw pyrolysis: Comparison of two different three-pseudocomponent models. *Bioresource Technology*. **99**, pp.7616-7622

Liang Z., Marshall M. and A.L. Chaffee. 2009. Comparison of Cu- BTC and zeolite 13X for adsorbent based CO_2 separation. *Energy Procedia*. **1**, pp.1265- 1271

Lin S.- Y., Suzuki Y., Hatano H. and M. Harada. 2002. Developing an innovative method, HyPr-RING to produce hydrogen from hydrocarbons. *Energy Conversion and Management*. **43**, pp.1283- 1290

Liu H. and K. Sims Gallagher. 2010. Catalyzing strategic transformation to a low-carbon economy: A CCS roadmap for China Energy Policy. **38**(1), pp.59-74

Liu K., Song C. and V. Subramani (Sircar S. and T. C. Golden), Chapter 10 Adsorbents for Hydrogen PSA Processes, Hydrogen and Syngas production and purification technologies, WILEY AICHEME, 2010.

Lopez- Oritz A., Perez- Riveria N. G., Reyes Rojas A. and D. Lardizabal Gutierrez. 2004. Novel carbon dioxide solid acceptors using sodium containing oxides. *Separation Science and Technology*. **39**, pp.3559- 3572.

Luangkiattikhun P., Tangsathitkulchai C. and M. Tangsathitkulchai. 2008.

Non-isothermal thermogravimetric analysis of oil-palm solid wastes. *Bioresource Technology*. **99**(5), pp.986-997

Lyngfelt A., Leckner B. and T. Mattisson. 2001. A fluidized-bed combustion process with inherent CO_2 separation; application of chemical-looping combustion. *Journal of Chemical Engineering Science*. **56**(10), pp.3101-3113.

Lyon R. K. and J. A. Cole. 2000. Unmixed combustion: An alternative to fire. *Combustion and flame*. **121**, pp.249- 261.

Madhukar R. Mahishi and D. Y. Goswami. 2007. An experimental study of hydrogen production by gasification of biomass in the presence of CO_2 sorbent. *International Journal of Hydrogen Energy*. **32**, pp.2803- 2808

Magrini- Bair K.A., Czernik S., French R. and E. Chornet. 2003. Fluidizable catalysts for hydrogen production from biomass pyrolysis steam reforming. *Hydrogen, Fuel Cells and Infrastructure Technologies*. FY 2003 Progress Report.

Maher, K.D. and Bressler D.C. 2007. Pyrolysis of triglyceride materials for the production of renewable fuels and chemicals. Bioresources Technology. **98**(12), 2351- 2368.

Mahishi M.R. and D.Y. Goswami. 2007. An experimental study of hydrogen production by gasification of biomass in the presence of a CO_2 sorbent. *International Journal of Hydrogen Energy*. **32**, pp.2803- 2808.

Maitra S., A. Choudhury, H. S. Das, MS J. Pramanik. 2005. Effect of compaction on the kinetics of thermal decomposition of dolomite under non-isothermal condition. Journal of Material Science. **40**, pp.4749- 475

Majlan E.H., Daud W.R.W., Iyuke S.E., Mohamad A.B., Kadhum A.A.H., Mohammad A.W., Takriff M.S. and N. Bahaman. 2009. Hydrogen purification using compact pressure swing adsorption system for fuel cell. *International Journal of Hydrogen Energy*. **34**(6), pp.2771- 2777

Manovic V. and E. J. Anthony. 2008. Sequential SO_2/CO_2 capture enhanced by steam reactivation of a CaO-based sorbent. *Fuel*. **87**(8-9), pp.1564-

1573

Manovic V., Anthony E.J., and D. Loncarevic. 2009. CO_2 looping cycles with CaO-based sorbent pretreated in CO_2 at high temperature. *Chemical Engineering Science*. **64**, pp.3236-3245.

Marquevich M., Coll R. and D. Montané. 2000. Steam Reforming of Sunflower Oil for Hydrogen Production. *Industrial and Engineering Chemical Research*. **39**(7), pp.2140-2147.

Marquevich M., Farriol X., Medina F., Montane D. 2001. Hydrogen production by steam reforming of vegetable oils using nickel based catalysts. *Industrial and Engineering Chemistry Research*. **40**, pp.4757- 4766

Martavaltzi C. S. and A. A. Lemonidou. 2008. Development of new CaO based sorbent materials for CO_2 removal at high temperature. *Microporous and Mesoporous Materials*. **110**(1), pp. 119-127

Mastalir A., Patzko A, Frank B., Schomäcker A., Ressler T. and R. Schlögl. 2007. Steam reforming of methanol over Cu/ ZnO/ Al_2O_3 modified with hydrotalcites. *Catalysis Communications*. **8**, pp.1684- 1690.

Mastral A.M., Murillo R., Garcia T., Navarro M.V., Callen M.S. and J.M. Lopez. 2002. Study of the viability of the process for hydrogen recovery from old tyre oils. *Fuel Processing Technology*. **75**(3), pp.185- 199.

Mathews J. A. 2008. How carbon credits could drive the emergence of renewable energies. *Energy Policy*. **36**(10), pp.3633-3639

Matsumura Y. And T. Nakamori. 2004. Steam reforming of methane over nickel catalysts at low reaction temperature. *Applied Catalysis A: General*. **258**(1), pp.107- 114.

Mattisson T., Johansson M. And A. Lyngfelt. 2006. The use of NiO as an oxygen carrier in chemical looping combustion. *Fuel*. **85**(5-6), pp.736- 747.

McCauley R.A. and L.A. Johnson. 1999. Dicrepitation and thermal decomposition of dolomite. *Thermochimica Acta*. **185**, pp.271- 282

McIntosh R.M., J.H. Sharp and F.W. Wilburn. 1990. The thermal

decomposition of dolomite. *Thermochimica Acta.* **165**, pp.281- 296

McKenzie K.J. D. and R.H. Meinhold. 1993. Thermal decomposition of dolomite (calcium magnesium carbonate) studied by ^{25}Mg solid state nuclear magnetic resonance. *Thermochimica Acta.* **230**, pp.331- 337

Minerological Society of America- International Zeolite Association. 2009 (http://www.iza-structure.org/).

Modafferi V., Pangerra G., Paglio V., Fusteri F. and P.L. Antonucci. 2009. Applied Catalysis A: General. **334**, pp.1- 9

Molina- Sabio M., Munecas M.A., Rodrigues- Reinoso F. and B. McEnaney. 1995. Adsorption of CO_2 and SO_2 on activated carbons with a wide range of micropore size distribution. *Carbon.* **33**(12), pp 1777- 1782.

Montanari T. and G. Busca. 2008. On the mechanism of adsorption and separation of CO_2 on LTA zeolites: An IR investigation. *Vibrational Spectroscopy.* **46**(1), pp. 45-51.

Morin J.-X. and C. Béal, Ch 37, Chemical Looping Combustion of Refinery Fuel Gas with CO_2 Capture, Carbon Dioxide Capture for Storage in Deep Geologic Formations. 2005. pp.647-654.

Mosca A., Hedlund J., Ridha F.N., P. Webley. 2008. Optimization of synthesis procedures for structured PSA adsorbents. *Adsorption.***14**, pp.687–693

Mrowec S. and Z. Grzesik. 2004. Oxidation of nickel and transport properties of nickel oxide. *Journal of Physics and Chemistry of Solids.* **65**(10), pp.1651- 1657.

Mueller-Langer F., Tzimas E., Kaltschmidtt M. and S. Peteves. 2007. Techno-economic assessment of hydrogen production processes for the hydrogen economy for the short and medium term. *International Journal of Hydrogen Energy.* **32**, pp. 3797- 3810.

Muradov,T. and N. Veziroğlu. 2008. "Green" path from fossil- based to hydrogen economy: An overview of carbon- neutral technologies Review Article. *International Journal of Hydrogen Energy.* **33**(23), pp.6804- 6839

Myren C., Hoernell C., Bjornbom E. and K. Sjostrom. 2002. Catalytic tar decomposition of biomass pyrolysis gas with a combination of dolomite and silica. *Biomass Bioenergy*. **23**(3), pp.217- 227.

Nader S. 2009. Paths to a low-carbon economy—The Masdar example. *Energy Procedia*. **1**(1), pp.3951-3958

Nagaoka K., Sato K., Nishiguchi H. and Y. Takita. 2007. Highly active Ni/ MgO in oxidative steam pre- reforming of n- butane for fuel cell application. *Catalysis Communications*. **8**, pp.1807- 1810.

Ni M., Leung D.Y.C., Leung M.K.H. and K. Sumathy. 2006. An overview of hydrogen production from biomass. *Journal of Fuel Processing Technology*. **87**, pp.461-472.

Nikulshina V., Gálvez M.E. and A. Steinfeld, 2007. Kinetic analysis of the carbonation reactions for the capture of CO_2 from air via the $Ca(OH)_2$–$CaCO_3$–CaO solar thermochemical cycle. *Chemical Engineering Journal*. **129**, pp.75-83

Ochoa-Fernández E., Lacalle-Vilà C., Zhao T., Rønning M., Chen D. 2007. Experimental demonstration of H_2 production by CO_2 sorption enhanced steam methane reforming using ceramic acceptors. *Studies in Surface Science and Catalysis*. **167**, pp.159-164

Oliveira E. L.G., Grande C. A. and A. E. Rodrigues. 2008. CO_2 sorption on hydrotalcite and alkali modified (K and Cs) hydrotalcites at high temperatures. *Separation and Purification Technology*. **62**, pp.137-147.

Olszak-Humienik M. and J. Możejko. 1999. Kinetics of thermal decomposition of dolomite. *Journal of Thermal Analysis and Calorimetry*. **56**, pp.829-833.

Otsuka K. and T. Nakajima. 1986. Partial oxidation of methane over rare earth metal oxides using N_2O and O_2 as oxidants. *Inorganica Chimica Acta*. **120**, L27-L28

Otsuka K., Takashi R., Amakawa K. and I. Yamanaka. 1998. Partial oxidation of light alkanes by NOx in the gas phase. *Catalysis Today*. **45**, pp.23-

Ozao R., Ochiai M., Yamazaki A. and R. Otsuka. 1991. Thermal analysis on ground dolomites. *Thermochimica Acta.* **183**, pp.183- 198

Peace J. and T. Juliani. 2009. The coming carbon market and its impact on the American economy. *Policy and Society.* **27**(4), pp.305-316

Pellerano M., Pri P., Kacem M. And A. Delebarre. 2009. CO_2 capture by adsorption on activated carbons using pressure modulation. *Energy Procedia.* **1**, pp. 647- 653.

Petitpas G., Rollier J.- D., Darmon A., Gonzalez- Aguilar J., Metkemeijer R. and L. Fulcheri. 2007. A comparative study of non- thermal plasma assisted reforming technologies- Review. *International Journal of Hydrogen Energy.* **32**, pp.2848- 2867

Pimenidou P.[(a)], Rickett G.L., Dupont V. and M.V.Twigg. 2010. Chemical looping reforming of waste cooking oil in a packed bed reactor. *Bioresource Technology.* **101**(23) pp.6389- 6397.

Pimenidou P.[(b)], Rickett G.L., Dupont V. and M.V.Twigg.2010. High purity H_2 by sorption- enhanced chemical looping reforming of waste cooking oil in a packed bed reactor, Bioresource Technology. **101**(16), pp.9279- 9286

Pimenidou P., Rickett G.L. and V. Dupont, In- situ CO_2 capture for unmixed steam reforming. Oral presentation at WCCE8 (8^{th} World Congress of Chemical Engineering). August 23- 27 2009, Montreal, Canada

Plaza M. G., Pevida C., Arenillas A., Rubiera F. and J. J. Pis. 2007. CO_2 capture by adsorption with nitrogen enriched carbons. *Fuel.* **86**, pp.2204- 2212

Prasad Y.S. and Bakshi N.N. 1985. Effect of pretreatment of HZSM-5 catalyst on its performance in canola oil upgrading. Applied Catalysis. **18**, pp.71- 85.

Profeti L. P.R., Ticianelli E.A. and E. M. Assaf. 2009. Production of hydrogen via steam reforming of biofuels on $Ni/CeO_2–Al_2O_3$ catalysts promoted by noble metals. *International Journal of Hydrogen Energy.* **34**(12), pp.5049-5060.

Ramadhas A.S., Jayaraj S., C. Muraleedharan. 2004. Use of vegetable oils as I.C. engine fuels- A review. *Renewable Energy*. **29**(5), pp. 727- 742.

Rao A.B. and E.S. Rubin. 2002. A technical, economic and environmental assessment of amine- based CO_2 capture technology for power plant greenhouse gas control. *Environmental Science and Technology*. **36**, pp.4467- 4475.

Rawadieh S. and V. G. Gomes. 2009. Steam reforming for hydrogen generation with in situ adsorptive separation. *International Journal of Hydrogen Energy*. 34, pp.343-355.

Reina J., Velo E., Puigjaner L.. 1998. Thermogravimetric study of the pyrolysis of waste wood. Thermochimica Acta. **320**(1-2), pp. 161-167.

Ren T. and M. K. Patel. 2009. Basic petrochemicals from natural gas, coal and biomass: Energy use and CO_2 emissions. *Resources, Conservation and Recycling*. **53**, pp.513–528.

Rioche C., Kulkarni S., Meunier F.C., Breen J.P. and R. Burch. 2005. Steam reforming of model compounds and fast pyrolysis bio-oil on supported noble metal catalysts. *Journal of Applied Catalysis B: Environmental*. **61**(1- 2), pp.130-139.

Ritter J.A. Ebner A.D., McIntyre J.A., Reynolds S.P. and S.A. Gadre. 2004. Radically new adsorption cycles for carbon dioxide sequestration, University Coal Research Contractors Review Meeting, U.S. DOE National Energy Technology Laboratory, Pittsburgh, Pennsylvania, June 10, 2004

Rizeq, G., West, J., Frydman, A., Subia, R., Zamansky, V., Loreth, H., Stonawski, L., Wiltowski, T., Hippo, E., Lalvani, S., 2003. Fuel flexible gasification–combustion technology for production of H_2 and sequestration-ready CO_2. DOE Award no. DE-FC26-00FT40974 Quaterly Technical Progress Report no. 9, Reporting period October 1, 2002–December 31, 2002.

Robert P., Dr Adams. 2007. Identification of Essential Oil Components By Gas Chromatography/Mass Spectrometry. Allured Pub Corp. ISBN 1-932633-21-9.

Romeo L. M., Lara Y., Lisbona P. and A. Martinez. 2009. Economical

assessment of competitive enhanced limestones for CO_2 capture cycles in power plants. *Fuel Processing Technology*. **90**, pp.803- 811.

Rubin E. S., Chen C. and Rao A. B. 2007. Cost and performance of fossil fuel power plants with CO_2 capture and storage. *Energy Policy*. **35**, pp.4444-4454

Ruy J- H., Lee K-Y., La H., Kim H.- J., Yung J.- I., and H. Jung. Ni-catalyst wash- coated on metal monolith with enhanced heat- transfer capability for steam reforming. *Journal of Power Resources*. **171**, pp. 499- 505

Rydén M., Lyngfelt A., Mattisson T., Chen D., Holmen A. and E. Bjørgum. 2008. Novel oxygen-carrier materials for chemical-looping combustion and chemical-looping reforming; $La_xSr_{1-x}Fe_yCo_{1-y}O_{3-\delta}$ perovskites and mixed-metal oxides of NiO, Fe_2O_3 and Mn_3O_4. *International Journal of Greenhouse Gas Control*. **2**, pp.21-36.

Samtani M., D. Dollimore and K. Alexander. 2001. Thermal decomposition of dolomite in an atmosphere of carbon dioxide. *Journal of Thermal Analysis and Calorimetry*. **65**, pp.93- 101.

Samtani M., Dollimore D., Willburn F.W. and K. Alexander. 2001. Isolation and identification of the intermediate and final products of the thermal decomposition of dolomite in an atmosphere of carbon dioxide. *Thermochimica Acta*. **367- 368**, pp.285- 295.

Samtani M., Dollimore D. and K.S. Alexander. 2002. Comparison of dolomite decomposition kinetics with related carbonates and the effect of procedural variables on its kinetic parameters. *Thermochimica Acta*. **392- 393**, pp 135- 145.

Sánchez-Sánche, M. C, Navarro M.R. and J.L.G. Fierro.2007. Ethanol steam reforming over Ni/MxOy–Al2O3 (M=Ce, La, Zr and Mg) catalysts: Influence of support on the hydrogen production. *International Journal of Hydrogen Energy*. **32** pp. 1462-1471.

Sarkar S.C. and A. Bose. Role of activated carbon pellets in carbon dioxide removal, Energy conversion and management. **38**, pp. 105- 110

Sato K. and K. Fujimoto. 2007. Development of new nickel based catalyst for tar reforming with superior resistance to sulphur poisoning and coking in biomass gasification. Catalysis Communications. **8**, pp.1697- 1701

Shafiee S. and E. Topal. 2009. When will fossil fuels be diminished?. Energy Policy. **37**, pp.181- 189.

Shimada K., Tanaka Y., Gomi K. and Y. Matsuoka. 2007. Developing a long-term local society design methodology towards a low-carbon economy: An application to Shiga Prefecture in Japan. Energy Policy. **35**(9), pp.4688-4703.

Shimizu T., T.Hirama, H.Hosoda, K.Kitano, M.Inagaki and K.Tejima. 1999. A twin fluid-bed reactor for removal of CO_2 from combustion processes. *Chemical Engineering Research and Design*. **77**(1) 62-68.

Shu Q., Gao J., Nawaz Z., Liao Y., Wang D. and J Wang. 2010. Synthesis of biodiesel from waste vegetable oil with large amounts of free fatty acids using a carbon-based solid acid catalyst. *Applied Energy*. **84**(8) pp.- 2596.

Silaban A., M. Narcida and D.P. Harrison. 1996. Characteristics of the reversible reaction between CO_2 (g) and calcined dolomite. Chemical Engineering Communications, 146, pp.149- 162.

Singh R., Reddy M.K.R., Wilson S., Joshi K., Diniz da Costa J.C. and P. Webley. 2009. High temperature materials for CO_2 capture. *Energy Procedia*. **1**, pp.623- 630.

Smith J.W., Johnson D.R. and M. Müller-Vonmoos. 1974. Dolomite for determining atmosphere control in thermal analysis. *Thermochimica Acta*. **8**, pp.45-56.

Solieman A.A.A., Dijkstra J.W., Haije W.G., Cobden B. D. and R. W. van den Brink. 2009. Calcium oxide for CO_2 capture: Operational window and efficiency penalty in sorption- enhanced steam methane reforming. *International Journal of Greenhouse Control*. **3**(4), pp.393- 400.

Song C. 2006. Global challenges and strategies for control, conversion and utilization of CO_2 for sustainable development involving energy, catalysis,

adsorption and chemical processing. *Catalysis Today*. **115**, pp.2–32.

Squire A.M.. 1967. Cyclic use of calcined dolomite to desulfurize fuels undergoing gasification. *Advances in Chemistry Series*. **69**, pp.205–229

Stanmore B.R. and P. Gilot. 2005. Review- Calcination and carbonation of limestone during thermal cycling for CO_2 sequestration. *Fuel Processing Technology*. **86**(16), pp.1707- 1743.

Stefanescu A., van Veen A.V., Duval- Brunel E. and Mirodatos C. 2007. Investigation of a Ni- based steam reforming catalyst developed for the coating of microstructures. *Chemical Engineering Science*. **62**, pp.5092- 5096

Stefaniak E., Bilinski B., Dobrowolski R., Staszczuk P. and J. Wojcik. 2002. The influence of preparation conditions on adsorption properties and porosity of dolomite- based sorbents. *Colloids and Surfaces A: Physicochemical and engineering Aspects*. **208**, pp.337- 345

Stendardo S. and P. U. Foscolo. 2009. Carbon dioxide capture with dolomite: A model for gas–solid reaction within the grains of a particulate sorbent. *Chemical Engineering Science*. **64**, pp.2343-2352.

Stiegel G.J. and M. Ramezan. 2006. Hydrogen from coal gasification: An economical pathway to a sustainable energy future. *International Journal of Coal Geology*. **65**, pp.173- 190.

Sugiura K., Takei K., Tanimoto K. and Y. Miyazaki. 2003. The carbon dioxide concentrator by using MCFC. *Journal of Power Sources*. **118**(1-2), pp.218- 227.

Sun P., Grace J. R., Lim C.J. and E. J. Anthony. 2008. Determination of intrinsic rate constants of the CaO–CO_2 reaction. *Chemical Engineering Science*. **63**, pp.47-56.

Sun, J., Qiu X., Wu F., Zhu W., Wang W. and S. Hao. 2004. Hydrogen from steam reforming of ethanol in low and middle temperature range for fuel cell application. *International Journal of Hydrogen Energy*. **29**(10) pp.1075-1081

Takanabe K., Aika K., Seshan K., Lefferts L. 2004. Sustainable hydrogen

from bio- oil- Steam reforming of acetic acid as a model oxygenate. *Journal of Catalysis.* **227**(1), pp.101- 108.

Takehira K., Shishido T., Wang P., Kosaka T. and K. Takaki. 2004. Autothermal reforming of CH_4 over supported Ni catalysts prepared from Mg–Al hydrotalcite-like anionic clay. *Journal of Catalysis.* **221**, pp.43-54.

Thambimuthu K., Davison J. and M Gupta, IPCC workshop on carbon dioxide workshop Geneva, 17- 20April 2002

Toonssen R., Woudstra N. And A.H.M. Verkooijen. 2008. Exergy analysis of hydrogen production plants based on biomass gasification. *International Journal of Hydrogen Energy.* **33**, pp.4074- 4082.

U.S. Department of Energy: Energy Efficiency and Renewable Energy. Hydrogen Production – Natural Gas Reforming. (15/12/2008), http://www1.eere.energy.gov/hydrogenandfuelcells/production/natural_gas.html

UNFCCC (United Nations Framework Convention on Climate Change), Kyoto protocol, http://unfccc.int/kyoto_protocol/items/2830.php

Urbanovici, E., Popescu, C., Segal, E. 1999. Improved iterative version of the Coats- Redfern method to evaluate non- isothermal kinetic parameters. *Journal of Thermal Analysis and Calorimetry.* **58**, pp.683-700

Uzun B.B., Pütün A.E., Pütün E. 2007. Composition of products obtained via fast pyrolysis of olive- oil residue: Effect of pyrolysis temperature. *Journal of Analytical and Applied Pyrolysis.* **79**(1- 2), pp.147- 153

Vagia, C. E. and A.A. Lemonidou. 2008. Hydrogen production via steam reforming of bio-oil components over calcium aluminate supported nickel and noble metal catalysts. *Journal of Applied Catalysis A: General.* **351**, pp.111–121

Vágvölgyi V., Palmer S. J., Kristóf J., Frost R. L. and E. Horváth. 2008. Mechanism for hydrotalcite decomposition: A controlled rate thermal analysis study. *Journal of Colloid and Interface Science.* **318**(2), pp.302-308.

van de Broek M., Hoefnagels R., Rubin E., Turkenburg W. and A. Faaij. 2009. Effects of technological learning on future cost and performance of power

plants with CO_2 capture. *Progress in Energy and Combustion Science*. 35. pp.457- 480.

Verhelst S. and T. Wallner. 2009. Hydrogen- fuelled internal combustion engines- Review. *Energy and Combustion Science*. **135**. pp.490- 527.

Wang J., Yao Y., Cao J. and M. Jiang. 2010. Enhanced catalysis of K_2CO_3 for steam gasification of coal char by using $Ca(OH)_2$ in char preparation. *Fuel*. **89**, pp.310- 317.

Wang Y. and W. J. Thomson. 1995. The effects of steam and carbon dioxide on calcite decomposition using dynamic X-ray diffraction. *Chemical Engineering Science*. **50**, pp.1373-1382.

Wang Z., Pan Y., Dong T., Zhu X., Kan T., Yuan L., Torimoto Y., Sadakata M. and Q. Li. 2007. Production of hydrogen from catalytic steam reforming of bio-oil using C12A7-O^- based catalysts. *Applied Catalysis A: General*. **320**, pp.24- 34

Wee J-H. 2010. Contribution of fuel cell systems to CO_2 emissions reduction in their application fields. *Renewable and Sustainable Energy Reviews*. **14**, pp.735- 744.

Wei G., Y. Wang, C. Huang, Q. Gao, Z. Whang and L. Xu. 2010. The stability of MEAnin SPE water electrolysis for hydrogen production. *International Journal of Hydrogen Energy*. **35**, pp.3951- 3957.

Weinberger B., Darkrim Lamari F., Veziroglu A., Beyaz S. and M. Beauverger. 2009. Accurate gas – Zeolite interaction measurements by using high pressure gravimetric volumetric adsorption method. *International Journal of Hydrogen Energy*. **34**(7), pp. 3191-3196.

White C.M., Steeper R.R. and A.E. Lutz. 2006. The hydrogen fuelled internal combustion engine: a technical review. *International Journal of Hydrogen Energy*. **31**, pp.1292- 1305.

Whitehead J.C. 2010. Plasma catalysis: A solution for environmental problems. *Pure Applied Chemistry*. **82**(6), pp. 1329- 1336.

Wigmans T. 1989. Industrial aspects of production and use of activated

carbons. *Carbon.* **27**(1), pp.13-22.

Xiong R., Ida J., Y.- S. Lin. 2003. Kinetics of carbon dioxide sorption on potassium doped lithium zirconate. *Chemical Engineering Science.* **58**. pp.4377- 4385.

ya Nsakala N., Liljedahl G.N. and J. L. Marion, Alstom Power Inc. 2004. Technology Options for Controlling CO_2 Emissions from Fossil Fueled Power Plants, IEA APEC

Yamada N. and M. N. Anuar Mohamad. 2010. Efficiency of hydrogen internal combustion engine combined with open steam Rankine cycle recovering water and waste heat. *International Journal of Hydrogen Energy.* **35**, pp.1430- 1442.

Yong Z. and A. E. Rodriguez. 2002. Hydrotalcite like compounds as adsorbents for carbon dioxide. *Energy Conversion and Management.* **43**. pp.1865- 1876

Yong Z., Mata V. and A. E. Rodrigues. 2001. Adsorption of carbon dioxide on hydrotalcite like compounds (HTLcs) at high temperatures. *Industrial and Engineering Chemistry Research.* **40**, pp.204- 209.

Yong Z., Mata V. and A. E. Rodriguez. 2002. Adsorption of carbon dioxide at high temperature- a review. *Separation and Purification Technology.* **26**, pp.195- 205.

Zeman F. 2008. Effect of steam hydration on performance of lime sorbent for CO_2 capture. *International Journal of Greenhouse Gas Control.* **2**(2), pp. 203-209.

Zeng K. and D. Zhang. 2010. Recent progress in alkaline water electrolysis for hydrogen production and applications. *Progress in Energy and Combustion Science.* **36**(3) pp.307- 326.

Zhang Y., Ashizawa M., Kajitani S. and S. Hara. 2010. A new approach to catalytic coal gasification: The recovery and reuse of calcium using biomass derived crude vinegars. *Fuel.* **89**, pp.417- 422.

Zhang, Q; Chang, J; Wang, TJ. 2007. Review of biomass pyrolysis oil properties and upgrading research. *Energy conversion and management*. **48**(1), pp. 87- 92.

Zhao B., Zhang X., Sun L., Meng G., Chen L. and Y. Xiaolu. 2010. Hydrogen production from biomass combining pyrolysis and the secondary decomposition. *International Journal of Hydrogen Energy*. **35**, pp.2606- 2611.